

Bio2Cementation: A novel treatment coupling clay aggregation and bio-cementation in sand-bentonite porous media

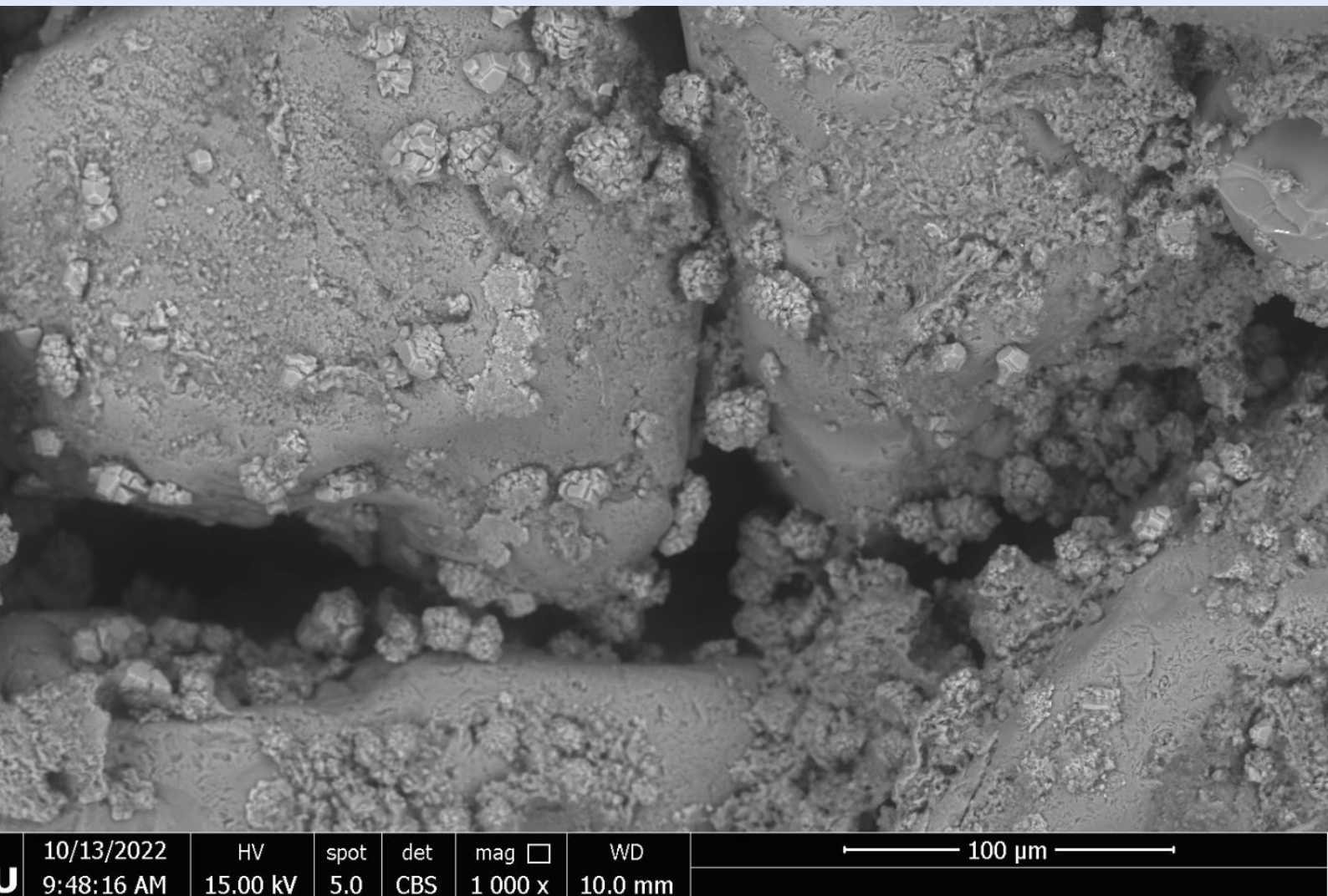
Master Thesis by Rocco Wennubst-Pedrini^a 5329728

^a*Technische Universiteit Delft, Postbus 5, 2600 AA, Delft, The Netherlands*

Supervised by Dr. Anne-Catherine Dieudonné (CEG, TU Delft)

Supported by thesis committee members Dr. Julia Gebert (CEG, TU Delft) and Dr. Henk Jonkers (3MD, TU Delft)

24th of November 2022



Abstract

The geo-technical quest to couple technical, environmental, and economic innovation, has increased recent attention towards bio-inspired soil strengthening techniques. This thesis presents a proof-of-concept for a coupled clay inhibition and bio-cementation treatment tested in sand-bentonite, referred to as *Bio2Cementation*. Fine particles are first aggregated using a nitrogen based compound. By binding the electrical double layer of clay minerals, the aggregates become chemically and physically stable. Thereafter, bio-cementation treatments hydrolyze urea to precipitate calcium carbonate crystals within the pore space. The crystals bind the mineral particles, increasing the strength and stiffness of the soil.

State of the art considerations regarding enzyme induced calcite precipitation and guanidinium hydrochloride research are used as the theoretical foundation for the treatment's design. A diverse sand-bentonite matrix is tested, comprised of 10% and 30% bentonite, to evaluate the applicability limits of the technique. The implementation is tested in flow-cells, whereby soils are injected with *Bio2Cementation* treatments. Experiments show the dominant role of guanidine for stabilizing clay particles – the matrix aggregates, hydraulic conductivity improves by two orders of magnitude, surface charge interactions are minimized, and swelling is halted irreversibly. Hydraulic conductivity calculations, unconfined compressive strength tests, image analysis of Micro-CT scans, and scanning electron microscope imaging evidence to notably improved bio-cementation following guanidine injections. Consistently, the optimized enzyme induced calcite precipitation was found to crystallize vigorously in 10% bentonite samples, but less successfully in optimally compacted 30% bentonite soils. The concept of *Bio2Cementation* is proven to work within certain limitations.

Future research should explore the role of different clay minerals such as kaolinite, in view of better defining the treatment's engineering applicability in-situ. Additional strength testing, soil-structure interaction analyses and environmental impact studies are also recommended

Contents

1	Introduction	9
1.1	Background	9
1.1.1	<i>Conventional Grouting and Mixing</i>	<i>9</i>
1.1.2	<i>Biopolymers and Nano Silica</i>	<i>10</i>
1.1.3	<i>Bio-Induced Cementation</i>	<i>11</i>
1.1.4	<i>Clay Inhibitors: Enhanced flow and swelling reduction</i>	<i>13</i>
1.2	Hypotheses and Research Questions.....	15
1.2.1	<i>Research Questions</i>	<i>15</i>
1.2.2	<i>General Hypothesis</i>	<i>16</i>
1.3	Method and Outline of the Thesis	17

Literature Review

2	Stabilization of clayey soils: a review of EICP and Guanidinium	18
2.1	Introduction	18
2.2	Bio-cementation	18
2.2.1	<i>Enzyme Induced Calcite Precipitation (EICP).....</i>	<i>19</i>
2.2.1	<i>Strengthening Soils by EICP.....</i>	<i>20</i>
2.2.2	<i>Microstructure and Bond Quality of EICP</i>	<i>21</i>
2.2.3	<i>Additives to Improve EICP</i>	<i>22</i>
2.2.1	<i>Reaction Rate Parameters of Bio-cementation.....</i>	<i>23</i>
2.3	Guanidinium and Clay Inhibition.....	26
2.3.1	<i>Guanidium and Protein Inhibition.....</i>	<i>26</i>
2.3.2	<i>Hydro-mechanical effects of Clay Inhibitors</i>	<i>26</i>
2.3.3	<i>Guanidinium as a Clay-Inhibitor.....</i>	<i>27</i>
2.4	Conclusions	29

Experimental Section

3	Materials and Methods.....	30
3.1	Introduction	30
3.2	Materials	30
3.2.1	<i>Treatment Solutions.....</i>	<i>30</i>
3.2.2	<i>Tested Soils.....</i>	<i>30</i>

3.3	Treatment Design.....	32
3.3.1	<i>EICP: Test Tube Experiments</i>	<i>32</i>
3.3.2	<i>Guanidinium Hydrochloride: Stability and Inhibition of EICP</i>	<i>36</i>
3.4	Soil Sample Preparation.....	40
3.4.1	<i>Sand-Bentonite Soil: Sample Hydration and Tamping</i>	<i>40</i>
3.5	Testing Program.....	42
3.5.1	<i>Injection Cell.....</i>	<i>42</i>
3.5.2	<i>Permeability Test.....</i>	<i>44</i>
3.5.3	<i>Mechanical Test</i>	<i>44</i>
3.5.4	<i>Microstructure Characterization</i>	<i>45</i>
3.6	Summary	45
4	Results and Data Interpretation	46
4.1	Permeability Testing	46
4.1.1	<i>KSat Falling Head Test.....</i>	<i>47</i>
4.1.2	<i>Barometer Equivalent Hydraulic Conductivity</i>	<i>50</i>
4.2	Strength Testing.....	55
4.2.1	<i>Unconfined Compressive Strength Test</i>	<i>55</i>
4.3	Microstructure Analysis	60
4.3.1	<i>Micro-CT.....</i>	<i>61</i>
4.3.2	<i>Scanning Electron Microscopy (SEM).....</i>	<i>73</i>
	Discussion and Conclusion	
5	Discussion	78
5.1	Crystal Morphology and Nucleation	78
5.2	Soil Type and Compaction.....	79
5.3	Grouting Engineering Applicability	80
5.4	Environmental Considerations and Knowledge Gaps.....	80
6	Conclusion.....	82
6.1	Summary of Findings.....	82
6.2	Concluding Remarks.....	83
6.3	Future Potential	84
7	References	86

8	Annex.....	91
8.1	Clay Theory: a review.....	91
8.1.1	Clay Minerals.....	91
8.1.2	Interlayer Cation Exchange Capacity (CEC).....	93
8.1.3	Double Clay Theory	93
8.1.4	Ionic Species - Interlayer and DDL Modification	94
8.2	Soil constituents: a review of EICP and Guanidinium research	95
8.2.1	Soils in EICP: a review of sand selection.....	95
8.2.2	Soils in Guanidinium Research: a review of clay mineral selection.....	96
8.3	Characterization of Sand-Bentonite: experimental data and empirical formulations	98
8.3.1	Density of Solids	98
8.3.2	Water Content.....	98
8.3.3	Dry Density.....	99
8.3.4	Summary	100
8.4	EICP recipes: a review	101
8.5	Experimental Procedures.....	102
8.5.1	Method: EICP Test Tube Optimization	102
8.5.2	Method: Guanidinium Hydrochloride Experiments.....	103
8.5.3	Method: Soil Sample Preparation	104
8.5.4	Flow Cell Iterative Design.....	105
8.5.5	Treatment Protocol	107
8.5.6	KSat Sample Preparation and Testing.....	108
8.5.7	Micro-CT – Image Analysis.....	109
8.6	Micro-CT - Image Analysis with Fiji ImageJ.....	113
8.6.1	Comparison of 3D Machine Learning Verification	113
8.6.2	Grain Scale Verification of Rendered Particles.....	113
8.6.3	Edge Detection and Systematic/Random Error.....	114
8.6.4	Big Data Limitations.....	115
8.6.5	Noise Comparison	115
8.6.6	Beam Hardening	116
8.6.7	Watershed 3D Artefacts.....	117
8.6.8	Complete 3D Rendering of Voids-Carbonate	118
8.6.9	Preprocessing - Area Calculation Macro.....	121
8.6.10	Preprocessing - Remove Background Macro.....	122

8.6.11	<i>Preprocessing - Match Histograms Beanshell (Java) Script</i>	122
8.6.12	<i>Preprocessing - Image Contrast and Noise Reduction Macro</i>	122
8.6.13	<i>Segmentation - Macro</i>	123
8.6.14	<i>Analysis – 3D ROI Calculations</i>	125
8.6.15	<i>Delft Blue Supercomputer</i>	126
8.7	SEM – Additional Images	127
8.7.1	<i>Sibelco M32 Sand</i>	127
8.7.2	<i>SEM Sample Preparation</i>	127
8.7.3	<i>Calcium Carbonate Polymorphs</i>	128
8.8	UCS – Additional Images	132
8.8.1	<i>UCS Sample Preparation</i>	132
8.8.2	<i>Failure of 30% Bentonite</i>	132
8.9	Equipment	134

Figures

Figure 1 - Soil improvements by grouting	10
Figure 2 - Calcite binding sand particles by EICP with casein	12
Figure 3 - Inhibition mechanism of a smectite.....	13
Figure 4 - GndCl treatment yielding open pores in Ca-bentonite	13
Figure 5 - Schematic of the EICP procedure.....	19
Figure 6 – Bio-cementation time dependency of pH	20
Figure 7 - Sand strength when treated by varying calcite precipitation methods	20
Figure 8 - Sand UCS treated with baseline and casein bearing EICP solutions.....	20
Figure 9 - SEM images of bridging calcite bonds between sand grains	22
Figure 10 - SEM images showing abundant nucleation of fine rhombohedral calcite	23
Figure 11 - Chemical speciation of ammonia and carbonic acid as a function of pH	24
Figure 12 – EICP rate of reaction (V), with increasing ammonium ions (P).....	24
Figure 13 - Resonant Guanidium Chloride conjugate acid.....	26
Figure 14 - Smectite interlayer cation exchange with guanidinium ions.	27
Figure 15 – Dispersed calcium bentonite washed with DI water and aggregate formation by Gnd.....	28
Figure 16 - Evolution of hydraulic conductivity during guanidine flow-through treatment	28
Figure 17 – Shear tests of guanidine treated sand-bentonite	28
Figure 18 - Cumulative grainsize distribution of sand and bentonite.	31
Figure 19 - Designing the bio-cementation and clay inhibition treatments.....	32
Figure 20 - Enzyme induced calcite precipitation (EICP) test tube experiments.....	33
Figure 21 - EICP Test tube recipe optimization as a function of pH.	34
Figure 22 - EICP Test tube recipe optimization as a function of EC.	34
Figure 23 - Sorption of guanidinium ions tested by Minder (2016).	36
Figure 24 - Guanidinium Hydrochloride pH and EC stability over time.....	37
Figure 25 - Test tube EICP reactions diluted with varying Guanidine Hydrochloride concentrations.....	37
Figure 26 - EICP Test tube in the presence of GndHCl as a function of pH and EC	38
Figure 27 – Schematic of characterizing and preparing a reproducible control artificial soil	40
Figure 28 –Texture visualization of a BC10 sand-bentonite mix.....	41
Figure 29 - MicroCT scans of untreated sand-bentonite (BC30) prepared at OMC	41
Figure 30 - Testing program of <i>Bio2Cementation</i>	42
Figure 31 - Machined inlet dimensions (DEMO Lab, EEMCS).....	43
Figure 32 – The finalized injection cell for cylindrical soil samples of either 30mm or 15mm	43
Figure 33 - The schematized research of sand-bentonite hydraulic conductivity modification by clay inhibition and bio-cementation treatments.....	46
Figure 34 - K _{Sat} sample preparation.....	47
Figure 35 - Failed water saturation due to excessive swelling for the dense BC30 sample	47
Figure 36 – Falling head tests of sand-bentonite mixtures saturated with water or guanidine	48
Figure 37 - Incompressible closed system of the injection cell.....	50
Figure 38 - Dynamic viscosity of the EICP 0.5M treatment solution	51
Figure 39 - Barometer readings during treatment injections in BC30 soils	52
Figure 40 - Barometer readings during treatment injections in BC10 soils	52
Figure 41 - Apparent hydraulic conductivity derived for K _{Sat} measurements (left) and apparent hydraulic conductivity calculation in the flow cell (right)	53
Figure 42 - The schematized process of researching the mechanical modification of sand-bentonite media by clay inhibition and bio-cementation treatments	55
Figure 43 - Unconfined compressive test peak load, indicating increasingly stiff (left to right) failure mechanisms of 10% bentonite specimens.	56
Figure 44 - Strength characteristics of treated samples	57
Figure 45 - Specific evolution of peak strength and E50 modulus for the UCS tests	58
Figure 46 - The schematized process of researching the microstructure of clay inhibition and bio-cementation in sand-bentonite	60
Figure 47 - Workflow of mineralogical classification then quantification, using Fiji ImageJ software.....	61

Figure 48 – Weka segmentation soil constituents of BC10 and BC30 samples for particles greater than 15µm 62

Figure 49 - Solid carbonate (solid line) and void (dashed line) proxies as markers for the modification of the porous media. 63

Figure 50 – Sand particle experimental sieved cumulative distribution (red) and numerically segmented cumulative distribution function (black dotted)..... 64

Figure 51 - Individual particle size analysis of carbonate, sand and void ROIs. 65

Figure 52 - Calcium carbonate ROI volume analysis 66

Figure 53 - Micro-CT calcium carbonate grains rendered in 3D –10% bentonite prepared at dry densities of 1.21g/cm³ 68

Figure 54 - Micro-CT calcium carbonate grains rendered in 3D – 10% bentonite prepared at dry densities of 1.47g/cm³ 69

Figure 55 - Micro-CT calcium carbonate grains rendered in 3D – 30% bentonite prepared at dry densities of 1.35g/cm³ 70

Figure 56 - Micro-CT calcium carbonate grains rendered in 3D – 30% bentonite samples prepared at dry densities of 1.56g/cm³ 71

Figure 57 - SEM imaging of EICP only (no guanidine pre-injection) treated soils 73

Figure 58 - SEM imaging of Bio2Cementation treatments (Gnd-EICP) treated soils taken at the base of the samples..... 74

Figure 59 - SEM imaging of Bio2Cementation treatments (Gnd-EICP) treated soils taken at the middle of the soil samples. 75

Figure 60 - SEM imaging of Bio2Cementation treatments (Gnd-EICP) treated soils taken at the top of the samples..... 75

Tables

Table 1 - Examples of potential applications for bio-improved soils relying on MICP. 12

Table 2 - Soil improvement results found in EICP studies, where only Gao et al. 2019 performed triaxial tests showing strain-hardening. 21

Table 3 - Reagents used in the preparation of Bio2Cementation treatments. 30

Table 4 - Sand-bentonite artificial soil upon which the two phase Bio2Cementation soil strengthening research is tested .. 31

Table 5 - Reduction in flow cell hydraulic conductivity for guanidine stabilized sand-bentonite. 54

Table 6 - Summary of Bio2Cementation microstructural evolution as enhanced by guanidine for treated BC10 and BC30 soils. 77

Abbreviations

EICP	Enzyme Induced Calcite Precipitation
Gnd-HCl	Guanidinium Hydrochloride
DDL	Diffusive double layer
CEC	Cation exchange capacity
EC	Electrical conductivity
BC	Bentonite content
OMC	Optimum moisture content
DI water	Demineralized water
$\rho_{dry,max}$	Maximum dry density
Micro-CT	Micro computer tomography
ROI	Region of interest (a single isolated particle segmented in 3D)
SEM	Scanning electron microscope
UCS	Unconfined compressive strength
$\sigma_{peak}, \sigma_{residual}$	Peak and residual compressive strength
E50	Secant stiffness modulus
Fine voids	Referred throughout the thesis as voids with diameter less than 15[µm] (reference defined by the Micro-CT resolution of one pixel)

1

Introduction

Problematic and weak soils display extremely diverse failure mechanisms and characteristics. To address the arising engineering problems, ground improvement research strives to develop innovative soil strengthening techniques targeting large soil masses in a low environmental impact and economically viable manner.

This chapter introduces the problematic, existing solutions and potential of this work. Firstly, this chapter introduces the concept of ground improvements; commonly used grouting methods and bio geomechanics as a recent and pertinent development in soil stabilization. Secondly, four alternative soil strengthening techniques are introduced as examples to identify the unresearched knowledge gaps. Thirdly, the chapter is guided towards the thesis' research plan, which includes the leading research questions and hypotheses.

1.1 Background

Society relies on stable subsurface in which to operate. Minimizing extensive deformations of soils is of primordial importance to civil engineers, mining operations, and other geotechnical applications. Likewise unwanted flow in excavations, tunnels and more also call for soil stability. Ground improvements in sensitive areas, such as under existing structures, requires non-invasive solutions. Dynamic and vibrating techniques are not always feasible. Additionally, scientific awareness of nature in the recent decade has pushed environmental concerns as necessary considerations during engineering practice. To this regard, many common in-situ techniques rely on invasive and toxic ground improvement solutions. This sparks the quest in civil and geo-technical engineering to innovate and propose alternative solutions.

This section is separated in three parts. Firstly, conventional grouting and mixing solutions are introduced. This transitions into the second sub-section, which a few examples of research seeking to strengthen soils in a new manner, albeit each marred with their own caveats. This leads to the third subsection, exploring the potential of bio-cementation for soil improvements.

1.1.1 Conventional Grouting and Mixing

Grouting is a process which injects suspended or dissolved substances, improving a soils' mechanical properties via a change in the physical parameters of the porous medium. Most often grouting techniques seek to reduce permeability and increase stiffness and strength. Applications targeting soils with a slow passive flow grouted in three ways (Figure 1) and by mixing the soil column.

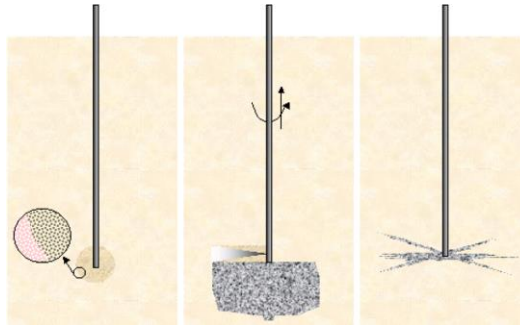


Figure 1 - Soil improvements using permeation grouting (left), jet-grouting (middle) and fracturing (right) (de Jong, 2021).

Permeation grouting - The chemical injection of either suspended cement, bentonite-cement or chemical fluids. Due to the reliance on large hydraulic conductivities, the method is limited to sand and gravel subsurface. The aim is primarily to reduce permeability with maximal spherical injections over 1-1.5[m]. Most notably, such methods are used in ground sealing solutions of building pits and the underpinning of foundations. The low pressures used range from 4-8bar and use flow rates of 4-8[L/min]. Acrylates and epoxy resins are expensive and toxic, likely inducing pollution of the water table (Zhao *et al.*, 2019).

Jet-grouting – A technique which relies on boring to the desired depth, injecting pressurized water and grout, to mix and replace the soil structure with maximal diameters of 1.3-5[m] diameter grout columns. This method reduces permeability and increases strength and stiffness parameters and is commonly used in many civil and geotechnical projects. The method is possible in all soils but uses extremely high pressures (30-50[mPa]) and high flow rates (125-300[L/min]). The energy consumption is notable, and the generated spoil must be disposed of.

Fracture grouting - Locally broken structures are formed by high pressure injections of cement grout. To ensure horizontal fracturing pre-stressing the soil and several charge injections are required. Such method seeks to increase the stresses in the soil, such as the friction between the soil and a pile foundation. Most useful is the settlement compensation ability of this method.

Deep dry soil mixing – Mixing of soft soils or other binders by a mechanical mixing tool. The soil loses its structure but remains in place, generating little to no spoil. Bearing capacity and trench stability is improved. The method is cost effective and generates less noise and vibration than injection grouting. It requires low air pressures of 0.4-0.8[mPa] and has an active radius of 1[m]. However, it is possible only in soft soils, requires re-consolidation of the target region, and its in-situ polyvalence is limited.

Such methods utilize a multitude of reagents; notably cement, bentonite, silicates, chemical additives (such as sodium silicates, phosphoric acids, etc.), lignosulfonates, plastic polymers, ferrous sulfates and more (Ivanov and Chu, 2008). Current environmental concerns regarding toxicity and invasiveness open the opportunity for innovative in-situ alternatives.

1.1.2 Biopolymers and Nano Silica

Increased attention towards alternative soil strengthening methods has spurred the research of diverse solutions. As an example of new techniques, this section proposes a short excerpt of two alternatives. They are primarily developed to improve silty sands, which are otherwise inaccessible for ultra-fine cements with 3-5[μ m] suspended particles (Zhao *et al.*, 2019). Their research relies primarily on minimizing liquefaction potential without obstructing existing structures by dynamic or vibrating

techniques. This preliminary literature investigation is by no means exhaustive, and yet it brings to light the potential to target increasingly finer soils with new methods.

Biopolymer-based Soil Treatment (BPST) – An environmentally friendly recent application of soil strengthening, and permeability control is the exo-cultivation of biopolymers, whereby viscoelastic aqueous solution interacts with the soil matrix by viscoelastic and electro-static interactions (Chang *et al.*, 2020). For example, experimental preparation ranges from Alginate micelles (Li *et al.*, 2015) to wheat husk purification (Buazar, 2019). Hydrogel swelling leads to increased unconfined compressive strength, moisture independent apparent cohesion increases shear strength, and Attenberg limits are improved. However, most biopolymers are hydrophilic, ergo the swelling of hydrogels leads to pore clogging and increasing suction potential. Most research relies on soil mixing, whereas injection in silty soils leads to minimal increases in strength (Kakavand, 2019). Its durability, reliance on unsaturated conditions and common deep mixing machinery, low global availability and toxicity of biopolymers renders the treatment hampers its polyvalence.

Colloidal Silica (CS) – Alternatively, colloidal silica has been applied in coarse grained material (gravel-sand) or fractures with large effective permeability. Solutions are prepared using alkaline (pH ~8) aqueous suspension of 7-22[nm] microscopic nano silica, from which the formation of *siloxane bonds* have generate a uniform network of chainlike structures constituting a rigid gel (Zhao *et al.*, 2019). Saturated solutions of silicic acid are stabilized against gelation by utilizing an alkaline solution (Conlee, 2010), and display slightly viscous behaviour (~200[Pa-s]) (Hadmeri and Gallagher, 2013). Its application remains specialized to fracture sealing against oil and chemical contamination, remaining less studied in the stabilization of loose, liquefaction prone soils (Conlee, 2010). Additionally, due to its extremely slow passive fluid flow, little research has been completed in fine grained media, *let alone* strengthening weak subgrade soils.

The methods are limited in certain regards: polymers often utilize toxic chemical additives and rely on invasive deep dry mixing, whereas colloidal silica is slightly viscous and remains a viable solution for loose liquefiable subsurface only (Zhao *et al.*, 2019). Additionally, the latter often still uses Portland cement as an additive to reach desired strength improvements (Vranna and Tika, 2019). Current environmental concerns regarding toxicity and invasiveness further open the opportunity for bio-inspired, less toxic, and economically viable solutions.

1.1.3 Bio-Induced Cementation

Taking natural phenomena as an example of energetic efficiency and maximal performance, bio-inspired geo-mechanics uses microorganisms to modify the physical properties of the soil skeleton.

Microbe Induced Calcite Precipitation (MICP) - MICP is a form of bio-mediated soil remediation, which combines calcium and urea to precipitate calcite crystals in the soil. The hydrolysis reaction is catalyzed by bacterial strains such as *Sporosarcina Pasteurii*, for which their metabolic pathways allow orders of magnitude faster reaction rates. The low viscosity, low temperature, remediation precipitates a mineral lattice of bonds over the timespan of a few hours to days (Terzis and Laloui, 2018). In this method, the wall electronegativity of the bacteria bounds them to sand grains, optimizing the bridging potential of growing calcite crystals. The resulting media retains its permeability (minor bio-clogging), and shows

improved cohesion, strength, and stiffness characteristics even in large scale applications (Terzis *et al.*, 2020). Tailoring the treated material properties is performed in-situ, showing great potential for non-intrusive low energy remediation. Nonetheless, although new cell free lyophilized approaches are recently developed (Terzis and Laloui, 2019), the endo-cultivation and need for bioreactors complexifies the entry point in the research branch. Additionally, the technique has yet to expand its novel performance to fine material. Complex charge interactions between clays and bacteria, as well as slow-flowing porous media limits its application (Cardoso *et al.*, 2018). For this reason, there is potential to explore the knowledge gap that is bio-mediated soil cementation in clay bearing soils.

Enzyme Induced Carbonate Precipitation (EICP) – Precipitation of enzyme induced calcium carbonate crystals is researched as alternative soil strengthening solution. Its' simple reliance on purified enzymes rather than from bacterial secretion, makes this method cheaper and more applicable than MICP (Cheng *et al.*, 2013; Terzis, 2016; Konstantinou *et al.*, 2021; and others). The biologically based soil process mixes aqueous calcium chloride, urea, and urease enzymes. Thereafter, the blended solution and catalytic agent (10^{14} rate increase, Terzis *et al.*, 2020) mobilize carbonate ions and increase the pH locally. In the alkali medium, calcite crystals precipitate in the soils' voids (Putra *et al.*, 2020). Binding the soils inter-grain voids, improves the mechanical properties, and the expense slower flowing medium. However, certain uncertainties remain. Although less viscous than cement, its efficiency is hindered in clayey soils, especially when interacting with charged mineral surfaces (Cardoso *et al.*, 2018). Likewise, Sun *et al.* (2019) found that kaolin clay and associated ions decrease enzyme activity in bio-cementation. Enzyme induced carbonate precipitation has been extensively studied for strengthening sandy soils (Figure 2). In fact, most EICP tests use Ottawa sand only (99% SiO₂) with large particle sizes ($D_{50}=0.6$ [mm]) (Almajed *et al.*, 2018)). Finally, ammonia, a known pollutant, remains a toxic biproduct of the reaction.

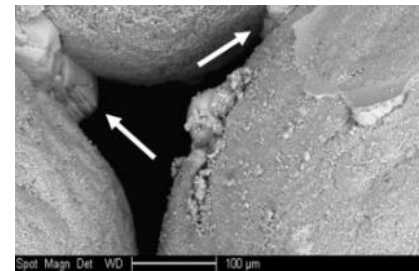


Figure 2 - Calcite binding sand (arrows) in EICP with casein (Almajed *et al.*, 2018)

Table 1 - Examples of potential applications for bio-improved soils relying on MICP and EICP.

Examples of Application Potential	Modification	Reference
Bearing capacity improvements	Increase stiffness and strength	(Cheng <i>et al.</i> , 2013)
Contaminant migration prevention	Decrease permeability	(Minto <i>et al.</i> , 2016)
Slope stability	Increase shear strength	(Terzis <i>et al.</i> 2020)
Surface runoff erosion protection	Strength and cohesion increase	(Jiang and Soga, 2017)
Wind erosion prevention	Reduce evaporation, increase cohesion	(Bick <i>et al.</i> , 2019)
Masonry and bio-bricks	Provide stiffness and strength	(Arab <i>et al.</i> , 2021)

In conclusion, such approaches all display notable advantages for in-situ applications. Diverse in their application potential, they spur an evolutionary branch of sub-surface engineering (Table 1). The method use readily available non-toxic reagents, is not invasive and polyvalent in its use. Nonetheless, although bio-cementing solutions are an order of magnitude less viscous than the finest cements, current EICP and MICP state of the art benefits from fast flowing porous media with little surface charge interactions (fine and coarse sands).

1.1.4 Clay Inhibitors: Enhanced flow and swelling reduction

The decreased performance of existing bio-cementation techniques to stabilize heterogeneous soil masses is linked to the small porosity, low permeability, and charged surface effects in soils. The opportunity presents itself in filling the knowledge gap; extending the applicability of bio-cementation to clayey soils by chemically stabilizing the clay mineralogical fraction.

Since the thesis' focus lies on the fundamental research of bio-cementation, the background of clay theory is not discussed herein, but rather presented as additional reading in annex 8.1 *Clay Theory: a review*. In summary, it is important to note that cation exchanges can be used to control a clay's molecular structure and physical properties. In fact, drilling and fracturing research has investigated the role of clay inhibitors, as means of modifying the rheological properties of clayey soils. To minimize the destabilization of operations, corrective additives seek to minimize clay hydration and inhibit swelling (Figure 3).

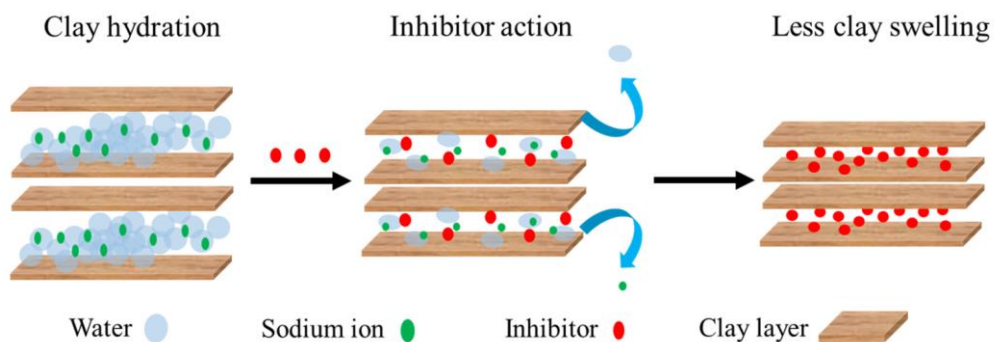


Figure 3 - Inhibition mechanism of a smectite (Qu et al., 2022)

Various compounds exist in common drilling and fracturing engineering practice:

Inorganic Salts – Inorganic salts such as potassium chloride were the first inhibitors, whereby interlayer cations are exchanged for the less hydratable potassium. However, the electrostatic attractions rely on highly concentrated brines, while not completely inhibiting the clay reactivity (Bergaya and Lagaly, 2011).

Organic Inhibitors – Organic salts are readily adsorbed upon clay surfaces, which fixes clay octahedral and tetrahedral sheets by electrostatic interactions. Potassium and caesium formats have small ionic radii, which reduce cationic hydration and thus swelling (Rahman et al., 2020). Surfactants and polymers (e.g. polyacrylamides) bind to the anionic surface of minerals, occupying the interlayer space, to prevent water sorption. These inhibitors provide increased success of “complete inhibition”, but are hampered by their toxicity, low biodegradability, and salinity intolerance (Quainoo et al., 2020).

Non-Conventional Methods – In the search for greener shale inhibitors, recent non-conventional methods have studied the use of saccharides, bio-surfactants, ionic liquids and nitrogen based compounds. Quainoo et al. (2020) study twenty-three inhibitors, concluding the superior performance potential of these compounds. In parallel, geo-technical research by Plotze and Kahr (2008) found the nitrogen based guanidine compound to intercalate smectite clays irreversibly; opening the door for its application in geotechnical problems of smectite soils (Minder, 2016). Guanidium treatment

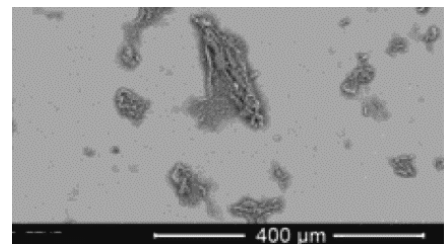


Figure 4 - GndCl treatment yielding open pores in Ca-bentonite (Minder et al., 2016)

of smectite clays (Figure 4) has shown increased shear strength and permanent flocculation of the soil matrix, leading to an increase in hydraulic conductivity (Minder *et al.*, 2016). The particle aggregation phenomena has also been researched on kaolinitic soils (Hu *et al.*, 2020). Nonetheless, little to no research has explored the molecule's mechanism alongside biocementation.

In conclusion, the thesis sees the potential of irreversibly aggregating swelling clays through the use of a clay inhibitor. Guanidine has been identified as a notable chemical stabilizer in clayey soils, with geo-technical engineering potential (Minder, 2016). Additionally, micro-biological research has studied the interaction between the organic molecule and urease enzymes (notably the catalyst of EICP), showing promise in developing a theoretical foundation of their coupled interaction in this thesis.

1.2 Hypotheses and Research Questions

The thesis investigates a coupled two-phase soil strengthening treatment. Clay inhibitors and bio-cementation treatments are identified as potentially mutually beneficial to strengthen clayey soils. The thesis artistically refers to the coupled technique as **Bio2Cementation**. Hereafter, the research questions are introduced, serving as guiding pillars for experimental tests performed in this thesis. Secondly, the research's central hypothesis is presented.

1.2.1 Research Questions

Coupled treatments of clay inhibition and bio-cementation have been rarely researched. This has formed a knowledge gap worth exploring. The thesis seeks to test the potential strengthening of sand-clay mixtures, in view of expanding the engineering applicability of bio-cementation to clayey soils. The ambition of strengthening large and heterogeneous soil masses, leads to the research question guiding the thesis:

“Can the microstructure and strength characteristics of a sand-bentonite soil be improved by combining guanidine hydrochloride clay stabilization and enzyme induced calcite precipitation?”

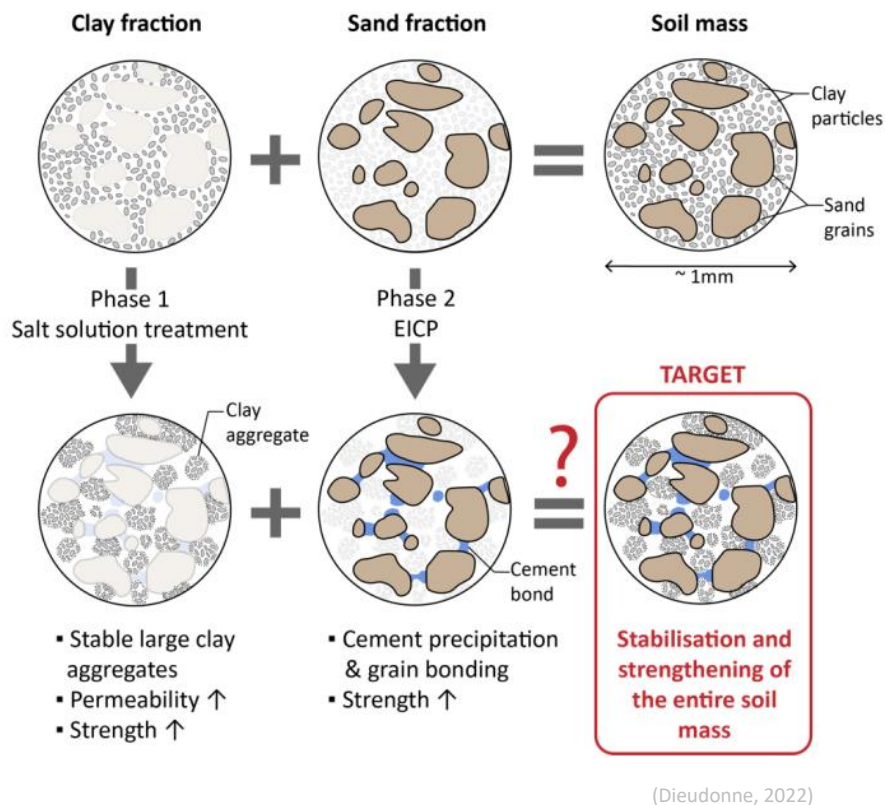
RESEARCH QUESTION

The research aims to gradually construct its complexity. Four research sub-questions organize the fundamental research of the *Bio2Cementation* technique. The first guides the treatment's design in test tubes. Whereas the last three research the treatments effect on permeability, strength and microstructure upon a clayey soil.

1. *What is the optimal enzyme induced calcite precipitation recipe to maximize yield at low concentration reagents? How stable is guanidinium hydrochloride, and does it's protein denaturing ability disrupt calcite precipitation solutions?*
2. *How does GndHCl improve the permeability and increase flow through potential of bentonite-sand soils? What role does it play in subsequent EICP injections?*
3. *How are the strength characteristics of a sand-bentonite altered using water saturated soils, GndHCl alone, or EICP-GndCl coupled treatment solutions?*
4. *With specific attention to soil matrix, grain morphology, and nucleation sites; how is the microstructure of a sand-bentonite modified by GndHCl alone and EICP-GndHCl treatment solutions?*

1.2.2 General Hypothesis

The thesis' relies upon the beneficial coupling of the two soil strengthening techniques. This interaction holds true under the following hypothesis:



“Individually treating the clay minerals and the sand fraction, leads to the combined effect of a stable and stronger clayey soil matrix.”

HYPOTHESIS

Hereafter, three additional research sub-hypotheses note the applicability limit of enzyme induced calcite precipitation alone, as well as stating the expected modification of a clayey porous media by the clay-inhibition treatments.

Hypothesis 1.1 Enzyme induced calcite precipitation’s success is hindered in sand-bentonite by too slow flow, insufficient coarse pores and excessive surface charge interactions.

Hypothesis 1.2 Guanidinium hydrochloride salt solutions modifies the clay matrix, opening the pore space and forming aggregates. This increases the hydraulic conductivity (K), shear strength (τ) and internal friction angle (ϕ) of the soil.

Hypothesis 1.3 Enzyme induced calcite precipitation and guanidinium hydrochloride treatments lead to a stronger and stiffer soil, increasing the compressive strength (σ_{max} , $\sigma_{residual}$) secant modulus (E_{50}).

To answer the research questions and test the leading hypotheses of *Bio2Cementation*, an experimental testing protocol is devised. This provides a diverse analysis of the treatments effect upon a reproducible porous medium.

1.3 Method and Outline of the Thesis

The proof of concept *Bio2Cementation* is designed, tested and evaluated in this thesis; the method seeks develop a fundamental understanding of the soil strengthening technique. Throughout the work, an artificial well defined soil is used, such that modifications of the porous system are attributed to the treatments. The chapters are subdivided according to a specific target, converging towards an experimental dataset suitable to evaluating the leading research questions. The work is outlined as follows:

Chapter	Aim
1. Introduction	<i>Problem definition and introduction of the innovative potential of the thesis.</i>
2. Stabilization of clayey soils: a review	<i>Development of a theoretical foundation using the state of the art.</i>
3. Materials and methods	<p><i>Designing Bio2Cementation “In-Vitro” and creating an experimental method to test the treatment in an artificial soil:</i></p> <div style="text-align: center;"> <p>In-Vitro Testing</p> <p>EICP: <chem>CaCO3</chem></p> <p>Guanidinium: <chem>[NH2+](C(=[NH2])N)N</chem></p> <p>Sand-Bentonite</p> <p>3.75mm</p> </div>
4. Results and data interpretation	<p><i>Development of a fundamental understanding of the treatment in a sand-bentonite soil by researching three aspects of the modified specimens:</i></p> <div style="text-align: center;"> <p>Soil Treatment Testing</p> <p>Permeability: <chem>Gnd</chem></p> <p>Strength: <chem>Gnd + CaCO3</chem></p> <p>Microstructure: <chem>CaCO3</chem>, Void, Sand Grains, Clay Particles ($\pm Gnd$)</p> </div>
5. Discussion	<i>Evaluation of the proof of concept technique, by gradually expanding from the grain scale considerations to a broader scale.</i>
6. Conclusion	<i>Summary of findings and future recommendations</i>

With this outline, the thesis strives to provide data of guanidinium and bio-cementation coupling treatments to strengthen clayey soils, evaluating its effectiveness and discussing its future potential.

2

Stabilization of clayey soils: a review of EICP and Guanidinium

2.1 Introduction

The first chapter of this thesis has identified EICP as relevant alternative to common grouting techniques. Although less viscous than cement, the applicability limit in clayey soils is expected to be hindered by the physical and chemical properties of clay minerals. Guanidinium has been identified as a rarely studied, yet strongly inhibiting, clay stabilizer. For this reason, the chapter explores the state of the art of both enzyme induced calcite precipitation (EICP) and Guanidinium (Gnd). Both sections attempt to present a knowledge base which accounts for their cross interactions in the pore fluid and matrix. This chapter is by no means an exhaustive analysis of other alternative soil strengthening options, but instead focuses on establishing a theoretical foundation for the design of *Bio2Cementation* treatments in clayey soils.

2.2 Bio-cementation

Bacterial biomineralization is a process found in natural environments, by which an organism precipitates mineralized elements as a byproduct of its natural activity. For example, calcite biomineralization is produced by ureolytic plant strains such as *Canavalia Ensiformis* (Nam *et al.*, 2015). These natural processes are defined by the diverse source of catalytic agents to allow mineral precipitation in aqueous solutions. Inspired by the latter, alternative soil strengthening solutions precipitate crystals in the porous media, by treatments of in-situ injections of aqueous solutions. The low energy requirements of in-situ solutions reduce costs and increase applicability in critical, hard to reach areas. The interdisciplinary method bridges biology, chemistry and geotechnics to increase strength, stiffness and reduce the permeability of a soil (Putra *et al.*, 2020).

Geo-engineered processes such as microbially induced carbonate precipitation (MICP) exploit the endo-cultivation of urease enzyme producing bacteria *S.Pasteurii* utilizing bioreactors on site which agitate and incubate cultures (Pham *et al.*, 2016). Various studies have shown that small pore sizes limit the distribution and growth of enzymes in MICP (Van Paassen, 2008). Developments by Terzis and Laloui (2018) have increased the flexibility of MICP preparation methods, by showing that urease enzyme efficiency does not vary with freeze-drying and rehydration cycles. Although new cell free approaches are being developed (Terzis and Laloui, 2019a), the process remains complex and expensive to engineer.

Enzyme induced carbonate precipitation (EICP) does not utilize bacteria to hydrolyze the urea, but rather directly utilizes purified urease enzyme reagents to precipitate calcite (Figure 5). EICP gains a comparative polyvalence of application in diverse soil types, by reducing the necessary considerations of parameters required for bacterial proliferation in-situ (Ross, 2018). Furthermore, it provides the opportunity to re-uptake biproducts of other industries. For example, purified urease enzymes can be derived from plant-based products such as *Canavalia Gladiata* (Khodadadi Tirkolaei *et al.*, 2020).

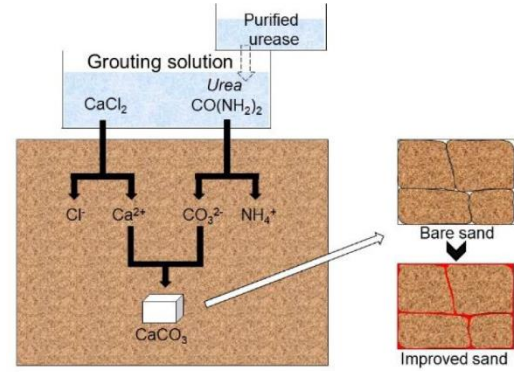


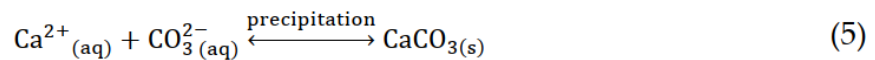
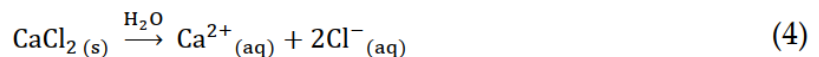
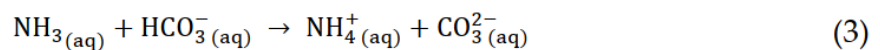
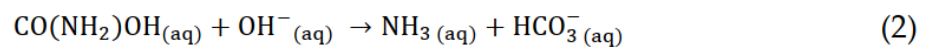
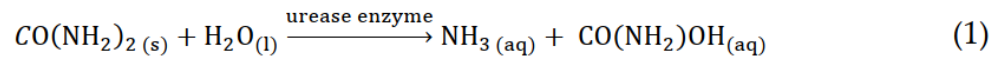
Figure 5 - Schematic of precipitation process and grouting procedure of EICP (Putra *et al.*, 2020)

To successfully bio-cement soils in this thesis, a review of EICP state of the art is explored in four subsections. The first briefly introduces the enzyme induced calcite precipitation (EICP) reaction. Thereafter, the role of the microstructure in achieving notable strength gains is discussed. The role of external parameters such as pH, equilibrium constants and temperature as means to control the treatments success are then discussed. Finally, the chapter terminates with examples of successful sand strengthening research by EICP.

2.2.1 Enzyme Induced Calcite Precipitation (EICP)

Enzyme induced calcite precipitation forms calcium carbonate crystals in the porous media, by treatment with the injection of an aqueous solution. Calcium carbonate solids are crystallized as an indirect product of urea hydrolysis from urea and calcium chloride reagents. Urease enzymes are used as the reaction's catalytic agent, increasing the reaction rate by 10^{14} times (Terzis *et al.*, 2020).

The chemical process of calcite precipitation is governed by the equilibrium reaction:



The reaction requires a source of dissolved calcium ions and carbonate ions to precipitate calcium carbonate solids (5). These are provided by the catalyzed urea hydrolysis (1-3), and dissociation of calcium chloride salts (4) (Putra *et al.*, 2020). Urea hydrolysis produces ammonium, increasing the pH locally, reducing proton availability in the aqueous solution. This generates an alkaline environment (pH=8-9), where the bicarbonate chemical speciation equilibrium shifts from HCO_3^- to CO_3^{2-} (Ahenkorah *et al.*, 2020). Nucleation and growth of solid calcite polymorphs ($\text{CaCO}_3 (\text{s})$) may occur once the solubility constant at 25°C is exceeded (Kirkland *et al.*, 2019). Whereby, the rate of reaction and CaCO_3 formation in EICP is proportional to the formation and decomposition of Ca^{2+} , CO_3^{2-} and NH_4^+ (Ahenkorah *et al.*, 2021):

$$\text{Saturation} = \frac{[\text{Ca}^{2+}][\text{CO}_3^{2-}]}{K_{\text{sol}}} \quad \text{where } K_{\text{sol}} = 5 \times 10^{-9}$$

Figure 6 schematizes the kinetics of the EICP reaction, showing the temporal evolution of pH.

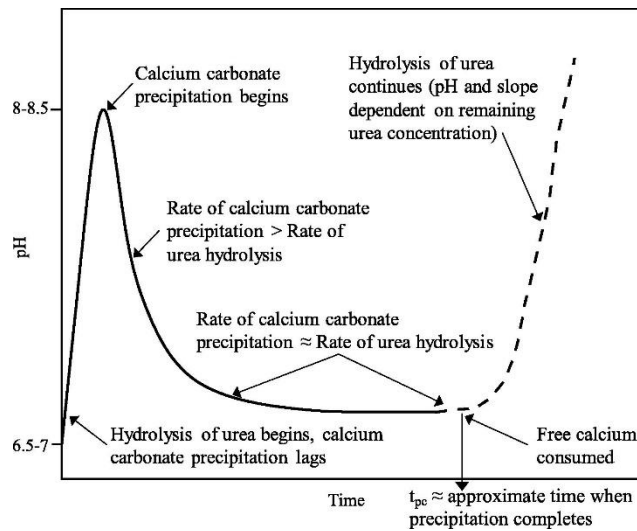


Figure 6 - Schematic kinetics of the treatment solutions pH and time dependent carbonate precipitation (Van Passen, 2009)

The precipitate formation depend on the limiting/excess concentration of the reagents produced in (3,4).

2.2.1 Strengthening Soils by EICP

Calcite precipitation bind the soils' grains, improving the mechanical properties (Figure 7), while decreasing the hydraulic conductivity of the medium (Putra *et al.*, 2020). When comparing bio derived urease to bacteria with the same initial activity, the reaction rate is slower, yet shows an improvement of the mechanical behavior compared to untreated soils (Gao *et al.*, 2019). More precisely, bio-cementation increases the dilative behavior, stiffness, and confers higher peak strength to soils.

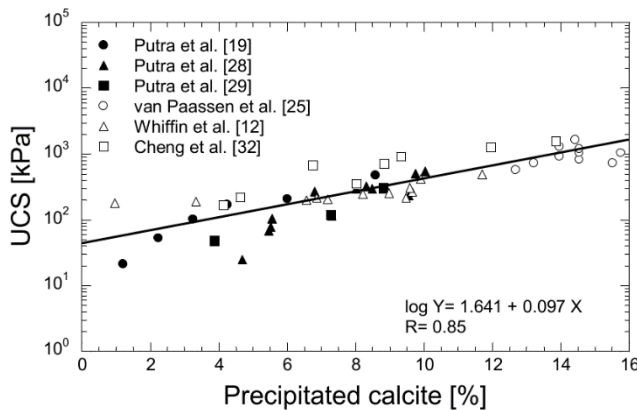


Figure 7 - Sand strength when treated by varying calcite precipitation methods. Calcite content ranges from 1-16% with strength ranging from 40kPa to 1MPa, as per Putra *et al.* (2020)

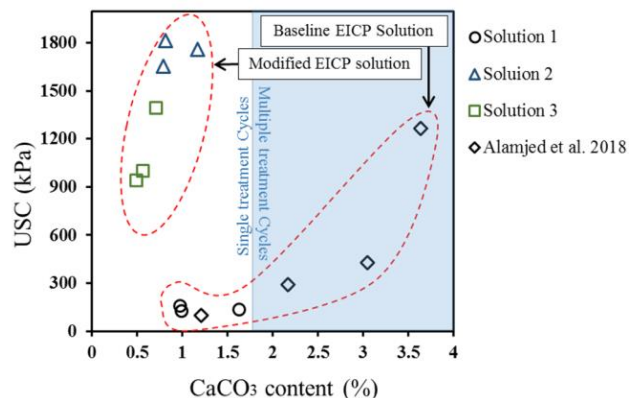


Figure 8 - Sand UCS treated with baseline and casein bearing EICP solutions (Almajed *et al.*, 2019)

Other experimental approaches aimed at reducing the required calcite content to strengthen soils, by improving the quality of inter-particle bonds. For example, adding chelating agents slow crystal growth, yielding 1.6-1.8MPa unconfined compressive strengths in Ottawa sands with only 1.5% carbonate content (Figure 8). Slowing the precipitation rate may improve interparticle bonds instead of forming small cladding crystals. Similarly, Yuan *et al.* (2020) also found that multiparticle clusters to be most efficient in increasing strength when utilizing the chelating and nucleating effects provided

by casein protein in the treatment solution. This optimization greatly improves strength gains over conventional EICP, even at low calcium carbonate contents.

State of the art mechanical improvements are summarized in Table 2:

Table 2 - Soil improvement results found in EICP studies, where only Gao et al. 2019 performed triaxial tests showing strain-hardening.

Author	Carbonate (%)	UCS (MPa)	Axial Stress	Elastic Modulus (MPa)	Peak-Failure Strain (%)	Initial-Final Permeability	Additional Reagents
Neupane et al., 2013	1-6						
Ross, 2018							
Almajed et al., 2018	1-1.5	1.6-1.8					Casein (skim milk)
Gao et al., 2019	2.6-10.7		q _{peak} 120-250 kPa				
Putra et al., 2020	10	0.6				4.5 - 1[cm/s]	MgCl ₂
Yuan et al., 2020		1.2-1.6 max. w. casein		80.5 (EICP) 1.65 – 1.25 (w. casein)	2.15 – 1.45 (EICP) 1.65 – 1.25 (w. casein)		Casein (skim milk)
Martin et al., 2021	3-6.9	>0.5					

Little is known of the behaviour of carbonate precipitation in fine grained media. In fact, Terzis and Laloui (2020) only tested MICP in fine material with a D₁₀ of 99[μm]. Most EICP ‘fine’ grained tests use silica Ottawa sand with D₅₀ of 0.6[mm] (Almajed et al., 2018), with only few reaching D₅₀ = 0.2mm (Terzis and Laloui, 2019). Few authors, such as Gao et al. (2019), studied the effect of utilizing crude urease enzyme for EICP in silty soils but were constrained by permeability limits. Additionally, Sun et al. (2019) found that kaolin clay and associated ions decrease ‘bacterial’ enzyme activity, and thus decreased calcium carbonate production rates in clay-sand mixtures. Finally, Cardoso et al. (2018) was unsuccessful in achieving significant strength gains in sand-kaolinite mixtures (<30%), attributing the lack of success to chemical interactions with the clay’s surface charges. For this reason, the desire to broaden both MICP and EICP’s application potential in clayey soils still requires successful experimental data in soils with active electro chemical surfaces.

2.2.2 Microstructure and Bond Quality of EICP

A decade of progress in MICP and recent development in EICP have shown the dependance of microstructure and grain interactions. State of the art work by Terzis and Laloui (2019) show the dominance of a soils response by the location of crystalline bonds, rather than the average bulk mass of CaCO₃ precipitate (total yield). Bridging bonds of large mesocrystals between grains, rather than distributed unbound crystals in the pore space, infer maximal strength gains to soils.

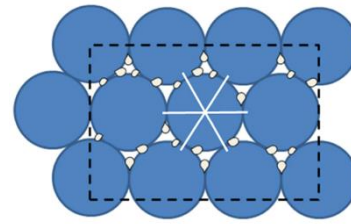
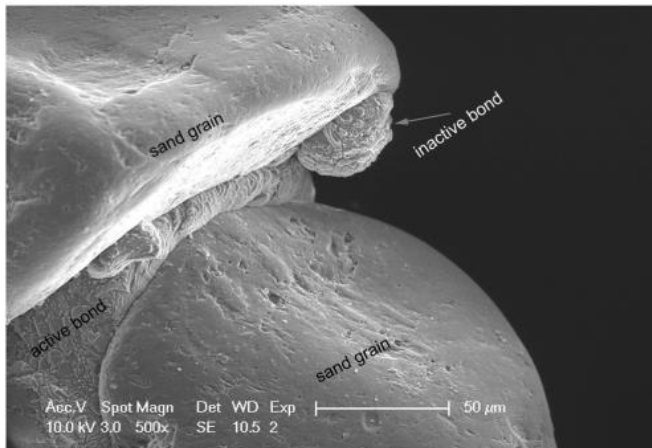


Figure 9 - Left: SEM bridging calcite bonds between sand grains (Terzis and Laloui, 2018). Right: Schematic grain contact points for densely packed grains, and white lines showing the intergranular contacts for idealized force transmissions. (Terzis and Laloui, 2016)

Desireable features, such as a homogeneous spatial distribution of bonds, are controlled by ureas enzyme type, reagent concentration, grain packing and saturation. Additionally, continued injections of fresh EICP solution, steadily grows existing calcium crystals in the pore voids. Their favoured nucleation site location occurs in low advection or unsaturated zones (Terzis and Laloui, 2019). Such properties shelter nucleation sites which preferentially yield binding calcite crystals, ultimately improving the physical properties of the porous medium (Figure 9). Lastly, MICP is successful in exploiting the cell wall to sand grain electronegative attraction of the *S. Pasteurii* bacteria. The catalytic urease enzyme is not diluted in the free pore space, but rather concentrated along the sand-fluid interface. This feature could be beneficially exploited in a clayey soil, where clay aggregates often retain a negative surface charge.

In microbial bio-cementation (MICP), the first precipitates of calcium carbonate generate spherical metastable vaterite, which thereafter transition to the desired stable cubic calcite (Terzis *et al.*, 2015). Cubic particles are followed by rhombohedral hierarchical plane expansion, which yield the strongest and largest bonds between soil grains (Terzis and Laloui, 2016). The polymorph precipitation mechanisms are controlled by pH, temperature, and pressure (Terzis and Laloui, 2018). The exact fabric characterization remains poorly studied in bacterial free precipitation methods. Nonetheless, EICP state of the art studies concur that the most stable, less soluble, CaCO_3 polymorph is calcite (Putra *et al.*, 2016, Gao *et al.*, 2020). Calcite microstructure which expands in an anisotropic manner, induces dislocation and defects, yielding weaker minerals than pure geological calcite (Terzis and Laloui, 2018). Re-growth and activation of existing nuclei is shown to extensively grow when provided with fresh calcium (Almajed *et al.*, 2019).

In conclusion, the success of bio-cementation is explained by microstructural details such as the crystal location, polymorph type, and precipitate yield. Solutions which favor large cubic-rhombohedral calcite crystals are deemed most optimal. Lower reaction rates have been shown to favor few nucleation sites of large calcite crystals, leading to large strength gains. Microstructural features are well researched in microbial bio-cementation (MICP), as seen by the work by Terzis *et al.* (2016), whereas it remains it remains rarely researched in EICP treatments.

2.2.3 Additives to Improve EICP

Additional reagents have been proposed as means to improve EICP performance, by reducing nucleation rates, controlling polymorph type, crystal morphology and more. Primarily, slowing initial hydrolysis rates allows for constantly renewed flow of reagents to growing crystals prior to clogging of the pore space, improving the crystal distribution and size. Putra *et al.* (2020) propose magnesium

compounds ($0.1[\text{mol/L}] \text{MgCl}_2$ and $0.05[\text{mol/L}] \text{MgSO}_4$) as means to reduce the calcite precipitation rate and differing the reaction onset. Although shown to increase distribution uniformity, these compounds promote the weaker dolomite (Mg-Ca carbonate) and vaterite (CaCO_3 polymorph) crystals, hampering the treatment's success. Almajed *et al.* (2019) and Yuan *et al.* (2020) achieved successful treatments, by including organic materials as chelating agents. The most efficient agent was found to be the proteins included in skim milk (Figure 10).

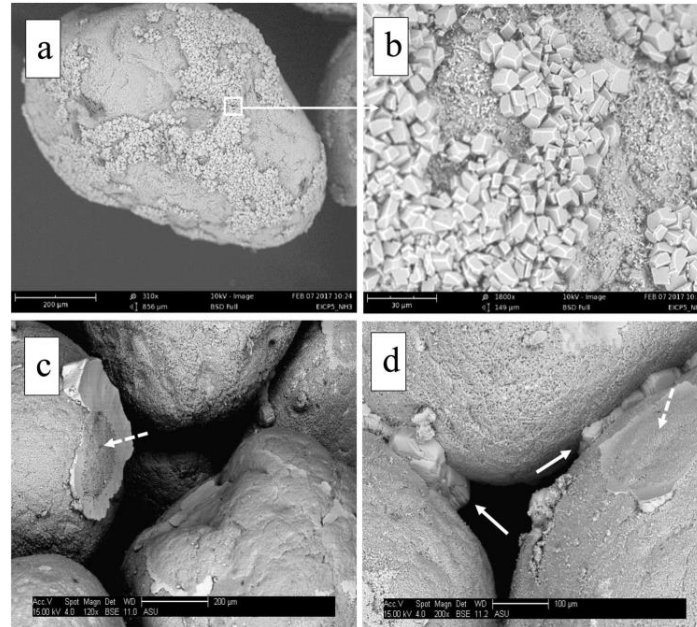


Figure 10 - SEM images of soil particles showing abundant nucleation of fine rhombohedral calcite crystals with baseline EICP treatments (a,b), versus casein modified solutions forming larger bridging crystals (c,d) (Almajed *et al.*, 2019)

The casein protein promotes the calcite polymorph over the weaker vaterite crystals, acts as a chelating agent to slow reaction rates, and favors nucleation sites along grain boundaries (Gao *et al.*, 2020). Seemingly, their action chelates Ca-ions, aggregating and acting as nucleation sites for calcite crystals. Therefore, such impurities seem to favor multiparticle clusters around singular nucleation sites, growing mesocryst's concentrically. The state of the art constantly seeks additional additives to improve EICP strength gains.

2.2.1 Reaction Rate Parameters of Bio-cementation

Urea hydrolysis modified the pH of the pore solution, precipitating calcium carbonate in alkali conditions. Various MICP studies have shown the dominance of carbonate ions CO_3^{2-} at pH's greater than 9.0 (De Jon *et al.*, 2006). Treatment solutions with these conditions allow for high carbonate ion concentrations, minimizing its role as a limiting reagent in the reactional pathway. Nonetheless, exceedingly basic pore solutions with pH greater than 9.5 have been also shown to be detrimental in MICP (Cheng *et al.*, 2014). In fact, urea hydrolysis and calcium carbonate precipitation are controlled by two primary equilibrium reactions. The carbonic dynamic equilibrium reaction and ammonia equilibrium in water, are strongly pH dependent acid-base reactions. Ammonia is a weak base ($\text{pKa}=9.25$), which when protonated increases the solution's alkalinity (Figure 11). Rising pH favors the dissociation of the weak Bronsted acid HCO_3^- ($\text{pKa}=10.34$), freeing carbonate ions in the basic aqueous treatment solution. Its supersaturation levels can therefore be modified by controlling the concentration of free protons; reducing the pH close to 8 will greatly reduce carbonate ion concentrations, reducing new nucleation rates and increasing crystal size (Figure 11).

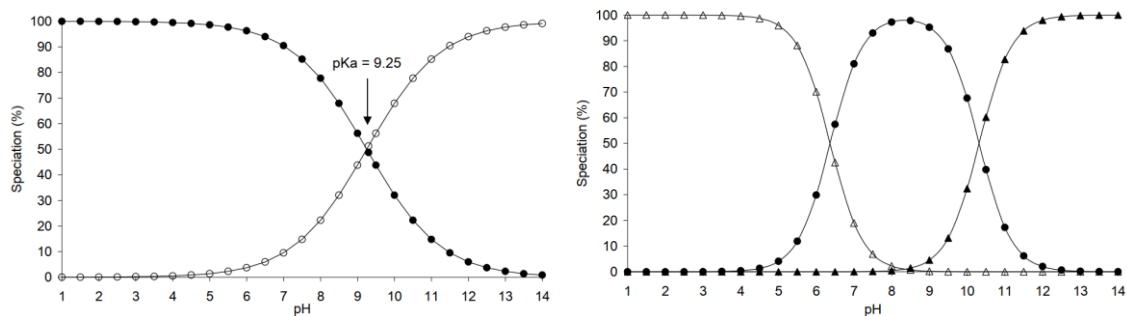


Figure 11 - Chemical speciation of ammonia and carbonic acid as a function of pH. Ammonium NH_4^+ as open white circles (left), and CO_3^{2-} as black triangles (right) (Whiffin, 2004)

Interestingly in EICP, non-equimolar (calcium chloride to urea) treatment solutions can be used to modify the pH; a larger urea concentration will increase alkalinity due to the abundance of NH_3 . This favors an equilibrium shift, causing excess $\text{CO}_3^{2-}(\text{aq})$ reagents. Whereas, lower calcium chloride concentrations renders $\text{Ca}^{2+}(\text{aq})$ ions a limiting reagent. This parameter slows the precipitation rate of calcium carbonate (Ahenkorah et al., 2021). In fact, Gao et al. (2020) and Yuan et al. (2019) attempted to slow the initial reaction rate in highly concentrated EICP treatments, by utilizing 2 [mol/L] CaCl_2 to 3 [mol/L] urea reagent ratios. Nonetheless, the solutions yielded lower strength improvements than less concentrated treatments.

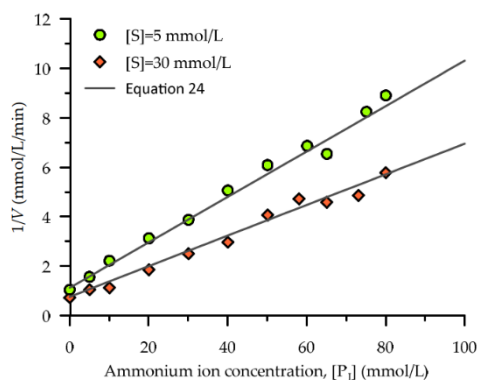


Figure 12 – One over the rate of reaction (V), with increasing ammonium ions (P). The latter act as non-competitive inhibitors of urease enzymes (S), reducing the reaction rate of urea hydrolysis. Whereas the red squares show that increasing the enzyme concentration speeds up the reaction. (Ahenkorah et al., 2021)

The kinetic reaction rate of urease enzymes is influenced by pH (Ahenkorah et al., 2021). In fact, bacterial urease enzymes display the most vigorous activity in pH ranges of 7 to 8 (Whiffin, 2004). As urea is hydrolyzed, the equilibrium reaction favors the production of toxic ammonium ions $\text{NH}_4^+(\text{aq})$, increasing the pH in ranges of 8 to 8.5 (Van Passen, 2009). Ahenkorah et al. (2021) performed kinetic calculations, showing that increasing ammonium concentration slows the rate of reaction (Figure 12). This would serve as a self-regulating mechanism, slowing urease activity in the solution once calcium carbonate precipitation occurs. Additionally, the use of buffers to maintain the pH between 7 to 8 is therefore sub-optimal for EICP, since the fastest reaction rate tendentially crystallizes small, non-bridging, calcite-vaterite (Gao et al., 2019).

Finally, temperature directly affects the rate of reaction; whereby higher energy lower completion times. Unsurprisingly, Ahenkorah et al. (2021) show direct correlations between the kinetic rate of reaction and temperature. Cheng et al. (2016) found that MICP achieved optimal strength gains at 25°C . This optimum allows for sufficient urease activity (proportional to temperature), while slower

nucleation rates yield sufficiently coarse, bridging, calcite grains (inversely proportional). Lastly, at higher temperatures, the less stable vaterite polymorph is favored (Van Paassen, 2009).

In conclusion the reaction rate of bio-cementation is controlled by pH, reagent concentration, and temperature. A slower reacting, high yield, EICP solution is achieved by three factors: allowing the solution to self-regulate without buffers (urease activity slows when ammonium concentration increases), utilizing non-equimolar solutions to render calcium a limit reagent, and maintaining the pore solution at 25°C.

2.3 Guanidinium and Clay Inhibition

Geo-technical research has seldom, yet successfully, utilized guanidine to inhibit clay swelling and enhance drainage in sand-bentonite soils. To further understand the topics treated in this chapter, an overview of clay theory is gathered for the reader in annex 8.1 *Clay Theory: a review*. Pertinent to the scope of the thesis, guanidium is introduced as protein inhibitor in micro-biology. Secondly, the role of hydromechanical coupling is discussed, identifying the geo-technical importance of clay inhibitors. Lastly, the state of the art of guanidine in smectite soil improvement treatments is discussed.

2.3.1 Guanidium and Protein Inhibition

Guanidium is a highly ionic and strongly exchanging organic cation, formed in an orthorhombic bipyramidal space (Figure 13). It is a weak acid (pKa=13.6, Biospectra) used extensively in physio-chemical studies of protein folding, due to its strong denaturing ability. The molecule used in the guanidine derivative salt, containing the guanidium conjugate acid. Its planar shape yields a very small ionic radius, and the three symmetric nitrogen covalent bonds induce an efficient resonance structure. This stabilizes the excess proton (+1 charge), further reducing its acidic potential. Additionally, the molecule is readily solved in water. The highly soluble molecule is nontoxic and biodegraded by naturally occurring species in surface waters (Mitchell, 1987).

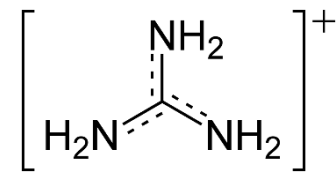


Figure 13 - Resonant Guanidium Chloride conjugate acid (Wikimedia)

Wang *et al.* (2021) state the “prevalence and biological significance of guanidine metabolism in nature”, thereafter studying genomic instability and toxicity of the molecule. More specific to this thesis, guanidine has also been studied in pathogenicity and ammonia production. Two domains where the underlying research analyses the disruption of urea hydrolysis. Guanidine derivatives have shown an inhibition of urease activity (catalyzer of the reaction) ranging between 20-30% (Mildner and Mihanovic, 1974), whereas pure guanidinium hydrochloride has shown none or milder inhibition of 2.5-9.3% at 0.1-1[mol/L] (Svane *et al.*, 2021). In fact, out of 84 studied compounds, guanidine hydrochloride was not listed as significantly inhibiting (Svane *et al.*, 2021). Nonetheless, the protein folding impact is non negligible; 0.9-1.5[mol/L] guanidinium hydrochloride was found to modify dissolved urease, forming aggregated fibril like structures of 6.5nm (McDuff *et a.*, 2004).

In conclusion, although the exact inhibitory action and kinetics of the urease-guanidine interaction remain beyond the scope of this research, their interaction must be addressed by experimental validation of EICP reactions *In-Vitro*.

2.3.2 Hydro-mechanical effects of Clay Inhibitors

The elastic and plastic responses of swelling smectite soils are strongly influenced by chemo-mechanical coupling. Soil strengthening in weak clayey soils can be achieved by increasing the resistive forces and decreasing the driving forces. For example, improving drainage through chemical alteration of clay platelets increases the shear resistance of a landslide prone lithologies (Minder and Puzrin, 2017). Additional processes, such as desorption/adsorption of fluids in the pore space, control swelling and plastic behaviour of clayey soils (Ghalamzan *et al.*, 2021). Soil strengthening treatments can seek to reduce excess pore pressures by draining water, leading to increased true effective stresses in the subsurface. Additionally, clay inhibitors form stable aggregates of clay particles (Minder and Puzrin, 2019), halting swelling and cyclic osmotic processes. The strongly binding and small ionic radii

compounds act by exchanging into and irreversible collapsing the interlayer space of clay minerals. Additionally, the aggregates display a modification of surface properties such as reduced repulsion between clay aggregates and increasing hydrophobicity (Hu *et al.*, 2020). Clay inhibitor compounds therefore directly modify the micro and macroscopic parameters of a clayey soil. Additionally, other clay minerals, such as kaolinite also undergo a compression of the electric double layer, forming aggregates when treated by electrolytes and surfactants (Hu *et al.*, 2020). The chemical stabilization is therefore key in improving the hydro-mechanics of a weak clayey soil, while potentially reducing the charge surface interaction which hampers bio-cementation in clays (Cardoso *et al.*, 2018).

2.3.3 Guanidinium as a Clay-Inhibitor

Interlayer cations determine the mechanical, chemical and thermal properties of clays. Clay inhibitors are molecules which collapse the interlayer space and reduce particle repulsion. The swelling potential and osmotic reactivity of the clay platelets is minimized. When treated by a clay inhibitor, homoionic exchanged smectites display lower reactivity and stabilized physical properties (Steudel and Emmerich, 2013).

Plotze and Kahr (2008) first proposed the use of guanidine carbonate as a promising non-conventional swelling inhibitor for analysis clays by x-ray diffraction. The highly ionic, strongly binding cation, is specifically intercalated in the interlayer space of stacked sheet-silicates, replacing water molecules and weaker charge density ions (Minder, 2016). Strong hydrogen bonding reduce inner crystalline swelling drastically. In fact, if free-swelling, a smectite's basal spacing ranges between 9.3 and 20[Å] (Ougier-Simonin *et al.*, 2016). However when inhibited by guanidine molecules, XRD analyses of the clay recorded fixed spacing of 13.0[Å] for vermiculite and 12.5[Å] for smectite (Figure 14), regardless the samples' relative humidity. Additionally, surface adsorption reduces the double diffusive layer of clay particles, reducing interparticle repulsion, and favoring aggregation (Minder, 2016). The molecule can irreversibly collapse clay particles in smectite bearing soils, such as bentonite, inhibiting swelling and favoring an aggregate matrix.

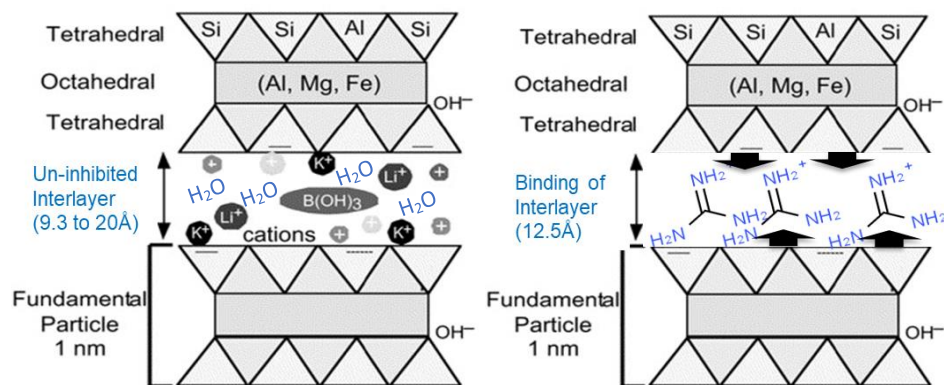


Figure 14 - Smectite interlayer cation exchange with guanidinium ions.

The first detailed use of guanidinium as a clay inhibitor for geo-engineering purposes is detailed in a patent filed by Canadian drilling companies operating in shales (McDaniel *et al.*, 2016). Thereafter, Minder (2016) studied the soil strengthening and drainage potential of the molecule. He measured the cation exchange and adsorption potential in bentonite by fluorescent spectrometry, concluding that 80% of exchangeable cations were readily replaced when saturating dry calcium bentonite with a 1[mol/L] guanidinium hydrochloride. Having quantified it's efficient uptake, Minder and Puzrin (2016) inhibited the clays in sand-bentonite soils by mechanical mixing and flushing, showing it's

suitability to injection based treatments. The treatment of clay with guanidium hydrochloride salt 0.5[mol/L] yields substantial aggregate formation and open pore structures (Figure 15), even when subjected to 800kPa loading (Minder *et al.*, 2016).

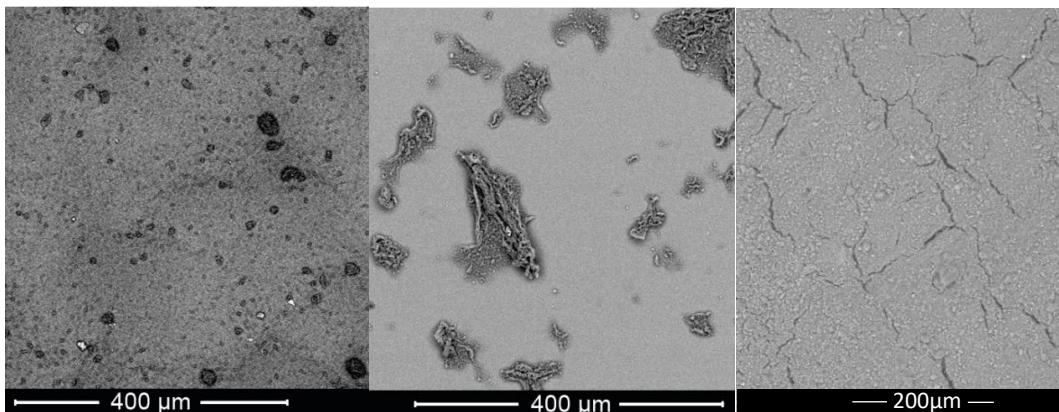


Figure 15 - Calcium bentonite washed with DI water remains finely dispersed (left), whereas guanidium ions yield aggregate formation (center) (Minder, 2016). Rough and blocky shear plane of a GndHCl treated natural soil (right) (Leik, 2020).

Falling head permeameter tests showed increased sample permeability by an order of magnitude when treated with guanidine (Figure 16). Additionally, the peak and residual shear strength increased with treatment. Microstructural imaging has shown increased shearing surface roughness (Leik, 2020). Minder and Puzrin (2017) measured guanidium treated samples to have 7-7.1° increase peak friction angle compared to control samples saturated with 0.01[mol/L] CaCl₂. Similarly, residual friction angles also increased (Figure 17).

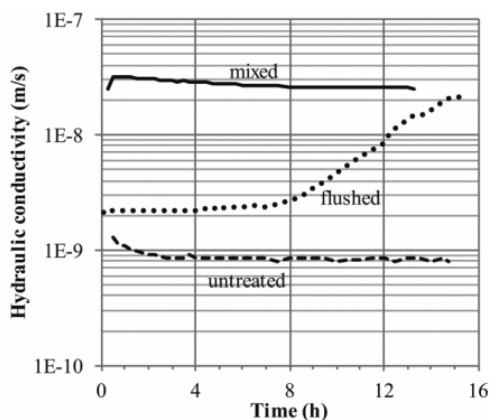


Figure 16 - Evolution of hydraulic conductivity during flow-through treatment (dotted line) (Minder *et al.*, 2016)

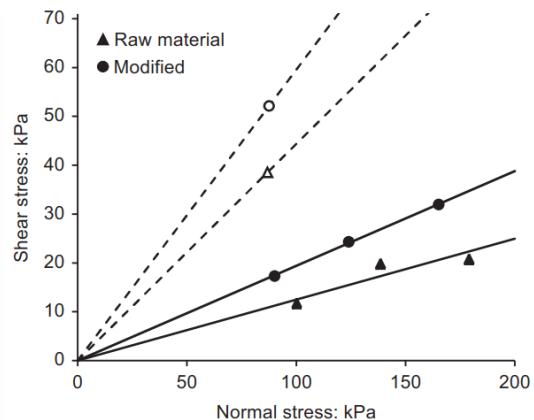


Figure 17 - Shear tests at 0.2mm/min. Empty symbols represent peak shear resistance. Filled symbols are the residual stress. (Minder and Puzrin, 2017)

To conclude, the aggregation of the clay particles enhances permeability and thus flow through potential, while improving mechanical properties (shear strength, friction angle) of the soil sample. The clay platelet aggregates are stable under loading, maintaining an opened pore structure (Figure 15). Swelling and hysteresis sensitivity decreases drastically. Stiffness does not majorly improve following treatment.

2.4 Conclusions

The literature review presented in this chapter develops a knowledge base on EICP and guanidinium. Using this theoretical foundation, the thesis' methodology attempts to account for the coupled interaction of the two treatments in the pore fluid and matrix.

Enzyme induced calcite precipitation has repeatedly shown promising strength gains when cementing sands, but fails to yield notable results in clayey soils. It's ease of preparation and novelty has garnered recent attention in alternative grouting research. Successful strength and stiffness gains derive from a calibrated low concentration solution, leading to voluminous calcium carbonate crystals, bonding adjacent sand grains. The activity of the catalyzing urease agent, the pH of the pore fluid, and density of the sand, are critical in achieving successful cementation. Building upon the abundant past EICP research, the bio-cementation solution for this thesis must be optimized for maximum yield at the lowest molarity. Currently, the state of the art lies in finding additives to control the reaction in favor of large crystals.

Guanidine is shown to act as an irreversible clay inhibitor, improving the strength parameters of smectite soils, while increasing their hydraulic conductivity. Microbiological research has exploited it's protein denaturing properties over the last decades, however the molecule remains rarely studied in geo-technical branches. It shows great potential in clays alone, but any residual molecules in the pore solution may interact with subsequent EICP treatments containing the urease enzyme. The coupled action must be experimentally researched in the thesis.

Following the literature review, engineering of weak sand-clay soils by bio-cementation, is identified as a recurring knowledge gap. Although rarely documented, guanidine shows significant potential as a clay inhibitor to improve strength and physio-chemical stability of such medium. If successful, the coupled treatment is expected to improve strength (shear and compressive) and increase stiffness, modifying the hydraulic conductivity and microstructure of the soil (aggregation of clays, crystallization of calcium carbonate in the voids).

3

Materials and Methods

3.1 Introduction

The materials and methods chapter researches *Bio2Cementation's* materials, treatment design and sample preparation, leading to a testing protocol in the soil skeleton. Test tube experiments are performed to research the optimal bio-cementation solution and guanidinium's potential inhibitor role in the coupled treatment. Thereafter, following the annexed impermeable liner literature considerations, the sand-bentonite soil sample preparation is verified for reproducibility and homogeneity. Following these initial considerations, the bio-cementation and clay inhibition testing program in the soil matrix is defined. In view of its realization, an injection cell is designed, capable of delivering treatments to sand-bentonite specimens. Finally, the envisioned tests are listed as hydraulic conductivity analyses, mechanical testing, and microstructural characterization.

3.2 Materials

3.2.1 Treatment Solutions

The treatment solutions are comprised of bio-cementation reagents and a diluted clay inhibitor molecule. The coupled treatments therefore utilize the following reagents (Table 3):

Table 3 - Reagents used in the preparation of *Bio2Cementation* treatments.

Treatment Type	Reagent Name	Specifications
EICP	❖ Urea	➤ <i>Alfa Aesar Urea 98+% by ThermoFisher GmbH</i>
	❖ Calcium Chloride	➤ <i>Granular CaCl₂ anhydrous, <7micron, >93% by Sigma-Aldrich</i>
	❖ Urease Enzymes	➤ <i>Jack Bean Urease 5g at 3[U/mg]. Lyophilized Canvalia Ensyformis 5g at 8[U/mg].</i>
Clay Inhibitor	❖ Guanidinium Hydrochloride	➤ <i>6M by Boomlab (aqueous)</i>
Flushing and Diluting	❖ Demineralized Water	

3.2.2 Tested Soils

This section defines two artificial sand-bentonite soils, at two void ratios, to test the range of *Bio2Cementation's* success at varying clay content and compaction. Additional reading concerning the selection of sand and bentonite as the artificial soil constituent (Figure 18) are included in annex 8.2 *Soil constituents: a review of EICP and Guanidinium research.*

In view of time and the thesis' scope, the soil is characterized by combining experimental data with empirical proctor formulations from impermeable liner state of the art research. The computation of the sand-bentonite density of solids (derived from He-pycnometer experiments), optimum water content (OMC) and maximum dry density ($\rho_{dry,max}$), are detailed in annex 8.3 *Characterization of Sand-Bentonite: experimental data and empirical formulations.*

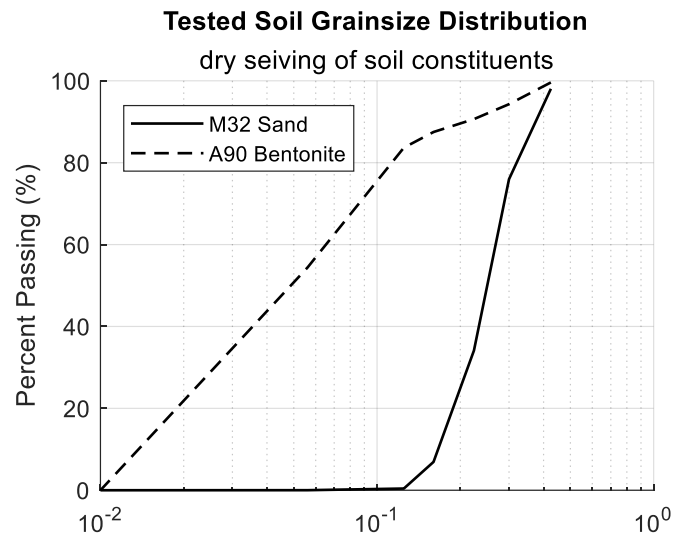


Figure 18 - Cumulative grainsize distribution of sand and bentonite.

A ten percent bentonite content (BC) soil is chosen, for which the sand fraction is expected to dominate the hydro-mechanic response of the porous media. On the other hand, a large thirty percent bentonite content soil is also selected to test the treatments' limit in quasi-impermeable, highly swelling, porous media (Biju and Arnepli, 2020). Additionally, varying compactions are also tested by preparing the two soils at ~95% and ~80% of the dry density maxima.

In summary, the tested clayey soils are detailed in Table 4:

Table 4 - Sand-bentonite artificial soil upon which the two phase Bio2Cementation soil strengthening research is performed. Bentonite content (BC) is a function of the total dry mass of sand to bentonite.

Bentonite Content	BC 10% $\rho_{dry,max}=1.55g/cm^3, OMC=19.2\%$		BC 30% $\rho_{dry,max}=1.64g/cm^3, OMC=14.6\%$	
	Dry Density	1.21g/cm³	1.47g/cm³	1.35g/cm³
% of $\rho_{dry,max}$	~80%	~95%	~80%	~95%
Void Ratio	1.22	0.83	1.01	0.75

3.3 Treatment Design

A successful treatment protocol requires functional treatments, which must be tested outside the soil mass before being injected in a porous medium. Two test tube experiments are performed (Figure 19). Firstly, the enzyme induced calcite precipitation recipe must be optimized (maximum yield at the lowest concentration) as a function of the available reagents. Secondly, the guanidinium solution is tested for temporal stability and its potential inhibition of the urease enzyme. A successful design will provide the basis to answer the following research sub-questions:

1. “What is the optimal enzyme induced calcite precipitation recipe to maximize yield at low concentration reagents? How stable is guanidinium hydrochloride, and does it’s protein denaturing ability disrupt calcite precipitation solutions?”

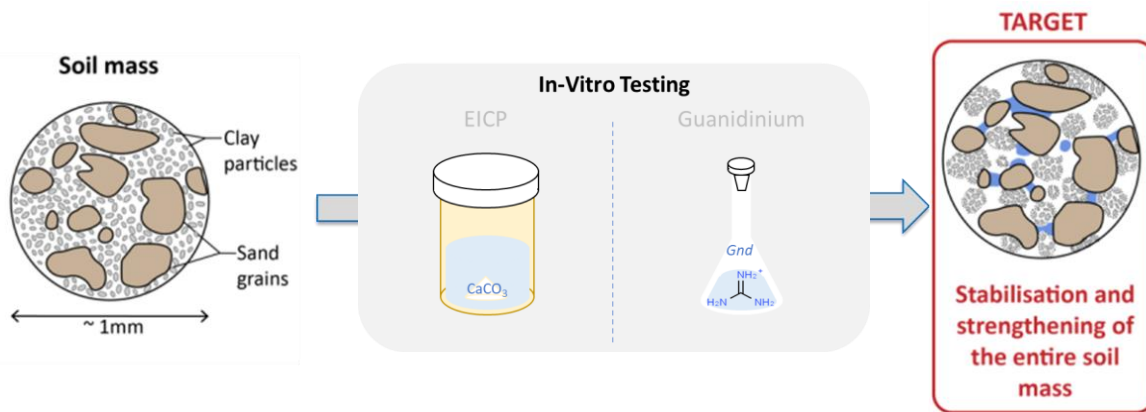


Figure 19 - The process of designing the bio-cementation and clay inhibition treatments; experimentally researching the first research sub-question of the thesis.

3.3.1 EICP: Test Tube Experiments

Soil improvements which bio-cement soils by enzyme induced calcite precipitation (EICP), require injection of calcium chloride, urea, and urease enzyme solutions. This sub-section proposes an optimization study conducted outside of the porous media. Reagent concentrations are varied in test tubes, seeking to maximize calcium carbonate yield at the lowest reagent concentration.

3.3.1.1 Background

The optimization of the cementation solution depends on the available reagents, type of dilutant used and urease activity. Past research has tested calcium chloride (CaCl₂) to urea ratios, yielding consistent results that the ratio of 1 to 1.5 ratio was the most efficient (Almajed *et al.*, 2018; Yuan *et al.*, 2020; Putra *et al.*, 2020). Large reagent concentrations led to the degradation of urease enzyme activity over time and the crystallization of weak vaterite crystals (Arab *et al.*, 2021). Almajed *et al.* (2018) concluded that 3[g/L] of urease, with an activity of 3.500 [mU/g], proved to be the threshold value after which calcium carbonate yield no longer increased. Cementing curing times were tested by Yuan *et al.* (2020), by quantifying the remnant calcium ion concentration in the pore solution. For solutions less concentrated than 1.6 [mol/L], they concluded that reactions reached 87-98% completion over twenty-four hours. The reaction no longer showed terminated after three days. For further reading, a review of the state of the art bio-cementation solutions is summarized in annex 8.4 EICP recipes: a review.

3.3.1.2 Results and Data Interpretation

The bio-cementation tests at varying concentrations and ratios are performed at constant volume, and agitated for forty-eight hours (Figure 20). Two catalyzing enzymes are tested: *Jackbean urease* (activity of 5mU/g) and the *Lyophilized Canavalia Ensiformis urease* (activity of 8mU/g). The testing protocol records the solutions' electrical conductivity (EC), hydronium ion concentration (pH), and precipitates mass (Figure 21 and Figure 22). The methodology is detailed in the experimental procedure of annex 8.5.1 Method: EICP Test Tube Optimization.

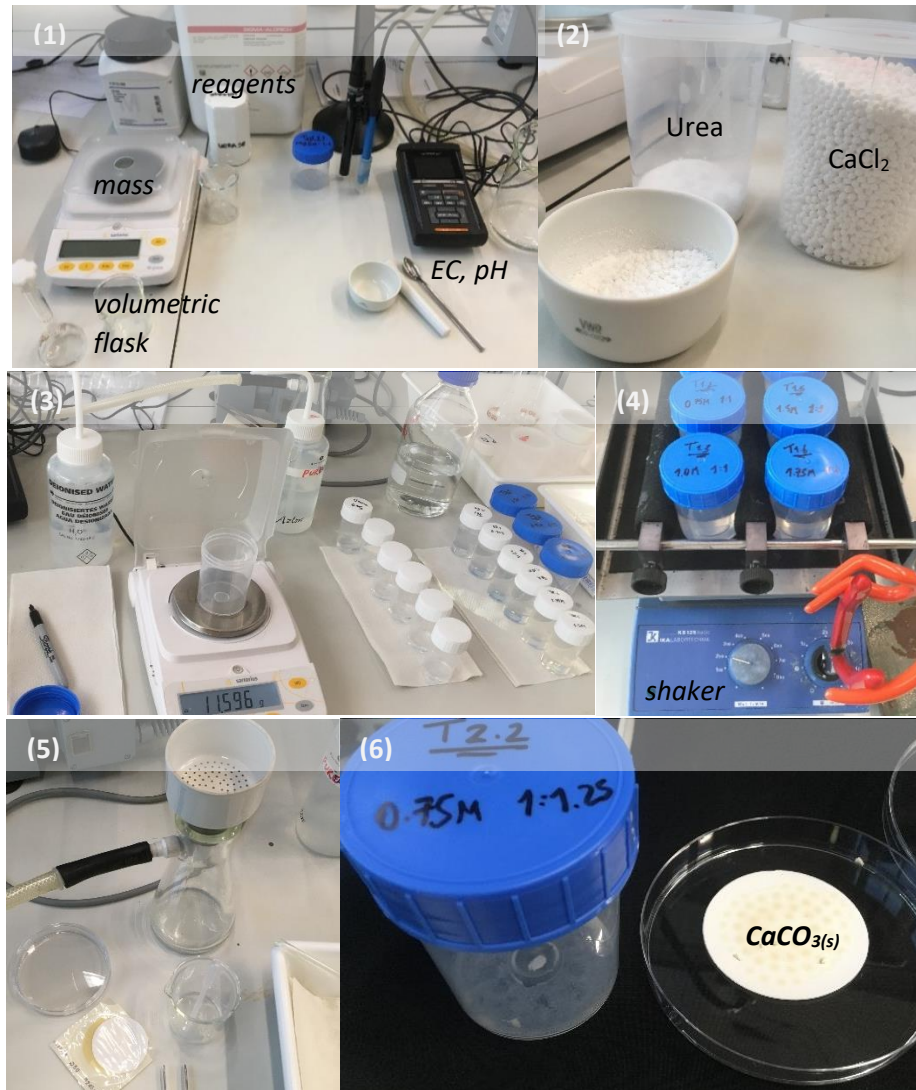


Figure 20 - Enzyme induced calcite precipitation (EICP) test tube experiments. From top left to bottom right: 1 - the measurement setup, 2 - the urea and CaCl₂ reagents, 3 - weighing recipients before cementation and dissolved urease enzymes (white cap ~10mL), 4 - shaker clamped to run indefinitely, 5 - filtering with 550kPa of underpressure, 6 - finally the resulting precipitation coating the tube and in suspension (here for Test 2.2 – 0.75M urea, with a ratio to CaCl₂ of 1:1.25).

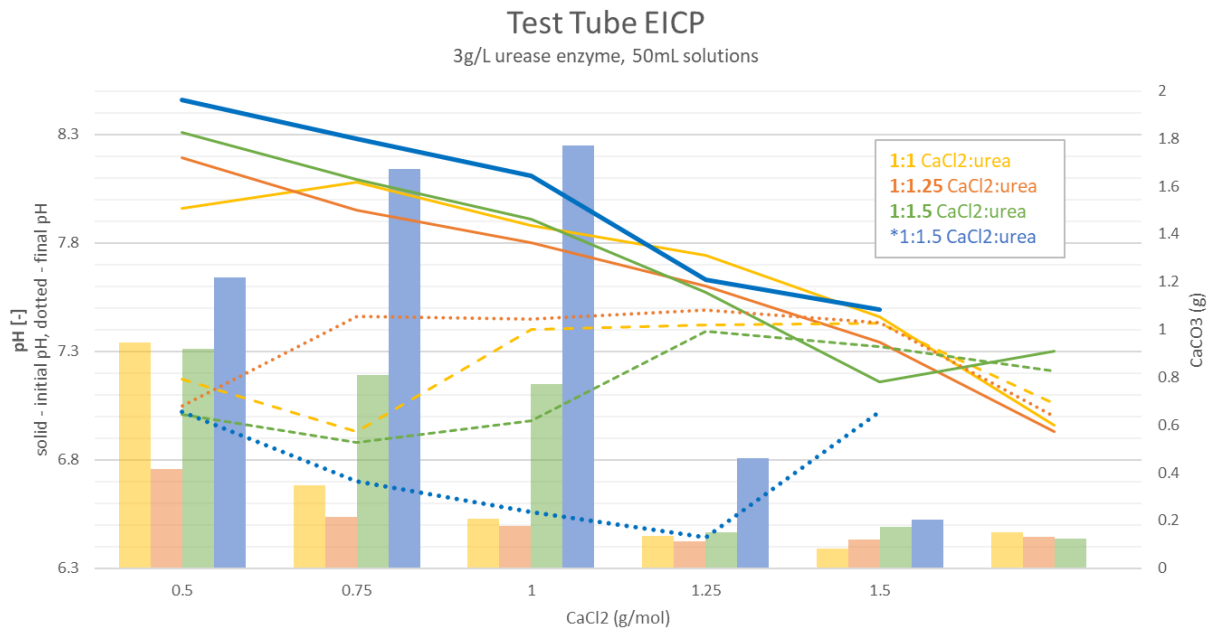


Figure 21 - EICP Test tube recipe optimization for three ratios of calcium chloride to urea reagents catalyzed by the Jackbean Urease with an activity of 5U/mg (1:1 yellow, 1:1.25 red, 1:1.5 green). Later experiments maintain the optimal ratio of 1:1.5, but verify the suitability of lyophilized *Canavalia Ensiformis* Urease with an activity of 8U/mg (*1:1.5 blue). Each ratio is tested at increasing CaCl₂ concentrations, ranging from 0.5 to 1.75 [mol/L]. The precipitated CaCO₃(s) of each bar graph is shown on the secondary vertical axis (right). The initial (solid line) and final (dotted line) pH are shown on the primary vertical axis (left).

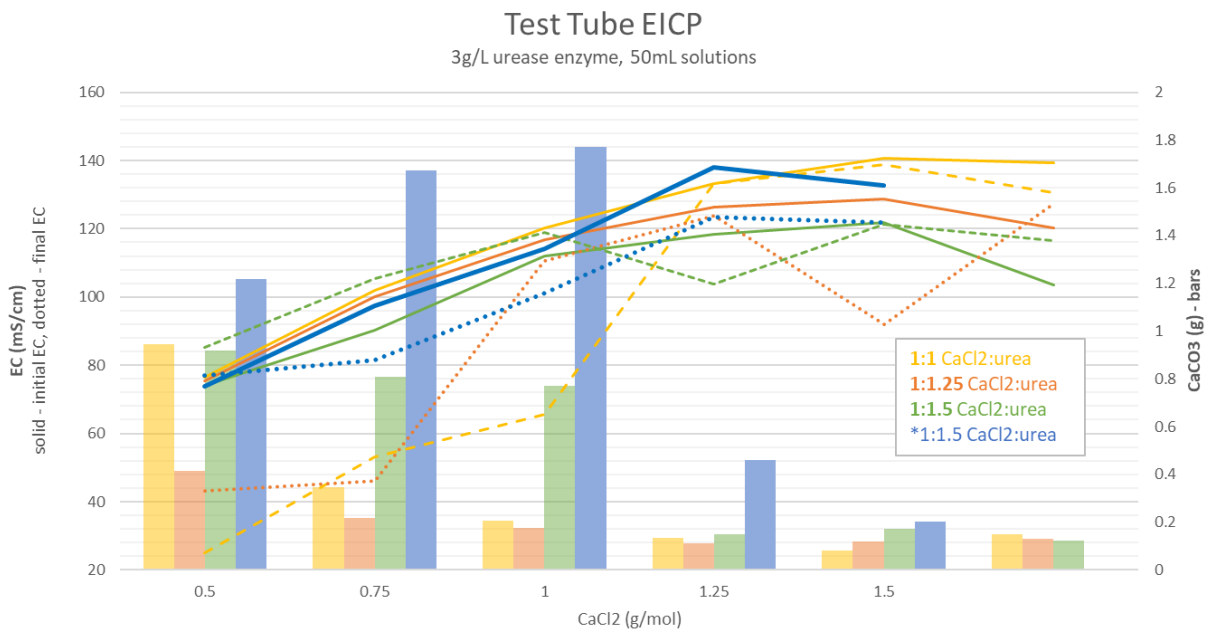


Figure 22 - EICP Test tube recipe optimization for three ratios of calcium chloride to urea reagents catalyzed by the Jackbean Urease with an activity of 5U/mg (1:1 yellow, 1:1.25 red, 1:1.5 green). Later experiments maintain the optimal ratio of 1:1.5, but verify the suitability of lyophilized *Canavalia Ensiformis* Urease with an activity of 8U/mg (*1:1.5 blue). Each ratio is tested at increasing CaCl₂ concentrations, ranging from 0.5 to 1.75 [mol/L]. The precipitated CaCO₃(s) of each bar graph is shown on the secondary vertical axis (right). The initial (solid line) and final (dotted line) EC are shown on the primary vertical axis (left).

Maximal calcium carbonate yield is achieved at concentrations of 0.5 [mol/L] for equimolar solutions, and at 1 to 1.5 ratios for calcium chloride concentrations of 1[mol/L]. Nonetheless, the latter shows a larger sensitivity of yield to increasing concentrations, potentially indicating a decreases solution stability. Such findings are visibly confirmed by calcium chloride cementation and suspension.

Expectedly, the higher activity catalysis rate by with the lyophilized Urease (8[U/mg], in blue), allows greater amounts of calcite to precipitate for any concentration less than or equal to one molar.

In the initial state, the low concentration solutions are most alkali, which Van Passen (2009) explains as the onset of calcium carbonate precipitation. More specifically, Figure 21 the most alkali one reaction occurs for specimen 0.5 [mol/L] CaCl₂ at a ratio of 1:1.5. Higher concentrations of reagents maintain neutral pH's, displaying a lack of bio-cementation initiation. After the curing time, neutral pH's are reached. This occurs at the end of the reaction, whereby the rate of calcium carbonate precipitation matches the rate of urea hydrolysis, until all free calcium is consumed. Assuming that neutral conditions are indicators of complete reactions, all solutions complete the EICP over forty-eight hours. Additionally, testing with the higher activity urease (blue), shows acidifying trends in final pore solutions (blue dotted line) for concentrations $\geq 0.75M$. This may hinder subsequent injections in a weakly acidic medium; suboptimal for calcite precipitation. Such argumentation corresponds well to the trend of precipitated solids.

The electrical conductivity (EC) profiles are measured at the start and end of the EICP reaction (Figure 22) Expectedly, at the reaction onset, the measure of total dissolved solids increases with increasing concentration. Whereas at the end, low concentration equimolar solutions are characterized by decreased EC values. This can be explained by the extraction of carbonate and calcium ions by calcite precipitation. Contrarily, the strongly reacting non-equimolar 1 to 1.5 ratio solutions at less than 1 molar concentration, yield greater final EC than initial readings. This is explained by continued urea hydrolysis (Van Passen, 2009), leading to excess ammonium ions in the solution. Such reading may therefore be a proxy of the beneficial alkaline conditions of non-equimolar solutions, allowing urease enzymes to thrive for longer at pH=7-8 (Ahenkorah *et al.*, 2021). In fact, many researchers have used such reagent ratios as means of optimizing EICP recipes (Yuan *et al.*, 2019; Gao *et al.*, 2020).

Additional continuous temporal measurements of EC and pH over twenty-four hours for varying *Lyophilized Canavalia Ensiformis urease* (activity: 8[U/mg]) concentrations are included in annex 8.7.3 *Calcium Carbonate Polymorphs*. Solutions using the 1[g/L] of the vigorous enzyme are found to yield the same initial peak pH as higher concentrations, indicating successful EICP, but are expected to beneficially reduce the rate of reaction over time.

3.3.1.3 Summary

This section tested the optimal EICP solution, aiming to maximize yield at the lowest concentration with the available reagents. The experiments comprised of bio-cementation test tubes prepared at varying concentrations and reagent ratios.

To conclude, the calcium chloride to urea solutions at 1 to 1.5 are most stable and precipitate abundant calcite. Specifically, 0.5[mol/L] to 0.75[mol/L] solution is deemed optimal. Jack Bean urease enzymes (activity: 3[U/mg]) are used at concentrations of 3[g/L]. Solutions using *Canavalia Ensiformis* urease (activity: 8[U/mg]) are used at concentrations of 1[g/L]. The low concentration non-equimolar solution and lower concentrations is expected to reduce reaction rates and improve crystal morphology for fewer nucleation sites (Almajed *et al.*, 2019). This is expected to improve the calcite crystal microstructure (polymorph, size, location) in the soil fabric. Such findings concur with the current state of the art EICP.

3.3.2 Guanidinium Hydrochloride: Stability and Inhibition of EICP

The clay inhibitor Guanidinium Hydrochloride (GndHCl) stabilizes the sand-bentonite matrix. This sub-section defines a treatment concentration according to the state of the art, which is then researched in two ways. Firstly, since the adsorption of ions in clays requires time, diffusion and cationic exchange must occur in stable conditions. A baseline study is performed to verify the temporal stability of pH and electrical conductivity (EC) of diluted guanidinium. Secondly, following the literature review's concern of guanidine's anti-ureolytic properties, the potential urease inhibition is researched by reacting EICP solutions with diluted guanidine.

3.3.2.1 Background

Impermeable liner research has identified salinity's role in reducing bentonite's swelling potential and increasing hydraulic conductivity (Komine *et al.*, 2009; Shirazi *et al.*, 2011). Although unwanted when isolating waste, such features are desirable in improving bio-cementation in clayey soils. In fact, guanidinium solutions have shown to aggregate colloidal kaolinite (Hu *et al.*, 2020), stabilize natural swelling plastic soils (Leik, 2020) and sand-bentonite mixtures (Minder *et al.*, 2016). The limited literature using guanidinium salts clay inhibition has used diluted solutions of 0.5[mol/L] or 1[mol/L] (Minder and Puzrin., 2017; Leik, 2020). For example, Figure 23 shows how suspending activated sodium bentonite in low concentration guanidinium chloride solutions, leads to the replacement of ~80% exchangeable cations. Additionally, seeking to minimize costs of the treatment, the lower 0.5[mol/L] concentration used in literature, is deemed desirable in the scope of this thesis. The experimental procedure is detailed in annex 8.5.2 *Method: Guanidinium Hydrochloride Experiments*.

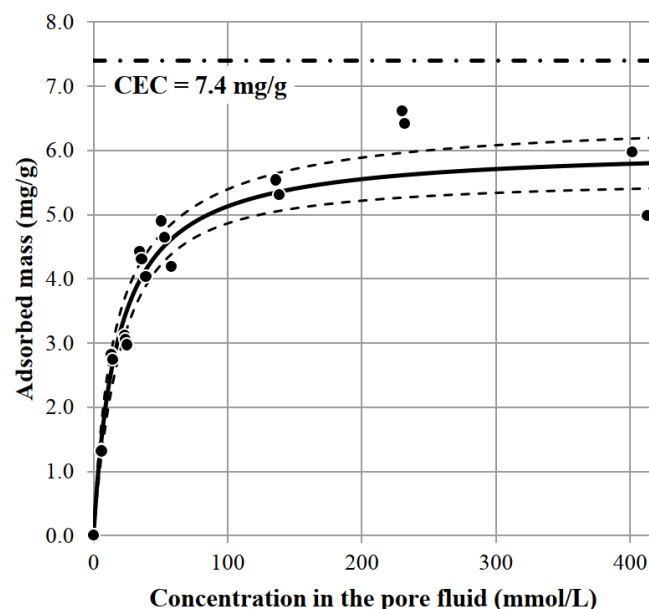


Figure 23 - Sorption of guanidinium ions tested by Minder (2016): The dash-dot line indicates the theoretical maximum CEC[mg/g] of the bentonite, whereas the Langmuir sorption isotherm (line, 95% interval: dashed) shows results yielding ~80% replacement of exchangeable cations by bentonite suspension in soil solutions (at concentrations of 0.4[mol/L]).

Guanidinium Hydrochloride Stability Test:

The test in Figure 24 shows extremely stable solution over time. The pH of the acidic solution increases by 0.04[-] when exposed to air for forty eight hours. Similarly, a monotonic increase in EC is also noted, with 400[$\mu\text{S}/\text{cm}$] gained over the same time. Following an initial thermal equilibration of the solution, a slow evaporation of the effluent in the climate room (20-21°C) may explain the increased electrical conductivity. Monotonic evaporation leads to increasing relative concentration of the effluent, whereby the relative proportion of total dissolved solids increases, leading to larger charge transport. Additionally, evaporation removes gaseous water molecules, whereby the equilibrium reaction utilizes hydroxyls from the strong acid and dissolves additional ones to form more water. This removes [H+] ions monotonically, explaining the increase in pH over time. No other phenomena except evaporation is discerned in the dataset.

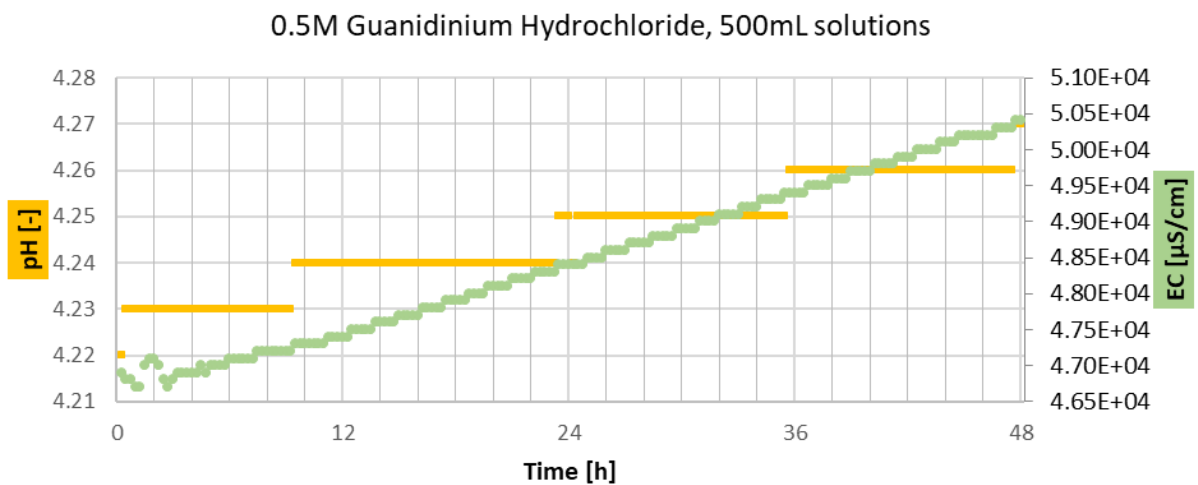


Figure 24 - Guanidinium Hydrochloride pH and EC stability over time.

Guanidinium Hydrochloride Inhibition Test:

Four tests are envisioned to mimic residual guanidinium ions in the pore solution. If adsorption is incomplete, and demineralized flushing is ineffective, the pore space treated by EICP may contain low concentrations of reactive guanidine. For this reason, this sub-section explores the sensitivity of calcite formation or lack-thereof in the presence of guanidinium ions.

Increasingly pessimistic scenarios are envisioned: no guanidinium followed by EICP occurring in with increasing guanidine concentrations (Figure 25 and Figure 26):

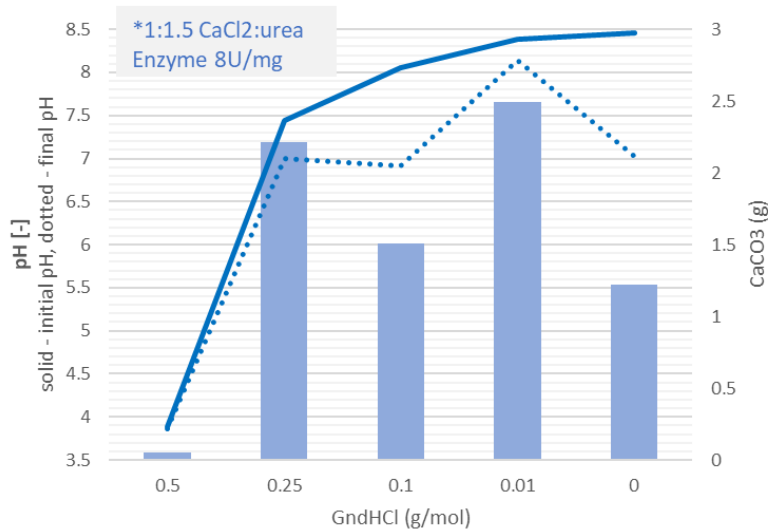


Figure 25 - Test tube EICP reactions diluted with varying Guanidine Hydrochloride concentrations, mimicking residual guanidine ions between the two treatment phases. Murky solutions and wall calcification show EICP occurring at $\leq 0.25\text{M}$ tests.

The highest concentration solution is strikingly different from the rest: the solution remains clear. No calcite precipitate form, leading to the hypothesis that urea hydrolysis is unsuccessful (Figure 25). This may be due to two factors: the highly acidic medium and/or denatured urease. In fact, a spiral of white material forms in suspension of the clear solution, potentially a result of protein folding in the highly concentrated guanidine. For any concentration less than or equal to 0.25[mol/L] guanidinium hydrochloride, the reaction is sufficiently vigorous to precipitate calcite, as seen by the murky solution and precipitation along the tube walls. Visually, the 0.01 and 0.1[mol/L] solution displays the largest amount of nucleation along the tube walls.

Test Tube Guanidinium in EICP

0.5M Calcium Chloride : 0.75M Urea, 3g/L urease , 50mL solutions



Test Tube Guanidinium in EICP

0.5M Calcium Chloride : 0.75M Urea, 3g/L urease , 50mL solutions

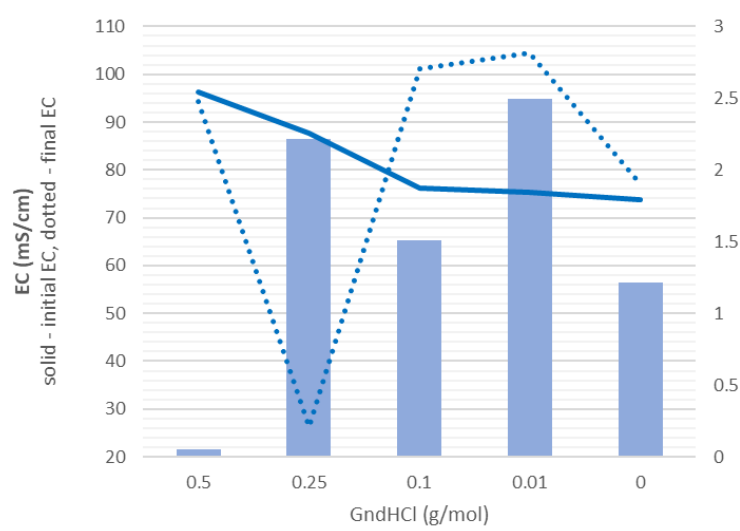


Figure 26 - EICP Test tube in the presence of GndHCl. These experiments maintain the optimal reagent ratio of urea:CaCl₂ of 1:1.5 and lyophilized *Canavalia Ensiformis* Urease with an activity of 8U/mg. Each bar shows varying guanidinium diluted in the EICP solution, ranging from 0.5 to 0 [mol/L]. The precipitated CaCO₃(s) of each bar graph is shown on the secondary vertical axis (right). Additionally, the initial (solid line) and final (dotted line) pH and EC are shown on the primary vertical axis (left).

Varying guanidine concentrations effect EICP yield and chemistry, as displayed in Figure 26. Inhibition of calcite precipitation occurs only in the overly acidic medium. The lack of reaction is further supported by unvarying readings of initial versus final pH and EC. Most interestingly, the highest precipitation efficiency occurs with residual Guanidinium ions in the solution. Tests containing less than or 0.25 [mol/L] of the clay inhibitor precipitate a larger amount of calcite than the pure EICP solution! In these experiments, a strongly reduced final EC of the 0.25 [mol/L] reaction outlies the rest. The latter two reactions display an opposite trend, recording an increase in final EC. When compared to the results of EICP alone (Figure 22), the former trend matches equimolar reaction trend, whereas the latter two concur non-equimolar solutions (which is also used in Figure 26).

Additional continuous temporal measurements of EC and pH over twenty-four hours for varying *Lyophilized Canavalia Ensiformis urease* (activity: 8[U/mg]) concentrations are included in Figure 84 of annex 8.7.3 *Calcium Carbonate Polymorphs*. EICP solutions using 0.25[mol/L] guanidine dilutant and 3[g/L] of the vigorous enzyme are found to not generate a peak in alkalinity during EICP onset, but rather favor slow reactions with monotonic pH and EC increases over twenty-four hours.

The visual and quantified data is interpreted as the following:

1. Visual coiling in the test tubes supports the theory of protein folding and denaturation in the most concentrated test (Figure 25). The dilution at 0.25[mol/L] contains abundant basal precipitates and little suspension. Differently, bio-cementation solutions with low guanidine concentrations are murky, containing molecules in suspension and large amounts of wall calcification. These cues indicate different reaction rates/pathways between the two.
2. It is postulated that at low guanidine concentrations, the vigorous urease is not denatured, allowing for continued urea hydrolysis over time. Therefore, the solution remains non-equimolar, and excess ammonium ions ($\text{NH}_4^+_{(\text{aq})}$) induce a larger final EC than at the start of the reaction (Figure 26, right).
3. Guanidine induces a partial urease degradation or kinetic modification of calcite precipitation (annex 8.7.3). Free charge transporting $\text{NH}_4^+_{(\text{aq})}$ ions are limited, as shown by low initial pH and gradual monotonic evolution over twenty-four hours. The partial hydrolysis of urea is not blocked by guanidine's protein inhibition, but allowed to progress slowly over time. Further research is needed to explore the molecules beneficial potential as an EICP additive.

In conclusion, the impact on the treatment's optimization is interpreted as follows:

Enzyme induced calcite precipitation is sensitive to guanidine, successfully occurring, and even improving yield in solutions. For the proposed clay inhibition guanidinium treatment of 0.5[mol/L], it is necessary to reduce the residual guanidine of the pore solution below 0.25[mol/L]. The dilution factor of two can be easily achieved by clay adsorption (and CEC), demineralized water flushing and subsequent EICP injections. Additionally, the inclusion of guanidine as a bio-cementing additive is shown to improve calcium carbonate yield and minimize residual free ammonia ions.

3.3.2.2 Summary

Guanidinium Hydrochloride Stability Test:

The demineralized water and Guanidinium Hydrochloride solutions are deemed stable over time in terms of EC and pH, unless undergoing evaporation. For this reason, all guanidinium hydrochloride treatment solutions are stored in airtight glass jars.

Guanidinium Hydrochloride Inhibition Test:

The current treatment protocol treats the clay fraction with 0.5[mol/L] guanidinium hydrochloride. Its concentration is reduced over time by adsorption, flushing and subsequent EICP injections. Any expected residual ions will not hinder bio-cementation. In fact, guanidine shows promise of acting as an additive to improve EICP. However, temporal effects, crystal polymorph and microstructural features must be further studied by imaging techniques before its acceptance.

3.4 Soil Sample Preparation

The thesis novel treatment protocol aims to stabilize and strengthen a clayey soil mass. To test the performance of *Bio2Cementation* in soils, a reproducible soil sample preparation must be tested prior to injecting treatment solutions (Figure 27). This section tests a controlled soil sample preparation exploring the role of sand-bentonite artificial soils as a crucial control variable throughout the thesis.

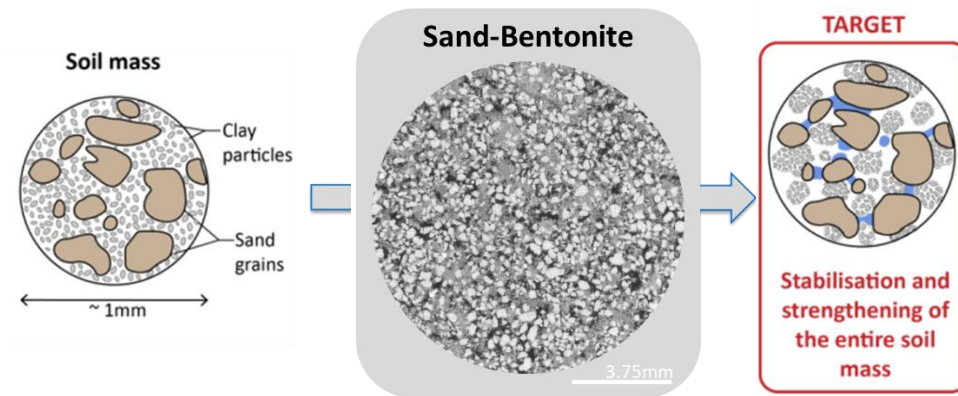


Figure 27 – Schematic representing the characterization and preparation of a reproducible control artificial soil, upon which to test the strengthening treatments.

3.4.1 Sand-Bentonite Soil: Sample Hydration and Tamping

The artificial soil is comprised of readily available, well documented, and previously researched soil constituents. The sand-bentonite characterization is based upon impermeable liner research. At varying bentonite content and compaction, this section tests the sample preparation for homogeneity and reproducibility. The approach is verified in two ways: visually and through the aid of non-destructive x-ray imaging.

3.4.1.1 Background

Soil density and homogeneity directly affect the binding lattice bonds and grain contact points of bio-cementation (Terzis and Laloui, 2019). Additionally, the clay fraction dominates the fine pores, total permeability, and sample cohesion of smectite soils (Minder, 2016). For these reasons, the characterization of sand-bentonites is described and justified according to impermeable liner research of annex 8.3 *Characterization of Sand-Bentonite: experimental data and empirical formulations* and the methodology detailed in annex 8.5.3 *Method: Soil Sample Preparation*. In summary, the sand-bentonite mixture is hydrated to the optimum moisture content (OMC) for twenty four hours. Then, in function of literature based proctor characteristics, cylindrical soil samples are compacted to the target density in five equal-mass layers.

3.4.1.2 Results and Data Interpretation

The soil shows contrasting macroscopic features when saturated either demineralized water (DI) or guanidine (Figure 28). In fact, if DI water is added, the paste is coarse, yet homogeneously smooth under the spatula. Clay plasticity dominates its texture. Whereas when hydrated with 0.5[mol/L] guanidinium hydrochloride, the soil displays a predominantly aggregated texture, immediately less homogeneous and smooth.

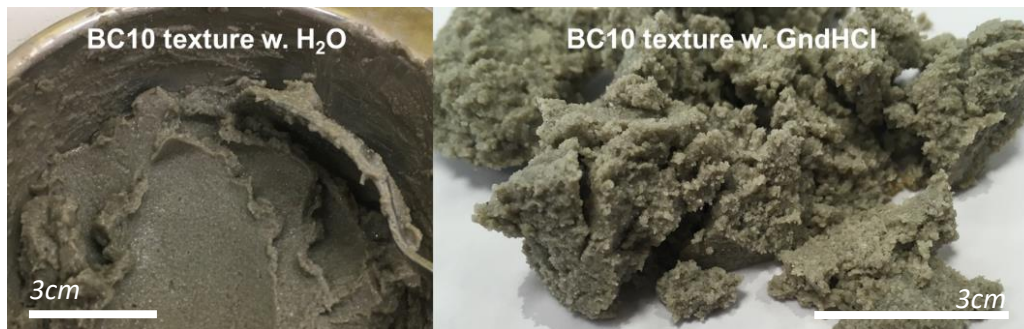


Figure 28 – Texture visualization of a saturated BC10 sand-bentonite mix. On the left water saturation creates a plastic, smooth paste, visibly moist. On the right, saturation with guanidinium aggregates the soil fabric creating a sandy texture, which crumbles rather than smearing when disturbed.

Grayscale micro-computer tomography (Micro CT) imaging of the samples confirm the visual and textural cues proposed previously. The samples prepared with DI water are homogeneous (Figure 29-*left*,). Quartz grains (very light) are surrounded by a diffused matrix of bentonite (gray), with poorly interconnected fine pores (black). Furthermore, homogeneity does not visibly vary with compaction. This is starkly contrasted in the heavily aggregated GndHCl sample preparation (Figure 29 – *right*). The unpredictable structure may induce preferential pathways, and randomly influence the soils strengthening treatments.

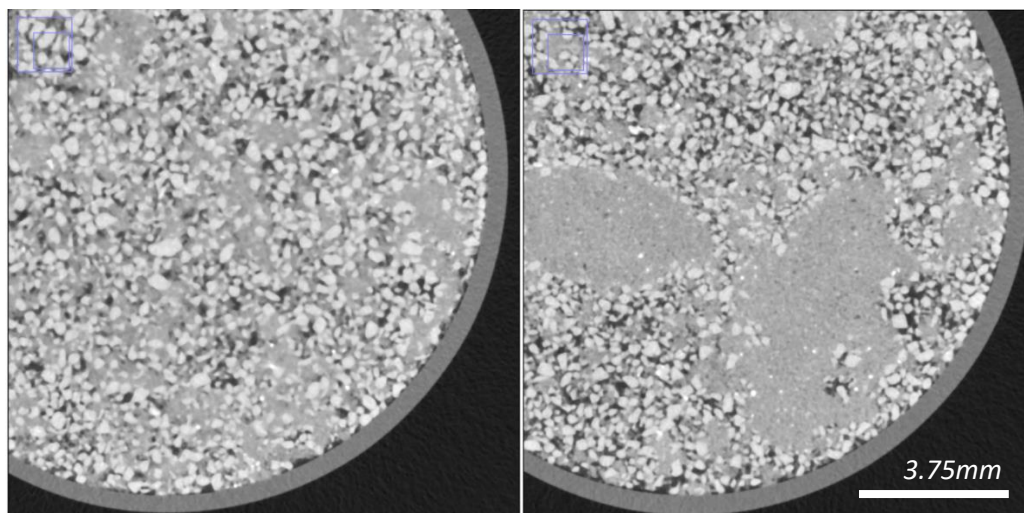


Figure 29 - MicroCT scans of untreated sand-bentonite (BC30) samples, compacted to dry densities of $1.57\text{g}/\text{cm}^3$. Left: Samples prepared at OMC with DI water. Right: Samples prepared at OMC with 0.5M GndHCl.

Therefore the sample preparation with demineralized water, at the two bentonite contents and compactions, yields satisfactory specimens upon which to execute the testing program.

3.4.1.3 Summary

The current chapter tests a methodology to prepare the sand-bentonite specimens. This is done by hydrating soils with varying fluids and compacting cylindrical specimens, aiming to produce a homogeneous porous medium.

The proposed literature characterization and methodology, using demineralized water, yield homogeneous and sand-bentonite samples. The cylindrical specimen preparation is simple and reproducible for any volume. Doing so reduces experimental error linked to the artificial soil role as a control variable.

3.5 Testing Program

Bio2Cementation seeks to ambitiously bio-cement and strengthen clayey soils. In view of engineering applications, such as in-situ chemical grouting, the treatments are injected into the sand-bentonite porous medium. To do so, an injection cell is created, capable of withstanding high pressures and accommodating samples of different sizes. Once created, the treatments effect upon sand-bentonite samples is researched by performing hydraulic conductivity measurements, strength tests, and microstructural analyses (Figure 30).

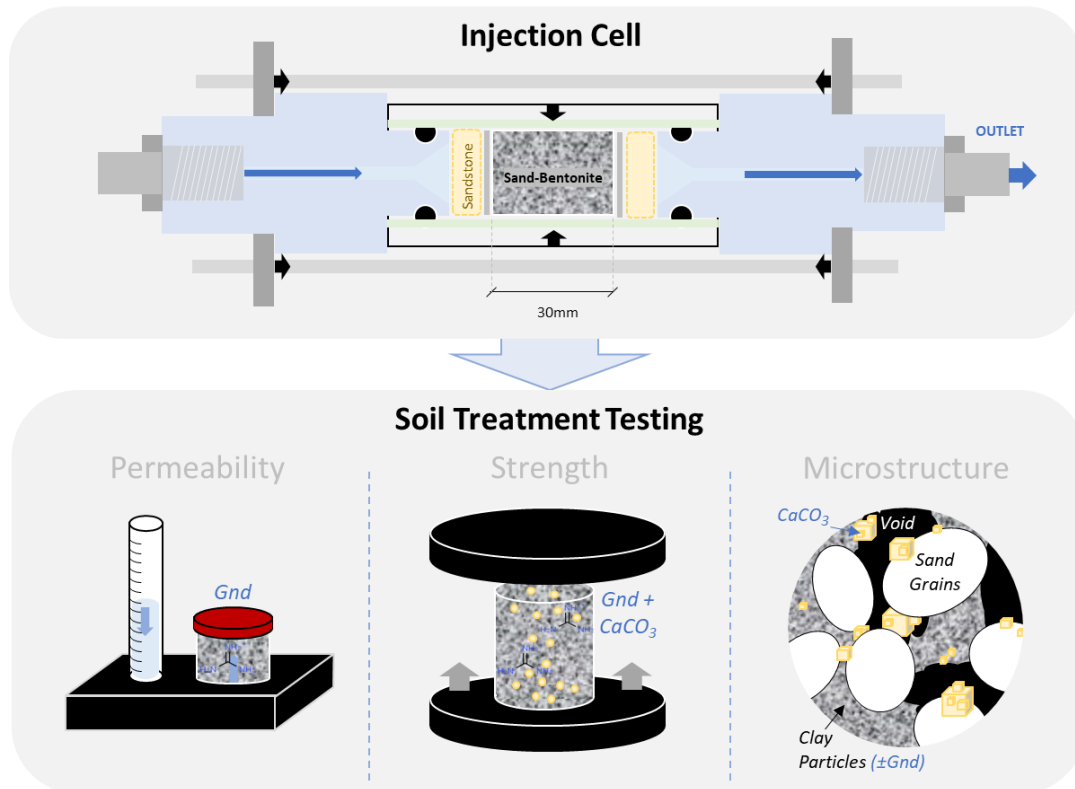


Figure 30 - Testing program of *Bio2Cementation*, whereby samples are suitable for injection treatments clay inhibition and bio-cementation.

3.5.1 Injection Cell

This section addresses the concrete implications of designing and building a cell capable of injecting the treatments in soil samples of different bentonite content, compaction and size. The design must withstand high pressures and swelling of smectite clays.

3.5.1.1 Target Properties

The injection cell is envisioned to successfully reproduce comparable high pressure treatments, while minimize experimental error during sample extraction. This ensures a credible comparative analysis of the treatment's results. To ensure this, abundant time was devoted in the laboratory to create a cell which matches the following target properties:

Target Properties:

- ✓ Two cylindrical flow cell sizes (D15mm and D30mm, 2:1 length to diameter ratio)
- ✓ Minimize the time between EICP solution preparation and injection
- ✓ Simultaneous injection in all four soils (optimization due to the long treatment curing times)

- ✓ No cementation or disruption of pumps and tubing, ensuring subsequent injections
- ✓ Insight on flow regime during the injection
- ✓ No swelling of samples (vertical, horizontal constrain)
- ✓ No preferential flow, no leakage
- ✓ Extraction of cylindrical specimens for destructive testing (eSEM and UCS)

The cell was iteratively constructed, analyzed for suitability, and reproduced until a satisfactory setup was reached. The process can be visualized in the annexed images of 8.5.4 Flow Cell Iterative Design.

3.5.1.2 Resulting Design

The flow through cell maintains a 15mm for optimal Micro-CT resolution and a 30mm diameter for UCS standard specimens as per ASTM-2166 (2016). The column height is two times the diameter, is sealed by a rubber O-ring, filter, and 5mm sandstone disk. The latter two prevent loss of fines and equalize the pressure gradient at the solution-soil interface due to the order of magnitude larger permeability (Figure 31).

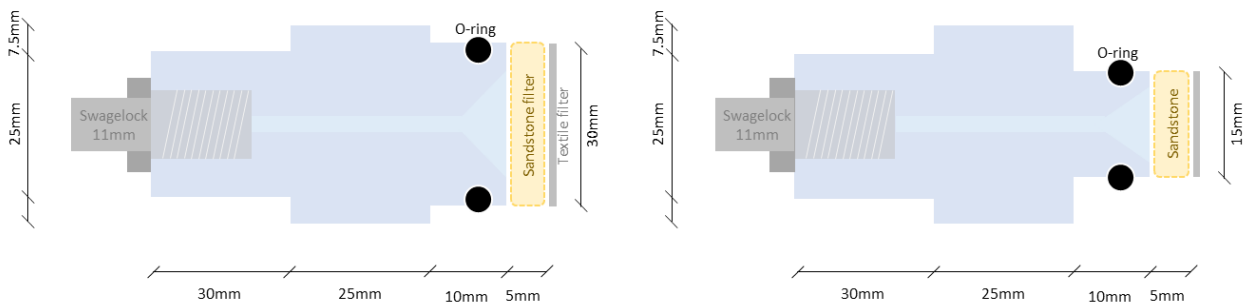


Figure 31 - Machined inlet dimensions (DEMO Lab, EEMCS). On the left the large D30mm inlet, and on the right the smaller D15mm. The cylindrical soil samples are twice the diameter in length, such that the cell height is 60mm and 30mm respectively.

Prior to testing, the soil specimens are compacted and prepared in accordance with annex 8.5.3 Method: Soil Sample Preparation. Finally, the complete injection cell successfully meets the target properties (Figure 32). It is designed to confine the sand-bentonite samples, while still allowing for a rapid extraction of specimens.

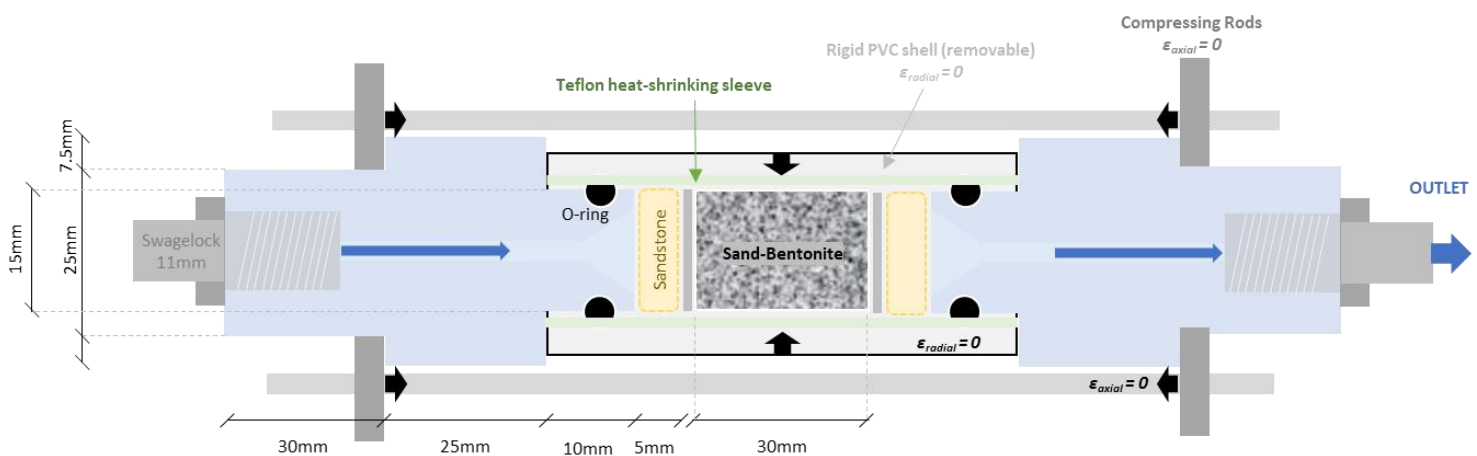
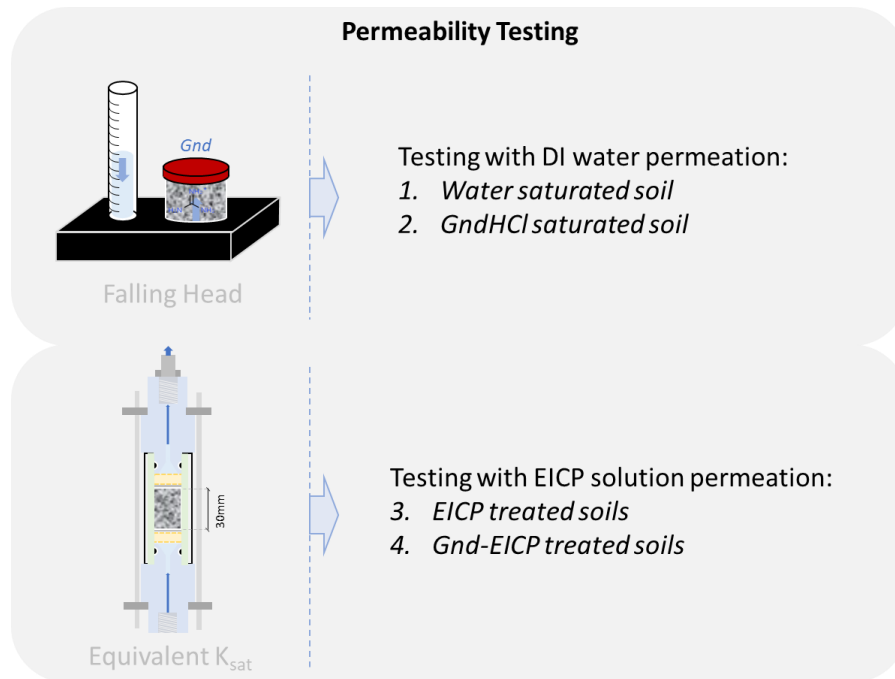


Figure 32 – The finalized injection cell for cylindrical soil samples of either 30mm or 15mm (pictured) diameter. Sand-bentonite soil samples are confined to impede axial and radial strain. The rigid shrink sleeve can be vertically cut with a razor, the PVC shell is slotted lengthwise for easy removal, and the compression rods are readily unscrewed.

3.5.2 Permeability Test

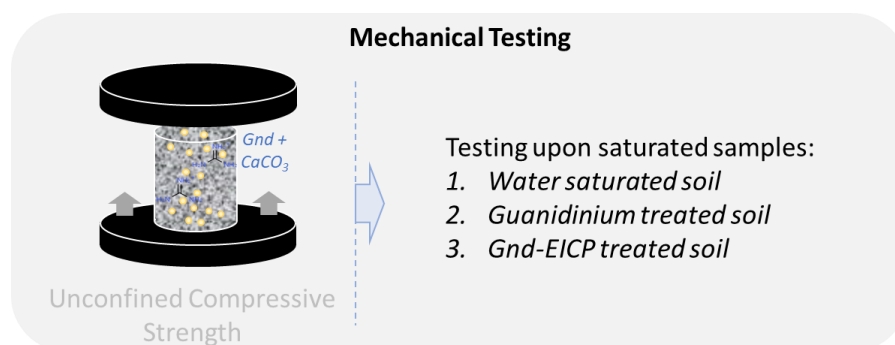
The hydraulic conductivity research quantifies the impact of the various treatments on porous flow regime. Two apparatuses are utilized: a falling head permeameter and a back calculation of equivalent permeability of the saturated injection cells. The detailed testing is organized as follows:



The tests provide quantitative data of flow modification and permeability enhancement during the falling head permeameter experiments, followed by the flow rate reduction by bio-cementation treatments.

3.5.3 Mechanical Test

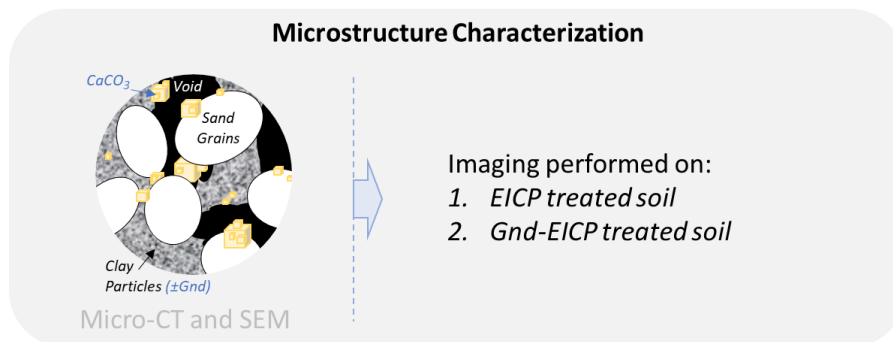
Strength experiments are a central pillar in the scope of the thesis. In conjunction the previous section, the mechanical testing provides data on the response of the sand-bentonite matrix to clay inhibition and bio-cementation:



Samples' saturation is maintained constant to minimize suction effects of partially saturated clayey soils. This is achieved by rapid extraction from the injection cell.

3.5.4 Microstructure Characterization

Microstructural characterization is achieved by two imaging techniques: micro-computer tomography scans (Micro-CT) and scanning electron microscope images (SEM):



The techniques provide complimentary data. The lower resolution Micro-CT provides three-dimensional scans of the entire soil samples, whereas SEM images provide extremely detailed but local insight on the micron-scale mineralogical features.

3.6 Summary

The materials and methods used in bio-cementation and clay inhibition treatments are summarized in this chapter. Test tube experiments concluded that EICP is optimized for the highest yield at low concentration, with solutions of 0.5[mol/L] calcium chloride to 0.75[mol/L] urea (urease enzyme activity of 3[U/mg] and 8[U/mg]). Guanidinium solution of 0.5[mol/L] are stable over time, and are found to not hamper, but even to improve the yield of EICP when diluting bio-cementation solutions at less than 0.25[mol/L]. The sand-bentonite sample preparation is verified as being simple and successful, consistently reproducing homogeneous cylindrical specimens. Finally, the chapter concludes by describing the testing program of *Bio2Cementation* in the porous media; hydraulic conductivity analyses, mechanical testing and microstructural characterization.

Results and Data Interpretation

4.1 Permeability Testing

Sand bentonite mixtures in impermeable liner research aim to reproducibly measure the hydraulic conductivity of sand-bentonite mixtures. Most commonly, the permeameters utilize rigid wall molds compacted at optimum moisture and maximum dry density (Ameta and Wayal, 2008; Osmanlioglu, 2016). Waste disposal research has shown bentonite to dominate the soil-fabric above bentonite contents (BC) contents of 15% by clogging preferential flow paths in between coarse grains (Biju and Arnepalli, 2020). These soil mixtures have coefficients of permeability ranging from $1e-7$ to $1e-10$ [m/s] (Osmanlioglu, 2016; Proia *et al.*, 2016). Additionally, the branch has researched the risk of increase of flow rates induced by clay aggregating polymers and electrolytes (Biju and Arnepalli, 2020). Other studies, seeking to inhibit clay swelling and increase chemical delivery, have tested hydraulic conductivity modification by salt solutions. For example, Minder *et al.* (2016) tested guanidine clay inhibition by comparing water saturated and aggregated soils, noting an order of magnitude faster flow in the guanidine treated matrix.

To explore the *Bio2Cementation* treatment's technique modification of slow in clayey soils, permeability testing is carried out in two apparatuses. Firstly, direct permeability measurements are performed using a KSat apparatus on water and guanidinium saturated samples. Secondly, an apparent hydraulic conductivity of injection cell samples is estimated from the barometer readings. The experimental dataset provides the basis to answer the following research sub-questions:

2. "How does GndHCl improve the permeability and increase flow through potential of bentonite-sand soils? What role does it play in subsequent EICP injections?"

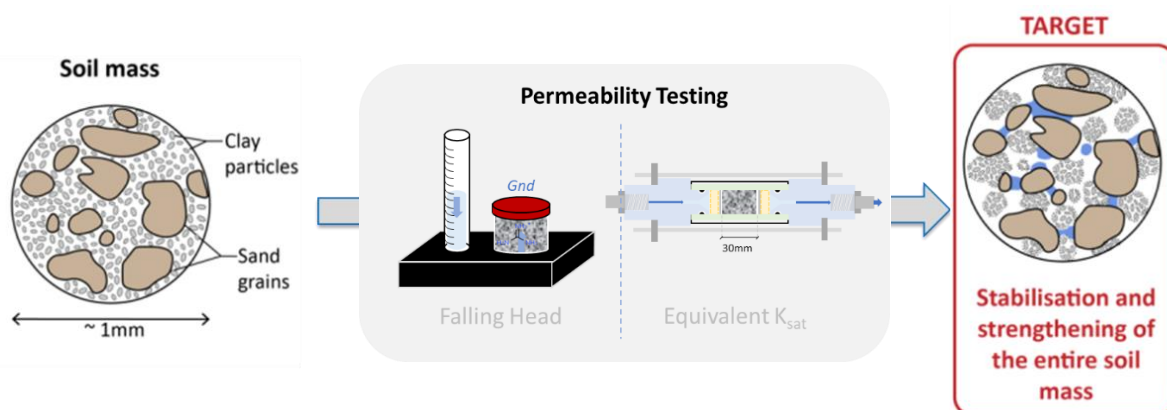


Figure 33 - The schematized process of researching the modification of sand-bentonite hydraulic conductivity by clay inhibition and bio-cementation treatments; experimentally researching the third research sub-question of the thesis.

4.1.1 KSat Falling Head Test

Hydraulic conductivity defines the soils' ability for fluids, and thus treatment solutions, to permeate the porous medium in a timely manner. For this reason, this section aims to quantify the flow rates in untreated and guanidinium enhanced sand-bentonite fabric. Additionally, as a secondary scope, the swelling inhibition by guanidine saturation is tested during the sample hydration. These are key in establishing guanidinium hydrochloride's success as an irreversible flocculant; seeking stabilization and enhanced flow in 10-30% bentonite specimens.

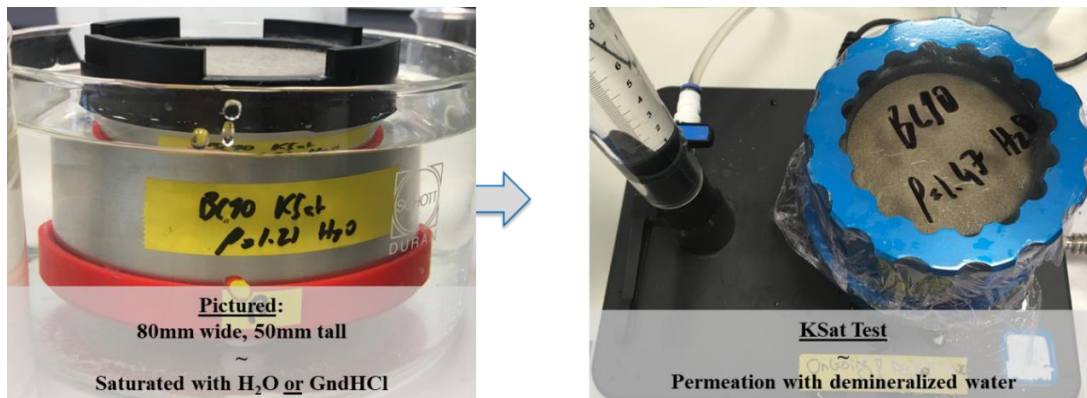


Figure 34 - KSat sample preparation before placing the 65kPa overburden (left), and a sealed falling head permeation test (right). The complete procedure is detailed in annex 8.5.6..

4.1.1.1 Results and Data Interpretation

The sample saturation takes considerable time in the highly impermeable soils, ranging from four to ten days of preparation per data point. Most samples saturated successfully, when confined by an overburden of 65[kN]. The sole failed sample preparation was the water saturated densest and highest bentonite content sample (Figure 34, BC30 $\rho_{dry}=1.57g/cm^3$). The swelling pressures led to the separation of the sample and filter plate (red), inducing preferential flow and unsuitable results. This specimen shows the limits of the KSat apparatus, whereby saturation procedure and apparatus hardware (filter plates bulging) struggle to cope with the high swelling potential of near optimally compacted 30% bentonite.

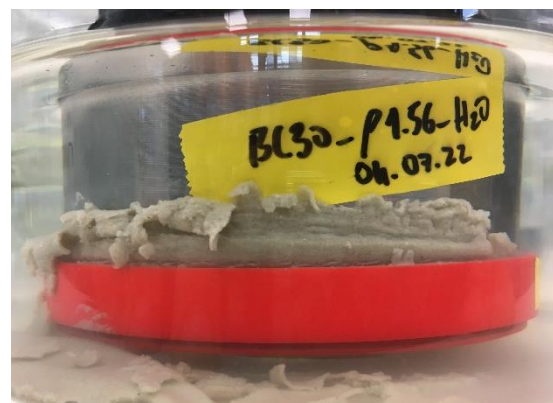


Figure 35 - Failed water saturation due to excessive swelling for the dense BC30 sample, leading to vertical strains beyond the accepted limit of $\epsilon_v = 0.4\%$ according to ASTM D5084-61a (2016).

The area normalized flow rate through the sand-bentonite is calculated from falling head levels. A capillary tube (small cross-sectional area) was used in the water saturated, slowest flowing samples. All other tests were sufficiently sensitive to the normal falling head KSat apparatus using the standard burette. This distinction was reached by trial and error. Using demineralized water (DI) as a constant permeation fluid, the falling head permeameter results are shown in Figure 36. Additional data points show existing data which is directly comparable literature; one using commercial swelling clays in the same sand-bentonite proportion. Impermeable liner research samples are prepared at

maximum dry density, whereas this study investigates treatment efficiency also as a function of packing density. Minder *et al.* (2016) provides the only data on guanidinium hydrochloride (Figure 36, green prisms).

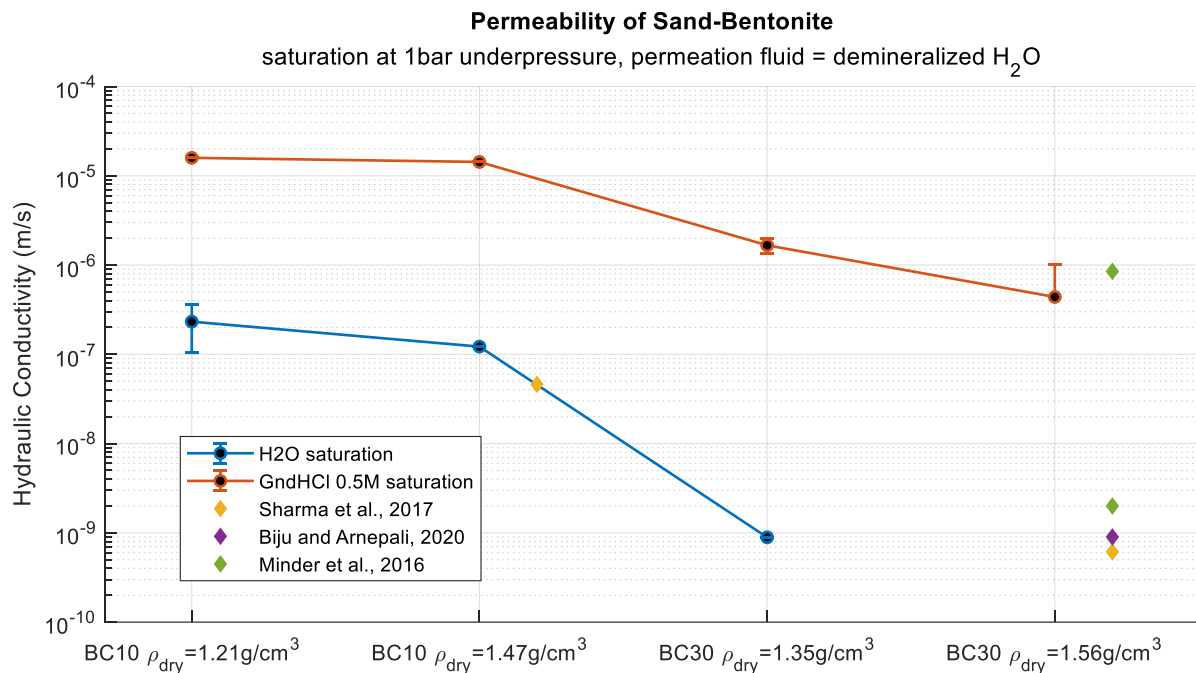


Figure 36 - Permeability of sand-bentonite mixtures, measured with the KSat apparatus. Two saturation solutions are tested: demineralized water (blue) and guanidinium hydrochloride (dark orange). Measurement errors are displayed as one standard deviation over three tests.

Water saturated samples of display hydraulic conductivities ranging approximately between 1e-7 to 1e-9 [m/s]. As expected, the fine fraction dominates the flow response, whereby BC30 flows two orders of magnitude slower than BC10. This concurs with existing literature review. Water saturated BC30 is considered almost impermeable, even at a looser compaction state. However, treating the soil by saturating specimens with guanidinium leads to striking modification of the soil matrix. Swelling is reduced significantly; all samples are prepared successfully. Additionally, constant increase in flow rates are recorded for the inhibited clayey soils. The diffused guanidinium ions increase hydraulic conductivity by one-and-a-half orders of magnitude BC10 and three orders of magnitude in BC30. The effect is notable; the modified dense BC30 specimen flows faster than the loosest water saturated BC10 sample.

The individual permeability back calculations of each run yielded an R² fit of greater than 98%. The accuracy of the sample preparation and tests are verified by two additional runs for three samples. In Figure 36, all error bars indicate a maximum variability of five times the mean over a 64% confidence interval ($\pm 1\sigma$ assuming a gaussian distribution around the mean). Small errors are assumed to arise in two instances: during the soil preparation and during the experiment. The former may include slight inhomogeneous five layer tamping, varying saturation times, etc. The latter regards random experimental error. Soil de-saturation during the mounting of samples is unlikely, due to extremely proximal transport and very large water retention of sand-bentonite. However, the fast-flowing filter plate may have partially drained as it's placed in the KSat, introducing minimal gas bubbles and suction forces. To counteract this, the tests were run over a duration of ten minutes.

4.1.1.2 *Summary*

Guanidinium is successful in stabilizing the bentonite swelling at low vertical confining pressure. The soil matrix undergoes notable modifications to the flow regime, whereby both the 10 and 30% bentonite soils flow orders of magnitude faster than untreated samples. Guanidinium hydrochloride treatments at 0.5[mol/L] efficiently targets the clay fraction, undoubtedly increasing coarse porosity in the matrix significantly. This can be as seen by the larger relative increase in hydraulic conductivity of the inhibited 30% bentonite soil, in comparison to the 10% one.

In this study, the guanidinium treatment solution is therefore verified as extremely suitable in inhibiting clay swelling and increasing the hydraulic conductivity. It is expected that the clay inhibition and opening the pore structure reduces the resistance to cementation solution injections in subsequent treatments. Future research may optimize guanidine's concentration in function of bentonite content. More specifically, lower concentrations of the clay inhibitor could achieve the modification of 10% sand-bentonite specimens.

4.1.2 Barometer Equivalent Hydraulic Conductivity

Barometers provide live monitoring of injected samples, while simultaneously quantifying the saturated flow in the cylindrical specimens. In this regard, this section analyzes the flow regime of EICP and Gnd-EICP treated soils for each subsequent injection. Firstly, the procedural approach and Darcy's Law is introduced. Secondly, the results are discussed. By doing so, the section aims to compare the effect of bentonite stabilization as well as carbonate precipitation on saturated flow in the sand-bentonite matrix.

4.1.2.1 Design

The flow cells are connected by a T-shaped junction to the barometer cells; measuring the relative pressure increase (Figure 37). Purging in between injections ensures an absence of air bubbles or crystals, ergo the flow between the syringe and base of the flow cell is assumed to be an incompressible closed system.

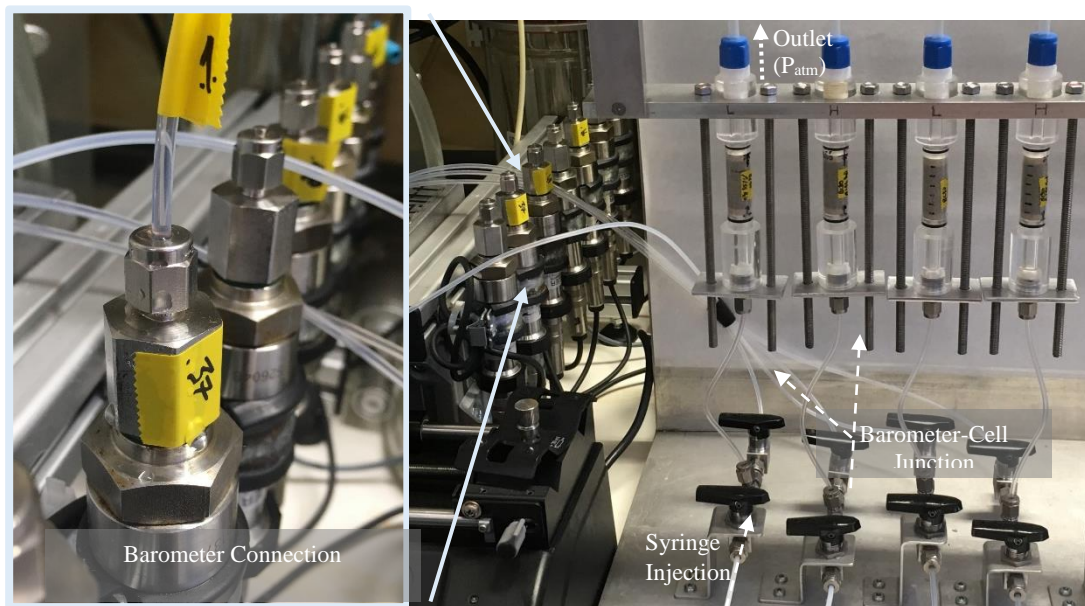


Figure 37 - Incompressible closed system between the syringe injection port, the barometer and the flow cell (here D15mm samples). The only decompression occurs at the flow cell outlet (blue cap).

The pressure sensors are used to monitor the transition from unsaturated to saturated flow; steady state pressures occur at soil saturation for a given injection rate. Additionally, knowing the relative pressure gradient between the barometer and atmospheric pressure (ΔP) across the cylindrical soil sample, an equivalent hydraulic conductivity can be calculated as per Darcy's law. Additionally, as the falling head permeameter readings are corrected for the increased viscosity of the percolation fluid in this experiment. The considerations and assumptions made are listed herein:

1. Constants: Length = 40[mm] including filter plates, Diameter = 15[mm], Total discharge (Q) = 0.3 [mL/min]
2. Measurements: Dynamic viscosity of the EICP treatment solution (μ_{EICP})
3. Assumptions: In a layered injection cell with perpendicular flow, the limiting hydraulic conductivity dominates the total hydraulic conductivity. Flow in the injection tubes is orders of magnitude faster than through the soil, ergo the pressure gradient is attributed to the soil and filter plates only.

$$k = Q * \frac{\mu L}{A \Delta P} \quad \text{and} \quad k_{KSat,corr} = k_{KSat} * \left(\frac{\mu_{EICP}}{\mu_{water}} \right)$$

4.1.2.2 Results and Data Interpretation

Prior to calculating the hydraulic conductivity in the cell by Darcy's law, rheometer tests are performed to quantify the dynamic viscosity of the EICP solution (Figure 38). Two tests are performed: a sweep through varying shear rates to account for the unknown shear forces during injection, and a time dependent viscosity measurement with the urease enzyme actively precipitating calcite crystals.

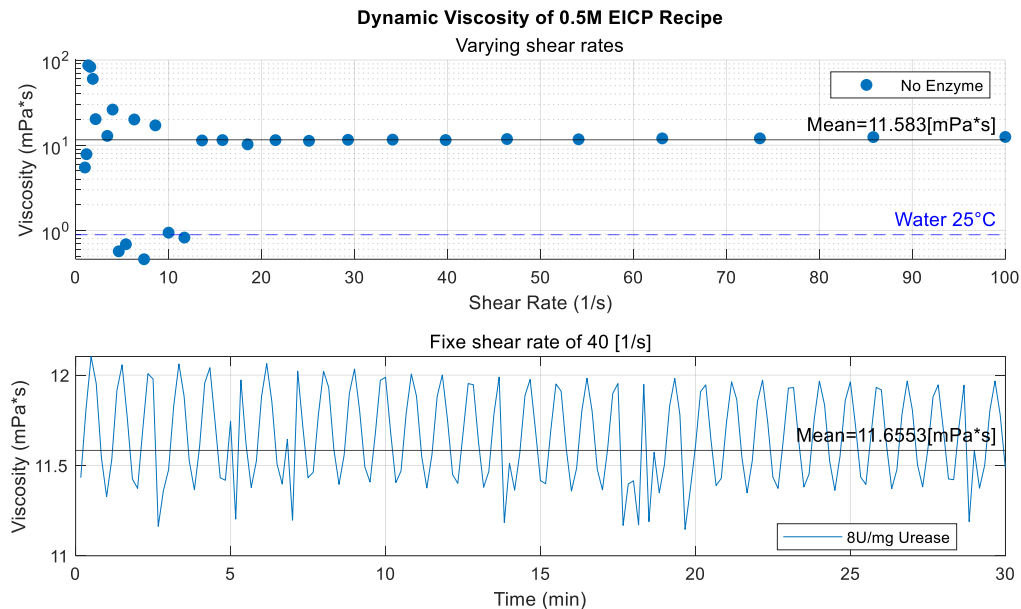


Figure 38 - Dynamic viscosity of the EICP 0.5M treatment solution. Enzyme activity shows little time dependency of the solutions' viscosity.

The EICP solution contains an abundance of dissolved reagents, which characterizes the solution by a ten time more viscous flow than water. This is constant for all shear-rates. Measurement error noise of poorly viscous specimens sheared at low rates is ignored in this work (less than $10[s^{-1}]$). Additionally, precipitating calcite leads to a very slight decrease in viscosity, which is considered negligible for the purpose of this application.

The proof of concept behind the dual treatment hypothesis states that the sand-bentonite must be targeted separately in two phases, and that the joint treatment yields to improved soil properties. To address the concept of complementing treatments, two tests are recorded: firstly, the artificial soils are treated exclusively using EICP. Secondly, specimens are subjected to a Guanidinium hydrochloride injection and pure water flushing prior to the EICP treatment. In this subsection, indirect quantitative insight on the soil matrix's absolute pressure gradient is recorded by barometers. Thirty percent bentonite barometer readings are shown in Figure 40, and ten percent bentonite content in Figure 39. Saturated pressure gradients are assumed to occur during the pressure plateau after 2-4 minutes of injection (Figure 38 and Figure 39). The delay increases for subsequent injections; most notably for the third injection of BC30.

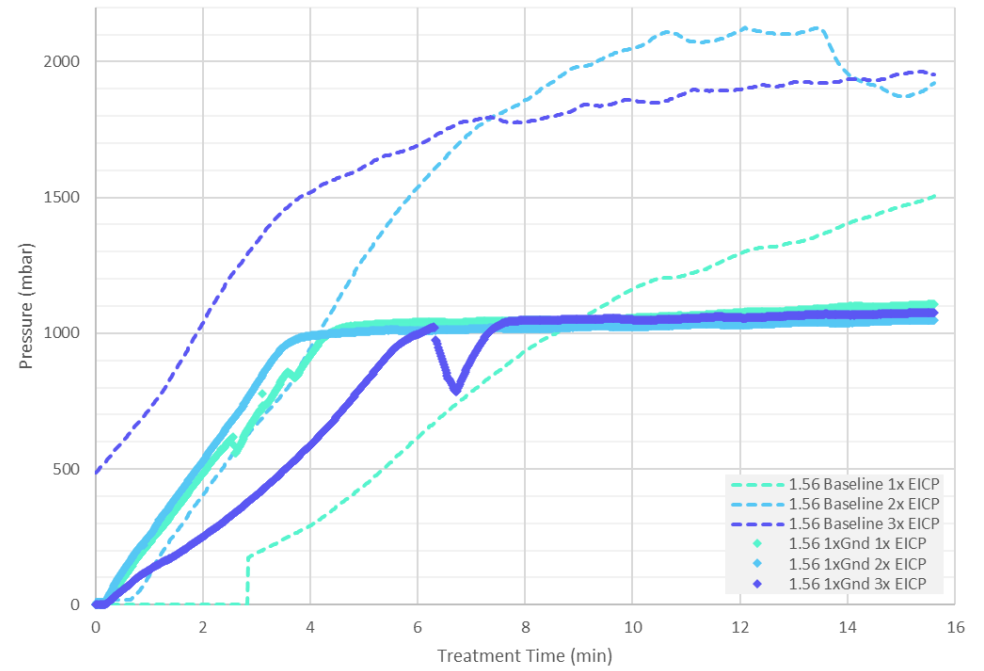
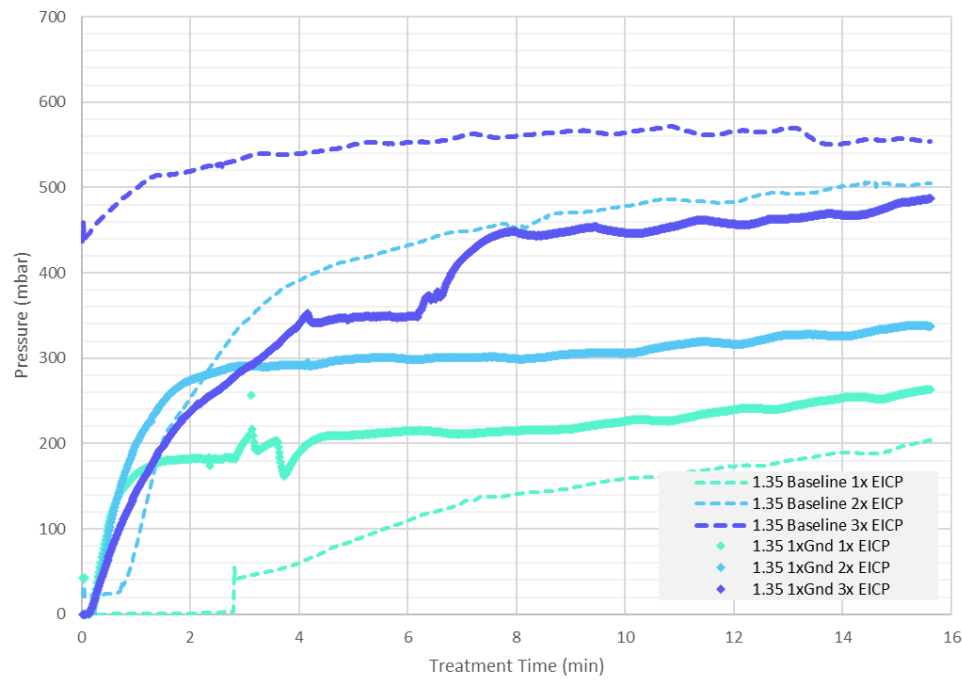


Figure 40 - Treatment injection barometer readings for soil BC30. The baseline EICP treatment (dotted lines) and guanidinium enhanced EICP treatments (full circles) are shown for two dry densities.

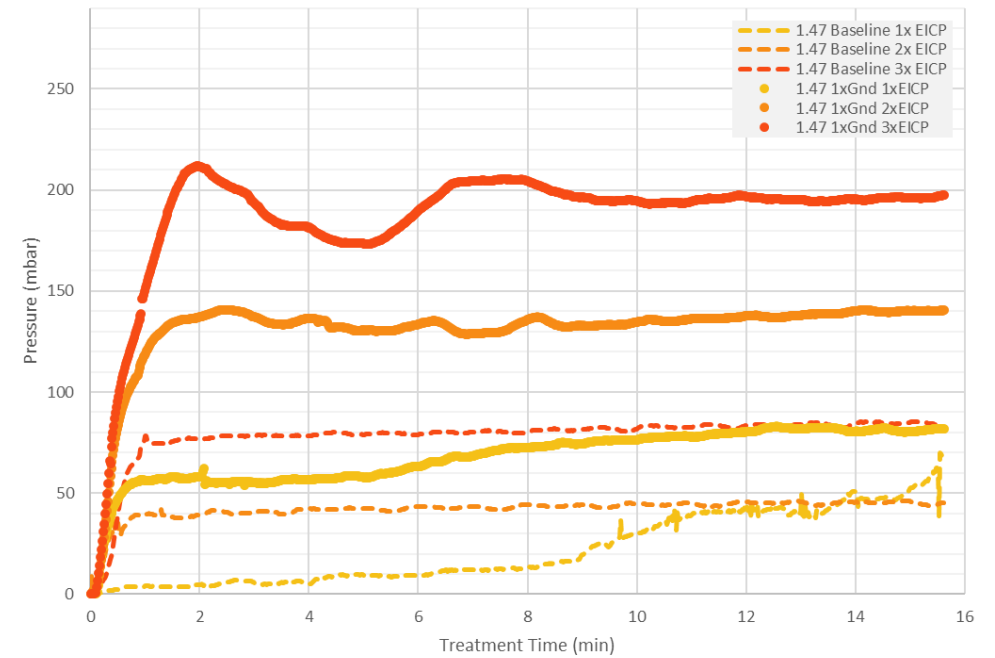
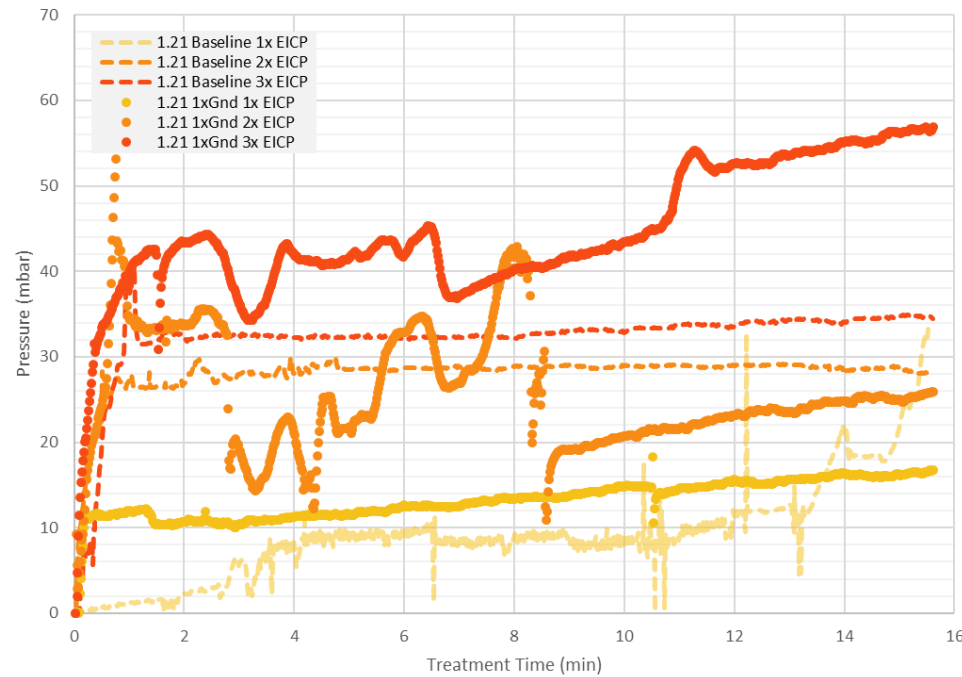


Figure 39 - Treatment injection barometer readings for soil BC10. The baseline EICP treatment (dotted lines) and guanidinium enhanced EICP treatments (full circles) are shown for two dry densities.

Baseline sample swelling is expected to occur in the 24-48[h] following saturation (Sharma *et al.*, 2017), which can be seen by the relatively low pressures measured during the 1st Baseline injection versus the following ones. Contrarily guanidine treated samples are already saturated for the 1st EICP injection (Figure 40 and Figure 39). This dichotomy is most notable in higher bentonite content samples, whereby the clay dominates the soil matrix response. Contrarily, 10% bentonite specimen swelling (Figure 39 – Baseline 1-2xEICP) yield pressures only between 50-100mbar. Additionally, injections in loose sand-bentonite (Figure 39 - left) records pressure variations under constant flow rates, akin to changing preferential flow evolving over the injection period (Di Maio *et al.*, 2004). Guanidine affects BC10 and BC30 drastically. Pre-treated specimens show near constant increase in barometer readings with subsequent EICP treatments and curing times. Notably, 10% bentonite samples yield drastically increased pressures compared to the baseline (no Gnd). This is most visible by a two-and-a-half times larger cell pressure gradient in $\rho_{1.47}$ [g/cm³] (Figure 39 – right, red lines). Although marred by greater variability, final readings of the loose BC10 also display near two-times pressure increase (Figure 39 – left, red lines). The un-stabilized 30% bentonite samples record consistently greater cell pressures (Figure 40 – dotted line > solid line). The residual pressure from prior injections is minimal in Gnd-EICP injections (Figure 40). Interestingly, the third injection during BC30 Gnd-EICP treatments records an evident longer time required to reach steady state (Figure 40 – dark blue solid line).

Finally, the knowledge gained on the viscosity of treatments (Figure 38), the fixed cell dimensions, and relative pressure gradients (Figure 40 and Figure 39) are used to calculate an apparent hydraulic conductivity for each injection (Figure 41 - right). Additionally, the falling head hydraulic conductivity results performed with water permeation, are adapted to EICP's solution viscosity at 25[°C] (Figure 41 - left).

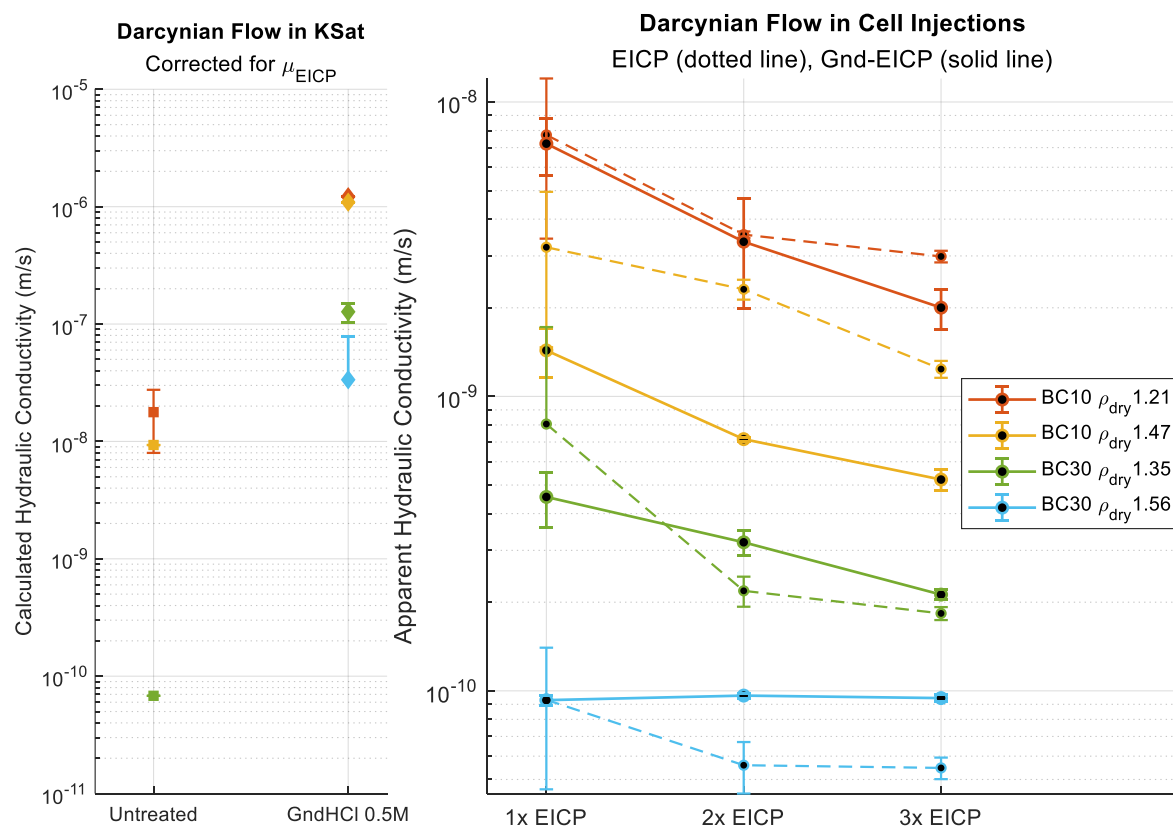


Figure 41 - Apparent hydraulic conductivity derived for KSat measurements as $k_{KSat} * \frac{\mu_{EICP}}{\mu_{water}}$ (left) and barometer readings in the D15mm flow through cell (right). In the latter, both soils are treated using EICP only (dotted) and the complete Gnd-

EICP treatment (solid). Flow rates of cemented samples decrease by two orders of magnitude. Nonetheless, the GndHCl effect is sufficient for the final flow rates to be one order faster than water saturated soils.

Table 5 - Reduction in flow cell hydraulic conductivity for guanidine stabilized sand-bentonite. The relative reduction of K_{sat} is calculated between the 1st-2nd and the 2nd-3rd EICP injection (Figure 41 - right).

Gnd-EICP Treatments	K_{sat} Reduction (EICP 1 to 2)	K_{sat} Reduction (EICP 2 to 3)	Average
BC10 1.21	-53.6%	-40.3%	-45.5%
BC10 1.47	-50.1%	-27.1%	-38.6%
BC30 1.35	-29.9%	-33.6%	-31.8%
BC30 1.56	-3.6%	-1.9%	-2.8%

Injections of EICP only (dotted lines), show a large drop in hydraulic conductivity following saturation of the sand-bentonite by 1st Baseline EICP injection. Additionally, for this first injection, the permeability range reaches one order of magnitude (error bar). Subsequent injections, shown by 2x EICP and 3x EICP datapoints, are less influential in reducing flow rates in the medium.

Differently, guanidine pre-treated specimens (solid line) yield consistently log-linear reductions in hydraulic conductivity. The most efficient reduction is found in the first three specimens (Table 5); additionally coupled to lower data range during all treatments (error bar). Ten percent bentonite is extremely sensitive to 1st-2nd EICP injections, as shown by 50% slower flow. Conversely, loose thirty percent bentonite injections ($\rho=1.35 \text{ g/cm}^3$) yield constant permeability reductions of 30%. Contrarily, the densest BC30 sample retains near constant flow rates throughout, while remaining stable post guanidine injection and curing.

Finally, the falling head tests delimit the range of hydraulic conductivity calculations (Figure 41 - left). In fact, the slow flowing bound is defined by water saturated K_{sat} samples (*Untreated*), whereas the upper bound of fast flow is the guanidine saturated K_{sat} tests (*GndHCl 0.5M*). All flow cell injection permeability values (Figure 41 – right) are elements included inside that range. In comparison to the permeability maxima, EICP injections of all soils lead to consistently 2-2.5 orders of magnitude slower flow. Interestingly however, the values of combined treatments still remain 0.5-1 order of magnitude faster flowing than the water saturated falling head tests.

4.1.2.3 Summary

Increasing the bentonite content (BC30 versus BC10) results in higher pressure gradients across the cell. The barometer data concurs with Biju and Arnepli's (2020) measured 15% threshold sand-bentonite content; bio-cementation without guanidine leads to a dominant swelling responses of 30% bentonite and additional injections yield little modifications of the flow field. This finding matches the existing impermeable liner research, which prepares 30% sand-bentonite at optimum compaction (Proia *et al.*, 2016). Excessive swelling, poor connectivity and charged surface interaction hamper bio-cementation in this matrix. The latter has fully impeded calcite nucleation in un-stabilized clay soils (Cardoso *et al.*, 2018).

However as hypothesized, guanidine pre-treatments lead to log-linear reductions of hydraulic conductivity following subsequent EICP injections (Figure 41) in all 10% and the looser 30% bentonite specimen. Such feature is indicative of successful calcite precipitation, greater nucleation and pore throat clogging. Cladding carbonate crystals are expected to increase tortuosity and reduce inter-void connectivity. Ergo, the barometer data supports the theory of clay aggregation and improved bio-cementation in neutralized charged surfaces by *Bio2Cementation*. Guanidine improves EICP performance in sand-bentonite mixes.

4.2 Strength Testing

Guanidinium hydrochloride has been shown to increase the shear strength, internal friction angles and compression coefficients of sand-bentonite mixtures (Minder *et al.*, 2017). Bio-cementation forming bridging calcite bonds between grains, has been shown to increase sand cohesion, strength and stiffness (Cheng *et al.*, 2019). To explore the combined effect of *Bio2Cementation* on the strength of sand-bentonite, cylindrical soil samples were subjected to unconfined compressive strength (UCS) tests. Soils were tested in three states: water saturated, treated by guanidinium hydrochloride, and finally the coupled Gnd-EICP technique. The experimental dataset provides the basis to explore the following research sub-question:

3. “How are the strength characteristics of a sand-bentonite altered using water saturated soils, GndHCl alone, or EICP-GndCl coupled treatment solutions?”

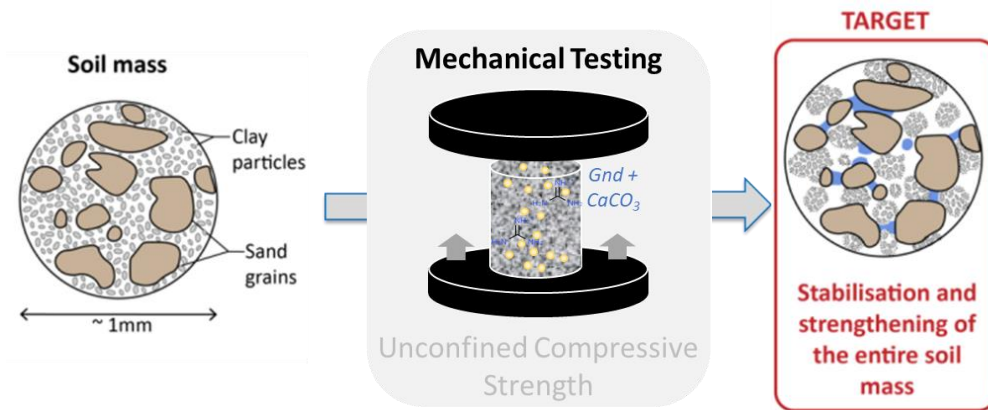


Figure 42 - The schematized process of researching the mechanical modification of sand-bentonite media by clay inhibition and bio-cementation treatments; experimentally researching the fourth research sub-question of the thesis.

4.2.1 Unconfined Compressive Strength Test

The samples are saturated and treated in 30mm wide injection cells, using EICP recipes catalyzed by the vigorous *Canavalia Ensiformis* urease at 1[g/L]. To allow a comparative base between all soils, the tests are performed in saturated conditions to minimize suction effects. Samples are extracted just prior to testing by slitting the Teflon sleeves vertically with a razor. Thereafter, the UCS tests are performed according to ASTM standard D2166, by loading the specimens at fixed strain rates of 0.3[mm/min].

4.2.1.1 Results and Data Interpretation

Four soils are loaded in saturated conditions using DI water, EICP treatments or coupled Gnd-EICP treatments. Failed samples are visualized in Figure 43 and annex 8.8.2, marked as the moment of peak compressive strength recorded by the apparatus. The continuous load-displacement data is used to calculate the representative UCS stress-strain response (Figure 44), upon which the secant moduli (E₅₀) are calculated as a measures of elasticity. These are defined as the secant-slope's inverse, taken at half the peak strength or 3[%] axial strain. Finally, a comparative analysis of the three treatments' effect on specimen strength is displayed in Figure 45.





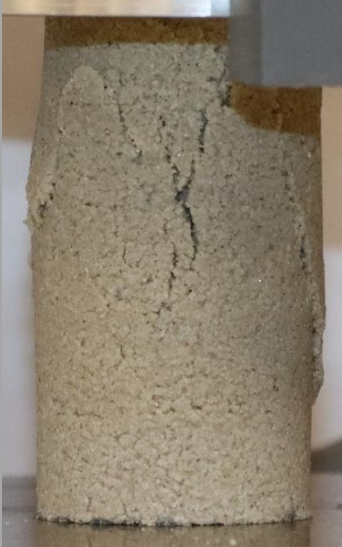

<i>Treatment Type</i> →	Water Saturated	Guanidinium Hydrochloride	Bio2Cementation
<p>10% Bentonite 80% compaction ρ_{dry} 1.21 [g/cm³]</p>			
<p>10% Bentonite 95% compaction ρ_{dry} 1.47 [g/cm³]</p>			

Figure 43 - Unconfined compressive test peak load, indicating increasingly stiff (left to right) failure mechanisms of 10% bentonite specimens.

Guanidine yields visibly aggregated structure to the soil specimens, with decreased distributed fine pores in the matrix. The evolution of failure mechanisms stems from plastic strain and bulging of water saturated specimens, to increasingly stiff fracturing failure in unconfined guanidine and samples (Figure 43, Figure 44). Guanidine modifies the failure mechanism considerably, whereby sand-bentonite displays radial fracturing of cohesive flakes. Coupled Gnd-EICP treatments display similar deformation features, while further reducing the radial bulging in the failure zone's vicinity. Additionally, bio-cemented soils fail farther from the treatment inlet, potentially indicating inhomogeneous calcite precipitation throughout the soil cylinder. In fact, EICP in sands has found UCS to be governed by EICP heterogeneity, whereby failure planes are favored through the weakest zones of low calcium carbonate content (Ma *et al.*, 2021). Water saturated specimens of 30% bentonite soils failed to saturate due to the formation of preferential flow paths and low hydraulic conductivity.

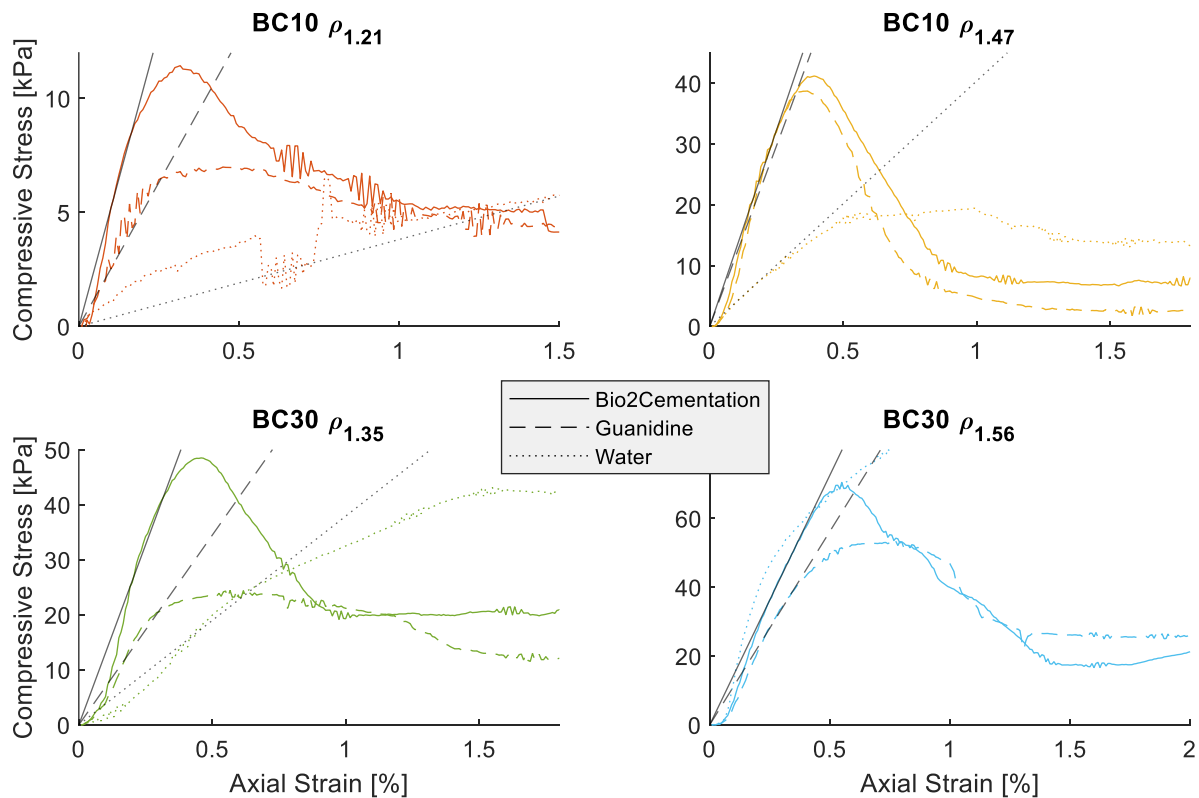


Figure 44 - Strength characteristics of treated samples, for 10% bentonite soils (top) and 30% bentonite soils (bottom). The samples are prepared at two compactions, as shown by their dry density in the sub-plot titles. Secant moduli are shown by the black linear fit.

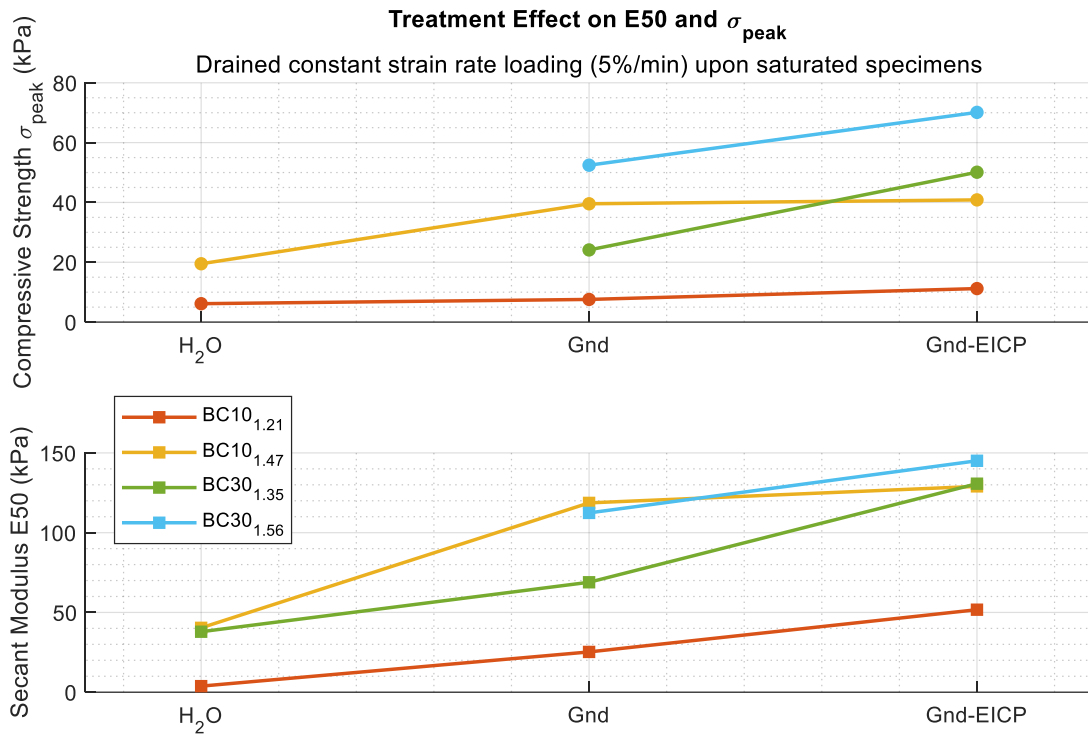


Figure 45 - Specific evolution of peak strength and E50 modulus for the UCS tests. Only successfully saturated samples are shown (exempt in this figure: water saturated 30% bentonite).

The stress-strain behaviour of saturated specimens records improved peak strength and stiffness by *Bio2Cementation* (Figure 45). Part of the strength gains are attributed to guanidine alone, which by aggregating the clayey matrix, increases peak strength and stiffness notably in 10% bentonite and looser 30% bentonite samples. Guanidine's effect in 10% specimens increases peak compressive strength, albeit reducing the residual strength at increased axial strain. The inhibited clayey samples display extremely stiff responses. Failure occurs at significantly reduced axial strains that water saturated samples, resulting in a greater secant modulus (E50). Thereafter, bio-cementation cumulates the effect modifying the soil matrix towards even stiffer and stronger soils. Notably, the peak strength increases, and radial strain at failure decreases (E50 increases). Additionally, the residual strength of EICP treated samples is improved compared to guanidine only injections.

Compaction plays a large role in the sand-bentonite loading response. Loose soil specimens are extremely responsive to bio-cementation, doubling peak strength and gaining one-to-two order magnitude stiffer E50 compared to guanidine specimens. Similar stiffness gains, are recorded in comparison to untreated loose sand-bentonite. The tested technique of *Bio2Cementation's* greatest added value in terms of strength gains occurs in less compacted soil matrices. Near optimally compacted soils are nonetheless strongly modified by guanidine, as seen by the dense 10% bentonite loading experiments.

It must be noted however that all water saturated soils, except the loose 10% bentonite, display greater residual compressive strength over large deformations ($\sigma_{residual}$) than treated samples. Additionally, the trend is exacerbated in unsaturated untreated 30% bentonite soils, whereby suction forces occurring in the bentonite's fine pores confer notable strength, even at extremely large axial strains (ϵ_{axial} greater than 3-5%). Therefore, under partial saturation, the untreated highly compacted 30% sand-bentonite soils are stronger than the tested techniques.

The physical behaviour of 10% bentonite soils is controlled by the granular constituent, which resides below the 15% limit after which the matrix is dominated by the clay fraction (Biju and Arnepali, 2020). In these specimens, the medium's strength is conferred by inter-particle friction (large friction

angle), while primarily remaining non-cohesive (Bouchemella and Taibi, 2022). For example, shear strength of sand-kaolinite is dominated by the granular phase at sand contents greater than 25% (Bouchemella and Taibi, 2022). The untreated media is subjected mainly to weak capillary cohesion in sands generated by the water meniscus between particles, resulting in weak plastic behavior (Figure 43). Unconfined loading of untreated 10% bentonite reflected the low peak strength and stiffness, whereas clay aggregation (induced by guanidine) and bio-cementation treatments resulted in increased compressive strength and stiffness (Figure 44, Figure 45). The tested treatments drastically improve the physical parameters of medium. Clay aggregation and crystal cladding is likely to improve the particle friction, while bridging calcite crystals are likely to confer cementation cohesion to 10% sand-bentonite soils. Notably, the loosely compacted soil benefits the most from EICP, whereby the weak coarse inter-grain voids provide ample room for calcite nucleation and growth. To conclude, this soil benefits greatly from *Bio2Cementation* treatment, especially if in a loosely compacted state. Alternatively, the 30% bentonite specimens display behaviors controlled by the cohesive phase. In this soil, the clay content is sufficient to fill the voids of the granular sand, conferring the medium strong cohesive forces, large plasticity, and lower shear strength (Cabalar *et al.*, 2018). The dominance of clay matrix reduces pore sizes, garnering greater cohesion than 10% bentonite mixtures. Additionally, unsaturated clayey samples are subjected to large suction forces (negative pressures), increasing capillary cohesion and thus material strength. Therefore, the UCS testing of unsaturated bentonite records stronger mechanical parameters (UCS and E50) (Bouchemella and Taibi, 2022). The tests record similar findings, with untreated 30% bentonite soils displaying extremely strong plastic behavior over large strains (Figure 44). Whereas, *Bio2Cementation* treatments aggregated the clay matrix and were successfully saturated, reducing the strength gains induced by partial saturation (physical parameter) and suction (mechanical parameter). Nonetheless, loosely compacted samples resulted positive net gains of peak strength and stiffness (Figure 45). It remains however important to note, that at the tested partial saturation, optimally compacted 30% bentonite soils are weakened by both treatments. The saturation rate of very clayey soils must be further investigated in future research of *Bio2Cementation*.

4.2.1.2 Summary

In conclusion, this section researches the mechanical properties of 10% bentonite and 30% bentonite soils treated by *Bio2Cementation*. The unconfined compressive strength tests are performed on saturated samples, to provide controlled physical properties between treatments. Untreated soils display plastic behavior over large deformations, whereas coupled clay-inhibition and bio-cementation treatments confer the medium stiff stress-strain responses. Most successfully, the loading of bio-cemented 10% bentonite specimens yielded doubled peak strength and one-two order of magnitude increased stiffness over the control. The strength parameters of granular soil are dominated by inter-grain friction, which is greatly increased by the coupled technique. Both 10% bentonite and 30% bentonite loosely compacted soils (80% of the optimum density), display large mechanical improvements (doubled σ_{peak}) by bio-cementation over guanidinium treatments. The increased coarse porosity facilitates the growth of calcium carbonate in the coarse inter-particle voids, likely inducing an increase in cementation cohesion. Lastly, unsaturated untreated 30% bentonite specimens displayed strong plastic deformation over large axial strains. Large suction forces and capillary cohesion of the optimally compacted specimen are neglected, and thus weakened when treated. Finally, *Bio2Cementation* confers successful mechanical improvements to clayey soils; the strengthening is found to be viable in loosely compacted porous media and 10% bentonite soils (any compaction).

4.3 Microstructure Analysis

This section presents quantitative and qualitative data analyses and images aimed at producing fundamental insight on the soil matrix modification by clay inhibition and bio-cementation techniques. The use of guanidine as a necessary constituent of the *Bio2Cementation* is explored by comparing the effect of EICP only and Gnd-EICP treatments. More specifically, two tools are proposed: firstly micro computer tomography (Micro-CT) 3D scans and secondly scanning electron microscope (SEM) images. The former provides large datasets by quantifying geometrical factors and spatial distribution of soil constituents, whereas the latter yields high resolution surface insight of the mineralogy.

The experimental dataset provides the basis to answer the following research sub-questions:

4. “With specific attention to soil matrix, grain morphology, and nucleation sites; how is the microstructure of a sand-bentonite modified by GndHCl alone and EICP-GndHCl treatment solutions?”

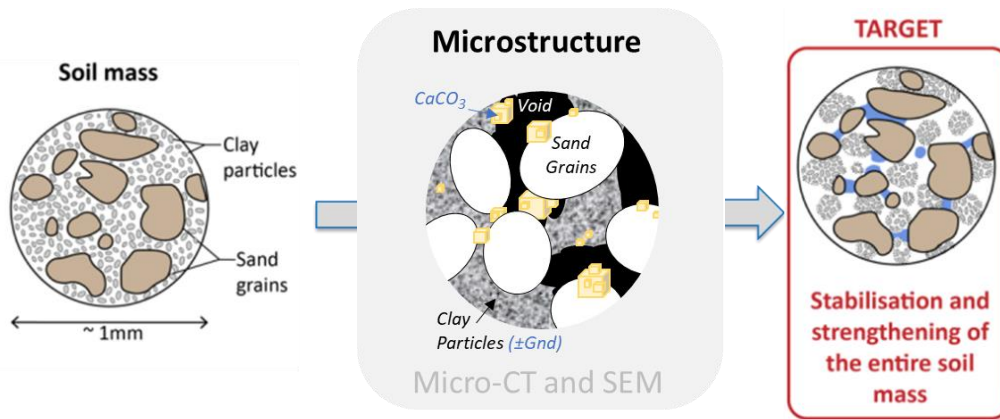


Figure 46 - The schematized process of researching the microstructure of clay inhibition and bio-cementation in sand-bentonite; experimentally researching the fifth research sub-question of the thesis.

4.3.1 Micro-CT

Differing attenuation of X-rays by the soil fabric constituents generate grayscale images, through which the grains and matrix are discernible. In this study, the research approach simplifies the matrix to four control variables: silica sand, bentonite, voids and the calcite cement. All four attenuate x-rays differently, and thus are discernible from one another. In fact, geomaterial Micro-CT analyses by Strzelecki *et al.* (2021) yielded increasingly light pixels for voids, bentonite, quartz and carbonates. Such features are used in addressing the microstructural changes between treatments. The extracted data can be used to analyze grain geometry and spatial variability of the treatments.

4.3.1.1 Design

This section outlines the image analysis steps to quantify the effect of GndHCl and EICP using X-ray imaging and the Fiji ImageJ software (Schindelin *et al.*, 2012; Schneider *et al.*, 2012). In the workflow overview of Figure 47, Micro-CT image stacks are handled to characterize the microstructure using numerical data and volume reconstruction images. Firstly raw image stacks are pre-processed, then segmented according to mineral/void type, and finally quantified.

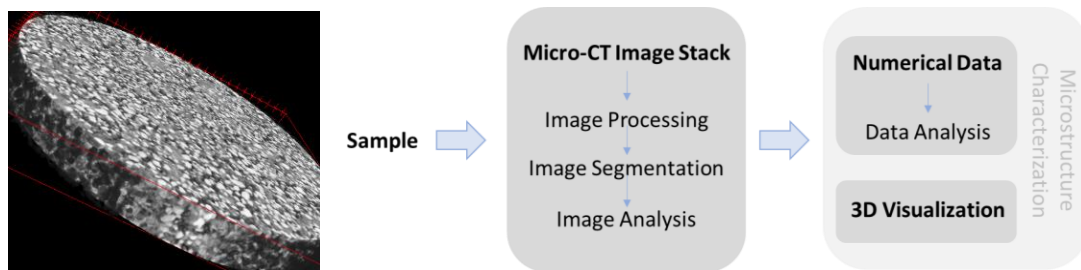


Figure 47 - Workflow of mineralogical classification, then quantification, using Fiji ImageJ software. On the left a grayscale untreated image stack as an example. The full Implementation details are included in Annex 8.6. Micro-CT specifications are displayed in Annex 8.9.

Through iterative process optimized upon smaller image stacks, the process named *Micro-CT Image Stack* (Figure 47) is run as an automatized process for all scans. Such method ensures reproducibility, reduces human bias, and allows for comparative analyses between all twelve samples. The procedure, including physical specifications of the method, is discussed in detail in annex 8.6 *Micro-CT - Image Analysis with Fiji ImageJ*. Reading this annex is strongly recommended to understand the intricacies of this chapter.

4.3.1.2 Results and Data Interpretation

The image analysis serves as the first insight on the microstructure of the soil specimens. As introduced in Figure 39, the process yields a numerical analysis and three-dimensional renderings of the soil matrix. Following this logic, the results are presented in three sections. Firstly, a whole volume analysis is presented as means to quantify the treatments effect over the entire soil column. Secondly, the segmented particles in three dimensions aim to provide insight on the microstructural modifications. Thirdly, the spatial distribution and result of the treatment is visually inspected using 3D renders of carbonate grains and voids (greater than the 15 μ m resolution limit).

Whole Volume Analyses

The porous media of the complete soil column is scanned, processed, and analyzed in this subsection. *Bio2Cementation* modification of the fine porous media is numerically quantified in

comparison to the unsaturated-untreated samples and EICP only treatments. The treatment targets the sand and bentonite fractions, are reflected in varying calcium carbonate and void volumes between samples. Firstly, Figure 48 displays the stacked whole volume analysis, for which specimens N.1-6 pertain to soil BC10 and N.7-12 are BC30.

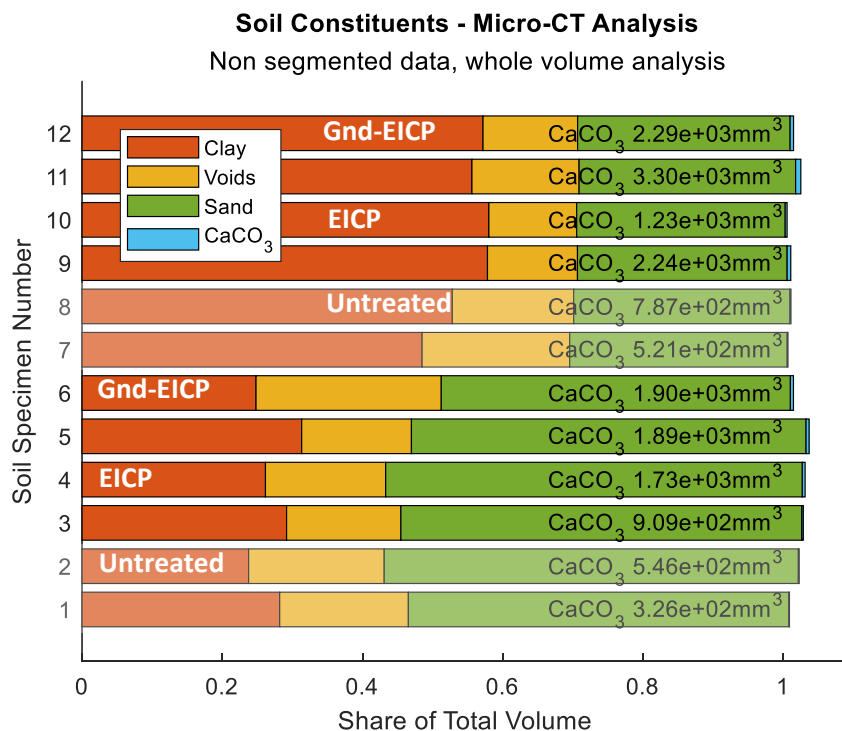


Figure 48 – Soil BC10 specimens N.1-6 and soil BC30 samples from N.7-12. Odd numbers are loosely compacted soils, even numbers are near optimally compacted specimens. All constituents are identified by machine learning Weka Segmentation in 3D for particles greater than the limiting 15 μ m resolution of one pixel.

The whole volume analysis presents an overview of the sand-bentonite matrix for cylindrical samples tested in this research. The two soils, each prepared at two dry densities, are easily discerned in Figure 48. It is notable that the sand fraction in Figure 48 is constant for BC30 (as expected), whereas soil BC10 strangely shows large variability of sand volume. Although prepared at 10% and 30% BC by weight, the samples are prepared at optimum moisture content, which lead to a significant volumetric contribution by the bentonite. Notably, the large surface area and swelling of clays during the injections, yield ~25-30% clay volume for BC10 and ~55% for BC30 soil specimens. It can therefore be expected that the clay fraction dominates the volume and porous microstructure of BC30. Guanidine pre-injections reduce the swelling effects, and thus reduce the discerned saturated clay volume for three-quarters of clay-inhibited specimens compared free-swelling EICP injections (BC10 1.47[g/cm³], BC10 1.35[g/cm³], BC10 1.56[g/cm³]). In expected conjunction, the final detectable void volumes augment for all specimens stabilized with guanidine. The sole identified outlier, which does not match the described trends is Gnd-EICP treated BC10 1.21[g/cm³]. Special attention is brought to this sample in the SEM chapter.

In evaluating Figure 48, BC10_{1,21} void ratios are unexpectedly and systematically too low (~5%vol). This could be explained by the histogram matching algorithm calibrated to the dense N.6 BC10 1.47[g/cm³] specimen, which generates noisy dark-gray (non-black) void regions when matching the “soft” BC10 1.21[g/cm³] specimens. This systematic error would overestimate the clay classification at the expense of void volume. Future work must take this into consideration by matching histograms to the four densities to reduce noise artefacts and/or training four different machine learning classifiers.

Secondly, the calcium carbonate and voids (greater than the 1 pixel resolution limit of 15 μm) are used as proxies to comparatively analyze the untreated soil, the non-stabilized clay fraction in EICP injections, and the coupled *Bio2Cementation* technique (Figure 49).

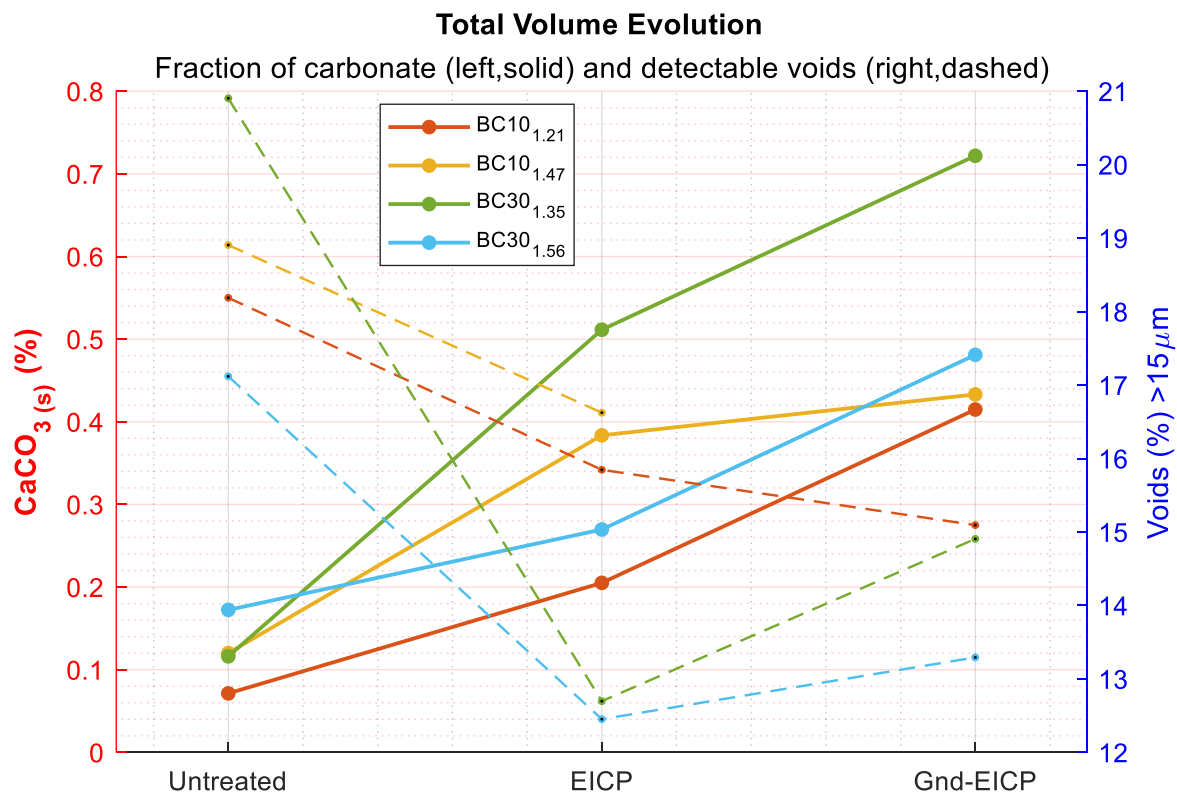


Figure 49 - Solid carbonate (solid line) and void (dashed line) proxies as markers for the modification of the porous media. Note the non-negligible carbonate constituents which are included in the sand (Sibelco M32, Silica >99) and Na-bentonite soil prior to treatment. This is used as a benchmark for additional calcite grains discerned in the treated matrix.

Untreated soils seem to contain between 0.08-0.18% highly attenuating grains such as CaCO_3 , or heavier such as iron oxides (Figure 49). The same samples are comprised of 17-21% voids greater than 15 μm in the unsaturated optimum moisture content. Bentonite saturation by EICP treatment leads to a decrease in soil porosity of 2% in BC10 specimens, and 7% in BC30 mixtures. The swelling response likely leads to an increase in fine pores below the resolution limit. Interestingly, the guanidine pre-treatment effect is overlain by the crystallization effects. In 30% bentonite, the clay inhibition and minimized swelling records a 1-2% greater coarse pore volume compared to EICP only. Additionally, such pre-stabilization improves the calcium carbonate precipitation by $\sim 0.2\%$ vol, detectable by decreased coarse porosity in loose 10% bentonite. To this regard, Figure 48 shows that soils injected with EICP only contain 1000-2000 mm^3 of CaCO_3 , versus Gnd-EICP treatments yielded 1500-3000 mm^3 . Nonetheless, at less than one percent of the soil matrix volume (Figure 49), it is approximated that the crystals must be sparse, filling a small fraction of the permeable void. For this reason, nucleation locations and crystal mineralogy must be further explored at higher resolutions.

Particle Analysis

The labelled grain ROI's are analyzed, leading to large datasets of microstructural features. Nonetheless, the additional image processing required may introducing additional numerical errors, which are thus cross verified to other sections.

The numerical grainsize distribution of sand is compared to manual sieving results in Figure 50 as an initial benchmark to verify the accuracy of the image analysis. Additional grain scale verifications performed on 3D renderings on sand and void ROIs are included in the Annex 8.6.2.

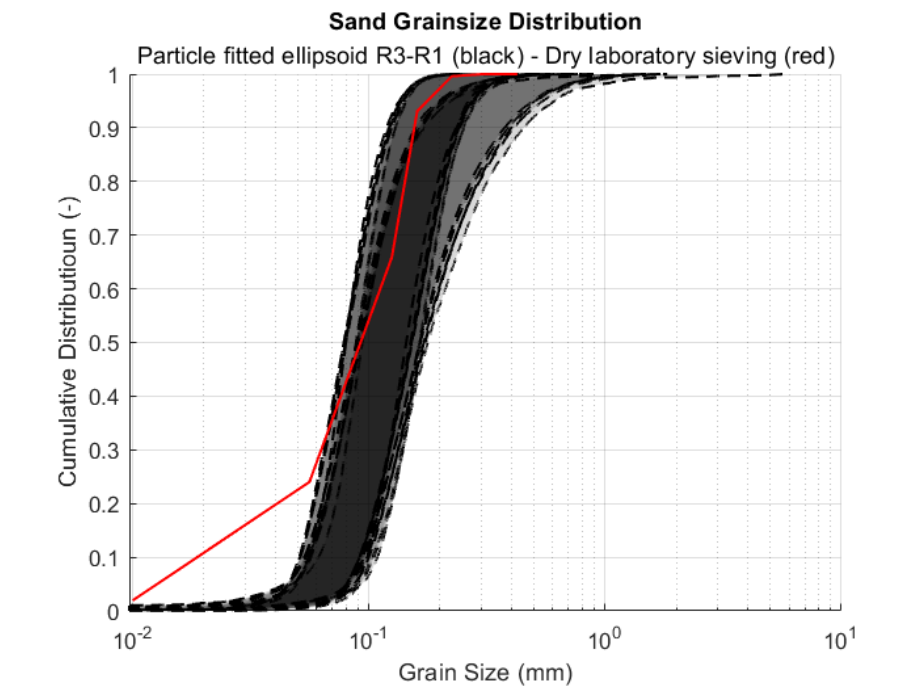


Figure 50 – Sand particle experimental sieved cumulative distribution (red) and numerically segmented cumulative distribution function (black dotted). The upper and lower bounds are computed by the major and minor fitted ellipsoids of each grain. Leftmost cluster are BC30 samples, whereas the BC10 cluster shows larger grains on the right.

The numerical grainsize distribution displays two clustered group, both of which match the experimental results well (Figure 50). This provides the necessary benchmark of the successful 3D automatized segmentation of individual grains in the soil cylinders. The smallest grain cross-section (R1) is expected to be the limiting factor when sieving mechanically, which is reflected in the closer fit to the experimental distribution. Nonetheless, although the laboratory sieving “resolution” is limited to stepwise increments of the fine meshes, the numerical analysis leads to a slight grain size overestimation for particles $<80[\mu\text{m}]$. Additionally, it is interesting to note that two distinct clusters are formed by the different bentonite contents. In fact, the higher contrast BC30 fits the experimental data perfectly (Figure 50 – left cluster), whereas the lower contrast BC10 shows a deviation and overestimation of the fourth quartile of the distribution (Figure 50 – right cluster). Two factors are likely the cause of such overestimation: systematic error of the image analysis or undiscerned calcite grains. It is expected that the very bright sand (90%_w) grains dominate the grayscale over the dark bentonite matrix (10%_w), leading to a poorer edge detection. A systematic tendential overestimation may occur when image reduction filters are applied. Additionally, the calcite crystal cladding may imprint bright voxels upon the sand grain surface, of which the distinct signal is lost due to resolution limitations, also inducing minimal systematic error. It must be noted however, that lone bright voxels of calcite are (or noise) are not lost when analyzing those binary masks alone, since manual thresholding was performed on unfiltered and un-adjusted Micro-CT images.

Continuing the microstructural size investigation, Figure 51 displays the median ellipsoid fitted around each ROI. Notably, the comparison is shown between EICP only (dashed line) or Gnd-EICP treatment (solid line). Additionally, the volume of individual carbonate grains of the treated samples is compared in Figure 52.

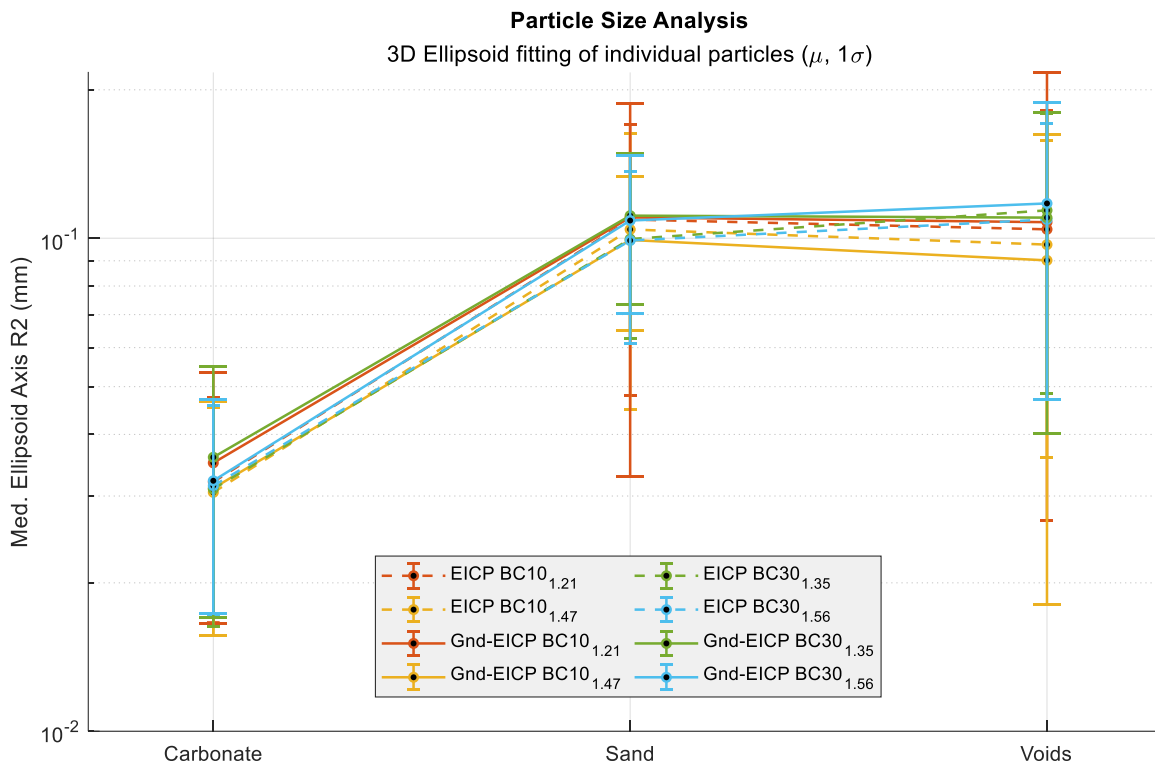


Figure 51 - Individual particle size analysis of carbonate, sand and void ROIs; all targets of the Bio2Cementation treatment. The guanidine enhanced Gnd-EICP voids greater than $15\mu\text{m}$ (solid) display a broader R2 distribution (2σ) that the un-stabilized EICP treatments (dashed). Sand grains and voids are similarly sized, whereas carbonate grains tend to be half the size.

Individual grain analyses show the similarity of sand and void region of interest size, whereas calcium carbonate grains are approximately three times smaller (Figure 51). More specifically, the mean sand and void size ellipsoid R2 is around $100[\mu\text{m}]$, whereas the carbonate grains are around $30[\mu\text{m}]$ in size. The latter is in fact the limiting resolution of $2[\text{pixels}]$ of the Micro-CT images. Additionally, although the mean detectable void volume of EICP and Gnd-EICP specimens is very similar, guanidine injections yield a broader range. The tail distributions indicate an increase in both coarse and fine porous space ($>15[\mu\text{m}]$), whereas the mean remain relatively constant. To be noted the dual effect of guanidine; hypothesized to collapse the clay double layer (increase coarse voids), while improving the precipitation of calcite (decrease void volume, increase surface roughness). Interestingly, the sand grains of BC10 1.21 [g/cm^3] show a large variability in the segmented ROI size, perhaps due to the increased surface roughness of calcite crystals smaller than the resolution limit. Such hypotheses are verified via SEM imaging at the nano scale in the next chapter.

Thereafter, the individual carbonate grains show little to indiscernible mean (star) and median (line) volumes (Figure 52). However, it is interesting to note that for a given soil type, the denser the sample the smaller the calcium carbonate. This is especially notable broader range of coarse calcite in BC10 1.21 [g/cm^3] versus the denser BC10 1.47 [g/cm^3] (broader quartile bars, larger kernel density distribution). The same features are also present in 30% bentonite content soil, albeit to a less obvious extent. This may be a microstructural feature of a soil with decreased coarse voids, which incites higher nucleation and smaller cladding crystals.

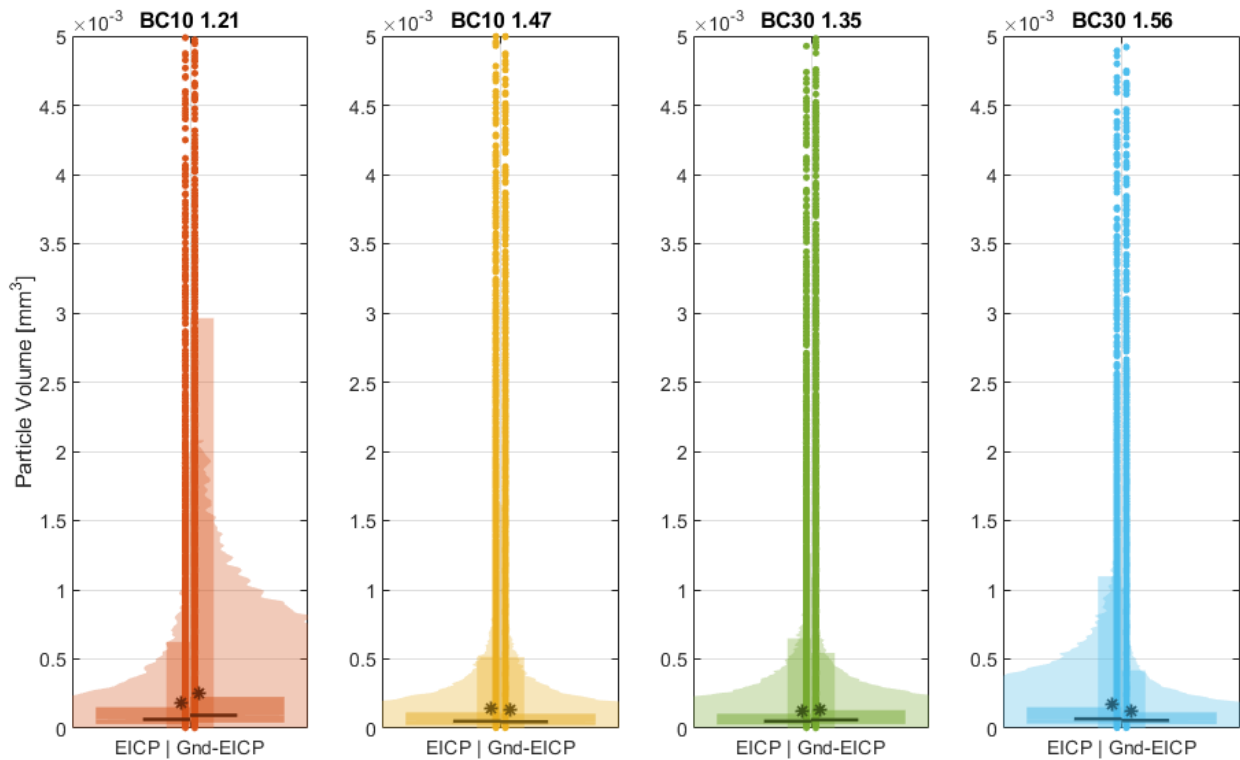


Figure 52 - Calcium carbonate ROI volume analysis, comparing the median (line), mean (star), quartile distribution of the grains (bars) and kernel density (volume). For each soil type the EICP only grains (left) and the guanidine EICP treatment results (right) are shown. The total precipitated volume is discussed in the previous section.

3D Visualization by Volume Rendering

Three-dimensional rendering visualizes the distribution and location of calcium carbonate crystals throughout the soil column. The non-destructive reconstruction is the final outcome of the image analysis procedure, and serves as an overview of *Bio2Cementation's* modification of the porous media. Additionally, renderings containing the void fraction are included as annex 8.6.8. The proposed reconstruction of cylindrical 15[mm] wide, 30[mm] long, displays the spatial evolution for untreated to EICP and Gnd-EICP treated specimens.

The calcium carbonate grains are reconstructed for the 10% bentonite content samples in Figure 53 and Figure 54, whereas the 30% bentonite specimens are displayed in Figure 55 and Figure 56.

As identified in the previous sub-sections, all untreated baseline specimens are shown to contain a fraction of highly x-ray attenuating crystals. Amongst them are aluminosilicates, carbonates, iron and manganese oxides and more. The exact mineralogy of the trace minerals remain beyond the scope of this work, but their distribution is homogeneous and preferentially comprised of coarser grains (light pink). As expected, with increasing sample density for a given bentonite content, the number of coarse grains and noise (dark purple) increases homogeneously (e.g. compare the untreated specimens of Figure 53 and Figure 54). These renderings form the base of the comparative analysis for EICP treatments.

The quantity and distribution homogeneity of enzyme induced calcite precipitation is consistently improved in soils which are pre-treated with guanidine. Additionally, two mineralogical effects are discerned: increased mesocryst quantity (light pink) and increased nucleation of microcrysts (dark purple).

Mesocryst formation is abundant and visibly improved in the looser soil samples. In fact, it dominates the microstructure and perimeter of the looser 10% bentonite specimen treated with Gnd-EICP (Figure 53). The crystal density along the injection axis is improved in the dense 10% bentonite Gnd-EICP (Figure 54). Whereas in the looser 30% bentonite sample it seems to modify the crystallization mechanism; homogeneous mesocryst growth is favored over rare macro-pore clustering (Figure 55). The matrix of microcrystals (dark purple), conically extend from the base and top of the specimens in all EICP treated soils. However, the highly nucleated soil volume extends consistently farther in the guanidine stabilized soils. The effect is most notable in the 30% bentonite soils treated with Gnd-EICP (Figure 55 and Figure 56).

In conclusion, mesocryst quantity and distribution is improved for Gnd-EICP treatments. This effect dominates calcite precipitation in the 10% bentonite soil. Similarly, microcrystals successfully nucleate deeper and at increased rates for the stabilized soils. This occurs most visibly in the dense and 30% bentonite specimens.

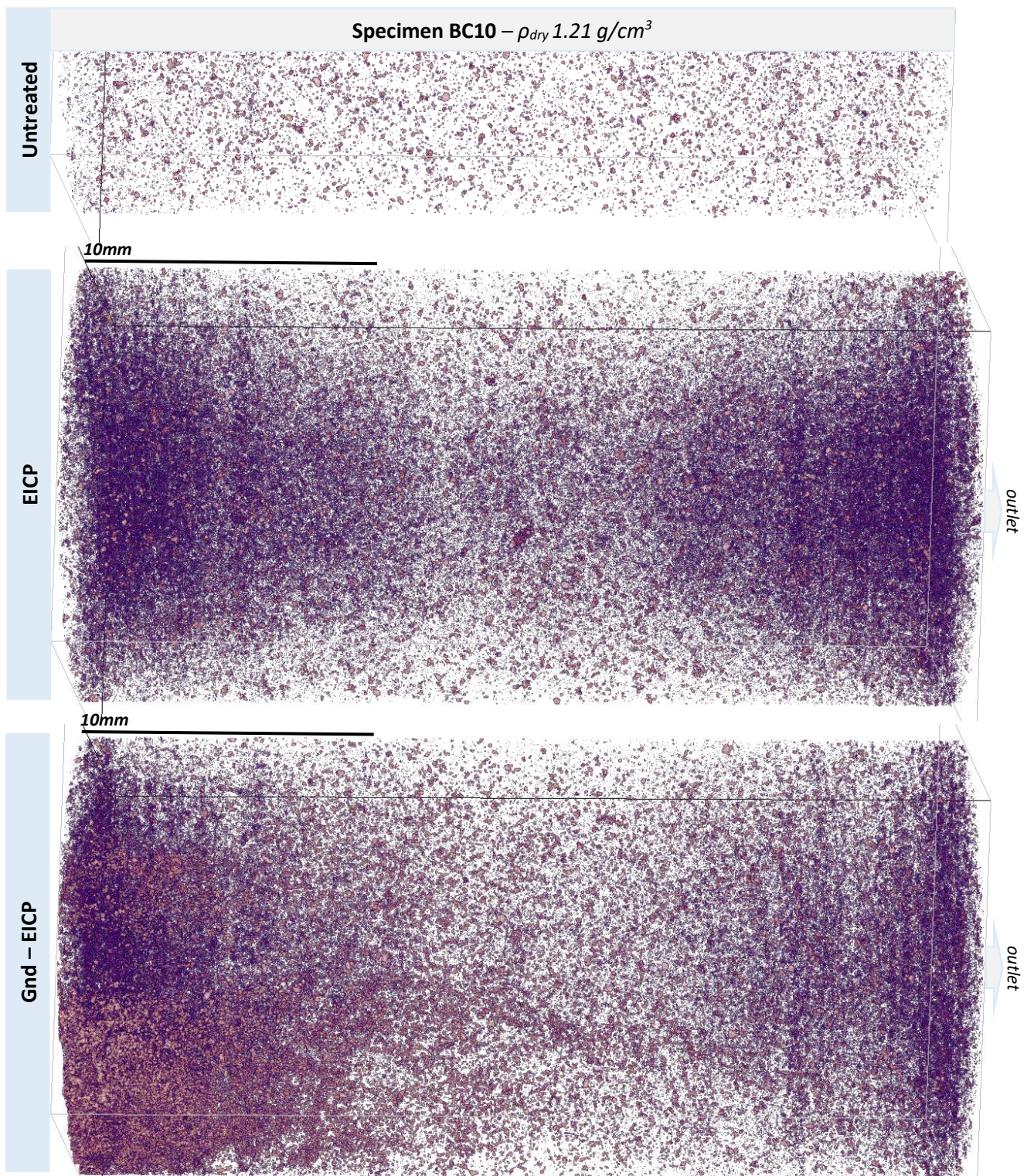


Figure 53 - Micro-CT calcium carbonate grains rendered in 3D – here the 10% bentonite samples prepared at dry densities of 1.21 g/cm^3 . Larger volume particles are represented by lighter pink hues. Dark purple clusters indicate large nucleation of microcrystals. The limit resolution is of 15-30microns.

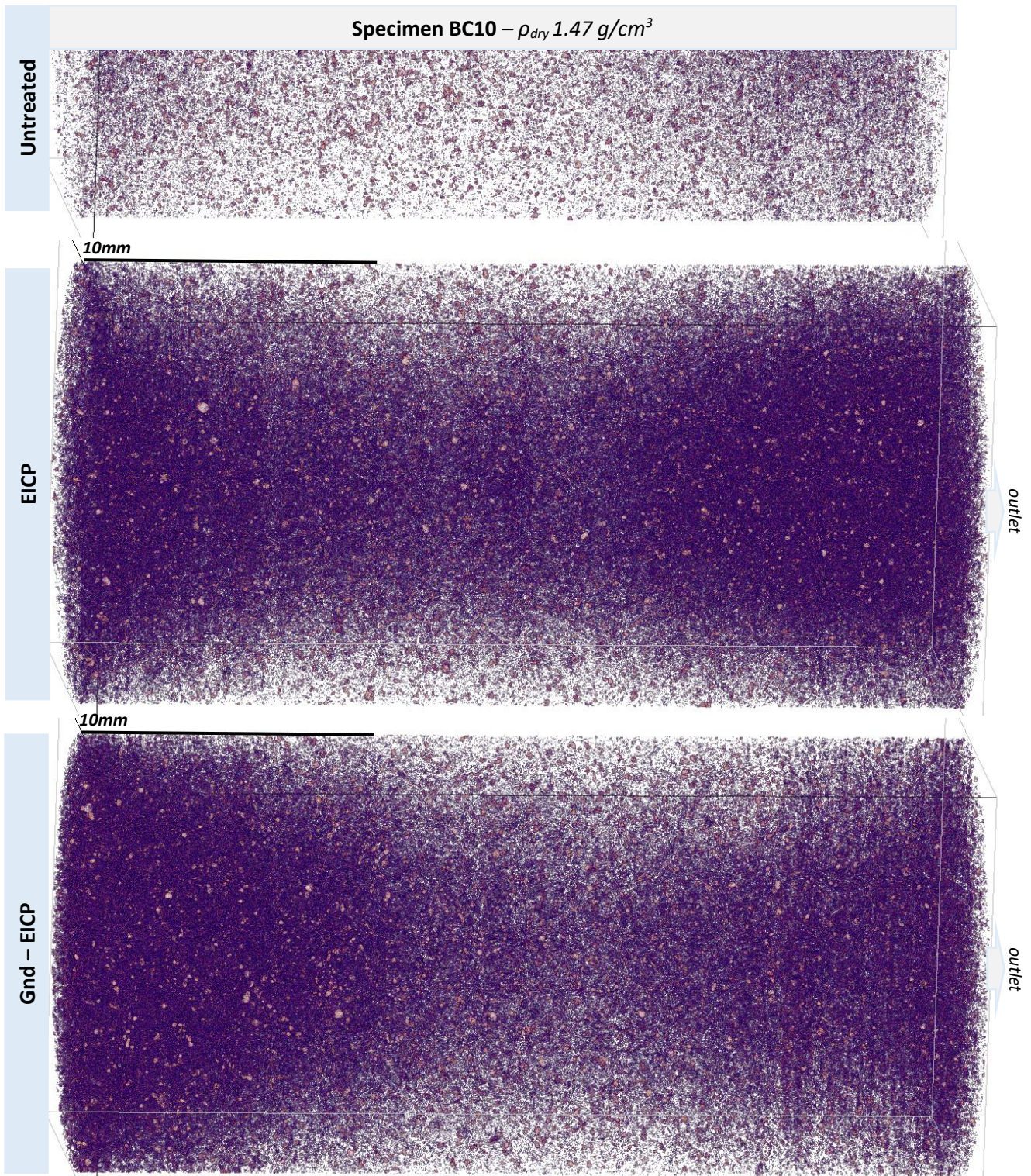


Figure 54 - Micro-CT calcium carbonate grains rendered in 3D – here the 10% bentonite samples prepared at dry densities of 1.47 g/cm^3 . Larger volume particles are represented by lighter pink hues. Dark purple clusters indicate large nucleation of microcrystals. The limit resolution is of 15-30microns.

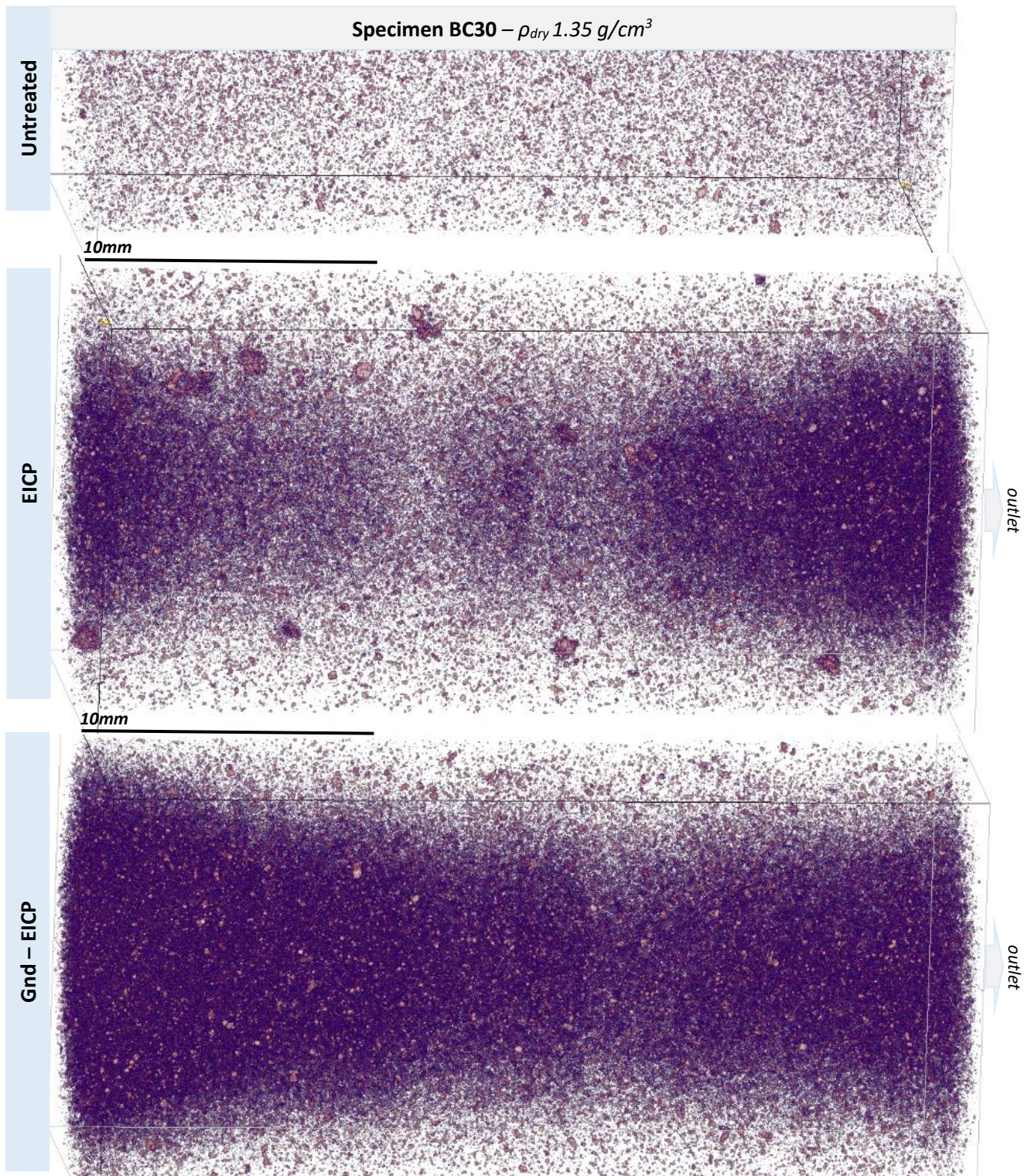


Figure 55 - Micro-CT calcium carbonate grains rendered in 3D – here the 30% bentonite samples prepared at dry densities of 1.35 g/cm^3 . Larger volume particles are represented by lighter pink hues. Dark purple clusters indicate large nucleation of microcrystals. The limit resolution is of 15-30microns.

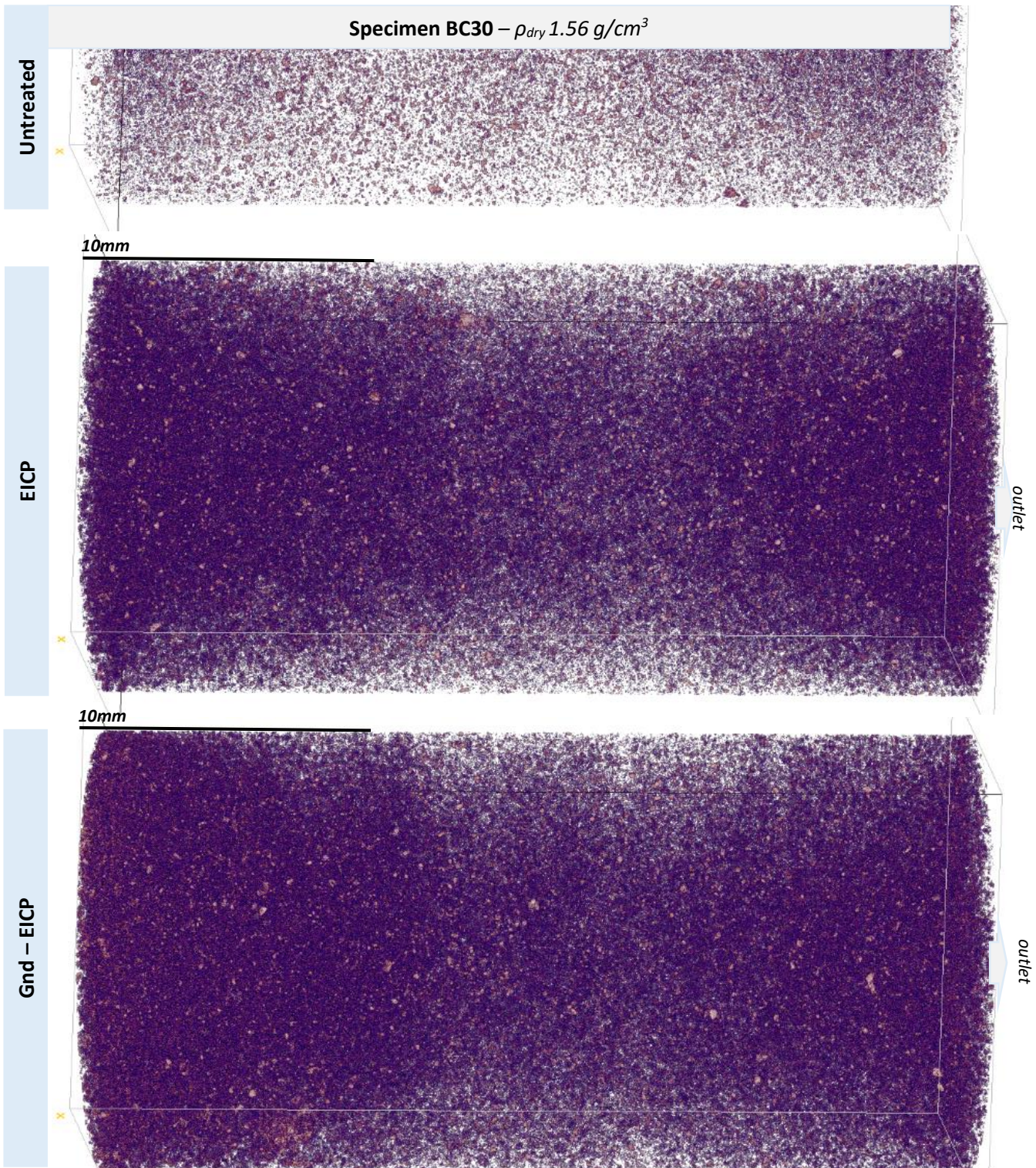


Figure 56 - Micro-CT calcium carbonate grains rendered in 3D – here the 30% bentonite samples prepared at dry densities of 1.56 g/cm^3 . Larger volume particles are represented by lighter pink hues. Dark purple clusters indicate large nucleation of microcrysts, or in this sample may be induced by noisier greyscale imaging (see annex Micro-CT - Image Analysis). The limit resolution is of 15-30microns.

Micro-CT scans are analyzed using Fiji ImageJ, of which the results are organized in three subsections. The chapters findings are summarized hereafter.

Whole Volume Analyses

The whole volume analysis shows that the use of guanidine to enhance EICP increased the total volume of soil CaCO_3 from 1000-2000 mm^3 to 1500-3000 mm^3 . In fact, the volume in comparison to the entire soil cylinder increased by +0.2%. Additionally, the flushing of guanidine, even with the increased performance of calcite precipitation, yields reduced swelling and increased share of coarse voids.

Particle Analysis

The segmentation and analysis of particles is verified by comparing the experimental and numerical sand cumulative distribution function. Physical resolution limits and image processing are acknowledged as potentially inducing minor systematic errors. In summary the sand and void ROI's are similarly sized at 100 micron, whereas the calcium carbonate precipitates smaller grains around 30micron. The range of void sizes is larger for guanidine enhanced EICP, with both coarser voids and fine ones ($>15\mu\text{m}$) increasingly dominating the matrix. For a given bentonite content, the denser the sample, the smaller the calcium carbonate crystal. The microstructural limitations of a densely compacted soil with decreased void volume, for which crystal growth is limited, favors higher nucleation rates and smaller cladding crystals. This is most evident in *Bio2Cementation* treatment of the near optimally compacted 10% bentonite sample.

3D Volume Rendering of Carbonates

Three dimensional renderings of *Bio2Cementation* treatments show a consistent improvement in enzyme induced calcite precipitation. Two microstructural mechanisms are modified. Firstly, mesocrystal quantity and homogeneity is increased (most notable in 10% bentonite soils). Secondly, microcrystals nucleation rate and volume increases (notably in dense samples or all 30% bentonite specimens).

Evaluation of Error

Abundant sources of random and systematic error are prevalent in image analysis techniques making use of microscale x-ray tomography. It is expected that sample BC30 1.56 $[\text{g}/\text{cm}^3]$ is most subjected to uncertain image analysis. This must be accounted for when considering the quantitative findings of this chapter. Most notably, this research's voxel resolution is limited to 15 μm (hardware maximal resolution is 5 $[\mu\text{m}]$), which limits details at that scale. Additional errors and challenges include big data handling, histogram matching algorithms, pre-processing filters, noise, edge detection limits, and watershed induced artefacts. A thorough evaluation on the precision and accuracy of these considerations are detailed in annex 8.6.

In conclusion, abundant insight is gained on the evolution of the sand-bentonite matrix when treated with both guanidine and enzyme induced calcite precipitation. Guanidine reduces the swelling effect of clays, increasing detectable voids ($>15\mu\text{m}$), while significantly improving the precipitation of calcium carbonate. Column specimens are vigorously cemented, showing extensive precipitation for all 10% and the looser 30% bentonite samples. Consistently, both meso and microcrystal performance is improved when the clay fraction is treated with guanidine. Such findings support guanidine's pivotal role in stabilizing the bentonite and fine pores, which leads to significantly improved bio-cementation.

4.3.2 Scanning Electron Microscopy (SEM)

The scanning electron microscope imaging generates insight of the microstructural details of *Bio2Cementations* effect. Such imaging is necessary to verify the calcium carbonate crystal type (polymorph), their size and distribution, and guanidine's effect on the porous media. This microstructural chapter provides abundant qualitative insight. The sand-bentonite soil specimens are imaged for EICP only and *Bio2Cementation* injections. Additionally, the calcium carbonate polymorph's mineralogy in the presence of 0.25[mol/L] guanidinium is interpreted in annex 8.7.3 *Calcium Carbonate Polymorphs*. As an outcome, guanidine's role as a beneficial additive is argued.

4.3.2.1 Results and Data Interpretation

The microstructure sand-bentonite's treated by EICP (no guanidine) is analyzed, providing a reference performance of bio-cementation in un-stabilized clayey soils (Figure 57).

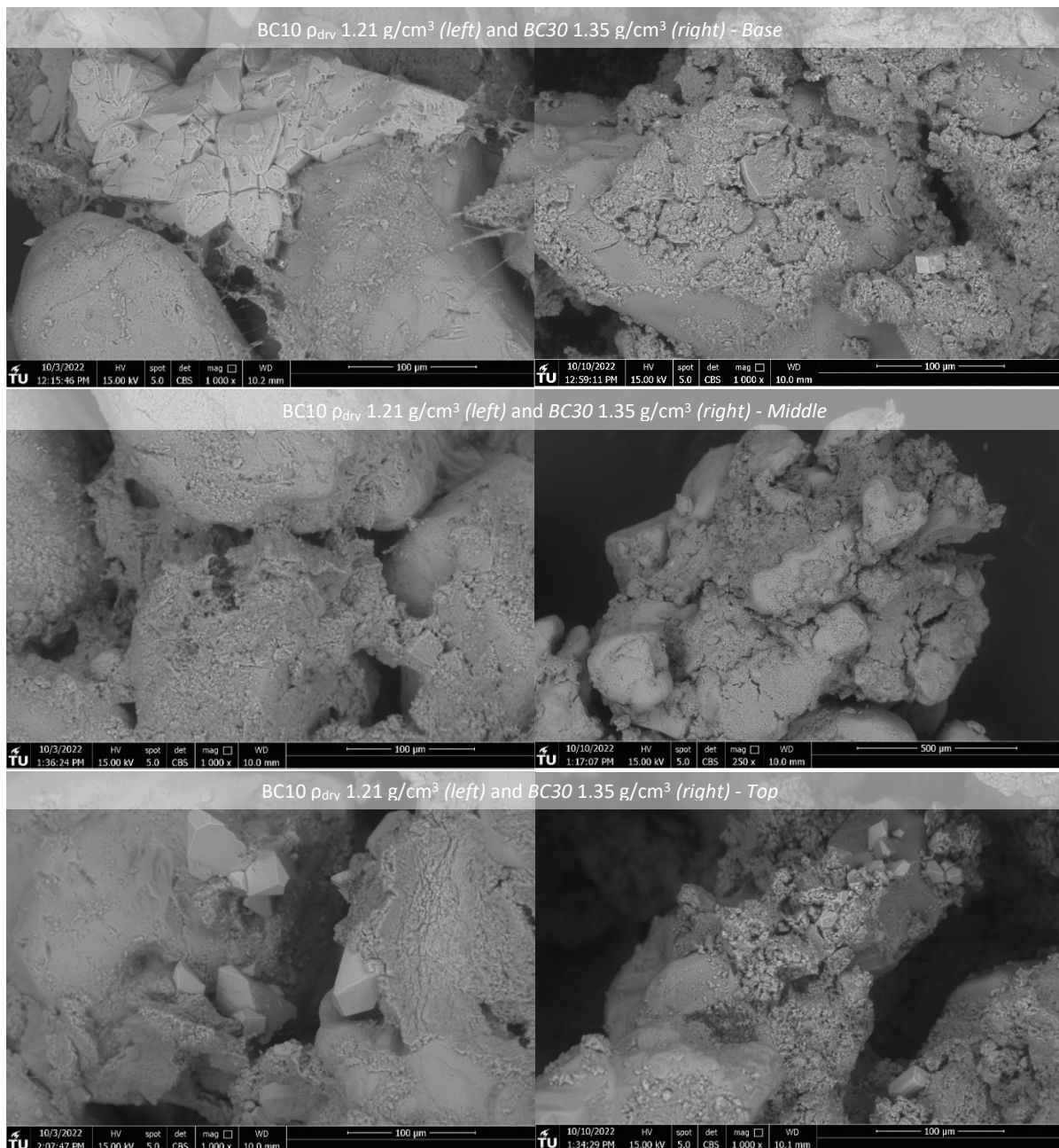


Figure 57 - SEM imaging of EICP only (no guanidine pre-injection) treated soil. On the left the 10% bentonite soil, on the right the 30% one. Images are taken at the base, middle and top of the sample.

In 10% bentonite soils, rhombohedral calcite mesocrystals $\sim 20\text{-}50\mu\text{m}$ (\pm small vaterite flowers) precipitate throughout, with large $\sim 300\mu\text{m}$ agglomerates occasionally growing sub-amorphously (Figure 57– *top left*). Additionally, the crystals are surrounded by abundant stringing of polymerlike fibers connected to the bentonite matrix. Sparse locations display very few crystallization features, with only occasional small $\sim 15\mu\text{m}$ rhombohedral calcite crystals coated in bentonite nucleating upon the silica grains. The clay matrix displays plastic deformation microstructural features, coating the sand grains and reducing the coarse void interconnectivity (Figure 57– *mid left*). Additionally, the no binding calcium carbonate grains were discerned. The porous media is dominated by the bentonite, whereby clays coat support the sand grains.

Very few calcium carbonate crystals are discerned in 30% bentonite specimens, with none being larger than $\sim 20\mu\text{m}$. Most occurrences are thin aragonite/vaterite flakes, perhaps early nucleation sites of the flower-like less stable polymorph (Figure 57– *top right*). The bentonite is dispersed and dominating the inter-particle media, coating the silica grains, dominating coarse and fine pores alike. This is extremely apparent at the center of the treated specimens (Figure 57– *mid right*). Occasionally, heterogeneous calcium carbonate crystal clusters are found. Nucleation occurs in microcrystalline mats, primarily containing flowerlike micro vaterite and few rhombohedral calcite grains (Figure 57– *top left*). Such crystal cladding was never found to bind sand grains, and visibly only alters the surface roughness of the finer voids.

The pre-stabilization of the bentonite matrix by guanidine, and residual ions in the pore solution, modify the EICP process in clayey soils. The microstructural effects of *Bio2Cementation* are analyzed hereafter (Figure 58, Figure 59 and Figure 60).

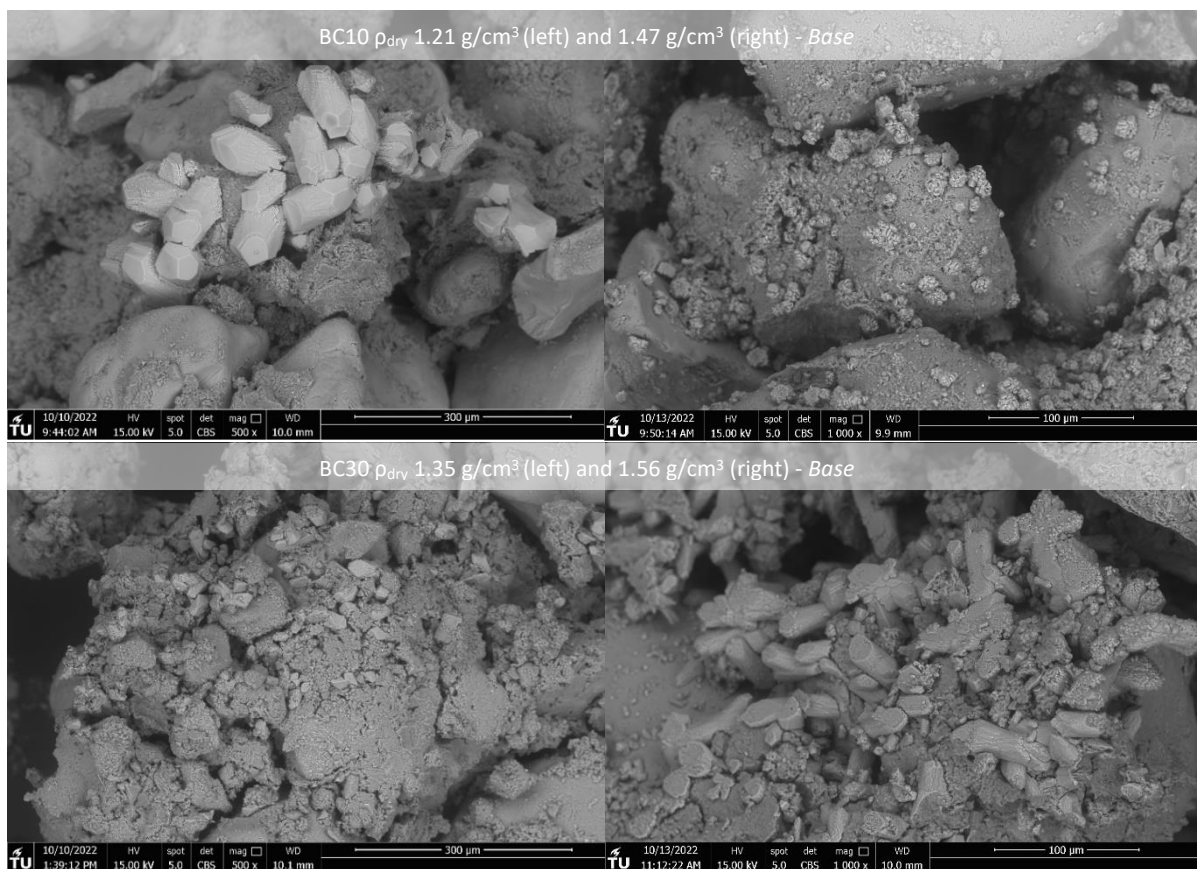


Figure 58 - SEM imaging of *Bio2Cementation* treatments (*Gnd*-EICP) treated soil. On the top the 10% bentonite soil, on bottom the 30% one. Images are taken at the base of the sample.

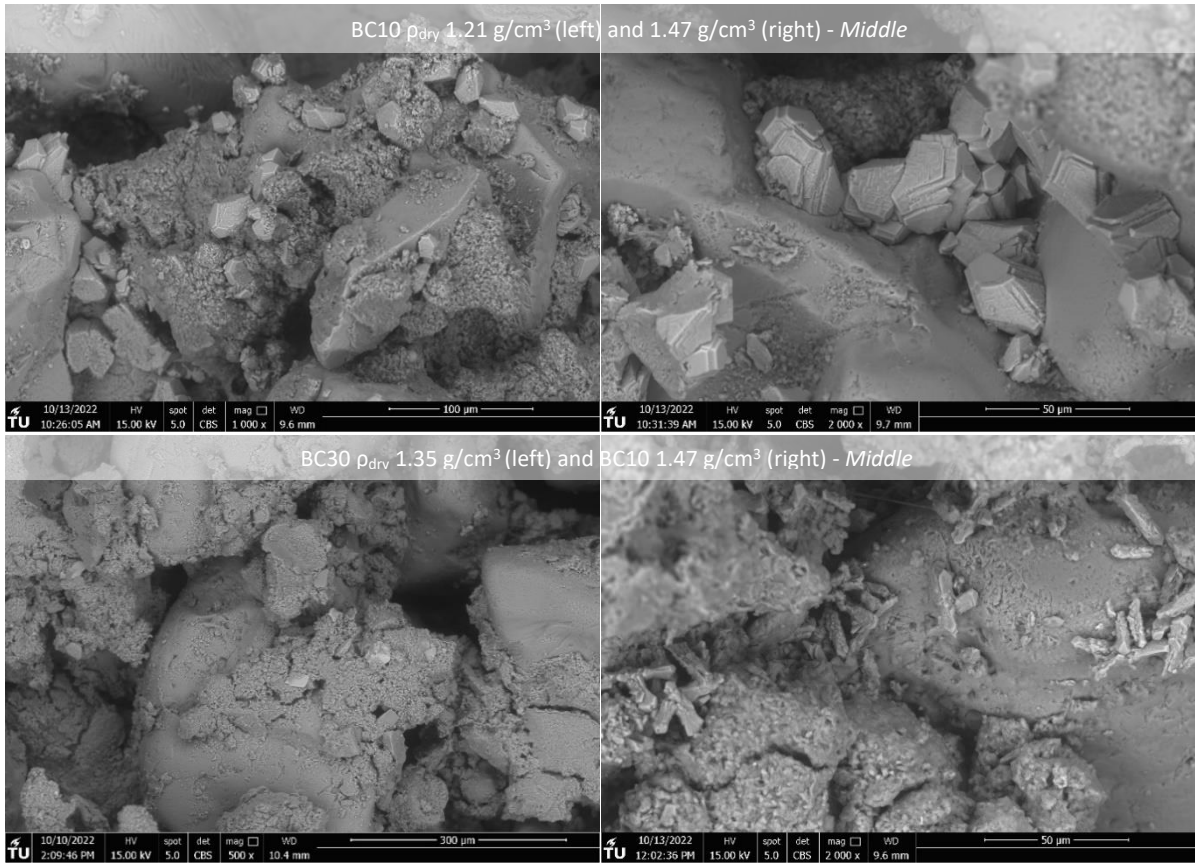


Figure 59 - SEM imaging of Bio2Cementation treatments (Gnd-EICP) treated soils taken at the middle of the soil samples.

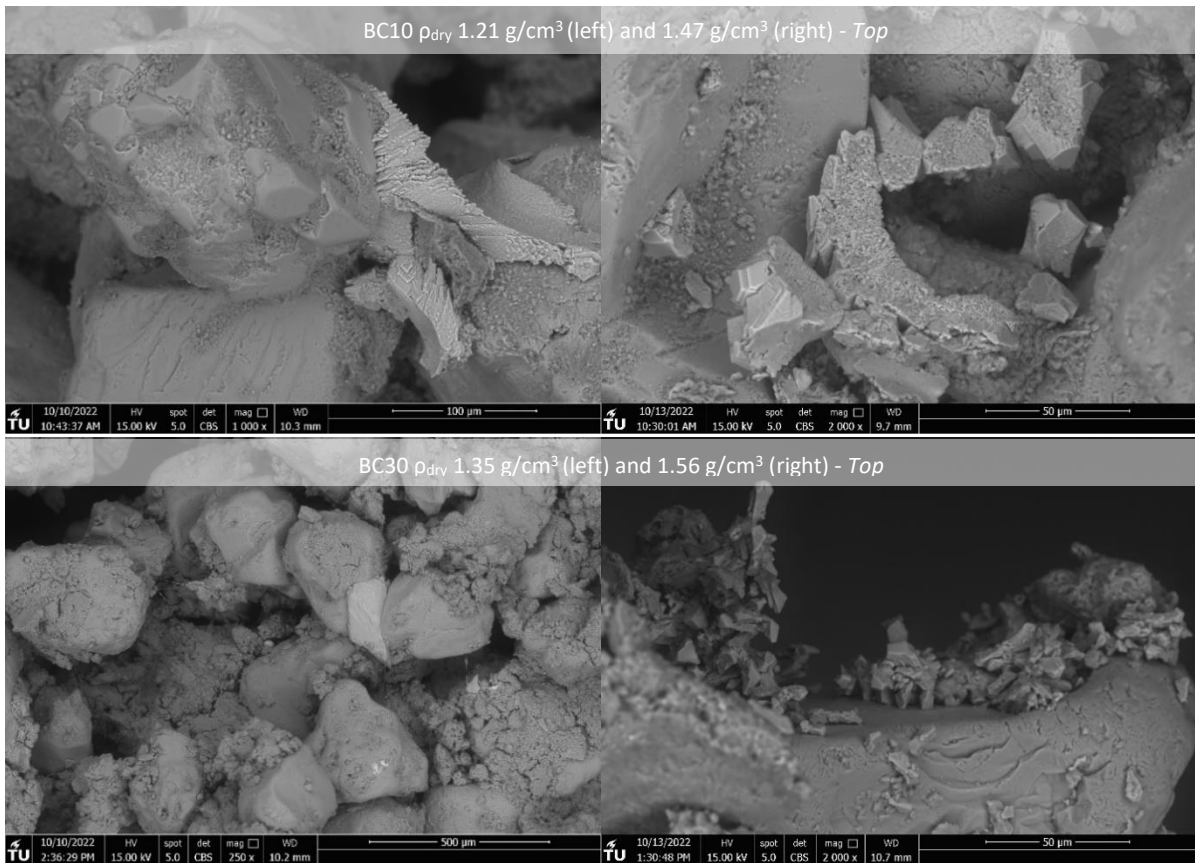


Figure 60 - SEM imaging of Bio2Cementation treatments (Gnd-EICP) treated soils taken at the top of the samples.

Soils comprised of 10% bentonite display prolific nucleation of calcium carbonate on sand and bentonite aggregates alike (Figure 58). Guanidine aggregates bentonite, increasing the coarse void size and interconnection. This allows for increased growth of stable calcium carbonate polymorphs. Less compacted specimens record modulated calcite mesocrystals. Firstly, large ~200micron bridging calcite as seen by the remnant sand grain imprint (Figure 60). Bentonite surrounds and underlies these large crystals without hampering the crystal morphology. The mineralogical evolution is visible upon the face of small octahedral calcite crystals, showing clear hierarchical plane expansion originating from nucleation sites upon sand and bentonite particles alike (Figure 59– *top right*). Optimally compacted specimens often display partial clustering and smaller cubic calcite, which also form bridging cemented bonds. The bentonite matrix displays low plasticity features, such as remnant imprints of sand grains throughout the samples. It often coats silica grains without hampering EICP, likely remnant from the sample preparation OMC water coating (see annex 8.7.1). The agglomerates are “brittle-like”, as seen via occasional cracking features. Finally, polymer like filaments are not present in the 10% bentonite soils stabilized by guanidine.

Specimens comprised of 30% bentonite display similar clay-inhibition and stability, albeit with decreased bio-cementation vigor and size. Calcium carbonate precipitates nucleate both in the clay matrix and sand grain surfaces. Rhombohedral calcite crystals of ~50-100micron dominate homogeneously the loosely compacted matrix (Figure 58), whereas cementation features between particles are not evident. Mesocrystal homogeneity decreases drastically in optimally compacted 30% bentonite specimens. Nonetheless, highly nucleated ~10micron stable calcite mats increase the surface roughness of all specimens, cladding sand grains and clay aggregates alike. Their morphology is akin to rhombohedral and cubic calcite, yet they occasionally contain intercalations of less stable flower/needle-like vaterite polymorphs. Carbonate precipitation is less frequent, and no binding crystals are discerned. In fact, the 30% bentonite porous media is dominated by the clayey fraction. Guanidine induces an impressive aggregation of clay platelets forming stacked clusters, forming angular fracture planes and maintaining stiff imprints of sand grains. The porous media seems “brittle” rather than diffused and plastic. Nonetheless, optimally compacted soils occasionally contain polymerized filaments in the clayey matrix, akin to non-enhanced soils. Furthermore, spherical vaterite crystals are heterogeneously enclaved in the bentonite fine voids (<15µm).

4.3.2.2 Summary


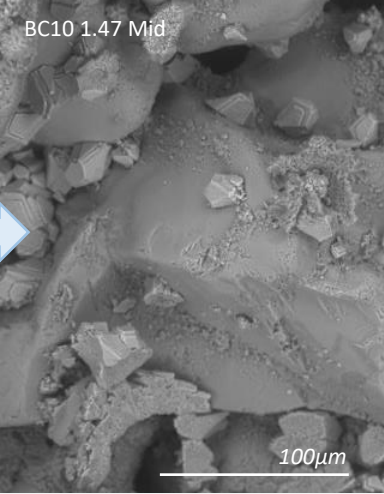
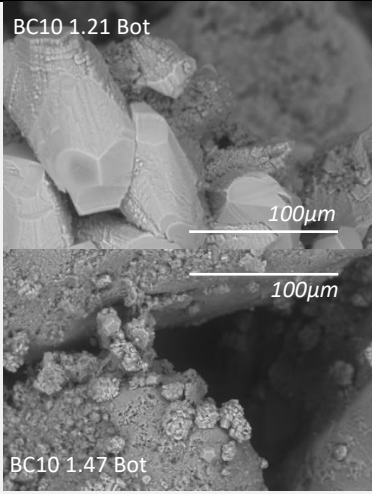
The scope of the SEM imaging was to gather insight on *Bio2Cementations* microstructural modification of sand-bentonite specimens. Bio-cementation is compared to clay-inhibition treatments coupled to EICP.

Firstly, guanidine is found to act as a beneficial additive to EICP in test-tube experiments, diluting EICP reagents with 0.25[mol/L] GndHCl. The favored calcium carbonate polymorphs are modulated mesocrystals calcite and rodlike aragonite. It is postulated that the biomolecule preferentially adheres to the calcite crystal surface, rather than denaturing the urease enzyme, facilitating slower reaction rates and large crystals.

Secondly, in the sand-bentonite soils, *Bio2Cementation* successfully inhibits clays and bio-cements particles. The use of clay inhibitors is shown to improve bio-cementation of clayey soils. In 10% bentonite specimens, large modulated calcite and vigorous octahedral/cubic crystals nucleate of silica grains and bentonite aggregates alike. In loosely compacted 30% samples, rhombohedral calcite crystals nucleate homogeneously, whereas optimally compacted specimens display less prolific bio-cementation and contain features akin to guanidine free EICP. Nonetheless, for all soil types the guanidine treatment confer the bentonite strong aggregation and non-plastic behavior.

In conclusion, the interpreted outcome of the SEM microstructural analysis is summarized in Table 6. Guanidine hydrochloride improves the crystal morphology of EICP, both in vitro and in the pore solution. Additionally, it stacks bentonite forming aggregates and drastically reducing charged surface interactions. *Bio2Cementation* is most successful in all 10% bentonite and loosely compacted 30% bentonite specimens.

Table 6 - Summary of Bio2Cementation microstructural evolution as enhanced by guanidine for treated BC10 and BC30 soils.

Microstructural Evolution			
	<p>Description Polymerized strands, no bentonite aggregation but coats silica, amorphous or rare calcium carbonate, either agglomerates or no crystals, no nucleation on bentonite, rare spherical vaterite</p> <p>Interpretation No guanidine hydrochloride in the soil matrix or pore solution</p>	<p>Description Cubic or rhombohedral calcite, little charge surface interaction with bentonite, few polymerized strands, sparse large bridging calcite bonds, nucleation mainly on sand grains, rare vaterite at sample summit</p> <p>Interpretation Little guanidine hydrochloride (postulated 0.01-0.1M) in the soil matrix or pore solution and well aggregated bentonite.</p>	<p>Description Large mesocrystals of modulated calcite with mesostep growth or extreme cladding of cubic calcite, strong aggregation of bentonite with visible stacking, no fibrous polymers, large nucleation on bentonite</p> <p>Interpretation Moderate guanidine hydrochloride (known $\leq 0.25M$) in the pore solution and/or uncharged clay surfaces.</p>
BC10 EICP	X		
BC30 EICP	Little to no bio – cementation		
BC10 Gnd-EICP		X	All soils
BC30 Gnd-EICP		Loosely compacted soil	X

5

Discussion

The experimental findings display the promising potential of the novel bio-cementation technique, while also bringing its limitations to light. This subsection expands upon the experimental knowledge base of *Bio2Cementation* by cross analyzing hydrological, mineralogical and strength considerations. The discussion is organized with by progressively expanding the focus from the crystal particle towards the soil scale. Then the techniques applicability as an in-situ grouting method is discussed. Finally the discussion is broadened towards potential environmental concerns and sources of uncertainty.

5.1 Crystal Morphology and Nucleation

Bio2Cementation uses clay inhibition to improve bio-cementation in the voids of sand-bentonite soils. The spatial distribution of calcium carbonate solids proved to be most homogeneous in loosely compacted samples and all 10% bentonite soils. This is clearly visible in the 3D volume rendering of carbonates from Micro-CT images. Additionally, this corresponds with decreased hydraulic conductivity and maximal strength gains under UCS loading, likely induced by successful calcium carbonate precipitation.

The growth of crystals occurred most successfully in the coarse voids of sand-bentonites pre-treated with guanidine. In fact, clay-inhibited specimens displayed continued reduced hydraulic conductivity for each subsequent EICP treatments, indicating continued growth of calcite crystals. This corresponds well with Micro-CT findings of increased total calcium carbonate volumes in soils pre-treated by guanidine.

The increased angularity and stiffness of the soil matrix was qualitatively found to be increased by the clay-inhibiting guanidine. Imaging shows crystal cladding of silica grains and bentonite aggregates alike, with grain size analyses recording an order of magnitude smaller calcite than the soil particles. UCS findings of stiffer guanidine modified soils reflected the cracking found in the SEM sample matrix.

The nucleation rate of calcite was found to be controlled by the enzyme activity, residual pore solution guanidine (see 8.7.3), clay aggregation and soil compaction. Micro-CT volume analyses and SEM imaging both found favored microcyst growth (<50[μm]) in highly compacted soils, due to the finer pores and less residual guanidine in the pore solution. The same methods identified large calcite crystals (>200[μm]) growing in the coarse voids of loosely compacted soils.

The crystal size increases with low soil compaction, presence of guanidine, lower reagent concentration, and repeated EICP treatment cycles. Imaging shows bridging mesocrystals in loose soils and increased modulated calcite growth in the presence of guanidine. In fact, samples containing large calcite crystals recorded the greatest increase in mechanical parameters, compared to water saturated specimens.

Finally, the crystal polymorph is controlled by the bentonite's inhibition, urease enzyme activity and guanidine additive. Imaging of test tube experiments and time dependent pH and EC results record favored stable calcite in the presence of guanidine (both in-vitro and in the soil matrix), whereas concentrated highly active enzymes or un-inhibited bentonite surfaces favored the growth of unstable vaterite polymorphs. SEM images in optimally compacted 30% bentonite showed heterogeneous and rare bio-cementation. In fact, occasional weak vaterite crystals were identified (unstable under the electron beam), which concur with the low strength gains after treatments in such media.

5.2 Soil Type and Compaction

The thesis explores the coupling of two strengthening techniques for clayey soils. To investigate *Bio2Cementation's* isolated effect, a commonly researched sand-bentonite mixture is used as a control variable. The fundamental understanding developed in this thesis serves as the basis to discuss the suitable target soil types for the soil strengthening solution.

The clay type used in this thesis exhibits multiple factors which usually hamper bio-cementation in soils. Charged surface interactions with EICP reagents, swelling characteristics hampering chemical delivery and plastic properties dominate the soil's mechanical response. These have been found to impair bio-cementation (Cardoso *et al.*, 2018). The proposed clay-inhibitor treatment chemically and physically stabilizes the matrix, improving EICP in clayey sands. Chemical modifications are interpreted indirectly by the SEM imaging of improved calcite polymorphs stability. Physical stability is directly measured by the mechanical parameter improvements from UCS tests. The clay-inhibition effect by guanidine is likely to occur in similar fashion in other clayey soils, for example containing kaolinite (Hu *et al.*, 2020).

The pH value of a soil's pore solution plays an important role in bio-cementation, since the EICP reaction must occur in an initially neutral or slightly alkali medium (Van Passen, 2009). This initial condition is experimentally verified by pH monitoring at the onset of EICP reactions in test tubes. Thereafter, the thesis strengthened sand-bentonite soils, as recorded by the neutral pore solution effluent. However, certain natural soils may not be suitable for bio-cementation. For example, acidic pore solutions residing in organic clays are likely to hamper calcite precipitation.

The clay percentages researched tested are limited to a two bentonite contents, and thus lack a continuous characterization of increasingly clayey soils. Nonetheless, the porous media displayed two physio-chemical responses; 10% bentonite was dominated by the sand constituents. *Bio2Cementation* modifies the hydraulic response and microstructure, leading to significantly improved mechanical parameters. Differently, the 30% bentonite soil's response was found to be controlled by the clay minerals. In optimally compacted media, bio-cementation's effect was found to be limited. Although beyond the scope of this thesis, in an unsaturated media the large suction and cohesion forces in unsaturated 30% bentonite soils are likely to outweigh the potential benefits of the technique.

The particle coating by bentonite has been shown to hinder urease activity, and thus reduce crystal precipitation in MICP and EICP (Arab *et al.*, 2022). However, the tested *Bio2Cementation* treatment stabilizes clay minerals, allowing vigorous nucleation and growth of calcite upon clay aggregates and coated silica grains alike.

The soil compaction has a large effect on the treatment's success. Looser compaction soils record large decreased hydraulic conductivity, increased strength characteristics and abundant calcite precipitation, attesting to *Bio2Cementations* soil strengthening success upon the tested loose media.

Differently, near optimally compacted 30% bentonite is sensitive to clay inhibition but fails to successfully bio-cement.

5.3 Grouting Engineering Applicability

The alternative soil grouting technique tested in the thesis shows promising potential for expanding bio-cementation's applicability in view of field applications, albeit with certain limitations. The suitable soil types strengthened by bio-cementation injections are successfully expanded beyond pure sands towards clayey soils. In-situ soil analyses are needed to maximize chemical distribution and cement homogeneity; loosely compacted soils containing neutral pore solutions ($\text{pH} \pm 0.5[-]$) in are deemed suitable target lithologies.

The grouting via water based cementation must occur in soils with sufficient water retention to prevent reagent leaching over the curing time of forty-eight hours. Nonetheless, the effect is deemed to limit bio-cementation of gravel-sands rather than clayey soils, even following the increase of hydraulic conductivity by guanidine pre-treatments.

The calcium carbonate precipitation was proven to increase with subsequent injections, whereby field applications will benefit from repeated bio-cementation injections. Reagent transport and the solution's preparation is rapid and simple, facilitating the on-site engineering for subsequent treatments.

The in-situ injectability by tube a manchette (TAM) has been shown to be a viable delivery method of EICP treatments (Martin *et al.*, 2021). The solution's low viscosity reduces energetic consumption and thus cost. Additionally, this may facilitate grouting near embedded structures or hard to reach soil masses at decreased pressure gradient. Nonetheless, pressure monitoring on site must prevent hydraulic fracturing of the matrix.

Some limitations remain before the possibility of researching Bio2Cementation at the field-scale. Most notably, the cost per cubic meter remains high. This work utilized micro-biological-grade reagents, whereas field applications would require industrial-grade economically feasible reagents.

Lastly, the range of applications expand beyond sub-surface grouting, such as slope stabilization and surface erosion mitigation. These techniques may benefit of the expanded applicability of bio-cementation towards clayey soils, but the effect of chemical grouting on biodiversity must be considered.

5.4 Environmental Considerations and Knowledge Gaps

The use of *Bio2Cementation* to strengthen clayey soils poses certain environmental upsides. compared to conventional Portland cement grouting. For instance, it is derived by the re-uptake of *Jackbean* as a bio-food industry bi-product, induces energy savings during chemical grouting, provides a neutral groundwater following the complete treatment, and residual free guanidine is biodegraded in the pore solution. Nonetheless, the bio-alternative poses notable environmental challenges.

The production of ammonium chloride is toxic when leached in the water table, for example impairing aquatic life if present at concentrations greater than 0.5[ppm] (Hora *et al.*, 2020). In this regard, the injections on-site may require downstream extraction wells, whereby the molecule could be recycled for industrial uses such as rice production. Furthermore, leaching effects are expected to be less

troublesome in clayey soils rather than the currently bio-cemented sandy soils. Notably, they benefit of lower permeability, reducing leaching rates and thus increasing its diluting factor. Nonetheless, this large concern must be further studied and mitigated prior to its wide application.

The oxidation of steel by chloride salts poses an additional challenge to EICP's mainstream acceptance. The effect of *Bio2Cementation's* effluent on steel reinforced embedded structures must be further researched. To this regard, it is possible to envision an alternative source of calcium ions to reduce the presence of toxic chlorinated compounds. This is highly desirable to improve the viability of the technique.

The research of EICP's long-term stability remains limited, and must be addressed. It is uncertain how stable calcite crystals are in natural groundwater prior to dissolving. For example, colder groundwater contains increased concentrations of CO₂, and thus carbonic acid, which may degrade bio-cementation over time. Therefore variations of the clayey soil's humidity, the cements susceptibility to freeze-thaw cycles, and infiltration of slightly acidic rainfall are knowledge gaps worth exploring.

The flexibility of *Bio2Cementation*, such as its ease of preparation and injection, provide multiple parameters to calibrate the proposed recipe. This may be exploited to improve its economic and environmental performance. This flexibility does however induce uncertainty in various aspects of the technique, and thus calls for additional experimental research.

6

Conclusion

Bio-based soil strengthening shows promise as an alternative grouting technique. Many natural soils contain clay minerals, which have been shown to hamper bio-cementation. This thesis researches a novel coupled approach named *Bio2Cementation*, aimed at expanding the applicability of bio-grouting to clayey soils. This is done by coupling two techniques: clay inhibition and bio-cementation. Guanidinium hydrochloride is used to target the clay minerals. By exchanging in the interlayer and binding to the electrical double layer of the platelets, it induces the formation of chemically and physically stable aggregates. Enzyme induced calcite precipitation treatments hydrolyze urea to form calcium carbonate crystals in the inter-particle voids. By cementing sand grains and clay aggregates alike, the mechanical properties of the medium are modified.

6.1 Summary of Findings

The testing program executed in this thesis provides a diverse analysis of the *Bio2Cementation* technique. Two artificial soils comprised of sand-bentonite are used to test the proof-of-concept treatment. In order to provide a comprehensive experimental investigation, four research sub-questions are posed to guide the thesis' experimental findings. They are thematically organized and summarized hereafter.

1. *What is the optimal enzyme induced calcite precipitation recipe? How stable is guanidinium hydrochloride, and does it disrupt calcite precipitation?*

Test-tube experiments with varying EICP reagents were performed to experimentally seek maximized calcium-carbonate yield at low concentrations. The optimal solutions are found to be non-equimolar solutions of calcium chloride 0.5[mol/L] and urea 0.75[mol/L]. This is found to be valid both for the lower activity *Jackbean urease* (3U/mg) and the higher activity lyophilized *Canvalia Ensiformis urease* (8U/mg). Such findings concur with successful EICP state of the art, seeking to improve crystal morphology and crystal distribution in the soil fabric.

Guanidinium Hydrochloride solutions are stable over time. Residual guanidine in the pore solution was found to increase yield and modify the calcium carbonate precipitation kinetics in test tubes. Its role as a beneficial additive occurred when combining EICP reagents with 0.25 [mol/L]. The surfactant led to modulated growth of large stable calcite polymorphs in the test tubes. Its role as an additive may also minimize excess ammonium bi-products.

2. *How does GndHCl improve the permeability and increase flow through potential of bentonite-sand soils?*

Guanidine clay-inhibiting treatments successfully increases flow rates by two orders of magnitude in 10% bentonite and 30% bentonite soils at any compaction. Additionally, swelling of the phyllosilicate interlayer is decreased significantly, which is critical in ensuring successful chemical delivery in the clayey soils. Visual inspection of guanidine saturated specimens reveals an open and aggregate pore

structure.

Guanidine pre-treatments included in the *Bio2Cementation* favored notable log-linear reductions of hydraulic conductivity with subsequent bio-cementation cycles. Specifically, 10% bentonite specimens at any compaction record reduced hydraulic conductivity by 50-30% per subsequent EICP injection. The decrease in hydraulic conductivity is explained by a modified matrix which facilitates crystal formation, whereby calcium carbonate precipitation increases tortuosity and clogs pore throats. The performance increase compared to the un-stabilized bio-cementation is explained by the successful clay-inhibitor treatment. However, the optimally compacted 30% bentonite soil displays little modification of flow by EICP in the *Bio2Cementation* technique, showing the upper limits of the bio-cementation of sand-bentonite.

3. How are the strength characteristics of a sand-bentonite altered using water saturated soils, GndHCl alone, or EICP-GndCl coupled treatment solutions?

The strength characteristics of *Bio2Cementation* treated samples improve significantly in successfully saturated tests. The failure mechanism changes from plastic bulging of untreated clayey soils, to brittle radial failure in guanidine and Gnd-EICP treated samples. More specifically, the coupled technique combines the added effect of bio-cementation and clay aggregation to strengthen the matrix. Peak strength and stiffness modulus are maximized for these tests. This can be explained by increased cohesion by calcite bridging bonds and increased interparticle friction.

Additionally, soil compaction has a large effect on the strength and stiffness gains of *Bio2Cementation*. Loose soils record doubled peak strength and various orders of magnitude increase in E50 modulus. The soil response is stronger and much stiffer than untreated specimens. However, in near optimally compacted soils, guanidine is the primary cause of increased strength.

Lastly, unsaturated samples display extremely cohesive and strong plastic behaviour. Untreated 30% bentonite soils, failed to saturate, but displayed significant peak strength conferred by large suction effects. The deformation is plastic over very large axial strains (>10%).

4. With specific attention to soil matrix, grain morphology, and nucleation sites; how is the microstructure of a sand-bentonite modified by GndHCl alone and EICP-GndHCl treatment solutions?

Column specimens treated via *Bio2Cementation* are vigorously cemented, showing extensive precipitation for 10% bentonite (any compaction) and the looser 30% bentonite samples. Guanidine treatments increase the share of coarse voids, significantly improving the precipitation of calcium carbonate. Soils pre-treated with guanidine display extensive nucleation on sand grains and bentonite aggregate alike. The largest proportion of bridging bonds occur in 10% bentonite soils. Calcium carbonate precipitates as rhombohedral, cubic and modulated calcite polymorphs. Aragonite rods are only occasionally found, with no vaterite detected. Mesocrystals (200[μm]) are favored in coarse pores of the low compaction samples, whereas microcrystals (~50[μm]) are consistently precipitated in propagated networks in any soil type. Additionally, in guanidine modifies the clayey matrix, favoring bentonite aggregation and low plasticity features. The technique fails to significantly bio-cement the optimally compacted 30% bentonite sample. Sparse crystals clad the sample heterogeneously, and the specimens share features more akin to the guanidine free EICP (fibrous textures, no nucleation on clays, traces of spherical vaterite, etc.).

6.2 Concluding Remarks

The two phase *Bio2Cementation* treatment proposes a simple, readily reproducible, soil strengthening solution. Reagent mixing, dilution and treatment injections are performed efficiently

with the proposed procedure. The thesis' research combines test-tube experiments and treatment of two artificial clayey soils (sand-bentonite), to test the following research hypothesis:

“Individually treating the complex clay fraction and the sand fraction, leads to the combine effect of a stable and stronger clayey soil matrix.”

To garner insight on *Bio2Cementation*'s effect, the testing program explores the modifications of hydraulic conductivity, strength parameters, and microstructural characteristics of the media. The hydraulic conductivity is greatly improved by guanidine, and the inhibited clays allow EICP to nucleate upon sand and bentonite aggregates alike. *Bio2Cementation* greatly alters the porous media of 10% bentonite-sand mixes at any compaction. Thanks to the clay-inhibitory treatments by guanidine, EICP injections homogeneously precipitate stable calcite-aragonite crystals in the matrix. Bridging calcium carbonate crystals cement sand grains and clay aggregates alike, increasing strength and stiffness of the medium. Additionally, loosely compacted 30% bentonite show successful bio-cementation, with homogeneous calcite growth in the coarse inter-grain voids. Nonetheless, *Bio2Cementation* is found to be unsuccessful in optimally compacted 30% bentonite. In such media, the clay fraction dominates the hydraulic response and microstructure. Bio-cementation is not successful, and the strength gains are unsatisfactory. The accumulated knowledge base is used to answer the main research question:

“Can the microstructure and strength characteristics of a sand-bentonite soil be improved by combining guanidine hydrochloride clay stabilization and enzyme induced calcite precipitation?”

This thesis successfully improves bio-cementation in sand-bentonite by proposing a novel approach named *Bio2Cementation*. The work shows that coupling clay inhibition by guanidine improves enzyme induced calcite precipitation. The findings display promise in expanding bio-cementation's applicability to natural clay bearing sands. However, the proposed technique does show limitations. It is found to be best suited for strengthening loosely compacted soils and coarse grain dominated media (expected to occur at <15% bentonite-sand content (Biju and Arnepali, 2020)).

6.3 Future Potential

Bio2Cementation is promising in successfully strengthen soils compositing of clay and sand fractions, by treating each component individually. The outcome has been shown to provide coupled potential in cumulatively improving a soils' physical properties. Additionally, the novel idea also opens the door to various knowledge gaps and concerns to be addressed. To summarize the future potential arisen in this work, an outline for a research proposal combining Bio-Geochemistry and Geomechanics is summarized below. It is organized in general considerations and two interdisciplinary branches:

General Considerations

The low concentration, non-equimolar *Bio2Cementation* technique is proven to precipitate calcium carbonate crystals in sand-bentonite soils. For this reason, the proposed methodology and reagent concentrations are recommended for future research.

The utilization of *Jackbean urease* 3[U/mg] activity is strongly recommended over the lyophilized *Canvalia Ensiformis* 8[U/mg]. The reaction rates vary dramatically, with the latter precipitating excessive calcite outside the soil matrix during two hour injections. Additionally, the former favors precipitation of stable calcite-aragonite polymorphs.

The artificial soil acts as a control variable throughout the thesis. Impermeable liner grade soils (30% bentonite) are realistically less susceptible to requiring soil strengthening engineering solutions. Therefore, future research using sand-bentonite should use 20% ratios to improve sample saturation,

reducing time constraints. Such clay content would potentially fill knowledge gaps of other unsuccessful MICP research in clayey soils.

This work results in successful bio-cementation of bentonite-sand media. It remains to be proved that such polyvalence is valid for other clay types, such as common kaolinite. Therefore, a standardized batch testing varying the clay constituents would expand the engineering applicability of the research.

Bio-geochemistry of *Bio2Cementation*

The proposed treatment supersaturates 10% bentonite specimens with guanidine. An cost-cutting optimization of the technique could envision to modify the clay-inhibitor concentrations in function of in-situ clay content. The investigation would comprise of a cation exchange analysis, which may envision an empirical correlation between the guanidine correlation and a soil's clay content. This would reduce cost and residual chemicals in the pore solution.

The time dependency of EICP is a key knowledge gap moving forward. Successful engineering practice would require greater control over the reaction rate. Greater injection volumes require slow or delayed reactions, to precipitate the cement in the soil only. This thesis sees future potential in integrating additives of 0.25[mol/L] guanidine hydrochloride in the EICP recipe as means to slow the reaction rate (tested only for *Canvalia Ensiformis* 8[U/mg], see 8.7.3). Test tube experiments should monitor pH and EC evolution over time as proxies of the EICP kinetics, whereas calcium carbonate polymorphs should be verified by SEM imaging following the reaction's completion.

In view of bio-cementing natural soils in an anthropic environment, the civil structure interaction should be researched. Residual chlorinates salts in the residual porous media may tend to strongly oxidize metallic compounds, such as steel reinforcements in embedded structures. Therefore, it is recommended to investigate the impact of pore fluid chemistry on civil structures.

Geomechanics of *Bio2Cementation*

This thesis displays the potential of bio-cementation to improve the mechanical parameters of peak strength and stiffness in clayey soils. Nonetheless, questions are raised regarding the shear and unsaturated behaviour at varying clay contents. The addressed knowledge gap is whether the improved shear strength of guanidine treated sand-bentonite (Minder, 2016) is significantly improved by coupling with bio-cementation. The injection of *Bio2Cementation* in larger cylindrical samples would allow the characterization of cohesion, undrained and drained response, friction angle in a triaxial apparatus.

Furthermore, it is recommended to complement strength tests with SEM imaging. Sampling is recommended along failure plane soil matrix to identify the mineralogy and microstructure of weaker regions. Additionally, this stimulates crossover research between the cement and geomechanics labs.

7 References

- Aaron, J., McDougall, S., & Nolde, N. (2019). Two methodologies to calibrate landslide runout models. *Landslides*, 16(5), 907–920. <https://doi.org/10.1007/s10346-018-1116-8>
- Agudo, E. R., & Putnis, C. V. (2012). Direct observations of mineral fluid reactions using atomic force microscopy: The specific example of calcite. *Mineralogical Magazine*, 76(1), 227–253. <https://doi.org/10.1180/minmag.2012.076.1.227>
- Agus, S. S., Schanz, T., & Fredlund, D. G. (2010). Measurements of suction versus water content for bentonite–sand mixtures. *Canadian Geotechnical Journal*, 47(5), 583–594. <https://doi.org/10.1139/T09-120>
- Ahenkorah, I., Rahman, M. M., Karim, M. R., Beecham, S., & Saint, C. (2021). A Review of Enzyme Induced Carbonate Precipitation (EICP): The Role of Enzyme Kinetics. *Sustainable Chemistry*, 2(1), 92–114. <https://doi.org/10.3390/suschem2010007>
- Almajed, A. A. (n.d.). *Enzyme Induced Carbonate Precipitation (EICP) for Soil Improvement*. 149.
- Almajed, A., Khodadadi Tirkolaei, H., & Kavazanjian, E. (2018). Baseline Investigation on Enzyme-Induced Calcium Carbonate Precipitation. *Journal of Geotechnical and Geoenvironmental Engineering*, 144(11), 04018081. [https://doi.org/10.1061/\(ASCE\)GT.1943-5606.0001973](https://doi.org/10.1061/(ASCE)GT.1943-5606.0001973)
- Almajed, A., Tirkolaei, H. K., Kavazanjian, E., & Hamdan, N. (2019). Enzyme Induced Biocementated Sand with High Strength at Low Carbonate Content. *Scientific Reports*, 9(1), 1135. <https://doi.org/10.1038/s41598-018-38361-1>
- Ameta, N., & Wayal, A. (2008). Effect of Bentonite on Permeability of Dune Sand. *Electronic Journal of Geotechnical Engineering*, 13.
- Arab, M. G., Alsodi, R., Almajed, A., Yasuhara, H., Zeiada, W., & Shahin, M. A. (2021). State-of-the-Art Review of Enzyme-Induced Calcite Precipitation (EICP) for Ground Improvement: Applications and Prospects. *Geosciences*, 11(12), 492. <https://doi.org/10.3390/geosciences11120492>
- Arab, M. G., Omar, M., Almajed, A., Elbaz, Y., & Ahmed, A. H. (2021). Hybrid technique to produce bio-bricks using enzyme-induced carbonate precipitation (EICP) and sodium alginate biopolymer. *Construction and Building Materials*, 284, 122846. <https://doi.org/10.1016/j.conbuildmat.2021.122846>
- Arganda-Carreras, I., Kaynig, V., Rueden, C., Eliceiri, K. W., Schindelin, J., Cardona, A., & Sebastian Seung, H. (2017). Trainable Weka Segmentation: A machine learning tool for microscopy pixel classification. *Bioinformatics*, 33(15), 2424–2426. <https://doi.org/10.1093/bioinformatics/btx180>
- Askarnejad, A. (n.d.). *Soil classification*. 34.
- Bendou, S., & Amrani, M. (2014). Effect of Hydrochloric Acid on the Structural of Sodic-Bentonite Clay. *Journal of Minerals and Materials Characterization and Engineering*, 02(05), 404–413. <https://doi.org/10.4236/jmmce.2014.25045>
- Bergaya, F., & Lagaly, G. (2011). Intercalation processes of layered minerals. In M. F. Brigatti & A. Mottana (Eds.), *Layered Mineral Structures and their Application in Advanced Technologies* (pp. 259–284). Mineralogical Society of Great Britain and Ireland. <https://doi.org/10.1180/EMU-notes.11.7>
- Bick, P., Bastola, H., Suleiman, M. T., Gu, J., Diplas, P., Brown, D. G., & Zouari, N. (2019). Minimizing Wind Erosion Using Microbial Induced Carbonate Precipitation. *Geo-Congress 2019*, 223–230. <https://doi.org/10.1061/9780784482117.022>
- Biju, M. S., & Arnepalli, D. N. (2020). Effect of biopolymers on permeability of sand-bentonite mixtures. *Journal of Rock Mechanics and Geotechnical Engineering*, 12(5), 1093–1102. <https://doi.org/10.1016/j.irmge.2020.02.004>
- Bouchemella, S., & Taibi, S. (2022). Effect of suction on the mechanical behaviour of unsaturated compacted clay–sand mixtures. *Studia Geotechnica et Mechanica*, 44(3), 175–189. <https://doi.org/10.2478/sgem-2022-0016>
- Buazar, F. (2019). Impact of Biocompatible Nanosilica on Green Stabilization of Subgrade Soil. *Scientific Reports*, 9(1), 15147. <https://doi.org/10.1038/s41598-019-51663-2>
- Cabalar, A. F., Khalaf, M. M., & Karabash, Z. (2018). Shear modules of claysand mixtures using bender element test. *Acta Geotechnica Slovenica*, 15(1), 3–15. <https://doi.org/10.18690/actageotechslov.15.1.3-15.2018>
- Cardoso, R., Pires, I., Duarte, S. O. D., & Monteiro, G. A. (2018). Effects of clay's chemical interactions on biocementation. *Applied Clay Science*, 156, 96–103. <https://doi.org/10.1016/j.clay.2018.01.035>
- Carraro, J. A. H., Prezzi, M., & Salgado, R. (2009). Shear Strength and Stiffness of Sands Containing Plastic or Nonplastic Fines. *Journal of Geotechnical and Geoenvironmental Engineering*, 135(9), 1167–1178. [https://doi.org/10.1061/\(ASCE\)1090-0241\(2009\)135:9\(1167\)](https://doi.org/10.1061/(ASCE)1090-0241(2009)135:9(1167))
- Chang, I., Lee, M., Tran, A. T. P., Lee, S., Kwon, Y.-M., Im, J., & Cho, G.-C. (2020). Review on biopolymer-based soil treatment (BPST) technology in geotechnical engineering practices. *Transportation Geotechnics*, 24, 100385. <https://doi.org/10.1016/j.trgeo.2020.100385>
- Charkley, F. N., Zhang, K., & Mei, G. (2019). Shear Strength of Compacted Clays as Affected by Mineral Content and Wet-Dry Cycles. *Advances in Civil Engineering*, 2019, 1–8. <https://doi.org/10.1155/2019/8217029>
- Cheng, L., Cord-Ruwisch, R., & Shahin, M. A. (2013). Cementation of sand soil by microbially induced calcite precipitation at various degrees of saturation. *Canadian Geotechnical Journal*, 50(1), 81–90. <https://doi.org/10.1139/cgj-2012-0023>
- Cheng, L., Shahin, M. A., Cord-Ruwisch, R., Addis, M., Hartanto, T., & Elms, C. (n.d.). *Soil Stabilisation by Microbial-Induced Calcite Precipitation (MICP): Investigation into Some Physical and Environmental Aspects*. 9.

- Ciardi, G., Bardotti, R., Vannucchi, G., & Madiai, C. (2020). Effects of high-diluted colloidal silica grouting on the behaviour of a liquefiable sand. *Geotechnical Research*, 7(4), 193–208. <https://doi.org/10.1680/jgere.20.00010>
- Claes, S., Van De Walle, W., Islahuddin, M., & Janssen, H. (2020). The application of computed tomography for characterizing the pore structure of building materials. *Journal of Building Physics*, 43(4), 254–276. <https://doi.org/10.1177/1744259119880927>
- Conlee, C. T. (2010). *Dynamic properties of colloidal silica soils using centrifuge model tests and a full-scale field test* [Doctor of Philosophy, Drexel University]. <https://doi.org/10.17918/etd-3248>
- Das, D., Kalita, T., & Chetia, M. (2020). Influence of Strain Rate on Unconfined Compressive Strength of Bentonite and Sand Mixes. In M. Latha Gali & R. R. P. (Eds.), *Geotechnical Characterization and Modelling* (Vol. 85, pp. 195–204). Springer Singapore. https://doi.org/10.1007/978-981-15-6086-6_16
- de Jong, E. (2021). *Soil improvement and deep excavations* [CEG Lecture].
- de Oliveira, J. A. T., Pires, L. F., Cássaro, F. A. M., Gaspareto, J. V., Posadas, A. N. D., & Mooney, S. J. (2022). Soil pore system complexity and heterogeneity as affected by contrasting management practices. *Soil and Tillage Research*, 224, 105497. <https://doi.org/10.1016/j.still.2022.105497>
- DeJong, J. T., Mortensen, B. M., Martinez, B. C., & Nelson, D. C. (2010). Bio-mediated soil improvement. *Ecological Engineering*, 36(2), 197–210. <https://doi.org/10.1016/j.ecoleng.2008.12.029>
- Di Maio, C., Santoli, L., & Schiavone, P. (2004). Volume change behaviour of clays: The influence of mineral composition, pore fluid composition and stress state. *Mechanics of Materials*, 36(5–6), 435–451. [https://doi.org/10.1016/S0167-6636\(03\)00070-X](https://doi.org/10.1016/S0167-6636(03)00070-X)
- Donker, R. S. (n.d.). *Experimental Characterization of the Constraints on Enzyme Induced Carbonate Precipitation*. 138.
- Doube, M., Klosowski, M. M., Arganda-Carreras, I., Cordelières, F. P., Dougherty, R. P., Jackson, J. S., Schmid, B., Hutchinson, J. R., & Shefelbine, S. J. (2010). BoneJ: Free and extensible bone image analysis in ImageJ. *Bone*, 47(6), 1076–1079. <https://doi.org/10.1016/j.bone.2010.08.023>
- Egli, M., Mirabella, A., Sartori, G., Giaccai, D., Zanelli, R., & Plötze, M. (2007). Effect of slope aspect on transformation of clay minerals in Alpine soils. *Clay Minerals*, 42(3), 373–398. <https://doi.org/10.1180/claymin.2007.042.3.09>
- Elhadj, S., Salter, E. A., Wierzbicki, A., De Yoreo, J. J., Han, N., & Dove, P. M. (2006). Peptide Controls on Calcite Mineralization: Polyaspartate Chain Length Affects Growth Kinetics and Acts as a Stereochemical Switch on Morphology. *Crystal Growth & Design*, 6(1), 197–201. <https://doi.org/10.1021/cg050288+>
- Elmashad, M. E., & Ata, A. A. (2016). Effect of seawater on consistency, infiltration rate and swelling characteristics of montmorillonite clay. *HBRC Journal*, 12(2), 175–180. <https://doi.org/10.1016/j.hbrj.2014.12.004>
- Gao, Y., He, J., Tang, X., & Chu, J. (2019). Calcium carbonate precipitation catalyzed by soybean urease as an improvement method for fine-grained soil. *Soils and Foundations*, 59(5), 1631–1637. <https://doi.org/10.1016/j.sandf.2019.03.014>
- Ghadr, S., Assadi-Langroudi, A., Hung, C., O’Kelly, B. C., Bahadori, H., & Ghodsi, T. (2020). Stabilization of Sand with Colloidal Nano-Silica Hydrosols. *Applied Sciences*, 10(15), 5192. <https://doi.org/10.3390/app10155192>
- Ghalamzan, F., De Rosa, J., Gajo, A., & Di Maio, C. (2022). Swelling and swelling pressure of a clayey soil: Experimental data, model simulations and effects on slope stability. *Engineering Geology*, 297, 106512. <https://doi.org/10.1016/j.enggeo.2021.106512>
- Glastonbury, J., & Fell, R. (2008). Geotechnical characteristics of large slow, very slow, and extremely slow landslides. *Canadian Geotechnical Journal*, 45(7), 984–1005. <https://doi.org/10.1139/T08-021>
- Guanidine HCl | Guanidine HCl GMP Denaturant—Bio Spectra. (n.d.). Retrieved 18 February 2022, from <https://www.biospectra.us/products/biological-buffers-and-denaturants-bulk-gmp/guanidine-hcl-gmp-denaturant>
- Hamdan, N., Kavazanjian, E., Rittmann, B. E., & Karatas, I. (2017). Carbonate Mineral Precipitation for Soil Improvement Through Microbial Denitrification. *Geomicrobiology Journal*, 34(2), 139–146. <https://doi.org/10.1080/01490451.2016.1154117>
- Hamderi, M., & Gallagher, P. M. (n.d.). *An optimization study on the delivery distance of colloidal silica*. 11.
- Handwerker, A. L., Roering, J. J., & Schmidt, D. A. (2013). Controls on the seasonal deformation of slow-moving landslides. *Earth and Planetary Science Letters*, 377–378, 239–247. <https://doi.org/10.1016/j.epsl.2013.06.047>
- Hicher, P., & Laloui, L. (n.d.). *OPEN Direct currents stimulate*. 15.
- Hora, P. I., Pati, S. G., McNamara, P. J., & Arnold, W. A. (2020). Increased Use of Quaternary Ammonium Compounds during the SARS-CoV-2 Pandemic and Beyond: Consideration of Environmental Implications. *Environmental Science & Technology Letters*, 7(9), 622–631. <https://doi.org/10.1021/acs.estlett.0c00437>
- Hu, Y., Yang, Q., Kou, J., Sun, C., & Li, H. (2020). Aggregation mechanism of colloidal kaolinite in aqueous solutions with electrolyte and surfactants. *PLOS ONE*, 15(9), e0238350. <https://doi.org/10.1371/journal.pone.0238350>
- Iravanian, A., & Bilsel, H. (2016). Tensile Strength Properties of Sand-bentonite Mixtures Enhanced with Cement. *Procedia Engineering*, 143, 111–118. <https://doi.org/10.1016/j.proeng.2016.06.015>
- Ivanov, V., & Chu, J. (2008). Applications of microorganisms to geotechnical engineering for bioclogging and biocementation of soil in situ. *Reviews in Environmental Science and Bio/Technology*, 7(2), 139–153. <https://doi.org/10.1007/s11157-007-9126-3>
- Jiang, N.-J., & Soga, K. (2017). The applicability of microbially induced calcite precipitation (MICP) for internal erosion control in gravel–sand mixtures. *Géotechnique*, 67(1), 42–55. <https://doi.org/10.1680/jgeot.15.P.182>
- Jozefaciuk, G., Skic, K., Adamczuk, A., Boguta, P., & Lamorski, K. (2021). Structure and Strength of Artificial Soils Containing Monomineral Clay Fractions. *Materials*, 14(16), 4688. <https://doi.org/10.3390/ma14164688>
- Kakavand, A. (2018). *Experimental Study of Applying Colloidal Nano Silica in Improving Sand-Silt Mixtures*. 17.

- Khodadadi Tirkolaei, H., Javadi, N., Krishnan, V., Hamdan, N., & Kavazanjian, E. (2020). Crude Urease Extract for Biocementation. *Journal of Materials in Civil Engineering*, 32(12), 04020374. [https://doi.org/10.1061/\(ASCE\)MT.1943-5533.0003466](https://doi.org/10.1061/(ASCE)MT.1943-5533.0003466)
- Kirkland, C. M., Norton, D., Firth, O., Eldring, J., Cunningham, A. B., Gerlach, R., & Phillips, A. J. (2019). Visualizing MICP with X-ray μ -CT to enhance cement defect sealing. *International Journal of Greenhouse Gas Control*, 86, 93–100. <https://doi.org/10.1016/j.ijggc.2019.04.019>
- Koestel, J. (2018). SoilJ: An ImageJ Plugin for the Semiautomatic Processing of Three-Dimensional X-ray Images of Soils. *Vadose Zone Journal*, 17(1), 170062. <https://doi.org/10.2136/vzj2017.03.0062>
- Komine, H., Yasuhara, K., & Murakami, S. (2009). Swelling characteristics of bentonites in artificial seawater. *Canadian Geotechnical Journal*, 46(2), 177–189. <https://doi.org/10.1139/T08-120>
- Konstantinou, C., Biscontin, G., Jiang, N.-J., & Soga, K. (2021). Application of microbially induced carbonate precipitation to form bio-cemented artificial sandstone. *Journal of Rock Mechanics and Geotechnical Engineering*, 13(3), 579–592. <https://doi.org/10.1016/j.jrmge.2021.01.010>
- Legland, D., Arganda-Carreras, I., & Andrey, P. (2016). MorphoLibJ: Integrated library and plugins for mathematical morphology with ImageJ. *Bioinformatics*, btw413. <https://doi.org/10.1093/bioinformatics/btw413>
- Leik, A. B. (2020). LABORATORY SCALE EVALUATION OF THE FEASIBILITY OF USING GUANIDINIUM SALTS AS A MEANS OF INSITU SOIL STRENGTHENING FOR WEAK CLAYS [Degree Master of Science, University of Saskatchewan]. <http://hdl.handle.net/10388/13075>
- Li, J., Ma, J., Jiang, T., Wang, Y., Wen, X., & Li, G. (2015). Constructing Biopolymer-Inorganic Nanocomposite through a Biomimetic Mineralization Process for Enzyme Immobilization. *Materials*, 8(9), 6004–6017. <https://doi.org/10.3390/ma8095286>
- Lormand, C., Zellmer, G. F., Németh, K., Kilgour, G., Mead, S., Palmer, A. S., Sakamoto, N., Yurimoto, H., & Moebis, A. (2018). Weka Trainable Segmentation Plugin in ImageJ: A Semi-Automatic Tool Applied to Crystal Size Distributions of Microlites in Volcanic Rocks. *Microscopy and Microanalysis*, 24(6), 667–675. <https://doi.org/10.1017/S1431927618015428>
- Ma, G., He, X., Jiang, X., Liu, H., Chu, J., & Xiao, Y. (2021). Strength and permeability of bentonite-assisted biocemented coarse sand. *Canadian Geotechnical Journal*, 58(7), 969–981. <https://doi.org/10.1139/cgj-2020-0045>
- Mahawish, A., Bouazza, A., & Gates, W. P. (2018). Improvement of Coarse Sand Engineering Properties by Microbially Induced Calcite Precipitation. *Geomicrobiology Journal*, 35(10), 887–897. <https://doi.org/10.1080/01490451.2018.1488019>
- Martin, K. K., Khodadadi Tirkolaei, H., & Kavazanjian, E. (2021). Mid-scale biocemented soil columns via enzyme-induced carbonate precipitation (EICP). *Soils and Foundations*, 61(6), 1529–1542. <https://doi.org/10.1016/j.sandf.2021.09.001>
- McDaniel, C. R., Shumway, W. W., & Davidson, E. (2016). CA2951241—GUANIDINE- OR GUANIDINIUM-CONTAINING COMPOUNDS FOR TREATMENT OF SUBTERRANEAN FORMATIONS (Canadian Patent Office Patent No. 2951241).
- McDuff, F.-O., Doucet, A., & Beaugregard, M. (2004). Low concentration of guanidine hydrochloride induces the formation of an aggregation-prone state in α -urease. *Biochemistry and Cell Biology*, 82(2), 305–313. <https://doi.org/10.1139/o03-072>
- Mildner, P., & Mihanovic, B. (1974). Inhibition of Urease by Some Triazole, Urea and Guanidine Derivatives. *Croatica Chemica ACTA*, CCA-822(46), 79–82.
- Minder, P. (2016). *Applications of Chemical Modification of Smectite Clays in Geotechnical Problems* (p. 1 Band) [ETH Zurich; Application/pdf]. <https://doi.org/10.3929/ETHZ-A-010700643>
- Minder, P., & Puzrin, A. M. (2013). Microstructural changes leading to chemically enhanced drainage. *Technical Committee 105 Geo-Mechanics from Micro to Macro*, 1027–1030.
- Minder, P., & Puzrin, A. M. (2017). Geotechnical applications of chemically enhanced drainage: Geotechnical Applications of Chemically Enhanced Drainage. *International Journal for Numerical and Analytical Methods in Geomechanics*, 41(15), 1541–1568. <https://doi.org/10.1002/nag.2685>
- Minder, P., Puzrin, A. M., & Plötze, M. (2016). Enhanced delivery of chemical agents in soil improvement applications. *Géotechnique*, 66(6), 469–480. <https://doi.org/10.1680/jgeot.15.P.127>
- Minto, J. M., MacLachlan, E., El Mountassir, G., & Lunn, R. J. (2016). Rock fracture grouting with microbially induced carbonate precipitation: ROCK FRACTURE GROUTING WITH MICP. *Water Resources Research*, 52(11), 8827–8844. <https://doi.org/10.1002/2016WR018884>
- Mitchell, J. K., & Soga, K. (2005). *Fundamentals of soil behavior* (3rd ed). John Wiley & Sons.
- Naeimi, M., & Haddad, A. (2018). Investigation on the Environmental Impact of Soil Improvement Techniques: Comparison of Cement Grouting and Biocement. In A. Farid & H. Chen (Eds.), *Proceedings of GeoShanghai 2018 International Conference: Geoenvironment and Geohazard* (pp. 483–490). Springer Singapore. https://doi.org/10.1007/978-981-13-0128-5_53
- Nam, I.-H., Chon, C.-M., Jung, K.-Y., Choi, S.-G., Choi, H., & Park, S.-S. (2015). Calcite precipitation by ureolytic plant (*Canavalia ensiformis*) extracts as effective biomaterials. *KSCE Journal of Civil Engineering*, 19(6), 1620–1625. <https://doi.org/10.1007/s12205-014-0558-3>
- Neupane, D., Yasuhara, H., Kinoshita, N., & Putra, H. (2015). Distribution of grout material within 1-m sand column in insitu calcite precipitation technique. *Soils and Foundations*, 55(6), 1512–1518. <https://doi.org/10.1016/j.sandf.2015.10.015>
- Neupane, D., Yasuhara, H., Kinoshita, N., & Unno, T. (2013). Applicability of Enzymatic Calcium Carbonate Precipitation as a Soil-Strengthening Technique. *Journal of Geotechnical and Geoenvironmental Engineering*, 139(12), 2201–2211. [https://doi.org/10.1061/\(ASCE\)GT.1943-5606.0000959](https://doi.org/10.1061/(ASCE)GT.1943-5606.0000959)
- Oral, Ç. M., & Ercan, B. (2018). Influence of pH on morphology, size and polymorph of room temperature synthesized calcium carbonate particles. *Powder Technology*, 339, 781–788. <https://doi.org/10.1016/j.powtec.2018.08.066>
- Osmanlioglu, A. E. (2016). *Evaluation on Mechanical Stabilities of Clay-Sand Mixtures Used as Engineered Barrier for Radioactive Waste Disposal*. 10(6), 4.

- Ougier-Simonin, A., Renard, F., Boehm, C., & Vidal-Gilbert, S. (2016). Microfracturing and microporosity in shales. *Earth-Science Reviews*, 162, 198–226. <https://doi.org/10.1016/j.earscirev.2016.09.006>
- Pham, V. P., Nakano, A., van der Star, W. R. L., Heimovaara, T. J., & van Paassen, L. A. (2018). Applying MICP by denitrification in soils: A process analysis. *Environmental Geotechnics*, 5(2), 79–93. <https://doi.org/10.1680/jenge.15.00078>
- Plotze, M., & Kahr, G. (2008). Diagnostic intercalation in clay minerals – use of Guanidine carbonate. *Mineralogia*, 33, 132.
- Proia, R., Croce, P., & Modoni, G. (2016). Experimental Investigation of Compacted Sand-bentonite Mixtures. *Procedia Engineering*, 158, 51–56. <https://doi.org/10.1016/j.proeng.2016.08.404>
- Putra, H., Yasuhara, H., Erizal, Sutoyo, & Fauzan, M. (2020). Review of Enzyme-Induced Calcite Precipitation as a Ground-Improvement Technique. *Infrastructures*, 5(8), 66. <https://doi.org/10.3390/infrastructures5080066>
- Qu, Y., Wang, R., Gao, S., Huang, H., Zhang, Z., Ren, H., Yuan, Y., Wang, Q., Wang, X., & Du, W. (2022). Study on the Shale Hydration Inhibition Performance of Triethylammonium Acetate. *Minerals*, 12(5), 620. <https://doi.org/10.3390/min12050620>
- Quainoo, A. K., Negash, B. M., Bavoh, C. B., Ganat, T. O., & Tackie-Otoo, B. N. (2020). A perspective on the potential application of bio-inhibitors for shale stabilization during drilling and hydraulic fracturing processes. *Journal of Natural Gas Science and Engineering*, 79, 103380. <https://doi.org/10.1016/j.jngse.2020.103380>
- Rahman, M. T., Negash, B. M., Moniruzzaman, M., Quainoo, A. K., Bavoh, C. B., & Padmanabhan, E. (2020). An Overview on the potential application of ionic liquids in shale stabilization processes. *Journal of Natural Gas Science and Engineering*, 81, 103480. <https://doi.org/10.1016/j.jngse.2020.103480>
- Ross, J. M. (n.d.). *For Soil Improvement for Finer-Grained Soils*. 95.
- Sarkar, A., & Mahapatra, S. (2012). Mechanism of unusual polymorph transformations in calcium carbonate: Dissolution-recrystallization vs additive-mediated nucleation. *Journal of Chemical Sciences*, 124(6), 1399–1404. <https://doi.org/10.1007/s12039-012-0339-9>
- Saur, H., Sénéchal, P., Boiron, T., Aubourg, C., Derluyn, H., & Moonen, P. (2020). First investigation of quartz and calcite shape fabrics in strained shales by means of X-ray tomography. *Journal of Structural Geology*, 130, 103905. <https://doi.org/10.1016/j.jsg.2019.103905>
- Schindelin, J., Arganda-Carreras, I., Frise, E., Kaynig, V., Longair, M., Pietzsch, T., Preibisch, S., Rueden, C., Saalfeld, S., Schmid, B., Tinevez, J.-Y., White, D. J., Hartenstein, V., Eliceiri, K., Tomancak, P., & Cardona, A. (2012). Fiji: An open-source platform for biological-image analysis. *Nature Methods*, 9(7), 676–682. <https://doi.org/10.1038/nmeth.2019>
- Schneider, C. A., Rasband, W. S., & Eliceiri, K. W. (2012). NIH Image to ImageJ: 25 years of image analysis. *Nature Methods*, 9(7), 671–675. <https://doi.org/10.1038/nmeth.2089>
- Schulz, W. H., Coe, J. A., Ricci, P. P., Smoczyk, G. M., Shurtleff, B. L., & Panosky, J. (2017). Landslide kinematics and their potential controls from hourly to decadal timescales: Insights from integrating ground-based InSAR measurements with structural maps and long-term monitoring data. *Geomorphology*, 285, 121–136. <https://doi.org/10.1016/j.geomorph.2017.02.011>
- Sharma, A., & R., R. (2016). Study on effect of Microbial Induced Calcite Precipitates on strength of fine grained soils. *Perspectives in Science*, 8, 198–202. <https://doi.org/10.1016/j.pisc.2016.03.017>
- Sharma, L. K., Singh, R., Ahmad, M., Umrao, R. K., & Singh, T. N. (2017). Experimental Evaluation of Geomechanical Behaviour of Bentonite-Sand Mixture for Nuclear Waste Disposal. *Procedia Engineering*, 191, 386–393. <https://doi.org/10.1016/j.proeng.2017.05.195>
- Shirazi, S. M., Wiat, S., Kuwano, J., & Kazama, H. (2011). Salinity effect on swelling characteristics of compacted bentonite. *Environment Protection Engineering*, 37(2), 65–74.
- Sivrikaya, O., Kilic, A. M., Yalcin, M. G., Aykamis, A. S., & Sonmez, M. (2008). The 2001 Adana landslide and its destructive effects, Turkey. *Environmental Geology*, 54(7), 1489–1500. <https://doi.org/10.1007/s00254-007-0930-4>
- Sposito, G. (2018). Gouy-Chapman Theory. In W. M. White (Ed.), *Encyclopedia of Geochemistry* (pp. 623–628). Springer International Publishing. https://doi.org/10.1007/978-3-319-39312-4_50
- Springman, S. M., Askarinejad, A., & Casini, F. (2009, October). Landslide triggering experiment in a steep forested slope in Switzerland. *Proceedings of the 17th International Conference on Soil Mechanics and Geotechnical Engineering*.
- Sridharan, A., & Prakash, K. (2000). Classification procedures for expansive soils. *Proceedings of the Institution of Civil Engineers - Geotechnical Engineering*, 143(4), 235–240. <https://doi.org/10.1680/jenge.2000.143.4.235>
- Stark, T. D., Baghdady, A. K., Hungr, O., & Aaron, J. (2017). Case Study: Oso, Washington, Landslide of March 22, 2014—Material Properties and Failure Mechanism. *Journal of Geotechnical and Geoenvironmental Engineering*, 143(5), 05017001. [https://doi.org/10.1061/\(ASCE\)GT.1943-5606.0001615](https://doi.org/10.1061/(ASCE)GT.1943-5606.0001615)
- Stephenson, A. E., DeYoreo, J. J., Wu, L., Wu, K. J., Hoyer, J., & Dove, P. M. (2008). Peptides Enhance Magnesium Signature in Calcite: Insights into Origins of Vital Effects. *Science*, 322(5902), 724–727. <https://doi.org/10.1126/science.1159417>
- Studel, A., & Emmerich, K. (2013). Strategies for the successful preparation of homoionic smectites. *Applied Clay Science*, 75–76, 13–21. <https://doi.org/10.1016/j.clay.2013.03.002>
- Strzelecki, P. J., Świerczewska, A., Kopczewska, K., Fheed, A., Tarasiuk, J., & Wroński, S. (2021). Decoding Rocks: An Assessment of Geomaterial Microstructure Using X-ray Microtomography, Image Analysis and Multivariate Statistics. *Materials*, 14(12), 3266. <https://doi.org/10.3390/ma14123266>
- Studds, P., & Stewart, D. (1996). The effect of ion valence on the swelling behaviour of sodium montmorillonite. *Proceedings of the 4th International Conference on Re-Use of Contaminated Land and Landfills, Engineering Technics*, 139–142.
- Sun, X., Miao, L., & Chen, R. (2019). Effects of Different Clay's Percentages on Improvement of Sand-Clay Mixtures with Microbially Induced Calcite Precipitation. *Geomicrobiology Journal*, 36(9), 810–818. <https://doi.org/10.1080/01490451.2019.1631912>

- Svane, S., Sigurdarson, J. J., Finkenwirth, F., Eitingier, T., & Karring, H. (2020). Inhibition of urease activity by different compounds provides insight into the modulation and association of bacterial nickel import and ureolysis. *Scientific Reports*, *10*(1), 8503. <https://doi.org/10.1038/s41598-020-65107-9>
- Terzis, D., Bernier-Latmani, R., & Laloui, L. (2016). Fabric characteristics and mechanical response of bio-improved sand to various treatment conditions. *Géotechnique Letters*, *6*(1), 50–57. <https://doi.org/10.1680/jgele.15.00134>
- Terzis, D., & Laloui, L. (2018). 3-D micro-architecture and mechanical response of soil cemented via microbial-induced calcite precipitation. *Scientific Reports*, *8*(1), 1416. <https://doi.org/10.1038/s41598-018-19895-w>
- Terzis, D., & Laloui, L. (2019a). Cell-free soil bio-cementation with strength, dilatancy and fabric characterization. *Acta Geotechnica*, *14*(3), 639–656. <https://doi.org/10.1007/s11440-019-00764-3>
- Terzis, D., & Laloui, L. (2019b). A decade of progress and turning points in the understanding of bio-improved soils: A review. *Geomechanics for Energy and the Environment*, *19*, 100116. <https://doi.org/10.1016/j.gete.2019.03.001>
- Terzis, D., Laloui, L., Dornberger, S., & Harran, R. (2020). A Full-Scale Application of Slope Stabilization via Calcite Bio-Mineralization Followed by Long-Term GIS Surveillance. *Geo-Congress 2020*, 65–73. <https://doi.org/10.1061/9780784482834.008>
- Triantafyllos, P. K., Georgiannou, V. N., Pavlopoulou, E.-M., & Dafalias, Y. F. (2022). Strength and dilatancy of sand before and after stabilisation with colloidal-silica gel. *Géotechnique*, *72*(6), 471–485. <https://doi.org/10.1680/jgeot.19.P.123>
- van Paassen, L. A., Ghose, R., van der Linden, T. J. M., van der Star, W. R. L., & van Loosdrecht, M. C. M. (2010). Quantifying Biomediated Ground Improvement by Ureolysis: Large-Scale BiogROUT Experiment. *Journal of Geotechnical and Geoenvironmental Engineering*, *136*(12), 1721–1728. [https://doi.org/10.1061/\(ASCE\)GT.1943-5606.0000382](https://doi.org/10.1061/(ASCE)GT.1943-5606.0000382)
- Van Passen, L. (2009). *Ground Improvement by Microbially Induced Carbonate Precipitation* [PhD Thesis, TU Delft]. <http://resolver.tudelft.nl/uuid:5f3384c4-33bd-4f2a-8641-7c665433b57b>
- Vardanega, P. J., & Haigh, S. K. (2014). The undrained strength – liquidity index relationship. *Canadian Geotechnical Journal*, *51*(9), 1073–1086. <https://doi.org/10.1139/cgj-2013-0169>
- Vranna, A., & Tika, T. (2019). Laboratory improvement of liquefiable sand via colloidal silica and weak cementation. *Proceedings of the Institution of Civil Engineers - Ground Improvement*, 1–37. <https://doi.org/10.1680/jgrim.19.00019>
- Wagner, S., Cattle, S. R., & Scholten, T. (2007). Soil-aggregate formation as influenced by clay content and organic-matter amendment. *Journal of Plant Nutrition and Soil Science*, *170*(1), 173–180. <https://doi.org/10.1002/jpln.200521732>
- Wang, B., Xu, Y., Wang, X., Yuan, J. S., Johnson, C. H., Young, J. D., & Yu, J. (2021). A guanidine-degrading enzyme controls genomic stability of ethylene-producing cyanobacteria. *Nature Communications*, *12*(1), 5150. <https://doi.org/10.1038/s41467-021-25369-x>
- Whiffin, V. S. (2004). *Microbial CaCO₃ Precipitation for the production of biocement*. [PhD Thesis, School of Biological Sciences and Biotechnology, Murdoch University]. <https://researchrepository.murdoch.edu.au/id/eprint/399/>
- Yin, Y., Xing, A., Wang, G., Feng, Z., Li, B., & Jiang, Y. (2017). Experimental and numerical investigations of a catastrophic long-runout landslide in Zhenxiong, Yunnan, southwestern China. *Landslides*, *14*(2), 649–659. <https://doi.org/10.1007/s10346-016-0729-z>
- Yuan, H., Ren, G., Liu, K., Zheng, W., & Zhao, Z. (2020). Experimental Study of EICP Combined with Organic Materials for Silt Improvement in the Yellow River Flood Area. *Applied Sciences*, *10*(21), 7678. <https://doi.org/10.3390/app10217678>
- Zhao, M., Liu, G., Zhang, C., Guo, W., & Luo, Q. (2019). State-of-the-Art of Colloidal Silica-Based Soil Liquefaction Mitigation: An Emerging Technique for Ground Improvement. *Applied Sciences*, *10*(1), 15. <https://doi.org/10.3390/app10010015>

8.1 Clay Theory: a review

The following chapter presents a rough overview of clay theory, and is organized in four subsections. The overview discusses clay minerals, cation exchanges, double layer theory and the role of ionic species in pore fluids.

8.1.1 Clay Minerals

Organized crystal structures yield stable arrangements, minimizing the energy per unit volume. This is achieved by reaching neutrality, in accord with bond directionality, while minimizing ion repulsion. The silica-oxygen polyhedral (SiO_4)⁴⁻ is comprised of a small silica cation of valence 4. Oxygen repulsion organizes the molecules in a tetrahedral structure. Joins at its corners form different associations with other tetrahedra, and thus different crystal structures. Sheet silicates polymerize along 3/4 oxygens, forming (Si_2O_5)²⁻ planar structures (Figure 61).

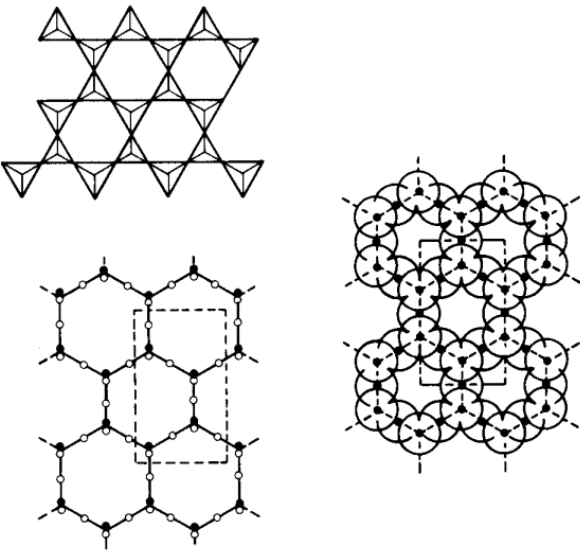
Combination of Tetrahedra	Diagrammatic Representation of Structure	Si-O Group and Negative Charge	Oxygen to Silicon Ratio	Example
Sheets		(Si_4O_{10}) _n ⁴⁻	5 : 2	Micas

Figure 61 - Silica tetrahedra organization in planar sheet mineral structures (Mitchell and Soga, 2005)

Differently, octahedral sheets are comprised of Mg/Al in octahedral coordination with oxygens or hydroxyls. Isomorphic substitutions occurring during crystal formation and alterations attribute net negative surface charges. For example, Mg²⁺/Al³⁺ ions in the octahedra are replaced by cations of lesser valence such as Fe²⁺, Mn²⁺ and more. Additional octahedral sheets include the gibbsite sheet (trivalent cation, mainly aluminum) and brucite sheets (divalent cation, mainly magnesium). Albeit less frequent, similar substitutions occur in the silica tetrahedra, by which Si⁴⁺ is replaced by Al³⁺. Clay minerals are grouped by idealized structures of stacked unit layers, generally sharing similar engineering properties.

Different bonds stack unit layers together; weak van der Waal forces (eg. neutral silicate layers), strong hydrogen bonding (eg. external oxygens bound to the silica tetrahedra form H-bonds with adsorbed water) and ionic bonds (eg. adsorbed cations both in the interlayer space and in the DDL). The force strength controls the interlayer distance (d-spacing). Such aggregates are known as clay minerals. They are predominantly small, contain net surface charges, exhibit plastic behaviour and are resistant to weathering. The synthesis of various clay minerals from oxygen and cations are shown in Figure 62.

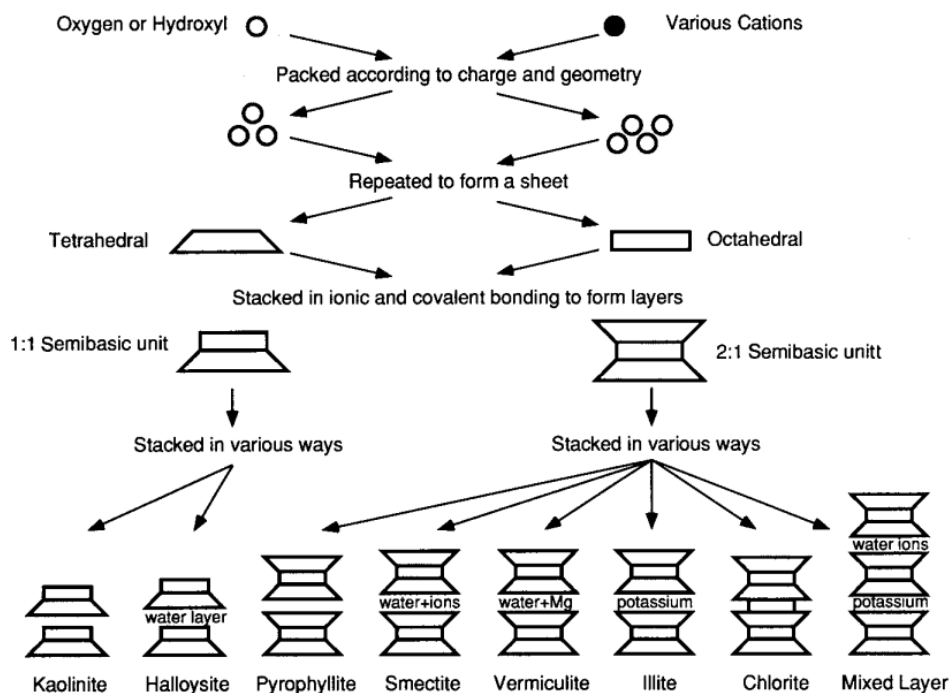


Figure 62 - Synthesis of clay minerals from its base components (Mitchell and Soga, 2005)

Smectite Group (2:1 TOT) – Characterized by extensive isomorphous substitutions, the cation exchange capacity (CEC) ranges large 80-150meq values. Van der Waal and ionic bonding is weak between TOT packets, in the interlayer region, ergo cations are readily exchanged and polar fluids are easily adsorbed (forming stronger H-bonds in the interlayer). Furthermore, the net charge deficiency allows thick double diffusive layers (DDL) at the surface of the mineral. Additionally, the high specific surface area is due to the large primary interlayer space (50-120m²/g), but dominated by the secondary expansion of the lattice (840m²/g), allowing polar molecules to penetrate between layers. A common mineral in the smectite group is Montmorillonite (Figure 80).

Bentonites – often comprised of large weight percentages of montmorillonite, they are highly plastic,

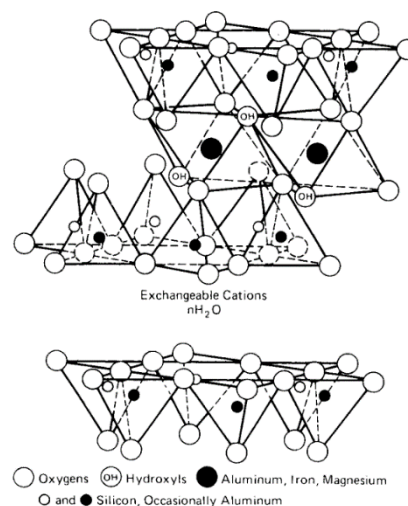


Figure 63 - Montmorillonite schematic TOT stacking, with interlayer cation and water molecules (Mitchell and Soga, 2005)

swell when hydrated/glycolated, and extremely impermeable. Their characteristics render them extensively used in geotechnical applications. Similar macro characteristics of smectite bearing soils often lead to weak soils.

8.1.2 Interlayer Cation Exchange Capacity (CEC)

Isomorphous substitutions attribute net negative surface charges to clay (phyllosilicates) molecules, allowing the adsorption of exchangeable cations. Charge deficiency amounting by isomorphous substitutions (eg Montmorillonite one Mg^{2+} per six Al^{3+}) leads to neutralization by uptake of exchangeable cations (eg. Na^+) in the interlayer space. The variety of compositions in the same basic crystal structure of smectite minerals leads to a large net negative surface charge. In combination with a large specific surface area and weak interlayer van der Waals and Ionic bonding, these minerals have a large cation exchange capacity (CEC= 80-150meq/g). For example, Montmorillonite may undergo 15% replacement of Si^{4+} with Al^{3+} (Mitchell and Soga, 2005). Ergo, smectites show a large cation adsorption potential/affinity.

Cation ease of replacement depends on valence, ionic radius, concentration and ion type. Increasing valency and charge density augments a species' displacement potential. In smectites, most CEC is located in the interlayer region, which renders the exchange in a salt solution time dependent (Mitchell and Soga, 2005). The complex's type dictates the selectivity and stability of the ion exchange from an aqueous environment (Studds and Stewart, 1996). Adsorption of water and swelling occurs when interlayer cation exchange capacity and hydration energy exceeds the existing attraction between unit layers.

In summary, the adsorption of ions and organic compounds in the interlayer space and clay surface are controlled by:

- **Clay Mineral:** Stacking structure, isomorphous substitutions, mineral type
- **Exchangeable Ion:** Polarity, polarizability, solution concentration, ion hydrated radius, and shape
- **Joint Effect:** Bond type in order of decreasing strength: H-bonds, Ionic, Van der Waals

8.1.3 Double Clay Theory

All clay minerals display a net negative charge, and this a diffusive double layer (DDL). This region of distributed charge is found at the surface of clay minerals, by which cations are electrostatically attracted while simultaneously extending away the surface by diffusion in the porewater. Simplified distribution theories such as Gouy-Chapman do not remain valid when the electrolyte solution is concentrated at $>0.001M$ (Sposito, 2018). Stern theory accounts for the hydrated radii of surface cations, which are postulated to form a rigid like layer of constant thickness, despite thermal motion. Evolutions of the DDL concept are referred to now as the DLVO theory, which apply the notion of repulsive forces and interactions to the stability of clay colloids. Although useful for physio-chemical considerations regarding flocculation and aggregation, its quantitative applicability remains questionable. Additional reference literature concerning DDL and DLVO theories are found in Mitchell and Soga (2005).

The attracted concentration of solution cations remains a function of valency, ionic radii, and concentration in the aqueous phase. 'Critical coagulation concentration' of monovalent ions leads to coagulation of colloids in suspension. As the interlayer collapses, water sorption/desorption process are halted, blocking the macroscopic swelling of smectite/montmorillonite rich soils. Therefore, cations in the free pore water solution are pivotal in controlling the soils' behaviour.

$$\frac{1}{K} = \left(\frac{\epsilon_0 D k T}{2 n_0 e^2 v^2} \right)^{1/2}$$

Figure 64 - DDL Thickness $1/K$ varies inversely with electrolyte concentration n_0 and cation valence v , but directly with dielectric constant D and temperature T

Figure 64's equation (Mitchell and Soga, 2005) shows that the thickness is inversely proportional to the valence and the square root of the cation concentration in the solution. Ergo, shortening the range of interparticle repulsive forces increases the flocculation potential and reduces swelling (tightly bounds particles, less water uptake). Additionally, increasing particle proximity increases the attractive Van der Waal forces.

Aggregation of a natural smectite bearing soil is controlled by chemical composition and interparticle forces. Based on the fundamentals of double clay theory, introducing a concentrated saline solution comprised of a highly ionic, strongly exchanging organic cation with a small, hydrated radius, is expected to reduce the DDL of negatively charged platelets. Doing so reduces repulsive forces and increases attractive forces. Aggregation augments, water uptake is reduced, and thus the true effective stress in clay particles increases. Macroscopic behaviors such as plasticity and swelling, should vary accordingly.

8.1.4 Ionic Species - Interlayer and DDL Modification

Leik (2020) argues that the interlayer ionic composition modification controls the DDL development. Ergo, cation valency and hydrated radii play a crucial role in the latter. Cations with a strong binding capacity effect the interlayer space of stacked sheet silicate structure of minerals such as montmorillonite and smectite (Minder *et al.*, 2016). Transformation of initially swellable clay platelets with large diffuse double layers occurs, binding the phyllosilicates into aggregate particles Minder (2016).

Additionally, increasing ionic solution concentration reduced swelling and plastic limits in Na-bentonite (Studds and Stewart, 1996). Monovalent ions show stabile behaviour even at high concentrations, inducing potential preferential pathways by particle aggregation. Di Maio (1996) tested the mechanical behaviour of Na-montmorillonite subjected to saturation by various salt solutions. Amongst NaCl, KCl and CaCl₂, the latter two showed irreversible mechanical response once flushed with demineralized water. More precisely, shear strength increased and volumetric strain was reduced. The K⁺ hydrated ion binds to the hexagonal voids between oxygens outside the silicate layer surface (interlayer TOT). Similarly, Egli *et al.* (2007) note that the preferential exchange of interlayer molecules is also strongest by monovalent cations, whereas dioctahedral cations such as Al³⁺ and Fe³⁺ were weakest. The time dependency of the mechanism remains unclear.

Further research concerning salt-water and montmorillonite interactions show that high concentration electrolyte solutions halter DLVO theory's repulsion mechanism, leading to flocculation and coagulation of platelets (Shirazi *et al.*, 2011, Elmashad and Ata, 2016, Komine *et al.*, 2009). However, the permanence depends on ion valency, hydrated radius and type. In alpine soils with abundant 2:1 phyllosilicates, K-saturation induced water desorption and collapse of d-spacing (Egli *et al.*, 2007). Plots and Kahr (2008) studied intercalation compounds to unequivocally collapse a clay specimen to its characteristic basal spacing (001), used for quantitative XRD Rietveld analysis. Polyhydric alcohol complexes were successful but reversed by evaporation, while the most efficient monovalent solution tested was Guanidium Chloride. Basal spacing becomes stable in the long run, independent of relative humidity changes (Plotze and Kahr, 2008). Leik (2020) confirmed similar findings by qualitative XRD analysis, such that 0.1-1M GndCl treatment yielded permanent interlayer collapse.

8.2 Soil constituents: a review of EICP and Guanidinium research

The research questions and a priori hypotheses lean on a soil mixture comprised of nonreactive coarser grains and plastic impermeable constituents. This annex provides additional literature context when considering the soil as a control variable (see Table 7). Removing additional complexity, it isolates the treatment research as the primary target.

Table 7 - Initial considerations used to design an artificial soil.

Soil and Selected Features	Motivation
<i>Fine Sand</i>	~ <i>Practical reason for homogeneous sample preparation, extensively used in existing EICP research</i>
<i>Swelling Clay</i>	~ <i>High plasticity, low permeability, and introduction of charged surfaces. This component limits EICP applicability, while being the target of the salt flocculation treatment.</i>
<i>Bimodal Grainsize Selection</i>	~ <i>Low to no additional complexity, allowing fundamental study of the treatment process. Fine sands are selected over coarse sand to reduce the bimodal grainsize gap.</i>
<i>Sibelco M32 and Colclay Na-Bentonite</i>	~ <i>Well characterized constituents, decreases complexity, providing rigorous control variables.</i>
<i>Oven Dried Sample Preparation</i>	~ <i>Constant hygroscopic water content (especially bentonite oven drying and additional handling), yields an aggregate microstructure, which may facilitate flow in the porous media.</i>

Past research has mostly aimed at targeting each soil independently from one another. Therefore, to organize the literature review concerning suitable artificial soil constituents, the following subsections analyze the role of sand and clay individually. Firstly, the sand fraction grainsize selection is discussed along with an existing carbonate precipitation strengthening solution. Secondly, attention is brought to the clay fraction and a specific flocculation research branch.

8.2.1 Soils in EICP: a review of sand selection

Sands are defined as grains of diameter between 63 microns to 2 millimeters. As commonly used in geotechnical research, a quartz sand is proposed as an unreactive phase, suitable for the testing of troublesome sandy soils. For example, soils prone to liquefaction under undrained cyclic seismic loading have successfully employed calcite precipitation to reduce risk (DeJong *et al.*, 2010). Additionally, Van Paassen *et al.* (2010) increased strength and stiffness of sands in large scale biogROUT experiments. Pure silica is chosen as a control variable. It's chemical stability and non-reactivity, ensure that mineralogical reactions do not influence the treatment research. In fact, treatment design studies which target weak sands often use >97-99% SiO₂ grains (Almajed *et al.*, 2018; Terzis and Laloui, 2018). Carbonate precipitation has been discussed in *Chapter 4* as an alternative multidisciplinary engineering solution for these soil types. In fact, although angularity, size and grain source vary, an extensive amount of research has been conducted in mono-mineralogical quartz sands (eg. Almajed *et al.*, 2018; Terzis and Laloui, 2019; Putra *et al.*, 2020; Konstantinou *et al.*, 2021). This is done to isolate study of calcite precipitation in the condition-sensitive pore solutions. More specifically, enzyme induced biogROUT solutions have tested grainsizes of d₅₀ between 720 and 210 μm (*Chapter 4, Table 1*).

In fact, microbially induced carbonate precipitation (MICP) in fine and medium quartz sands strengthens the soil fabric, as shown by increased peak strength under deviatoric loading. Terzis and Laloui (2019) validated existing trends in literature; medium sand (D₅₀=0.39mm) with greater void ratios, yielded larger unconfined compressive strength post treatment in comparison to fine sand

($D_{50}=0.19\text{mm}$). The pure silica sand they used (Figure 65) was uniformly distributed. The grains range from sub-angular to rounded (coefficient of curvature C_c 0.86 to 0.91). This soil sample example is similar to most used silica sands tested in enzyme induced carbonate precipitation research.

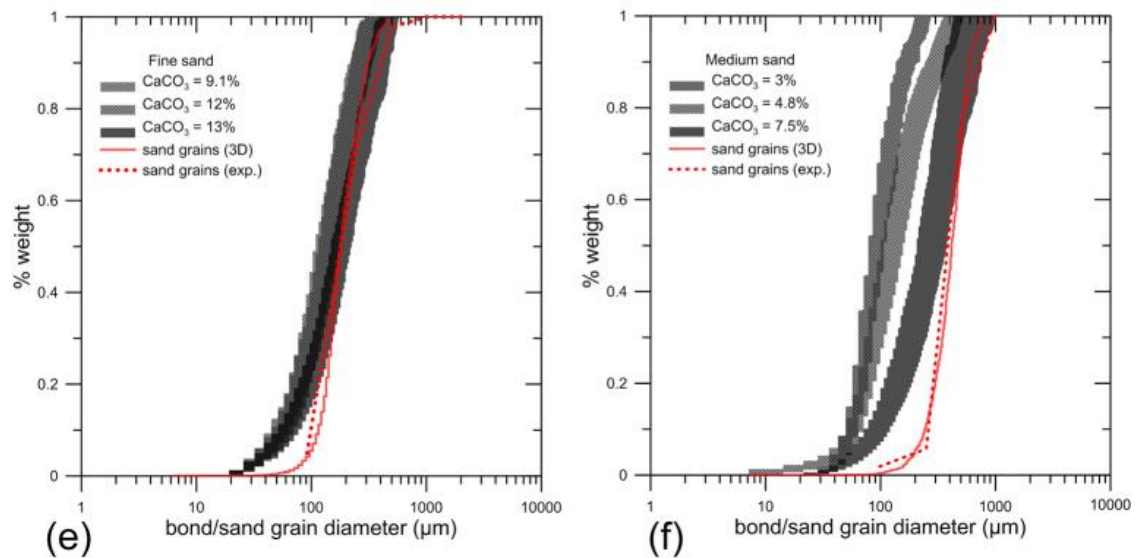


Figure 65 - Terzis and Laloui (2019) 3D structure micro-architecture and mechanical response of silica sands. The medium sand yields improved performance following treatment.

The strength and stiffness of bio-remediated sand samples vary in function of the physical properties (roughness, size, shape) of the parent material, where increased angularity leads to stronger and stiffer material (Konstantinou *et al.*, 2021). This is also due to greater interlocking of rough soil skeletons. Nonetheless, the direct role of roughness on nucleation sites for calcite growth remains poorly understood in enzyme induced calcite precipitation treatments. Microstructural analysis of calcite bonds provides a tool to qualitatively inspect the bridging of grains and their respective morphology.

In conclusion, a fine-medium quartz sand will be used. A unimodal $D_{50}=0.23$ silica sand is selected for this research. The fine sand is easy to handle, readily available, and is relevant as the fine sand artificial soil constituent. The second constituent, bentonite, will dominate the inter-grain contact points and soil matrix.

8.2.2 Soils in Guanidinium Research: a review of clay mineral selection

Little is known of the behaviour of carbonate precipitation in fine grained media. In fact, Terzis and Laloui (2020) only tested biogrout in ‘fine’ material of $D_{10}=99\mu\text{m}$, with only few enzyme induced calcite precipitation research reaching $D_{50} = 210\mu\text{m}$ (Neupane *et al.*, 2013). In fact, the prevalent role of active electro chemical surfaces in clay minerals remains less studied. Cardoso *et al.* (2018) concluded that the complex chemical interactions between clay minerals and MICP feeding solutions were dominated by osmotic consolidation and pore clogging in sand and white kaolinite <28wt% samples. Bio-cementation treatments in such soils yield mediocre results since the apparent cohesion of unsaturated clays and the poor crystallization failed to increase tensile strength significantly. Nonetheless, others such as Yuan *et al.*, 2020 have successfully strengthened alluvium silty soils using enzyme induced calcite precipitation. Due to the contrasting success of biogrout in clay bearing soils, premature stabilization of the clay fraction is proposed as means to stabilize charged surfaces and improve soil structure.

Electrolytes and surfactants have been studied as means to aggregate of colloidal kaolinite (Hu *et al.*, 2020). Following a similar principle, troublesome bentonite soils have been aggregated and stabilized by Guanidinium Chloride electrolyte solutions (Plotze and Kahr, 2008, Minder and Puzrin, 2017). According to double layer theory, ion adsorption in the interlayer space of clay minerals and the corresponding parallel platelet distance, controls osmotic deformations and mechanical response. Ergo, the guanidium treatment provides a solution to osmotic phenomena encountered in failing soils pertinent to the research.

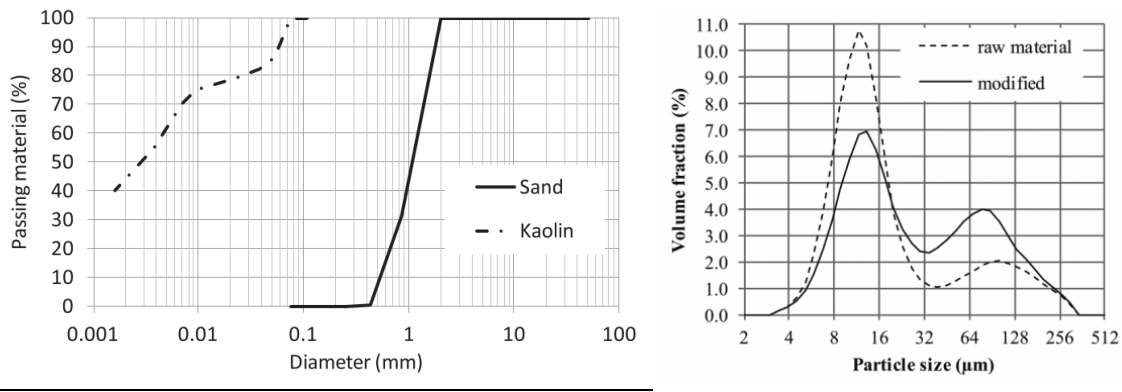


Figure 66 – **Left:** Cardoso *et al.* (2018) MICP with 20-28%w kaolinite mixture, treated at pH=7-9. **Right:** Minder *et al.* (2016) mixed 40% bentonite with 60% pure quartz sand prior to guanidine flow through treatment.

Bentonite is a commercial, readily available, dry clay easily mixed with the silica sand prior to wetting. Sodium bentonite has a larger plastic limit and liquid limit than the calcium one. Furthermore, the former also has greater sorption potential and are most appropriate for impermeable liner applications (most commonly used is the Na-activated bentonite MX-80). Alternatively, the Ca-activated bentonite provides a chemically favorable environment for percolation of artificial groundwater pore solutions (0.01[mol/L] $CaCl_2$), as well as for enzyme induced carbonate precipitation (EICP with $CaCl_2$ and urease enzyme solutions). In fact, previous works by Minder *et al.* (2016) tested Ca-bentonite soils (65wt% montmorillonite), while Minder and Puzrin (2016) tested Ca-bentonite (40%) and quartz sand (60%) mixtures (Figure 66).

In conclusion, bentonite will be used as the second constituent of the artificial soil. Natural sodium bentonite will be used due to the lab availability and extensive existing documentation.

8.3 Characterization of Sand-Bentonite: experimental data and empirical formulations

The characteristics of sand-bentonite are introduced in three subsections. Firstly, He-pycnometer readings are used to define the density of solids. Second and thirdly, the maximum dry-density and optimum water content (OMC) are defined. These considerations are the basis for the soil preparation.

8.3.1 Density of Solids

By oven drying 300g of both constituents at 105°C for 48 hours, the hygroscopic water content of the Portaclay bentonite at room moisture was calculated to be 7.51%, whereas the M32 sand retained only 0.01% water by mass. Back calculations of He-pycnometer readings verified the latter, whereby the moist reading of $\rho_{He-moist,MX80} = 2.62 [g/cm^3]$ and oven dried $\rho_{bulk,MX80} = 2.83 [g/cm^3]$ yield a bentonite water content 7.42%. For this reason, the samples are oven dried accordingly, prior to measuring the bulk density by He-pycnometer readings.

The total bulk density of sand-bentonite mixtures are calculated from the weighted constituent percentages and their specific gravity (He-pycnometer):

$$\rho_{s_{BC10}} = \rho_{MX80,He-pycn}(10\%) + \rho_{M32,He-pycn}(90\%) = 2.83(0.1) + 2.67(0.9)$$

$$\rho_{s_{BC30}} = \rho_{MX80,He-pycn}(30\%) + \rho_{M32,He-pycn}(70\%) = 2.83(0.3) + 2.67(0.7)$$

$$\rho_{s_{BC10}} = \mathbf{2.69 [g/cm^3]}, \quad \rho_{s_{BC30}} = \mathbf{2.72 [g/cm^3]}$$

8.3.2 Water Content

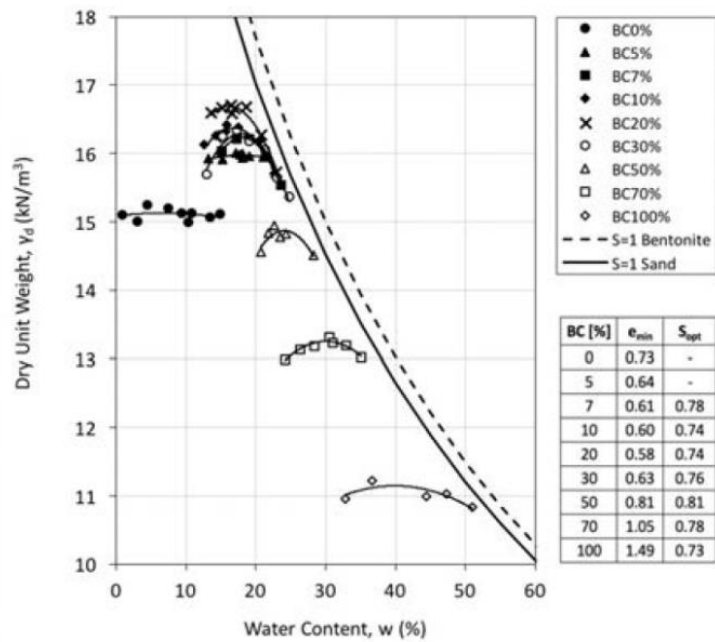
Sample compaction to maximum optimum water content is common practice, as facilitates test reproducibility (Charkley *et al.*, 2019). Sharma *et al.* (2017) propose an empirical formulation to compute optimum moisture content. Based on their tests, they propose an empirical approximation by the formula:

$$OMC = 0.005 * (BC)^2 - 0.43 * BC + 23, \quad \text{for } BC = 10\%, 30\%$$

$$\mathbf{OMC = 19.2\% \text{ and } 14.6\%}$$

Such value is comparable to other proctor compaction tests executed on sand-bentonite mixtures of similar BC (Figure 67; Iravanian and Bilsel, 2016; Osmanlioglu, 2016; Charkley *et al.*, 2019). It is therefore taken as a valid reference value for sample preparation, since additional lab tests go beyond the sub-research question scope and time constraints of this research.

Figure 67 – (right) Proctor compaction tests for varying bentonite content by Proia *et al.*, (2016). The void circles represent 30% BC. The saturation curve is shown by the S=1 lines. As seen, for a constant water content, reducing the dry unit weight will never exceed the saturation line.

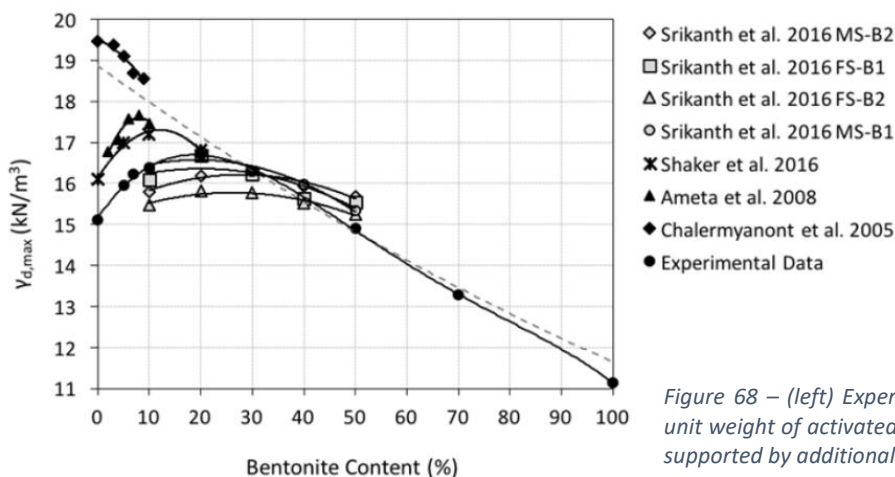


8.3.3 Dry Density

Sharma *et al.* (2017) suggest an empirical fitting of the maximum attainable dry density for coarse sand-Na-bentonite as a function of bentonite content (BC%):

$$\gamma_{d,max} = 0.0463 * BC + 15.05, \quad \text{for } BC = 10\% \text{ and } 30\%$$

$$\gamma_{d,max} = 15.51 \text{ and } 16.44 [kN/m^3]$$



These predicted values concur with existing literature as seen in Figure 68, and are taken as a baseline for the development of a control soil variable.

Figure 68 – (left) Experimental data of maximum dry unit weight of activated Na bentonite – sand mixtures, supported by additional literature (Proia *et al.*, 2016).

For any a given water content (in this case the OMC), reducing a specimens target dry density will never exceed the sand-bentonite saturation curve (Figure 67). Ergo, sample preparation at dry densities lower than optimum is still possible by reducing the compactive effort. This implies varying saturation rates, which is not problematic in view of saturated tests and treatments.

Two dry densities are proposed, whereby a loose sample at ~80% and a dense mixture at 95% of the maximum dry density:

$$\rho_{dry,10\%} = 1.21 \rightarrow 1.47 \left[\frac{g}{cm^3} \right], \quad \rho_{dry,30\%} = 1.35 \rightarrow 1.56 [g/cm^3]$$

The dense states correspond to void ratios greater than $e=0.75$. Proia *et al.* (2016) have found natural 30% bentonite to have minimum void ratios of $e_{min}=0.63$. Samples are prepared with similar void ratios of previous geotechnical research of sand-bentonite/kaolin mixtures.

8.3.4 Summary

Four soils are proposed as vectors upon which to treat the *Bio2Cementation* treatment process (Table 8). A lower bentonite content is proposed (BC10), for which the sand fraction is expected to dominate the porous media. On the other hand, a large bentonite soil is also tested (BC30), to test the treatments' limit in quasi-impermeable porous media. Additionally, both sand-bentonite mixtures are tested at two dry densities, corresponding to ~95% and ~80% of the dry maxima.

Table 8 - Sand-bentonite artificial soil upon which the two phase *Bio2Cementation* soil strengthening research is performed.

Bentonite Content	BC10 $\rho_{dry,max}=1.55g/cm^3, OMC=19.2\%$		BC30 $\rho_{dry,max}=1.64g/cm^3, OMC=14.6\%$	
	Dry Density	1.21g/cm³	1.47g/cm³	1.35g/cm³
% of $\rho_{dry,max}$	~80%	~95%	~80%	~95%
Void Ratio	1.22	0.83	1.01	0.75

8.4 EICP recipes: a review

Past research based treatment protocols on preliminary experimental test tube EICP solutions. This is done to optimize the calcium chloride - urea ratio and concentrations, for the available reagents. For example, Almajed *et al.* (2018) utilized a 1:1.5 ratio (0.67M CaCl₂, 1M urea and 3[g/L] urease). Others, such as Yuan *et al.* (2020) utilized the same ratio in more concentrated solutions (2.8[mol/L] CaCl₂, 4.2M urea and 4[g/L] urease). The most common ratios used by the state of the art tends to be either 1:1 or 1:1.5. Neupane *et al.* (2013) found that when using *Jack-bean* purified urease, the maximal precipitation ratio occurred at 3[g/L] and decreased thereafter. In EICP, reaction times occur over course of days. For example, when using a ratio of 1:1.5, 24h reaction times of yield 87-98% for EICP reagent combinations until 2.8[mol/L] CaCl₂ (Yuan *et al.*, 2020). Additionally, cycles of refreshed solution improve the treatment results (Putra *et al.*, 2020). The state of the art of EICP treatment solution recipes are summarized in Table 9.

Table 9 - State of the art of EICP treatment solutions.

Author	Density [g/cm ³]	Pore Space	Grainsizes Tested	CaCl ₂ : urea	Urease	Enzyme Activity	Treatment Volume	Time
Neupane <i>et al.</i> (2013)	$\rho=2.65$ RD=60%	$e_{max}=0.899$ $e_{min}=0.549$	$d_{50}=210-280 \mu m$	1:1 (0.5M)	2 g/L	2'950U/g	0.75 + 0.75 times the pore space	2 to 24h
Putra <i>et al.</i> (2016)	$\rho_{dry}=1.55$, RD=50%	$e_{max}=0.899$ $e_{min}=0.549$	silica sand, $d_{50}=300\mu m$, $d_{10}=180\mu m$	1:1 (0.5M)	1g/L +MgCl ₂ 0.1M +MgSO ₄ 0.05M	2'950 U/g	1 pore space	2-5d p. cycle, 3 cycles
Ross (2018)	$\rho_{dry}=1.70$, water=19%	-	Low plastic clay, $I_p=14$, $d_{50}=450\mu m$, $d_{10}=75\mu m$	1:1.5 (0.67M)	3g/L +4g/L skim-milk	-	-	2d
Almajed <i>et al.</i> (2018)	RD=45-63% (pluviation and hand tamped)	$e_{max}=0.742$ $e_{min}=0.502$	Ottawa 20-30, $d_{50}=720\mu m$, $d_{10}=650\mu m$	1:1.5 (0.67M)	3g/L	3'500 U/g	1 pore space	7d p. cycle, 4 cycles
Almajed <i>et al.</i> (2019)	RD=76% (pluviation and hand tamped)	$e_{max}=0.742$ $e_{min}=0.502$	$d_{50}=600\mu m$	1:1.5 (0.67M)	3g/L +4g/L skim-milk	3'500 U/g	1 pore space	3d p. cycle (20°C)
Gao <i>et al.</i> (2019)	$\rho_{dry}=1.62$ (5x layers in cylinder and hand tamped)	$e=0.62$	non-plastic silty soil (qtz powder, sand), 10% <0.005mm, 50% 0.005- 0.075mm	1:1 (0.5M)	40g/L soybean powder	6.5-13.2 mM/min	1.5 pore space	3d, vacuumed at -100Pa
Yuan <i>et al.</i> (2020)	$\rho_{dry}=1.68$, $\rho_{sample}=1.94$ water=15.2%	-	silty soil, 46% >0.075mm $I_p=9.96$, $d_{50}=260\mu m$	1:1 (low conc.) 1:1.5 (1.6M)	8 g/L (vaterite becomes calcite)	-	-	7d (25°C)

8.5 Experimental Procedures

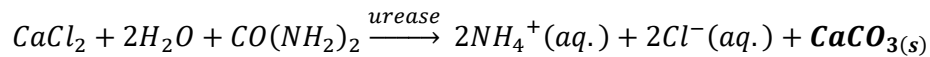
8.5.1 Method: EICP Test Tube Optimization

To test the solutions performance, a test tube experiment is performed to optimize the EICP recipe. Stemming from the design concentrations, the reagent masses are diluted in a total solution volume of 50mL, and are calculated as follows:

$$n = M_{d, reagent}(\text{mol/L}) * V_{sol}(\text{L}) \quad \text{and} \quad m = m_m(\text{g/mol}) * n(\text{mol})$$

$$m_{reagent} = m_{m, reagent} * [M_{d, reagent}] * 0.05(\text{L})$$

Furthermore, the calculated theoretical CaCO_3 (s) mass is a function of the limiting reagent. All tests are limited by the $[\text{Ca}^{2+}]$ since the ratio $\text{CaCl}_2:\text{urea}$ is greater than or equal to one. Precise equilibrium calculations (dependent on K_{eq} , pH, T, etc) lie beyond the scope of this research. The balanced simplified reaction is shown hereafter. The latter does not account for the acid-base equilibrium, and assumes an equilibrium shift completely to the alkaline side (right). Ergo the mass calculation of CaCO_3 defines a maximal theoretical yield for each test. This approach allows for the calculation of an 'efficiency ratio', which compares the experimental mass to the theoretical potential of each recipe.



$$\text{Precipitation Ratio} = \frac{m_{\text{CaCO}_3, \text{actual}}}{m_{\text{CaCO}_3, \text{theor}}}$$

The total solution's volume is 50mL, therefore $0.05\text{L} * 3\text{g/L} = 0.15\text{g}$ of urease are used as the catalyzing agent. To quantify the ionic strength and acidity of the solution the electrical conductivity, temperature and pH of the samples are measured. The cementation solution and urease enzyme powder is cured and agitated in the test tubes during 24h at 200rpm. Every 2 to 4 hours, visual checks are performed. Finally, upon the reaction's completion, all parameters are measured once again. This is repeated for varying concentrations and varying urea to calcium chloride molar ratios.

The pure water (PW) is measured to having a pH of 6.57 and an EC of $2.1[\mu\text{S}/\text{cm}]$.

Cementation Solution Shaker Tests:

1. Control Mass: The shaker tube weight (no lid), the petri dish base (no lid), and filter paper weight are measured to 0.001g accuracy. Labelling of each experiment is done on the respective lids.
2. Calcium chloride and urea are carefully extracted from their storage recipient. The aggregated urea is crushed into its crystalline form, the granular CaCl_2 (<7.0mm) is crushed in a hand mortar.
3. The urease enzyme is extracted from the fridge just prior to use, in order to minimize it's initial temperature dependent activity and avoid degradation
4. Urease is weighed to 0.150g (3g/L in 50mL solutions), and dissolved by shaking in a 50mL container (white cap) in approximately ~10mL of Pure water (PW)
5. The reagent mass according to each test is measured in a 50mL container. Both calcium chloride granules and urea are added dry to the design weight.
6. The two salts are dissolved with ~30mL of PW. By swirling and shaking is done until the reagents are entirely dissolved.

7. Using a funnel, the salt solution is transferred to a 50mL volumetric flask. The dissolved urease is combined in the volumetric flask, the funnel and PP rinsed with PW, and topped to precisely 50mL below the menisci. Rapidly!
8. The cementation solution is agitated rapidly for 4-5s, and immediately transferred to the 50mL shaker containers (blue cap) to avoid precipitation in the volumetric flask.
9. Initial measurements: EC and pH electrodes are rinsed with DI, and thereafter plunged in the cementation solution. Once stable the initial values are noted.
10. The solutions for each Test (x6) are prepared and set to shake and cure for approximately 24h at 200rpm.
11. Final measurements: EC and pH electrodes are rinsed with DI, and thereafter plunged in the cementation solution. Once stable the initial values are noted.

Weighing Samples:

1. Cellulose Nitrate filters (diameter 50mm, pore size 8 μ m, m) are placed upon the collecting apparatus and wetted with 4 drops of 'Pure Water'
2. The pump is activated, generating 80.0mBar of under pressure in the solution collection container.
3. Samples of 50mL shaker flasks are slowly drained through the Cellulose Nitrate filters, such that the precipitate is deposited on the filter. In order to not lose any precipitate, slow pouring ensures no later spillover outside of the 50mm diameter filter.
4. The filter paper is carefully lifted and placed in the appropriate labelled petri dish (D 85mm, mass of the base 7.400g \pm 0.003g)
5. In order to analyze the dissolved [Ca²⁺] concentration, the solution is transferred to 50mL PP tubes, labelled, and stored at room temperature.
6. Thereafter the drainage apparatus is rinsed with DI water, dried, and prepared for the subsequent sample.
7. Steps 1-6 are repeated six times per test. In total the three tests (Test 1 (1:1), Test 2 (1:1.25) and Test 3 (1:1.5)) yield 18 experiments. The shaker capacity is of six 50mL containers.
8. Each test iteration (six samples) is oven dried at 50deg C with ventilation for 24h.
9. Final Mass: Since the precipitated solids partially cement to the shaker tube, the actual final masses is defined by both the mass difference of the tube and of the filter. Ergo, the mass of each tube and petri dish + filter paper is measured and recorded.
10. Actual Mass of CaCO₃ (g): The precipitated calcite weight is therefore equal to the "Final Mass" minus the "Control Mass".

8.5.2 Method: Guanidinium Hydrochloride Experiments

Two procedures are envisioned for this section, respectively. The first is a dilution into monitoring of the treatment solution, whereas the second replicates EICP test tube experiments with the addition of guanidine.

Guanidinium Hydrochloride Stability Test:

1. All beakers are rinsed thoroughly with demineralized water (DI).
2. Guanidinium Hydrochloride 6M is diluted to the desired molarity. To prepare 0.5L of treatment solution at 0.5mol/L, the initial volume required is calculated as molarity (M) and volume (V) of the final solution compared to the molarity of the initial solution:

$$V_1 = \frac{M_2 * V_2}{M_1} (L)$$

3. The guanidium hydrochloride is extracted using a 0.7mm needle attached to a 50mL syringe.
4. The difference between the final and initial volume is calculated as the volume of DI water added as dilutant:

$$V_{H2O} = V_2 - V_1$$

5. The guanidinium hydrochloride (V_1) and diluting demineralized water solution (V_{H2O}) are combined in a 500mL glass flask.
6. A magnetic stirrer is introduced at the base. An electrical conductivity and pH probe are then inserted in the solution, continuously logging measurements for a period of 48h.

Guanidinium Hydrochloride Inhibition Test:

The same procedure as the methodology of 8.5.1 Method: EICP Test Tube Optimization is followed, such that a direct comparison can be made on the effect of guanidinium hydrochloride on calcite precipitation.

1. Weigh the necessary reagents for four test tubes.
2. Dissolve the $CaCl_2$:urea using appropriate volumes of 0.5M guanidinium hydrochloride and pure water, such that the final diluted concentration in 50mL amounts to 0.5M, 0.25M, 0.1M and 0.01M.
3. The EC, pH and precipitated calcite content are compared to the guanidinium free EICP solution (0.5M $CaCl_2$:urea in a ratio of 1:1.5, using the urease with an activity of 8U/mg. See Figure 21 – blue bar chart, leftmost dataset).

8.5.3 Method: Soil Sample Preparation

Impermeable liner research has extensively characterized sand-bentonite mixtures, where samples are usually prepared at optimum moisture content and maximal sample dry density (Sharma *et al.*, 2017; Charkley *et al.*, 2019). Diverse geo-technical strength research, such as tensile strength tests by Iravanian and Bilsel (2016), also utilize the same procedure to ensure reproducibility.

Due to its extremely large sorption potential, bentonite experiments often mix constituent percentages in an oven-dried state to control humidity (Cardoso *et al.*, 2018; Charkley *et al.*, 2019; etc). Free-water and capillary water can be removed by oven drying at 110°C for 12h (Lang *et al.*, 2017). Additionally, 2-3% water content is held in the interlayer space and adsorbed water particle surfaces, which requires 200°C for 12h (Lang *et al.*, 2017). Thereafter, water is added to reach a desired moisture content. For these reasons, a similar approach is taken in the scope of this research. Like the procedure utilized by Proia *et al.* (2016), a methodology is proposed as follows:

1. Forced-draft oven drying of sand and bentonite separately at 110°C for 12h (expected 2-3% water content remaining) (Lang *et al.*, 2016).
2. Dry specimens are weighed in a sand-bentonite ratio of 70-30%
3. Bentonite is crushed and sieved at 425µm to reduce the maximal aggregate size.
4. The sand (70% dry weight) is wetted with DI water to the OMC of ~15%, whereby the dry bentonite (30% dry weight) is added while mixing (Proia *et al.*, 2016). Treated pre-mixed samples are instead wetted using the same volume of 0.5M GndCl solution.
5. The soil mixture is sealed for 24h. This minimizes capillary condensation and allows interlayer hydration in an isolated container.

6. Cylindrical specimens are filled according to the desired bulk unit weight at OMC, for which the mold's volumes are used to calculate the required mass of soil. Manual tamping is done in 5 layers following D1557-02 (2003).
7. The mold and soil are sealed to prevent evaporation prior to treatment/testing.

The soils samples prepared for the D15mm and D30mm flow cells are to be prepared with the following soil masses:

Bentonite Content	BC10 $\rho_{dry,max}=1.55g/cm^3$, OMC=19.2%		BC30 $\rho_{dry,max}=1.64g/cm^3$, OMC=14.6%	
	Dry Density	$1.21g/cm^3$	$1.47g/cm^3$	$1.35g/cm^3$
D15 Bulk Mass	7.674g	9.314g	8.204g	9.492g
D30 Bulk Mass	61.395g	74.492g	65.615g	75.891g

8.5.4 Flow Cell Iterative Design

Hereafter, a visual aid of the iterative design of the flow cell is presented. It's aim is to display the considerations in the realization of a suitable cell to inject at pressures reaching 3[bar], preventing radial and axial strain, while facilitating non-destructive sample extraction for data acquisition.

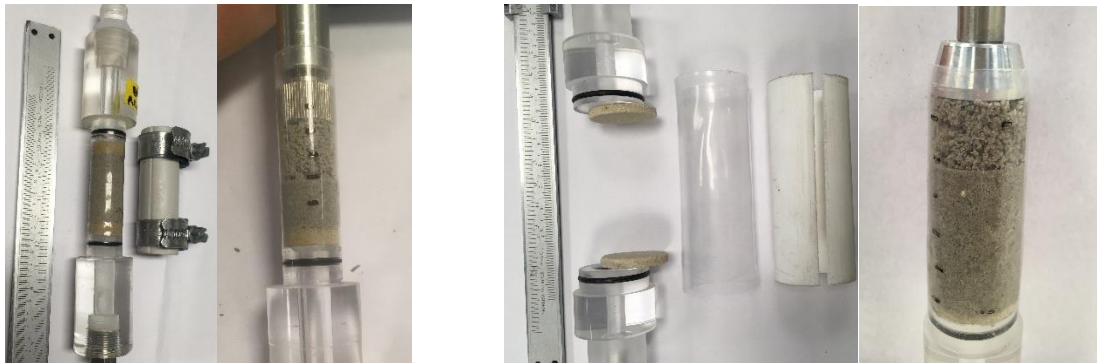


Figure 69 - Cylindrical flow cell in 2:1 length to diameter ratios, with m_{bulk} tamped in five equal volume layers. The 15mm wide cell (left) is used for imaging, the 30mm cell (right) for strength testing.



Figure 70 - Time minimization via rapid dilution in a 50mL volumetric flask of urea:CaCl₂ reagents (glass beaker) and dissolved urease (white cap). On the right, an immediate transfer of EICP solution to the DB 50mL syringe.

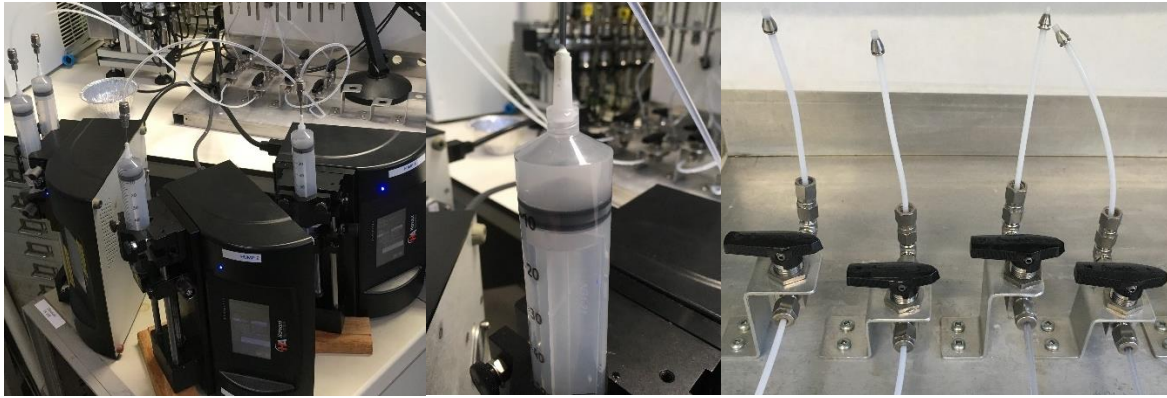


Figure 71 - Simultaneous injection of all four soils, allowing for optimization of the time-consuming treatment cycles. Three Harvard Ultra PHD fixed rate pumps are used to inject. Swagelok valves isolate the samples (right).

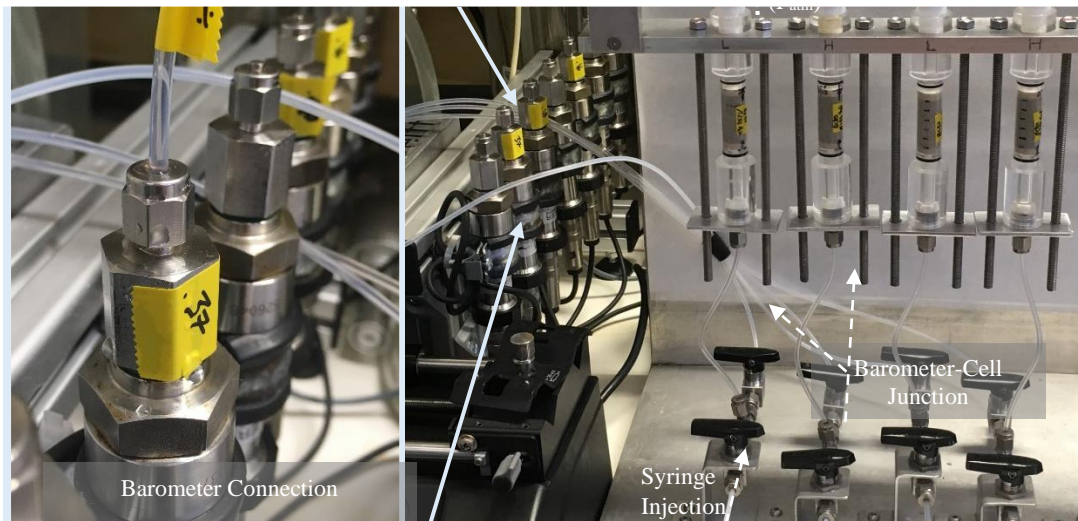


Figure 72 - Incompressible closed system between the syringe injection port, the barometer and the flow cell (here D15mm samples). The only decompression occurs at the flow cell outlet (blue cap).

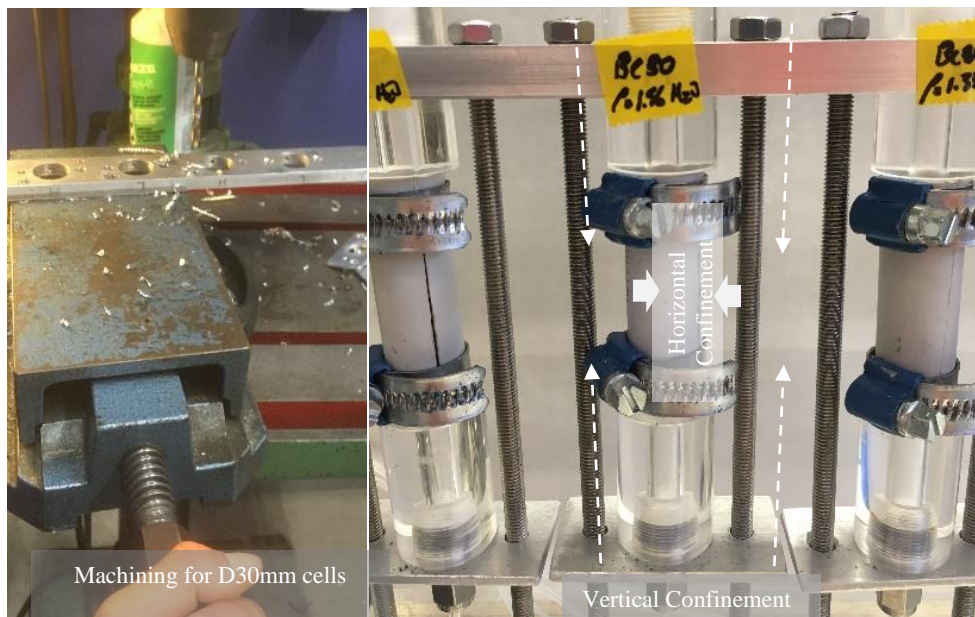


Figure 73 - (Left) Machining of aluminum plates. (Right) Horizontal confinement provided by a $D_{inner}=15\text{mm}$ PVC pipe, slit vertically to allow removal of samples, clamped via the hex screw. Vertical confinement provided by M4 rods compressing the top fixed plate to the individual basal plates. These solutions strive to provide a zero strain condition.

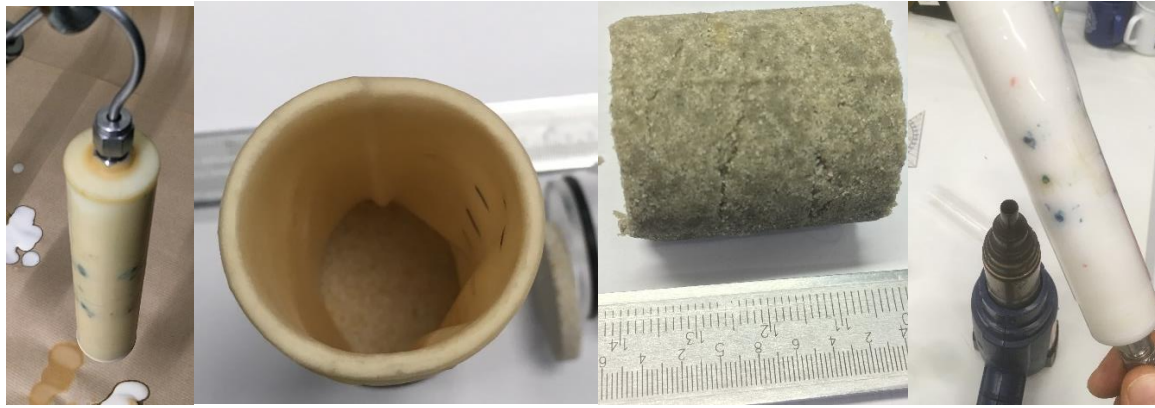


Figure 74 - Two sleeves are tested for the sample preparation. The parameters which must be met are easy sample extraction, no preferential flow, uniform sample preparation. Explicitly made latex membranes deform millimetrically, leading to unsuitable soil specimens (left three pictures), whereas heat shrinking teflon tubes provided a rigid structure yielding precise specimens.

8.5.5 Treatment Protocol

The following sub-section details the treatment procedure in view of injections in the soil columns. Firstly, the pressure sensors are calibrated and connected. Secondly, the treatment of samples is detailed.

Barometers

Once calibrated, the pressure sensors (barometer) and the connecting tubes must be flushed and saturated prior to treatment. Due to the incompressible nature of water (in absence of compressible air bubbles), any pressure increase in the adjacent soil samples, will lead to an equivalent reading in sensors and data logging software. These are used as “eyes” into the time dependent evolution of the flow regime, necessary to monitor against excessing pressure buildup. This may occur due to bentonite swelling and/or abundant cementation.

1. Isolate the tube which will connect to the syringes by closing the bottom front valve. Open the bottom rear valve, such that the top of the T junction can be connected to a 50mL syringe of demineralized water (later used as the basal connection of the flow cell).
2. Inject the water until all air has escaped the tubing, allowing a few drops to spill.
3. Remove the caps of the pressure sensors, plug the saturated pipe, and screw tight while avoiding air inflow.
4. Repeat the saturation for all four barometers (one per treatment cell).

Treatment Injections

The flow through cells must be mounted accordingly, to ensure horizontal and vertical confinement against the swelling of bentonite. Thereafter, the treatment and data acquisition begins. This procedure is performed both for the 15mm (detailed hereafter) and 30mm wide soil samples.

1. Remove the stoppers from the sample (used to maintain OMC constant), placing the screw ports sealed by the rubber O-rings. For consistency, the top port has a plastic connector, whereas the bottom one is metal.
2. Top Flow Cell: Insert the top port into the machine aluminum frame, screwing the blue plastic cap (connected to drainage tubes) with 2x 15mm Allen keys. Tighten the rear 1mm safety hex.

3. Bottom Flow Cell: Screw the bottom port to the treatment tube, using 2x 11mm Allen keys. Close both bottom black valves (rear: pressure sensor, front: syringe pump) to prevent evaporation.
4. Horizontal Confinement: Open the rigid external sleeve along the cutline. Slide it outside the sample, such that it will provide confinement against swelling when saturating (internal diameter of 16mm and 32mm respectively). Using a 7mm hex ratchet and clamp, screw tight the metal rings over the O-ring location to ensure water tightness.
5. Vertical Confinement: Slide on the 180mm long M6 rods and aluminum plate from below, tighten the bolts at the top and bottom of the thread using two 10mm Allen keys. Do so until the sample is immobilized.
6. Syringe Pump: Select the appropriate syringe (2x CD 50mL, inner diameter 25.594mm). For a 15mm wide samples select a 21mL (GndHCl or pure water for flushing) or 7mL (EICP) injection volume (~2x pore volume for 15mm) at a fixed rate of 0.3mL/min. Alternatively, for D30mm specimens the injected volumes correspond to 42mL (~2x PV).
7. Pressure Data Acquisition: Open the CSS application. Select a new measurement for the appropriate cells and sensors, recording mbar readings at 1s intervals. Name the test accordingly. All data is copied and exported once the injection is completed.
8. Cementation Solution: Prepare 50mL of 0.5M 1:1.5 cementation solution (or 4x 50mL for D30mm cells, see 8.5.1 Method: EICP Test Tube Optimization), rapidly filling ~12.5mL for D15mm cells (or 45mL for D30mm cells) in four syringes devoid of air. Connect the syringes to the treatment tubes, and place them in the constant rate pumps.
9. De-air Treatment Line: Open the bottom front valve, manually compressing the pump, such that both tubes are saturated with treatment solutions. Unscrew the basal cap of the flow cell. Connect the saturated treatment line to the base, tighten with 2x 11mm Allen keys.
10. Inject Treatment: Open the bottom rear valve (to the pressure sensors), start the data acquisition software, start the Harvard syringe pump protocol, and immediately open the top valve (to outflow).
11. Monitor Pressure: Ensure that the pressure resides below 2bar.
12. Curing Preparation. Once the injection is complete, curing of samples is done over ~1day (Gnd HCl) or ~2days (1x EICP). Close **all** valves, unscrew the bottom port, and seal the soil sample with a screw cap.
13. Clean Treatment Line: Open the bottom front valve, injecting 50mL of air from the top to drain the treatment tubes.
14. Export Data: Export the pressure data table to the joint data file.
15. Repeat steps 6-14 for subsequent EICP treatments. Otherwise, remove the samples by following in reverse order steps 5-1 and commence anew with new specimens.

8.5.6 K_{Sat} Sample Preparation and Testing

Rigid wall K_{Sat} rings are filled according to the sand-bentonite optimum compaction state (Biju and Arnepalli, 2020). The specimens are prepared according to D5084-61a (2016).

1. The soil is prepared at optimum moisture content. Either demineralized water or 0.5M guanidium solutions are used to wet the sand-bentonite.

$$V_{cell,30mm} = L * \pi r^2 = 5cm * \pi \left(\frac{8cm}{2}\right)^2 = 251.3274cm^3$$

2. Laboratory compacted specimens are placed in a KSat mold by hand tamping in 5 layers according to D1557-02 (2003). Each layer's surface is lightly scarified according to D5084-61a (2016).
3. Sample water content is calculated from trimmings, draft-oven drying at $110 \pm 5^\circ\text{C}$ for 12h.
4. The height, diameter and mass of specimens are determined prior to saturation.
5. The mold is placed upon the KSat filter plate inside a container.
6. A second filter plate is placed above the mold, loaded with a 65kPa surcharge (Minder *et al.*, 2016). This ensures sufficient effective stress against bentonite swell pressures.
7. The container is filled with demi-water or guanidium chloride solution.
8. Bottom-up saturation is aided by a partial vacuum of $<200\text{psi}$ ($<1'400\text{kPa}$) as per D5084-61a (2016). As verification of minimized volumetric strain, the axial strain must remain $<0.4\%$.

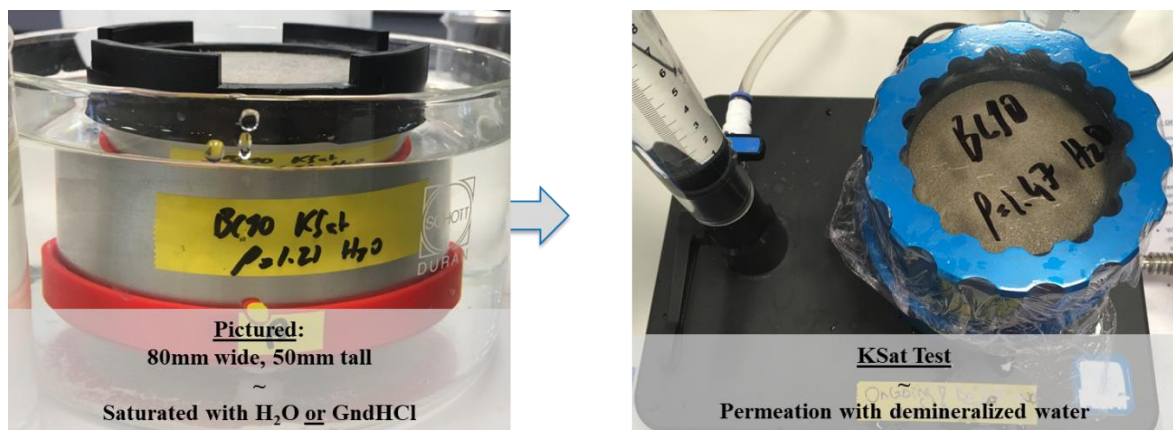


Figure 75 - KSat sample saturation before placement of the 65kPa overburden (left), and a sealed falling head permeation test (right).

9. The sample is placed in the KSat measuring device and the summit sealed with cling wrap to prevent evaporation. Low hydraulic conductivity falling head test, using a capillary tube, are performed for tests flowing slower than $1\text{e-}7[\text{m/s}]$.

8.5.7 Micro-CT – Image Analysis

This section outlines a methodology to quantify by X-Ray imaging the effect of GndHCl and EICP using the Fiji ImageJ software (Schindelin *et al.*, 2012; Schneider *et al.*, 2012). In workflow overviewed in Figure 47, the sub-section describes how Micro-CT Image Stacks are handled. Firstly raw image stacks are pre-processed, then segmented according to mineral/void type, and finally quantified.

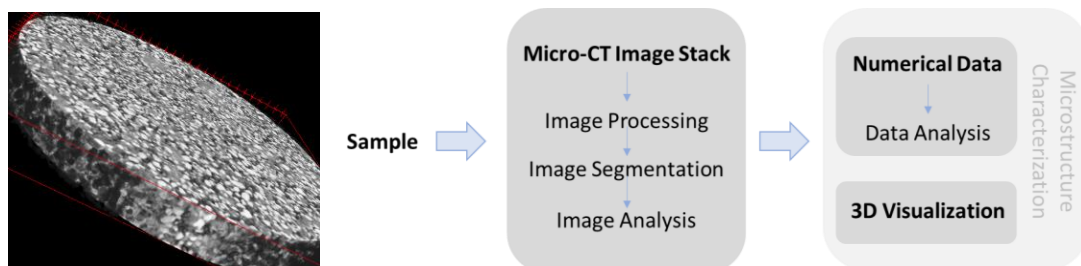


Figure 76 - Workflow of mineralogical classification, then quantification, using Fiji ImageJ software. On the left a grayscale untreated image stack as an example. The full Implementation details are included in Annex XX. Micro-CT specifications are displayed in Annex XX.

Through iterative process optimized upon smaller image stacks, the process named Micro-CT Image is run as an automatized process for all scans. Such method ensures reproducibility, reduces human bias, and allows for comparative analyses between all twelve samples.

1. **Image Processing:** Soil only cylinders are cropped to ~14mm width (ergo omitting the retaining plastic sleeve). A histogram matching function was developed to equate grayscale histograms between different scans (see code in annex 8.6.11). Thereafter, annex 8.6.12 shows how brightness and contrast are adjusted, and image noise is reduced by applying a median filter over two adjacent pixels (resolution of 1pixel = 15µm).

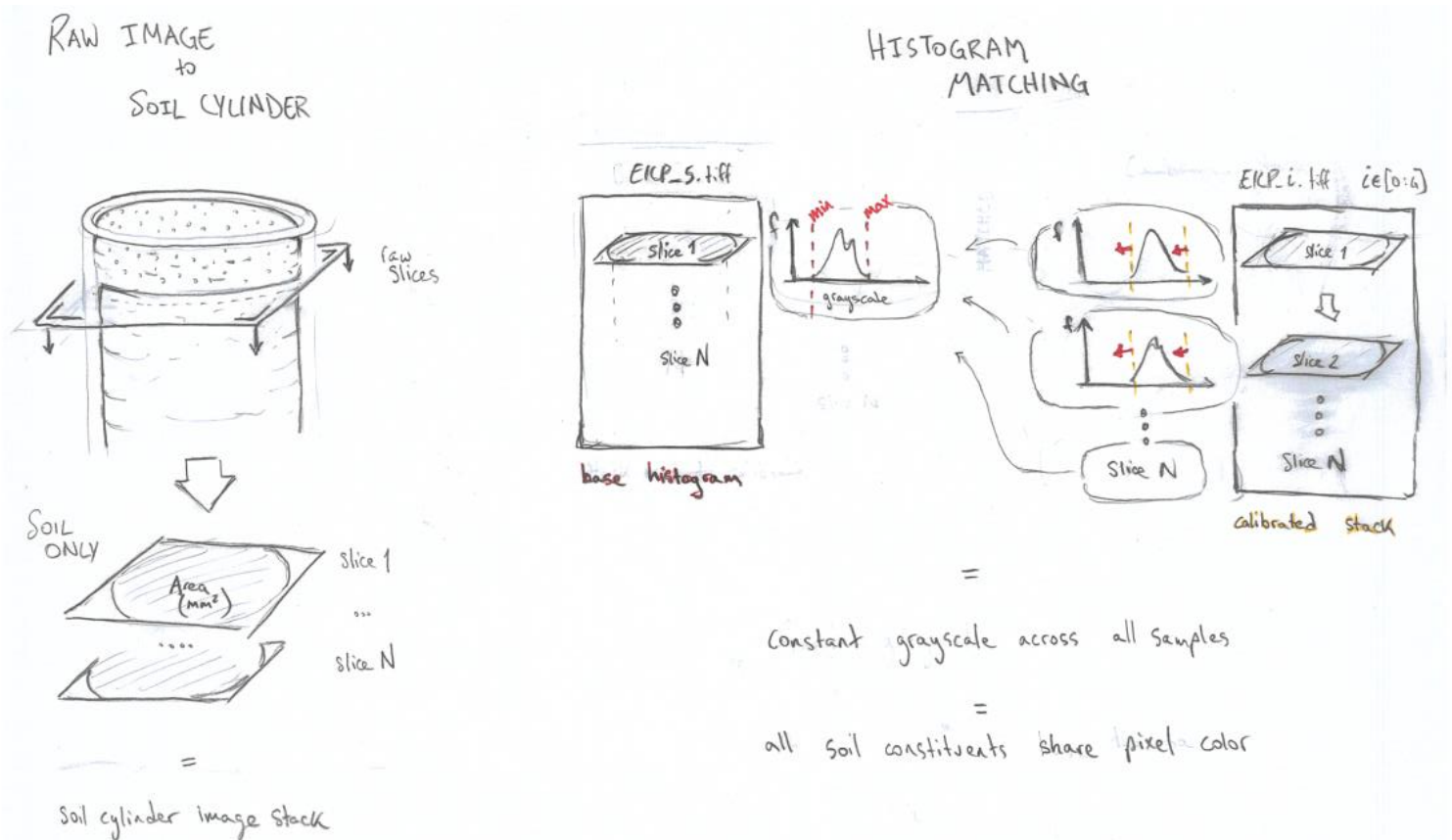


Figure 77 - Image Processing 1: Extraction of soil only cylinder (left), and histogram matching Java algorithm (right). The second step is necessary to equate the greyscale, such that soil constituents from every scan are directly comparable. This is critical in automatized analysis of image stacks.

2. **Image Segmentation:** Image segmentation was done by the machine learning 3D Weka Segmentation tool (Lormand *et al.*, 2018). This was done by training the neural network iteratively through a manual randomized classification of voids, silica grains, and bentonite matrix (see code in annex 8.6.13). Two classifiers are generated: one for BC10 and one for BC30. Meanwhile, carbonates are segmented via a set local thresholding technique due to their extremely high attenuation of x-rays (white pixels, chosen as voxels with an 8-bit grayscale value between 240-255). Boolean operations are run to assure that no overlap

occurs between voxels classified as sand or carbonate particles. The output is duplicated as four binary masks comprised of white voxels of sand, carbonate, voids, and clay.

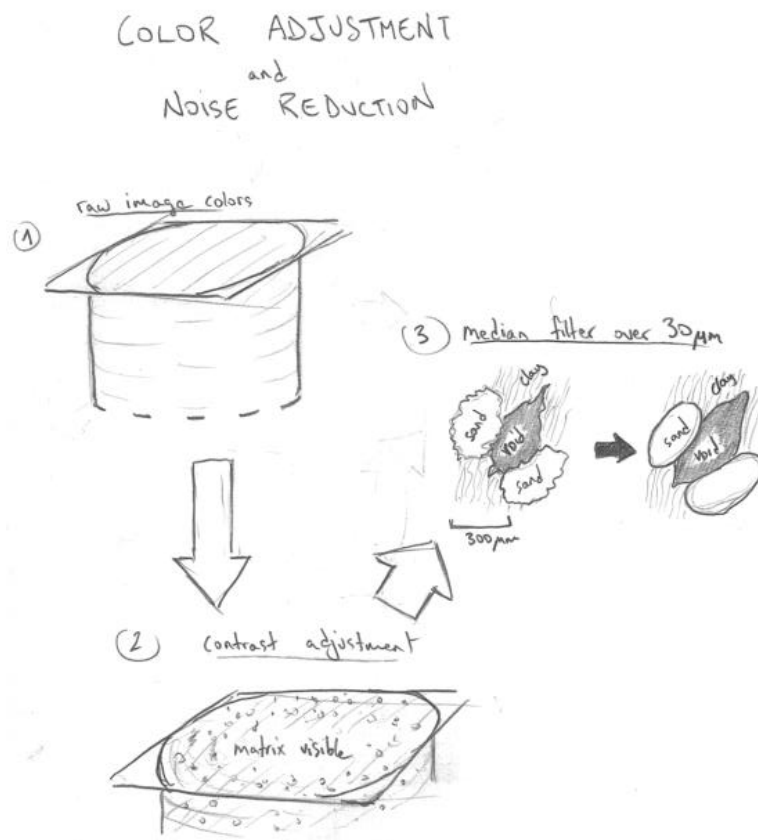


Figure 78 - Image Processing 2: Color adjustment by fixing contrast values in function of the histogram matcher reference image (see Image Processing 1, top right). Finally a median filter reduces noise and error in subsequent steps.

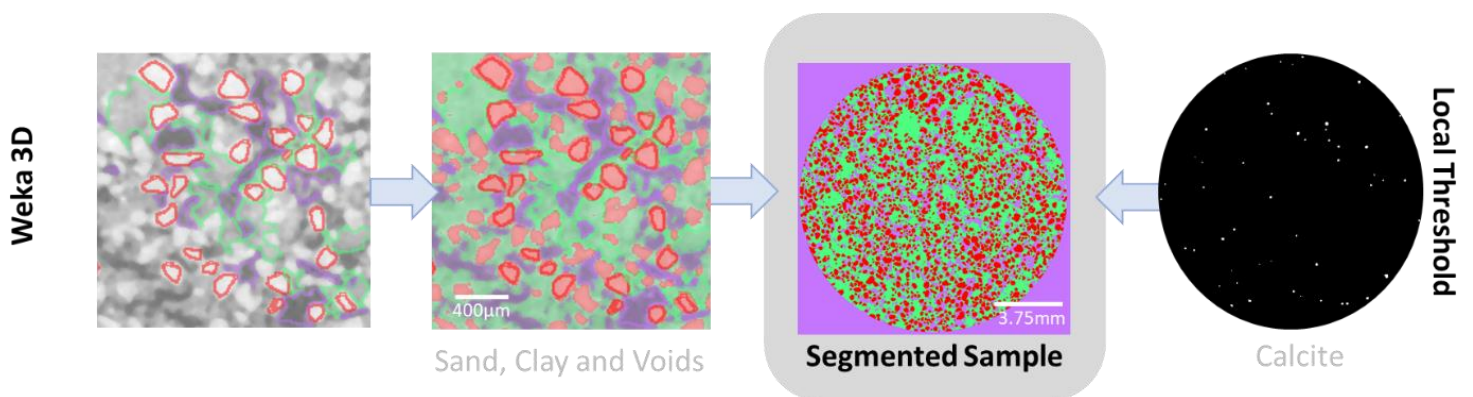


Figure 79 - Iterative training of the machine learning plugin 3D Weka Segmentation planar view (left), and local thresholding to isolate the extremely bright carbonate grains (right) on the raw Micro-CT greyscale image (16-bit, 15µm resolution). Polygons are drawn as training input for the voids (purple), the quartz sand (red), and bentonite matrix (green). Two classifiers are trained by feeding abundant and random 3D data to the neural network for all BC10 and BC30 scans.

Finally, it is imperative that the image analysis must identify and split individual grains and voids which appear “joint” in the 15-micron resolution (see code in annex 8.6.14). To do so, the center location of each grain is found by computing the inverse of a 3D Chamfer Distance Transform (maximal distance from grain’s border, computed towards the center region). This location is used as a “seed”, specifying where the flooding of black voxels by 3D Watershed Segmentation technique should separate grains. The output result is a label image of individual regions of interest (ROI) for each sand, carbonate and void particle.



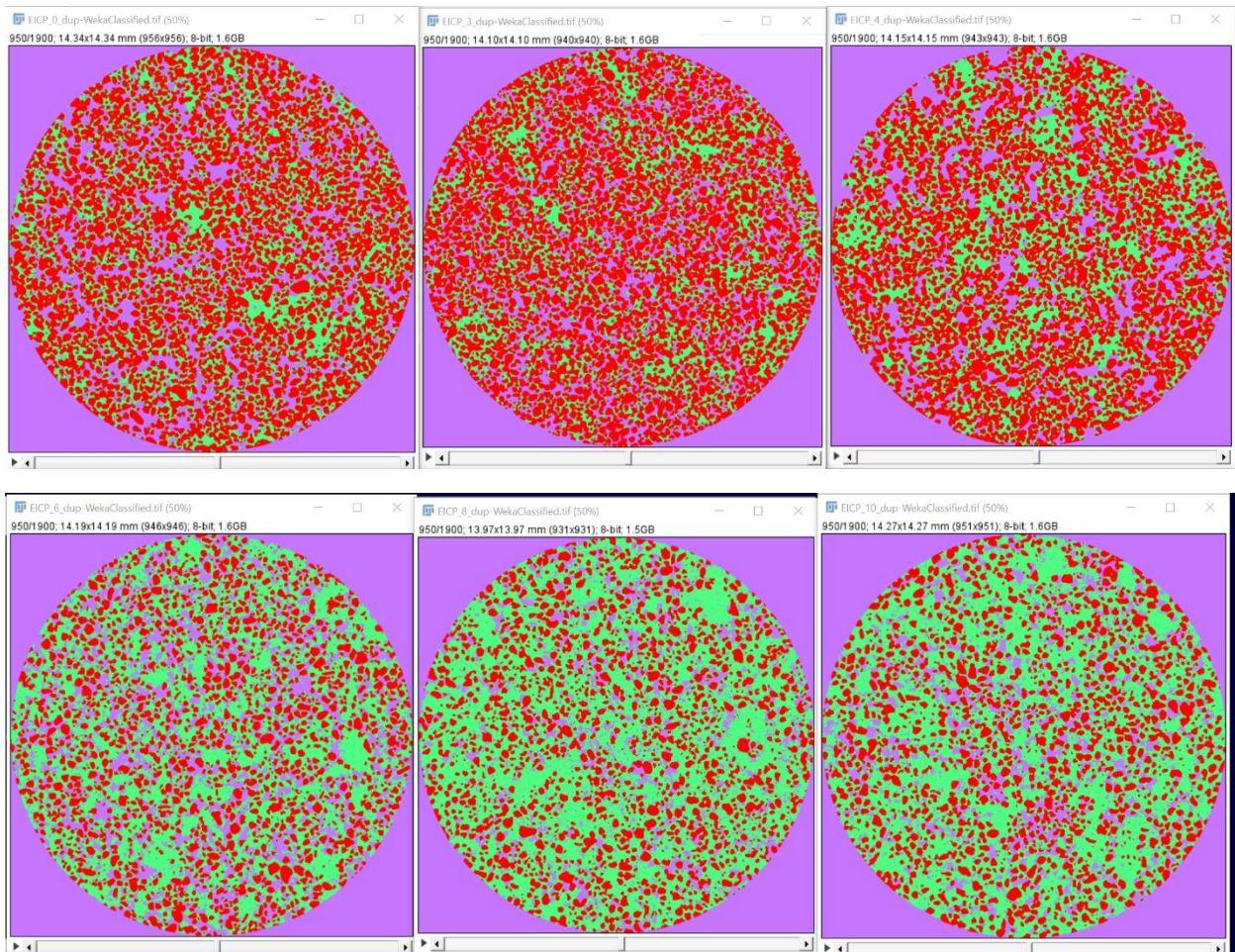
Figure 80 - Step process of individual grain segmentation. Firstly, a chamfer distance transform is applied to the binary (left) to locate the center of each sand/carbonate/void. Secondly, watershed flooding is performed towards the known center points of grains (middle), such that each grains are separated at the catchement split. Thirdly, a label image is generated containing all the regions of interest (right), ready to be analyzed.

3. Image Analysis: To address the microstructural changes between treatment phases, a quantitative methodology is proposed herein. The image quantification step consists in calculating the morphology and volume fraction of target elements using the MorphoLibJ plugin (Legland *et al.*, 2016). The labelled ROIs output from the image segmentation are used identified and analyzed according to various shape factors. These serve as proxies to spot geometrical microstructural evolutions in the data analysis phase.

8.6 Micro-CT - Image Analysis with Fiji ImageJ

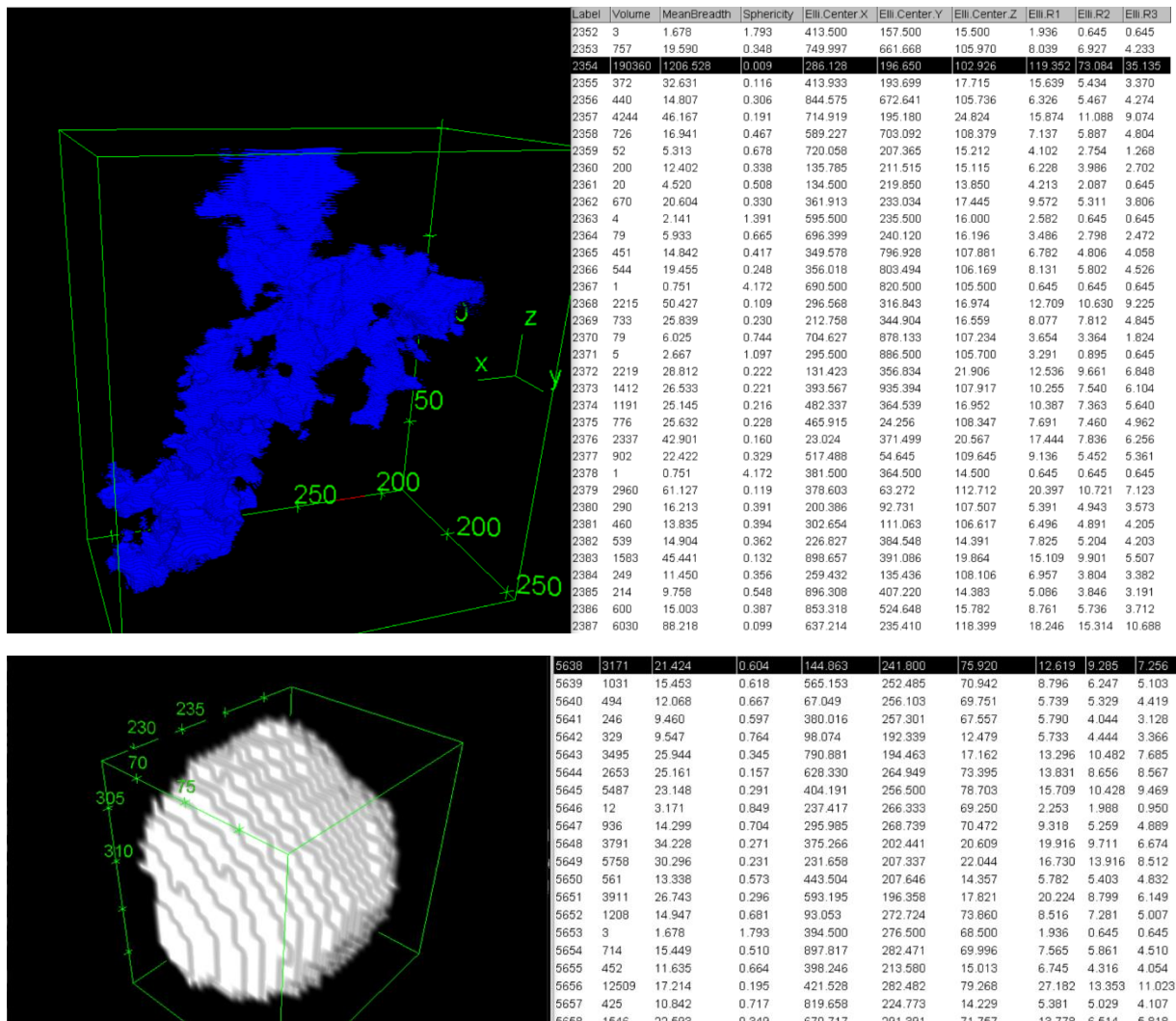
8.6.1 Comparison of 3D Machine Learning Verification

Stack still shots are taken at 950/1900 slices (middle). On the left are untreated (prior to swelling) samples, in the middle EICP only injections, on the right Gnd-EICP complete treatments. The top samples are soil specimen BC10 at $\rho_{\text{dry}}=1.21 \text{ g/cm}^3$. The lower are BC30 at $\rho_{\text{dry}}=1.35 \text{ g/cm}^3$. Untreated samples are visibly characterized by larger void ratios; expected from the optimum moisture content levels prior to saturation. Guanidine treatment displays a slight increase in coarse voids, reducing the sparse distribution of clay.



8.6.2 Grain Scale Verification of Rendered Particles

The rendering of individual particles is performed to verify the expected volume reconstruction of successfully segmented particles. Upon the voids (blue) and sand grains (white) a MorphoLibJ 3D particle analysis is performed to compute dimensions in pixels. Postprocessing of data converts the recorded measurements to millimeters, knowing that the Micro-CT resolution is that of 1 pixel = 1 micron.



Knowing a priori that the grainsizes of Sibelco M32 silica sand have a D_{50} of ~ 200 microns, it is well expected for particles to have ellipsoid axes between 75 to 300 micron (~ 5 pixels for R3, < 20 pixels for R1). Likewise, the rendered geometry and size of the blue void region of interest seems reasonable (eg y -width= $50\text{px} \times 15\mu\text{m} = 750\mu\text{m}$). Additionally, this verification clarifies that all analyses performed following the 3D Watershed Segmentation converts units to global pixel readings. Non segmented data analysis, such as the total volume computation, yield results in millimeters as per the specified image properties.

8.6.3 Edge Detection and Systematic/Random Error

It is notable that the sand fraction in Figure 48 is constant for BC30 (as expected), whereas soil BC10 strangely shows large variability of sand volume. Coating silica with bentonite forms films thinner than the Micro-CT resolution, leading to systematic error by which sand grains will gain "volume %". It is also expected that the images will not discern between surface cladding of calcium carbonate at the < 45 micron micron scale (< 3 pixels). The varying morphologies and nucleation mechanisms vary both with soil density and treatment type (samples N.3-6). This source of random error is enhanced in the silica dominated BC10 specimens, which have a lower greyscale range. More specifically, the low grayscale contrast (less dark bentonite) and noise reducing filters hamper the edge detection performance, inducing random segmentation errors. Contrarily with higher BC30 soils, the bimodal grayscale histogram leads to and increased contrast between grains, which facilitates the edge detection performance.

The histogram matching function is pivotal in automatized image analyses of same soil specimens. The calibration ensures the same quantification procedure, and matrix recognition, between all scans.

Nonetheless, the nature of "force fitting" greyscale values of the adjusted image to existing bins of the base image, induces non-negligible noise features. This inherent feature is targeted in two ways: an additional noise reduction feature over 30 microns (2px) is applied to the fitted image, and the machine learning is trained sufficiently to recognize the "noise" as intrinsic variability in a sole unique constituent. The combined effect successfully avoids "noisy" component segmentation.

However, in the future, an iterative java script may be envisioned, whereby all images are iteratively matched to the mean total grayscale histogram of all scans (not just using one baseline image slice). Additionally, careful calibration of the Micro-CT parameters was not explored in this study, and may present an easier

8.6.4 Big Data Limitations

The 1900 slice image stack of the D15mm*L30mm soil samples, scanned at 15µm resolution, required between 2GB (binary stacks) to 6.5GB (RGB stacks) solid memory. Therefore, the computational requirements of analyzing individual particles in such a medium are large. In this regard, the creation and storage of data for individual grains is attributed to individual regions of interest. These labels can be stored in 16-bit data types according to the 3D segmentation of MorphoLibJ. Ergo, particles are individually attributed a number: commencing at 1 and maximally until 65'553. In the prevalence of many small particles, or noisy signals, the segmentation of the entire image stack become unfeasible. Iterative back analyses led to understand an "overwriting" and appending of data to pre-existing label number. In other words if the stack requires 3*65'553 ROI's, each label would record the sum of three particles. For this reason, an analysis of the memory limit over the full stack shows which fraction requires a smaller volume of analysis (modification of the MorphoLibJ plugin lies beyond the scope of the research, whereas additional noise reduction was omitted in view of time constraints). A Gantt chart illustrates which analysis reached the memory limit, followed by an approximation of the accounted volume of the total soil cylinder.

EICP Sample	0	1	2	3	4	5	6	7	8	9	10	11	Accounted Volume Share	New ROI Stack Size
Sand ROIs	<i>Memory limit exceeded!</i>											~20%	200/1900	
Voids ROIs	<i>Memory limit exceeded!</i>											~60%	1000/1900	
Carbonate ROIs	<i>Memory limit exceeded!</i>											100%	No re-run	

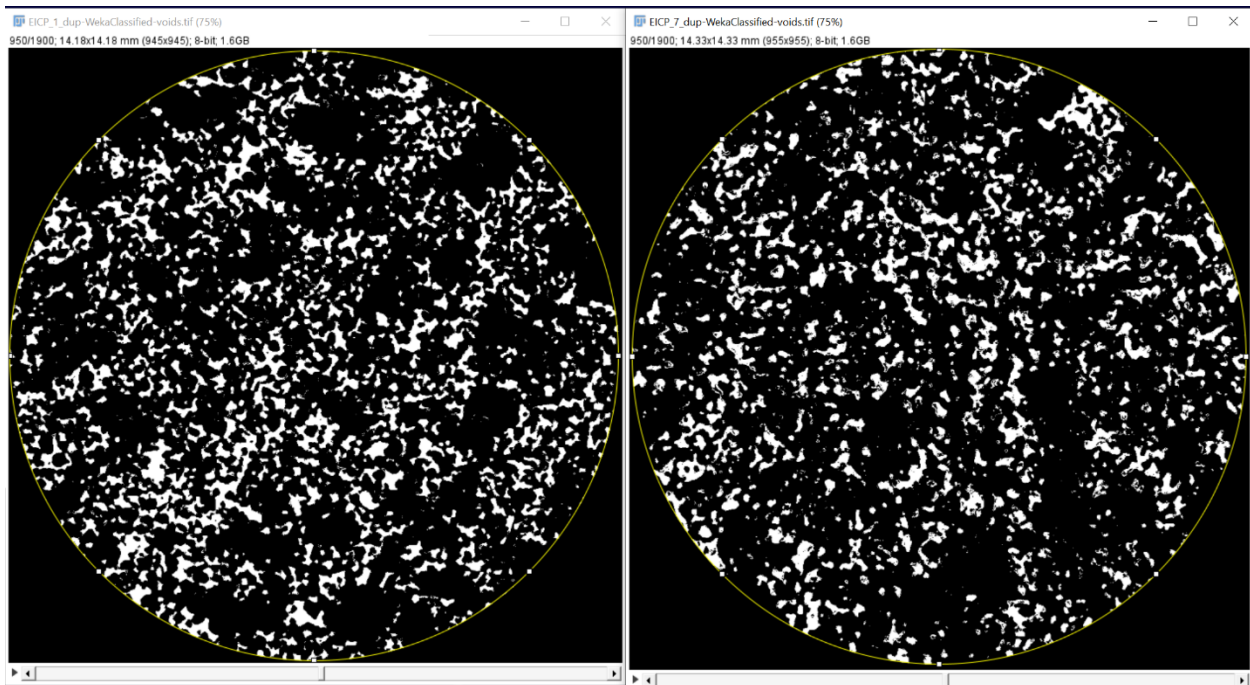
The only sample for which the voids did not exceed the storage limit over the full stack was the loose BC10 sample pre-treated with guanidine, ergo attesting to its effect on the porous media restructuration.

8.6.5 Noise Comparison

The noise increased in the denser BC30, in comparison to the looser BC10 specimens. In this regard, the Weka Segmentation is not the noise inducing factor, but rather the Histogram Matching function. By manually forcing a greyscale histogram into fixed bins calibrated to a specific image, yields inherent noisy signals akin to the data forcing. To complement this, the machine learning tool was trained to recognize noise as a potential "feature" of a soil component, for example discerning noisy bentonite as one element, instead of one containing many small voids.

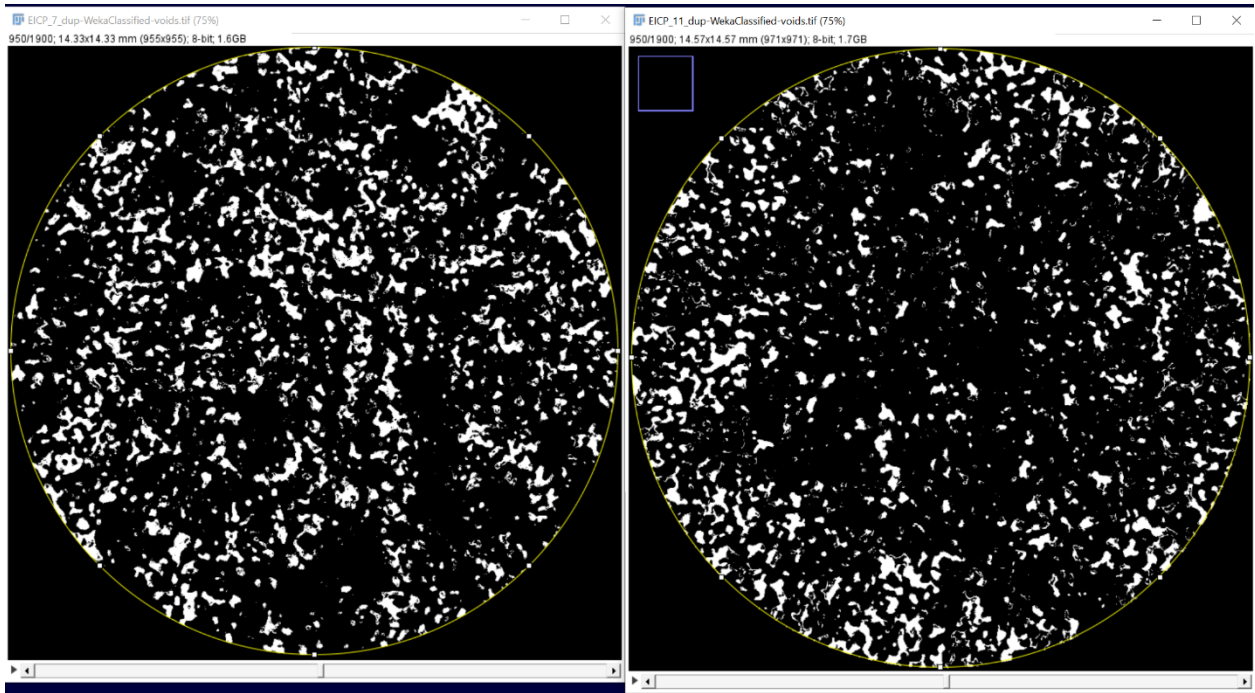
The histogram matching function is pivotal in automatized image analyses of same soil specimens. The calibration ensures the same quantification procedure, and matrix recognition, between all scans. Nonetheless, the nature of "force fitting" greyscale values of the adjusted image to existing bins of the base image, induces non-negligible noise features. This inherent feature is targeted in two ways: an additional noise reduction feature over 30 microns (2px) is applied to the fitted image, and the machine learning is trained sufficiently to recognize the "noise" as intrinsic variability in a sole unique constituent. The combined effect successfully avoids "noisy" component segmentation.

However, in the future, an iterative java script may be envisioned, whereby all images are iteratively matched to the mean total grayscale histogram of all scans (not just using one baseline image slice). Additionally, careful calibration of the Micro-CT parameters was not explored in this study, and may present an easier solution to reduce the grayscale variability between scans.



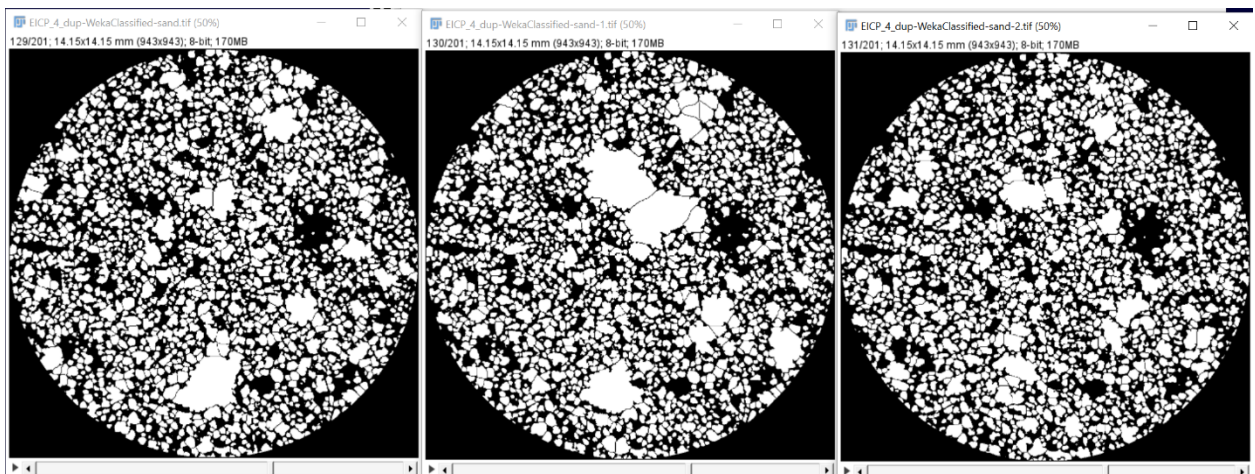
8.6.6 Beam Hardening

Additional complexity and error is introduced in the form of beam hardening, whereby the radial attenuation of X-rays in dense BC30 samples, lead to a “halo” effect in the Micro-CT images. This can be seen in the binary stack of the densest EICP_11 (treated BC30 $1.56\text{g}/\text{cm}^3$). New scans were performed, applying a new calibrated beam hardening parameter. Nonetheless, its effect cannot be taken as negligible on all $\rho_{\text{dry}}=1.56\text{g}/\text{cm}^3$ BC30 samples. This phenomenon is currently well documented, and source of state of the art post-processing scripts, but lies beyond the scope of this research.

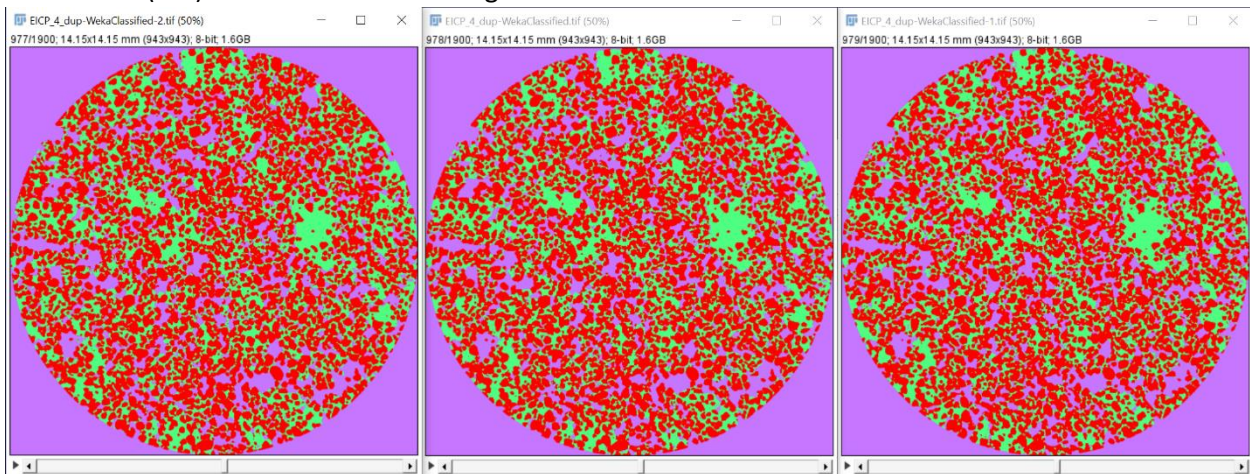


8.6.7 Watershed 3D Artefacts

Automatic watershed segmentation in 3D using the MorphoLibJ plugin (tested both with and without seed image indicating the center location of grains), occasionally included one image stack thick artefacts. Below is shown an example containing snaps of three stacked images, note the often disappearing artefacts. This is suspected to arise from unstable matrix operations over such large and noisy analysis domains in the out of plane direction. Nonetheless, the plugin's robustness and modification was beyond reach for this research, and this source of error is rather addressed in the data processing phase. Outliers of grain size, shape or morphology could be explained by such artefacts.

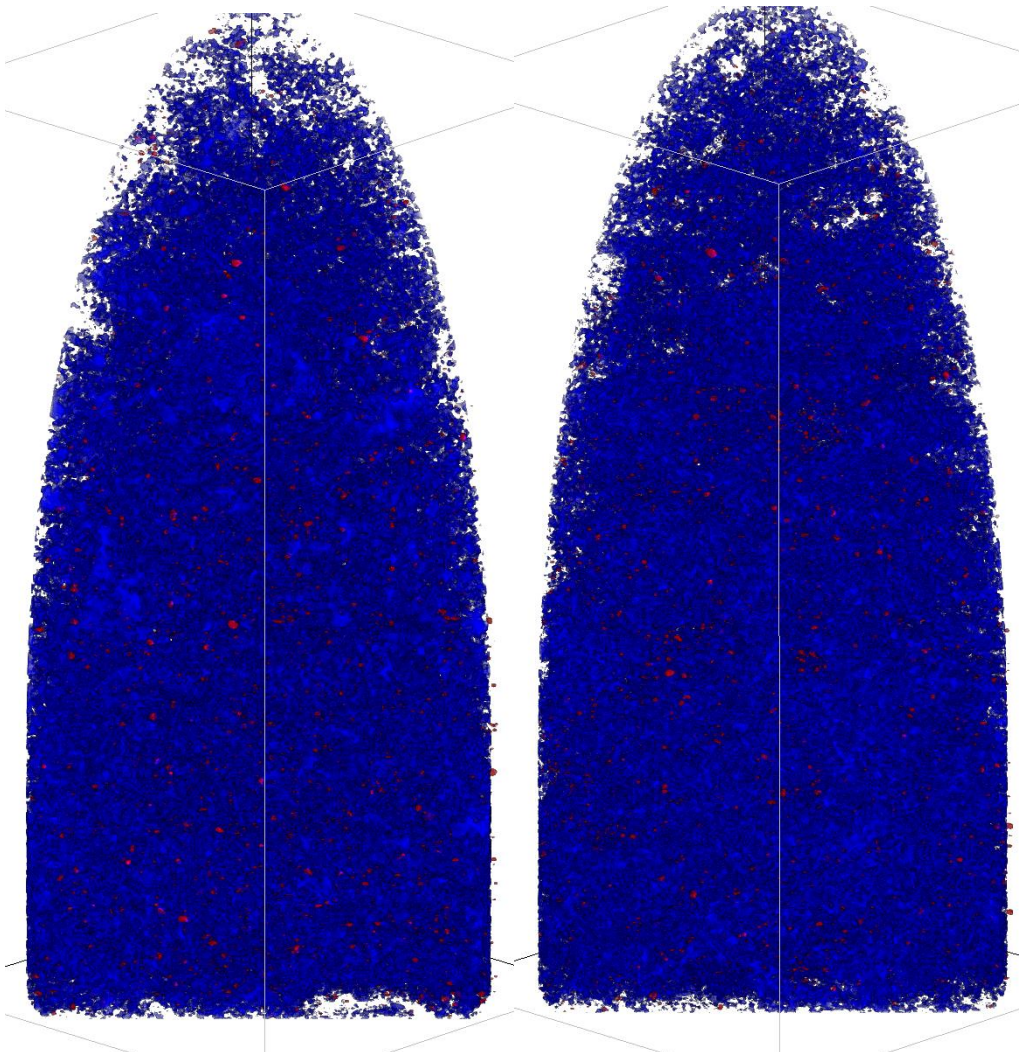


Note that such features are not present in the Weka Segmentation which identifies sand grain boundaries (red) for the same three images.

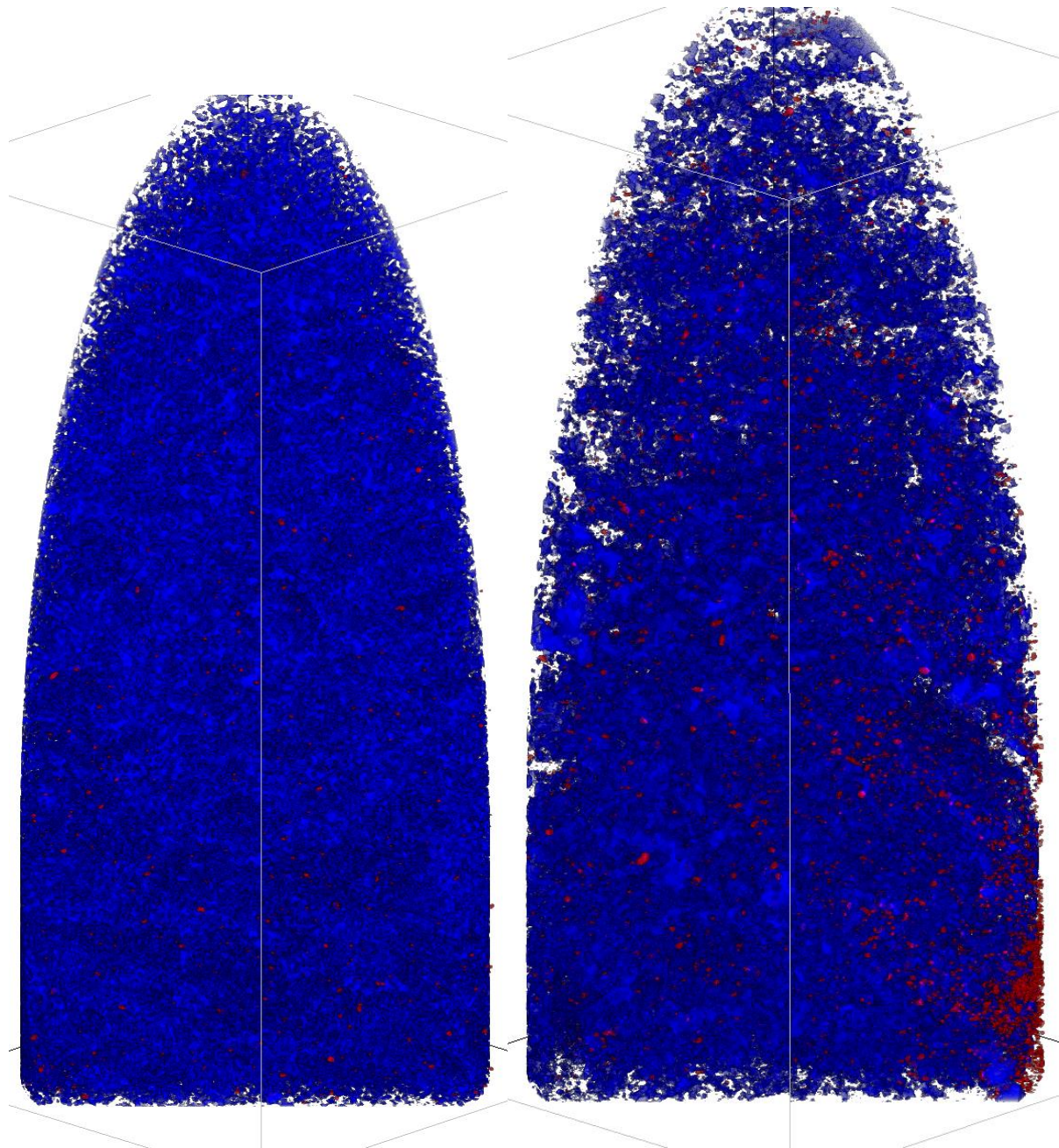


8.6.8 Complete 3D Rendering of Voids-Carbonate

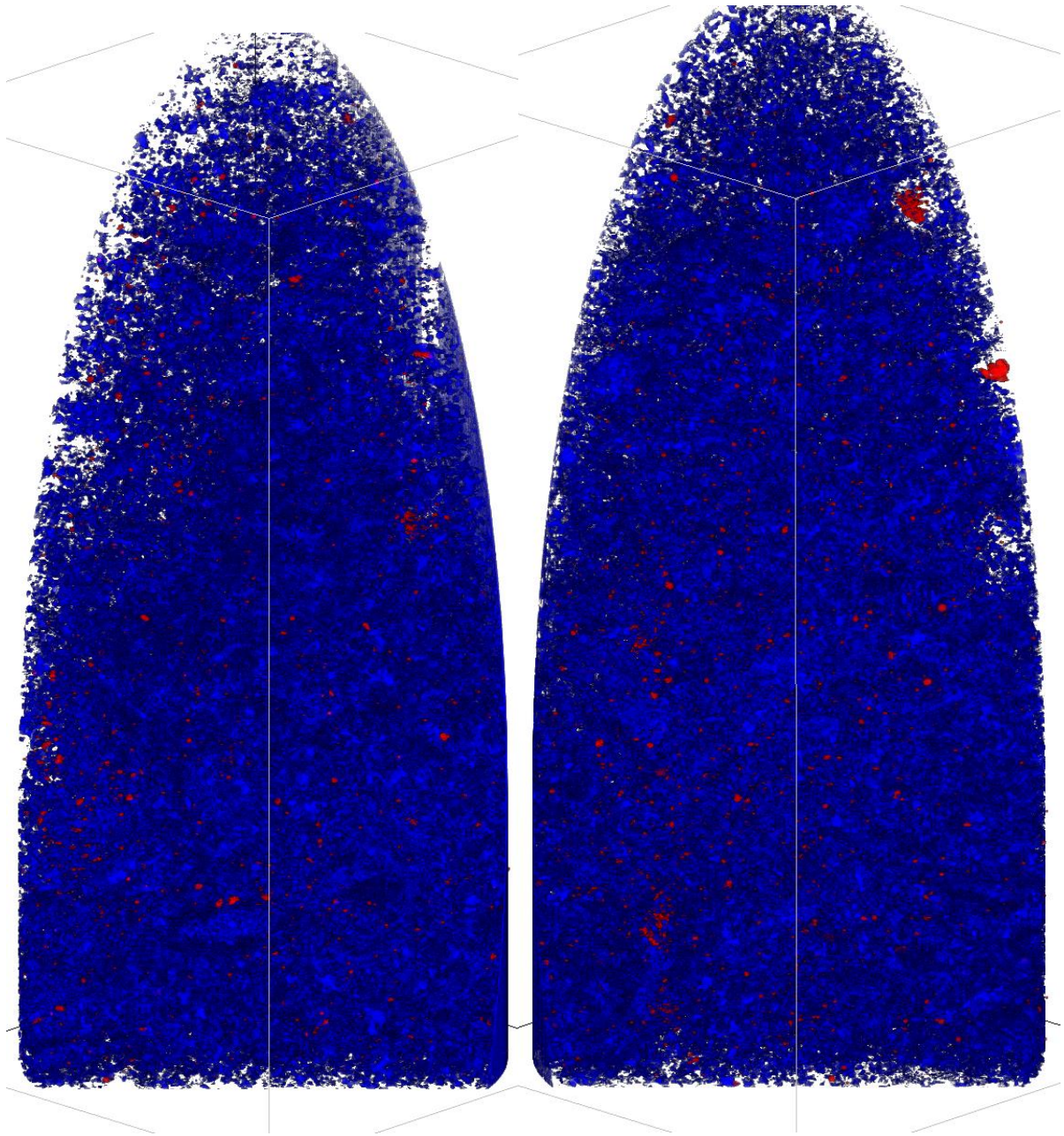
The following two renders are ~80% compacted specimens of BC10, with the left render being EICP only treatments and the right the coupled *Bio2Cementation* treatment.



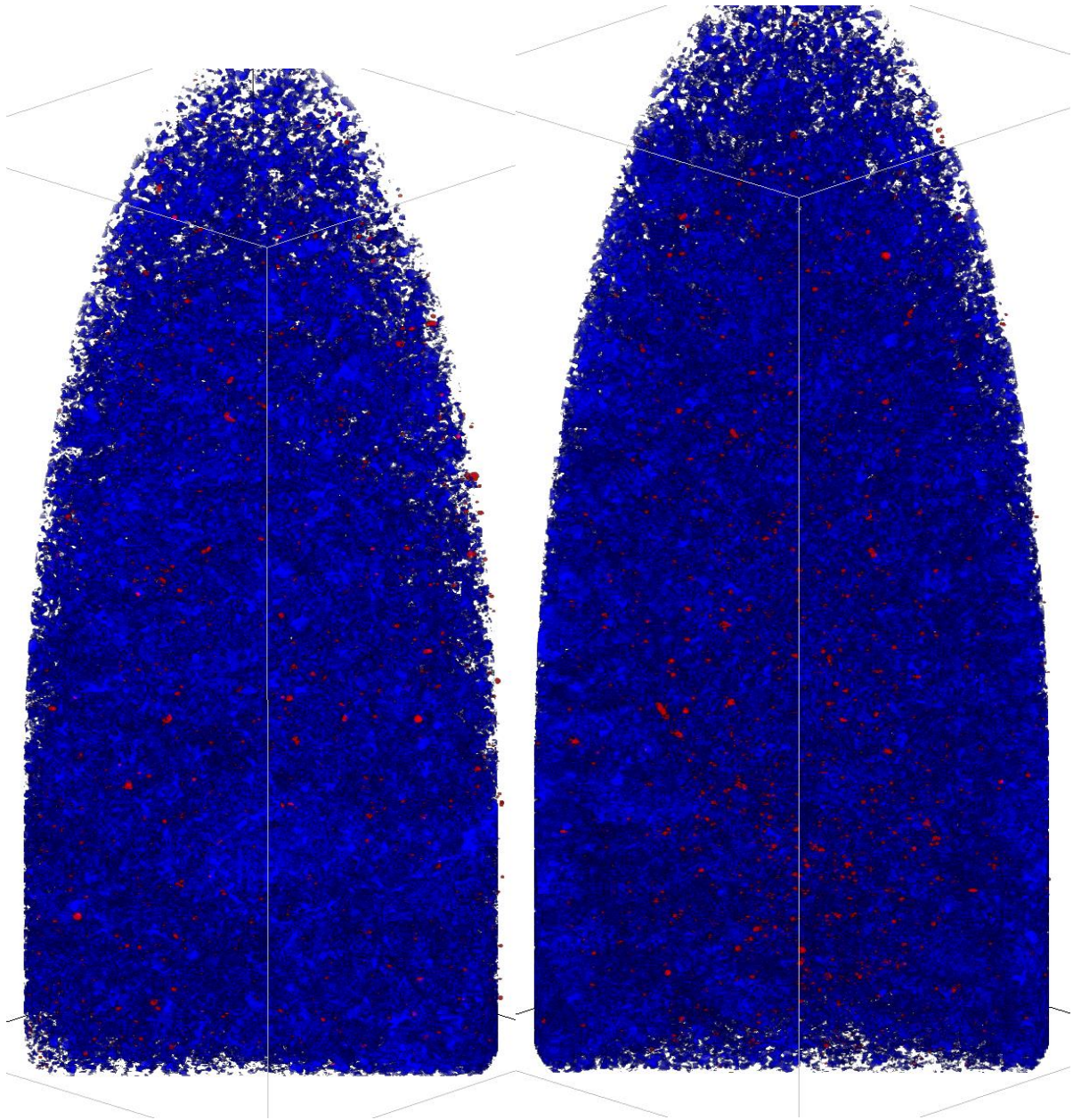
The following two renders are ~95% compacted specimens of BC10, with the left render being EICP only treatments and the right the coupled *Bio2Cementation* treatment.



The following two renders are ~80% compacted specimens of BC30, with the left render being EICP only treatments only and the right the coupled *Bio2Cementation* treatment.



The following two renders are ~95% compacted specimens of BC30, with the left render being EICP only treatments and the right the coupled *Bio2Cementation* treatment.



8.6.9 Preprocessing - Area Calculation Macro

```
// Simple Clear area macro
dir_output = "C:/Users/rwennubstpedri/EICP_Image_Analysis/DelftBlue_SLURM_wp/to/"
title = getTitle();
run("Measure");
Asection=getResult("Area", 0); //insert volume aswell?
print("Asection="+Asection) ;
setBackground(0, 0, 0);
saveAs("Results", dir+"/"+title+"_Area.csv");
run("Clear Outside", "stack");
run("Select None");
saveAs("Tiff", "C:/Users/Ram/Documents/MASTER/TU Delft
GeoEng/Thesis/Results/MicroCT/DelftBlue_SLURM_wp/from/"+title);
```

8.6.10 Preprocessing - Remove Background Macro

```
//Clear Backgrounds
dir = "C:/Users/rwennubstpedri/EICP_Image_Analysis/DelftBlue_SLURM_wp/from/";
for(i=0;i<12;i++){
    run("Fresh Start"); //clear ROI, close images
    open(dir+"EICP_"+i+".tif");
    run("Memory & Threads...", "maximum=500000 parallel=24 run");
    //PER STACK
    title = getTitle();    dotIndex = indexOf(title, ".");    title = substring(title,0,dotIndex);
    selectWindow(title+".tif");
    run("Auto Crop (guess background color)");    run("Save");
    selectWindow(title+".tif");    close();
}
}
```

8.6.11 Preprocessing - Match Histograms Beanshell (Java) Script

```
//Match Histograms Script
import ij.IJ;
import histogram2.HistogramMatcher;
folder = "C:/Users/rwennubstpedri/EICP_Image_Analysis/DelftBlue_SLURM_wp/from/";

//Soil BC10
base_image = IJ.openImage(folder + "EICP_5.tif"); //baseline image
base_processor = base_image.getProcessor();
base_histogramm = base_processor.getHistogram(); //baseline greyscale histogram
for( int i=0; i<5; i++ ) { //for all other BC10 scans
    IJ.log("image" + i); //state which img is modified

    current_image = IJ.openImage(folder+"EICP_"+i+".tif"); //open img to modify
    stack = current_image.getImageStack();

    for (int j=1; j<=stack.getSize(); j++){ //for each image in the stack loop
        IJ.log("slice" + j);
        processor = stack.getProcessor(j);
        h = processor.getHistogram();
        matcher = new HistogramMatcher(); //call base processor, match slice
        matched_histogramm = matcher.matchHistograms(h, base_histogramm);
        processor.applyTable(matched_histogramm); //fix table stored data bounds
        stack.setProcessor(processor, j); //apply process matching
    }
    IJ.save(current_image, folder+"EICP_"+i+"_matched.tif"); //once all slices are complete = save stack
}

//Soil BC30
base_image = IJ.openImage(folder + "EICP_6.tif");
base_processor = base_image.getProcessor();
base_histogramm = base_processor.getHistogram();

for( int i=7; i<12; i++ ) {
    IJ.log("image" + i);

    current_image = IJ.openImage(folder+"EICP_"+i+".tif");
    stack = current_image.getImageStack();

    for (int j=1; j<=stack.getSize(); j++){
        IJ.log("slice" + j);
        processor = stack.getProcessor(j);
        h = processor.getHistogram();
        matcher = new HistogramMatcher();
        matched_histogramm = matcher.matchHistograms(h, base_histogramm);
        processor.applyTable(matched_histogramm);
        stack.setProcessor(processor, j);
    }
    IJ.save(current_image, folder+"EICP_"+i+"_matched.tif");
}
}
```

8.6.12 Preprocessing - Image Contrast and Noise Reduction Macro

```
// Process Image Contrast and Median 2Px Filter - for Soil Type BC10 - BC30
dir = "C:/Users/rwennubstpedri/EICP_Image_Analysis/DelftBlue_SLURM_wp/from/"
dir_output = "C:/Users/rwennubstpedri/EICP_Image_Analysis/DelftBlue_SLURM_wp/to/"
run("Fresh Start"); //clear ROI, close images
run("Memory & Threads...", "maximum=500000 parallel=24 run");

//Soil BC10 with histogram matched to img5
for(i=0;i<6;i++){
    if(i<5)
        open(dir+"EICP_"+i+"_matched.tif");
    else {
        open(dir+"EICP_"+i+".tif");
    }
    //Get image name without .tif
    title_dup = getTitle();    dotIndex = indexOf(title_dup, ".");
    title_dup = substring(title_dup,0,dotIndex);
    run("Properties...", "channels=1 slices=1900 frames=1 pixel_width=0.0150000 pixel_height=0.0150000");
}
```

```

voxel_depth=0.0150000");
    setMinAndMax(2254, 6896); run("Apply LUT", "stack");
    run("Median...", "radius=2 stack");
    save(dir+"EICP_"+i+"_dup.tif");
}

//Soil BC10 with histogram matched to img6
for(i=6;i<12;i++){
    if(i>6)
        open(dir+"EICP_"+i+"_matched.tif");
    else {
        open(dir+"EICP_"+i+".tif");}
    title_dup = getTitle();    dotIndex = indexOf(title_dup, ".");
    title_dup = substring(title_dup,0,dotIndex);
    run("Properties...", "channels=1 slices=1900 frames=1 pixel_width=0.0150000 pixel_height=0.0150000
voxel_depth=0.0150000");
    setMinAndMax(3547, 8724); run("Apply LUT", "stack");
    run("Median...", "radius=2 stack");
    save(dir+"EICP_"+i+"_dup.tif");
}

```

8.6.13 Segmentation - Macro

```

//SEGMENTATION LOOPS - 2x Soils BC10(0:5) BC30(6:11)
// !! If NOT saving intermediate images then MUST remove Select Window ==> .tif <==

dirWeka = "C:/Users/rwennubstpedri/EICP_Image_Analysis/DelftBlue_SLURM_wp/scripts/"
dir = "C:/Users/rwennubstpedri/EICP_Image_Analysis/DelftBlue_SLURM_wp/from/"
dir_output = "C:/Users/rwennubstpedri/EICP_Image_Analysis/DelftBlue_SLURM_wp/to/"

for(i=1;i<6;i++){
    run("Fresh Start"); //clear ROI, close images
    open(dir+"EICP_"+i+"_dup.tif"); //color adjusted, filter, no background, matched histogram
    run("Memory & Threads...", "maximum=500000 parallel=24 run");

    //PER STACK
    title_dup = getTitle();    dotIndex = indexOf(title_dup, ".");    title_dup = substring(title_dup,0,dotIndex);
    run("Properties...", "channels=1 slices=1900 frames=1 pixel_width=0.0150000 pixel_height=0.0150000
voxel_depth=0.0150000"); // SET SLICE NUMBER!!

    //    // Create Corrected Image
    //    NOTE: Area and Histogram_Matching were always run separately to this Segmentation script (for stepwise
    //    checking of outputs)
    //    run("Sand Clay area2"); //Script computing the area of cylindrical soil sample inside the soil sleeve. Output
    //    is a cropped image and _Area.csv
    //    run("Remove Background"); //Script reducing image size (optimization) to limits of soil cylinder. Output is
    //    overwritten image
    //    eval("bsh", dirWeka+"old/Match_Histograms.bsh"); //Beanshell (~Java) script nested for Loop: matches
    //    greyscale histograms for both soils to a "base" image. Whereby EICP0>=5 is BC10 (EICP_5 = hist match ref) and
    //    EICP6>=11 is BC30 (EICP_6 = ref) !! != RUN when called from .ijm!!
    //    run("Image Contrast wFilter"); //Script adjusting color contrast, voxel size and noise reduction

    //===== SEGMENTATION =====
    // SEGMENTATION by Manual: Carbonate
    //selectWindow(title_dup+".tif");
    run("Duplicate...", "title="+title_dup+"-carbonate.tif duplicate");
    run("8-bit");
    setThreshold(240, 255, "red");
    setOption("BlackBackground", true);
    run("Convert to Mask", "method=Default background=Default black");
    run("Fill Holes", "stack");
    run("Dilate", "stack");
    saveAs("Tiff", dir_output + "/" + title_dup + "-carbonate.tif");
    // SEGMENTATION by Weka: Sand, clay, voids
    selectWindow(title_dup+".tif");
    run("Trainable Weka Segmentation 3D");
    wait(3000);
    selectWindow("Trainable Weka Segmentation v3.3.2");
    call("trainableSegmentation.Weka_Segmentation.setFeature", "Maximum=true");
    call("trainableSegmentation.Weka_Segmentation.setMaximumSigma", "4.0");
    call("trainableSegmentation.Weka_Segmentation.loadClassifier",
dirWeka+"/EICP_Classifier_sand-bent-void_BC10.model");
    wait(20000);
    call("trainableSegmentation.Weka_Segmentation.getResult");
    print("weka done");
    selectWindow("Trainable Weka Segmentation v3.3.2");
    close();
    selectWindow("Classified image");
    saveAs("Tiff", dir_output + "/" + title_dup + "-WekaClassified.tif");
    // SEGMENTATION: Sand, clay, voids
    selectWindow(title_dup+"-WekaClassified.tif");
    run("Duplicate...", "title="+title_dup+"-WekaClassified-sand.tif duplicate");
    run("8-bit");

```

```

selectWindow(title_dup+"-WekaClassified.tif");
run("Duplicate...", "title="+title_dup+"-WekaClassified-clay.tif duplicate");
run("8-bit");
selectWindow(title_dup+"-WekaClassified.tif");
run("Duplicate...", "title="+title_dup+"-WekaClassified-voids.tif duplicate");
run("8-bit");
selectWindow(title_dup+"-WekaClassified.tif");
close();

// THRESHOLD x3 Particles
selectWindow(title_dup+"-WekaClassified-sand.tif");
//setAutoThreshold("Otsu");
setOption("BlackBackground", true);
run("Convert to Mask", "method=Otsu background=Light calculate black");
run("Fill Holes", "stack");
//remove carbonate grains from sand (binary subtract)
// imageCalculator("Subtract stack", title_dup+"-WekaClassified-sand.tif", title_dup+"-carbonate.tif");
//watershed to split adjacent grains
run("Watershed", "stack");
saveAs("Tiff", dir_output + "/" + title_dup + "-WekaClassified-sand.tif");
print("Done: Sand Segmentation");
selectWindow(title_dup+"-WekaClassified-clay.tif");
setThreshold(140, 170, "red");
setOption("BlackBackground", true);
run("Convert to Mask", "method=Default background=Default black");
saveAs("Tiff", dir_output + "/" + title_dup + "-WekaClassified-clay.tif");
print("Done: Clay Segmentation");
selectWindow(title_dup+"-WekaClassified-voids.tif");
setThreshold(171, 255, "red");
setOption("BlackBackground", true);
run("Convert to Mask", "method=Default background=Default black");
saveAs("Tiff", dir_output + "/" + title_dup + "-WekaClassified-voids.tif");
print("Done: Voids Segmentation");
}
print("!BC10 done!");

for(i=6;i<12;i++){
run("Fresh Start"); //clear ROI, close images
open(dir+"EICP_"+i+"_dup.tif"); //color adjusted, filter, no background, matched histogram
run("Memory & Threads...", "maximum=500000 parallel=24 run");
//PER STACK
title_dup = getTitle(); dotIndex = indexOf(title_dup, "."); title_dup = substring(title_dup, 0, dotIndex);
run("Properties...", "channels=1 slices=1900 frames=1 pixel_width=0.0150000 pixel_height=0.0150000
voxel_depth=0.0150000"); // SET SLICE NUMBER!!

// // Create Corrected Image
// NOTE: Area and Histogram_Matching were always run separately to this Segmentation script (for stepwise
checking of outputs)
// run("Sand Clay area2"); //Script computing the area of cylindrical soil sample inside the soil sleeve. Output
is a cropped image and _Aarea.csv
// run("Remove Background"); //Script reducing image size (optimization) to limits of soil cylinder. Output is
overwritten image
// eval("bsh", dirWeka+"old/Match_Histograms.bsh"); //Beanshell (~Java) script nested for Loop: matches
greyscale histograms for both soils to a "base" image. Whereby EICP0>=5 is BC10 (EICP_5 = hist match ref) and
EICP6>=11 is BC30 (EICP_6 = ref) !! != RUN when called from .ijm!!
// run("Image Contrast wFilter"); //Script adjusting color contrast, voxel size and noise reduction

//===== SEGMENTATION =====
// SEGMENTATION by Manual: Carbonate
//selectWindow(title_dup+".tif");
run("Duplicate...", "title="+title_dup+"-carbonate.tif duplicate");
run("8-bit");
setThreshold(240, 255, "red");
setOption("BlackBackground", true);
run("Convert to Mask", "method=Default background=Default black");
run("Fill Holes", "stack");
run("Dilate", "stack");
saveAs("Tiff", dir_output + "/" + title_dup + "-carbonate.tif");
// SEGMENTATION by Weka: Sand, clay, voids
selectWindow(title_dup+".tif");
run("Trainable Weka Segmentation 3D");
wait(3000);
selectWindow("Trainable Weka Segmentation v3.3.2");
call("trainableSegmentation.Weka_Segmentation.setFeature", "Maximum=true");
call("trainableSegmentation.Weka_Segmentation.setMaximumSigma", "4.0");
call("trainableSegmentation.Weka_Segmentation.loadClassifier",
dirWeka+"EICP_Classifier_sand-bent-void_BC30New.model");
wait(20000);
call("trainableSegmentation.Weka_Segmentation.getResult");
print("weka done");
selectWindow("Trainable Weka Segmentation v3.3.2");
close();
selectWindow("Classified image");
saveAs("Tiff", dir_output + "/" + title_dup + "-WekaClassified.tif");
// SEGMENTATION: Sand, clay, voids

```

```

selectWindow(title_dup+"-WekaClassified.tif");
run("Duplicate...", "title="+title_dup+"-WekaClassified-sand.tif duplicate");
run("8-bit");
selectWindow(title_dup+"-WekaClassified.tif");
run("Duplicate...", "title="+title_dup+"-WekaClassified-clay.tif duplicate");
run("8-bit");
selectWindow(title_dup+"-WekaClassified.tif");
run("Duplicate...", "title="+title_dup+"-WekaClassified-voids.tif duplicate");
run("8-bit");
selectWindow(title_dup+"-WekaClassified.tif");
close();
// THRESHOLD x3 Particles
selectWindow(title_dup+"-WekaClassified-sand.tif");
//setAutoThreshold("Otsu");
setOption("BlackBackground", true);
run("Convert to Mask", "method=Otsu background=Light calculate black");
run("Fill Holes", "stack");
//remove carbonate grains from sand (binary subtract)
// imageCalculator("Subtract stack", title_dup+"-WekaClassified-sand.tif", title_dup+"-carbonate.tif");
//watershed to split adjacent grains
run("Watershed", "stack");
saveAs("Tiff", dir_output + "/" + title_dup + "-WekaClassified-sand.tif");
print("Done: Sand Segmentation");
selectWindow(title_dup+"-WekaClassified-clay.tif");
setThreshold(140, 170, "red");
setOption("BlackBackground", true);
run("Convert to Mask", "method=Default background=Default black");
saveAs("Tiff", dir_output + "/" + title_dup + "-WekaClassified-clay.tif");
print("Done: Clay Segmentation");
selectWindow(title_dup+"-WekaClassified-voids.tif");
setThreshold(171, 255, "red");
setOption("BlackBackground", true);
run("Convert to Mask", "method=Default background=Default black");
saveAs("Tiff", dir_output + "/" + title_dup + "-WekaClassified-voids.tif");
print("Done: Voids Segmentation");
}
print("!BC30 done!");

```

8.6.14 Analysis – 3D ROI Calculations

```

//ANALYSIS LOOPS
// !! If NOT saving intermediate images then MUST remove Select Window ==> .tif <==

dirWeka = "C:/Users/rwennubstpedri/EICP_Image_Analysis/DelftBlue_SLURM_wp/scripts/"
dir = "C:/Users/rwennubstpedri/EICP_Image_Analysis/DelftBlue_SLURM_wp/to/"
dir_output = "C:/Users/rwennubstpedri/EICP_Image_Analysis/DelftBlue_SLURM_wp/to/analysis"

for(i=0;i<12;i++){
    run("Memory & Threads...", "maximum=500000 parallel=24 run");
    //===== ANALYSIS =====
    // each grain is analyzed individually. Geodesic diameter 3D and Feret cannot be computed for voids (fatal errors),
    // thus no tortuosity info.

    //VOIDS - Microstructure 3D Analysis
    run("Fresh Start"); //clear ROI, close images
    open(dir+"EICP_"+i+"_dup-WekaClassified-voids.tif");
    run("Properties...", "channels=1 slices=1900 frames=1 pixel_width=0.0150000 pixel_height=0.0150000
voxel_depth=0.0150000"); // SET SLICE NUMBER!!
    selectWindow("EICP_"+i+"_dup-WekaClassified-voids.tif");
    title_voids = getTitle(); dotIndex = indexOf(title_voids, "."); title_voids =
substring(title_voids,0,dotIndex);
    run("Chamfer Distance Map 3D", "distances=[Svensson <3,4,5,7>] output=[32 bits] normalize"); //Distance
Transform 3D = center of mass of ROI
    setThreshold(3, 65535, "red");
    setOption("BlackBackground", true);
    run("Convert to Mask", "method=Default background=Default black"); // Binary Mask 3D = mask image of
centers of ROI, used to control segmentation Location
    run("Connected Components Labeling", "connectivity=6 type=float"); //Label/Seeds of ROIs 3D
    run("3D Watershed Split", "binary="+title_voids+" seeds="+title_voids+"-dist-lbl radius=2"); //Watershed
Split 3D (Geometry: Weka Sand Regions, Location: Seeds of ROIs in 3D)
    run("Analyze Regions 3D", "volume mean_breadth sphericity equivalent_ellipsoid ellipsoid_elongations
max._inscribed surface_area_method=[Crofton (13 dirs.)] euler_connectivity=6");
    saveAs("Results", dir_output+"/"+title_voids+"-3DRegions.csv");

    //CARBONATE - Microstructure 3D Analysis
    run("Fresh Start");
    open(dir+"EICP_"+i+"_dup-carbonate.tif");
    run("Properties...", "channels=1 slices=1900 frames=1 pixel_width=0.0150000 pixel_height=0.0150000
voxel_depth=0.0150000");
    selectWindow("EICP_"+i+"_dup-carbonate.tif");
    title_carb = getTitle(); dotIndex = indexOf(title_carb, "."); title_carb =
substring(title_carb,0,dotIndex);
    run("Chamfer Distance Map 3D", "distances=[Svensson <3,4,5,7>] output=[32 bits] normalize");

```

```

        setThreshold(3, 65535, "red");
        setOption("BlackBackground", true);
        run("Convert to Mask", "method=Default background=Default black");
        run("Connected Components Labeling", "connectivity=6 type=float");
        run("3D Watershed Split", "binary="+title_carb+" seeds="+title_carb+"-dist-lbl radius=2");
        run("Analyze Regions 3D", "volume mean_breadth sphericity equivalent_ellipsoid ellipsoid_elongations
max._inscribed surface_area_method=[Crofton (13 dirs.)] euler_connectivity=6");
        saveAs("Results", dir_output+"/"+title_carb+"-3DRegions.csv");

//SAND - Microstructure 3D Analysis
run("Fresh Start");
    open(dir+"EICP_"+i+"_dup-WekaClassified-sand.tif");
        run("Properties...", "channels=1 slices=1900 frames=1 pixel_width=0.0150000 pixel_height=0.0150000
voxel_depth=0.0150000");
        selectWindow("EICP_"+i+"_dup-WekaClassified-sand.tif");
        title_sand = getTitle(); dotIndex = indexOf(title_sand, "."); title_sand =
substring(title_sand,0,dotIndex);
        run("Chamfer Distance Map 3D", "distances=[Svensson <3,4,5,7>] output=[32 bits] normalize");
            setThreshold(3, 65535, "red");
            setOption("BlackBackground", true);
            run("Convert to Mask", "method=Default background=Default black");
            run("Connected Components Labeling", "connectivity=6 type=float");
            run("3D Watershed Split", "binary="+title_sand+" seeds="+title_sand+"-dist-lbl radius=2");
            run("Analyze Regions 3D", "volume mean_breadth sphericity equivalent_ellipsoid ellipsoid_elongations
max._inscribed surface_area_method=[Crofton (13 dirs.)] euler_connectivity=6");
            saveAs("Results", dir_output+"/"+title_sand+"-3DRegions.csv");

//CLAY - Microstructure 3D Analysis
run("Fresh Start");
    open(dir+"EICP_"+i+"_dup-WekaClassified-clay.tif");
        run("Properties...", "channels=1 slices=1900 frames=1 pixel_width=0.0150000 pixel_height=0.0150000
voxel_depth=0.0150000");
        selectWindow("EICP_"+i+"_dup-WekaClassified-clay.tif");
        title_clay = getTitle(); dotIndex = indexOf(title_clay, "."); title_clay =
substring(title_clay,0,dotIndex);
        run("Analyze Regions 3D", "volume mean_breadth sphericity equivalent_ellipsoid ellipsoid_elongations
max._inscribed surface_area_method=[Crofton (13 dirs.)] euler_connectivity=6");
        saveAs("Results", dir_output+"/"+title_clay+"-3DRegions.csv");
print(i);
}
print("!analysis done!");

```

8.6.15 Delft Blue Supercomputer

```

#!/bin/bash

#!/bin/bash
#SBATCH --job-name="EICP_Images"
#SBATCH --cpus-per-task=8
#SBATCH --mem=128G
#SBATCH --time=24:00:00
#SBATCH --partition=standard
#SBATCH --account=Education-CEG-MSc-AES

echo "EICP Micro-CT Image Analysis"

#run imagej script
echo "Running ImageJ ..."
/home/rwennubstpedri/DelftBlue_SLURM_wp/programs/Fiji_app/ImageJ-linux64 --headless -macro
/home/rwennubstpedri/DelftBlue_SLURM_wp/scripts/WennubstPedrini_Macro_ImageJ_DB.ijm

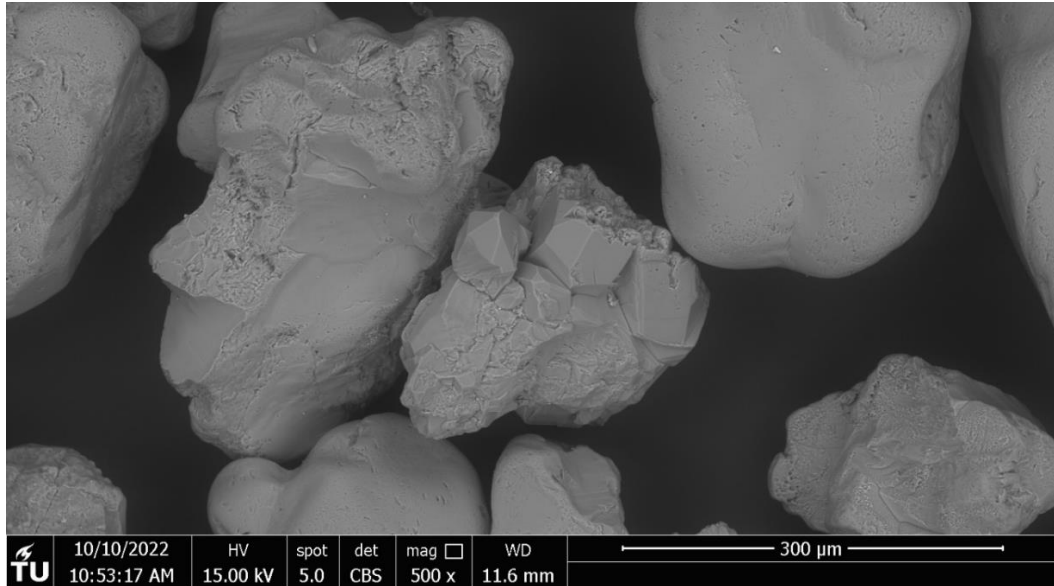
echo "End of Script"

```

8.7 SEM – Additional Images

8.7.1 Sibelco M32 Sand

Sibelco M32 sand is clean, washed, with no coating. Particles range in texture; most commonly sub-rounded crystals with micrometer long striations reminiscent of abrasion in suspension, or angular silica with visible quartz crystal planes.



8.7.2 SEM Sample Preparation

The SEM analysis requires thin sampling of minimal volume. Approximately, scooping extracts $\sim 1\text{mm}^3$ of soil mass from the D15mm cylinders. This is done at three intervals. One $\sim 2\text{mm}$ from the base, one halfway, and one $\sim 1\text{-}2\text{mm}$ from to top filter. This method is a very localized extraction, and thus partial view, of the soil column. For this reason, there is a risk that SEM imaging may be non-representative of the entire soil mass. Additionally, untreated swelling bentonite (eg. Dense BC30 EICP only) clogs pores, which minimizes depth perception and information in the third dimension. This is especially notable when soil samples are “smeared” upon the carbon sample holder, instead of “placed”.



8.7.3 Calcium Carbonate Polymorphs

SEM imaging provides extensive insight into the crystal growth and formation mechanisms. To construct a knowledge base of calcium carbonate mineralogy, imaging of EICP is performed outside of the soil matrix. This sub-section analyzes the crystal morphology and growth of pure EICP, and EICP containing 0.25[mol/L] guanidine additive. Doing so, yields insight in the hypothesized positive interaction of guanidinium and EICP.

Guanidine free 0.5[mol/L] EICP solutions crystallize calcium carbonate exclusively as the trigonal calcite polymorph. The stacking of grains is comprised of highly nucleated cubic and cuboctahedron $\sim 5\text{-}10\text{ }\mu\text{m}$ crystals, which display large stepwise propagation upon each other (Figure 81). In contrast, solutions including 0.25[mol/L] guanidine yields two calcium carbonate polymorphs: either extensive out of plane expansion aragonite rods (Figure 83), or large mesocrystals of modulated rhombohedral calcite (Figure 82). The weaker vaterite polymorph (often spherical at pH=8, or flower like in very alkali media (Oral and Ercan, 2018)) is not found in either test.

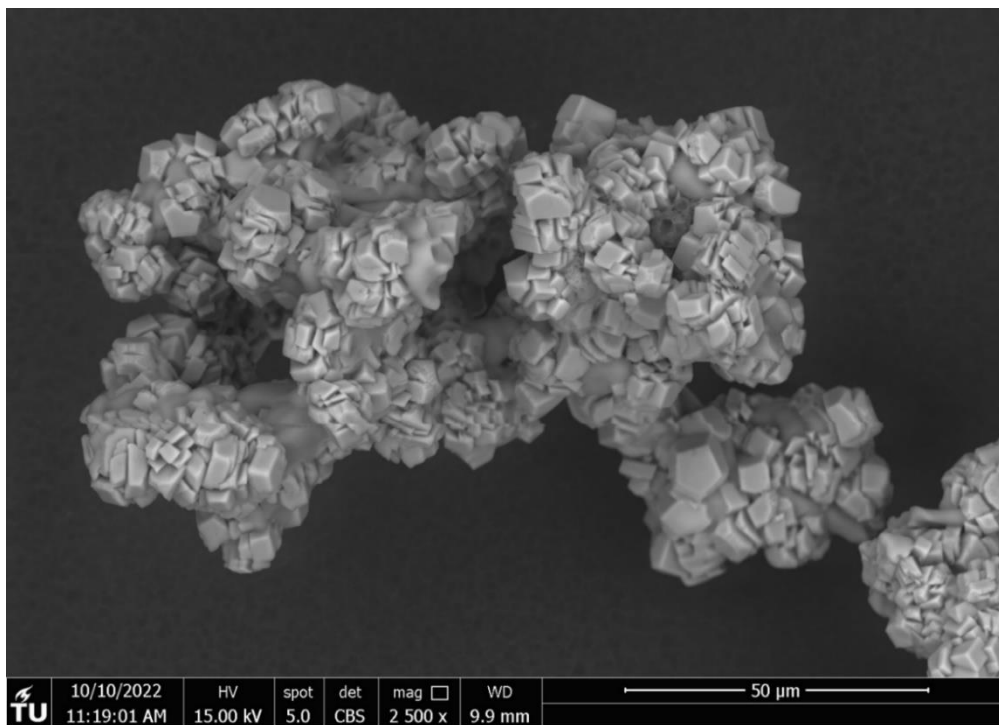


Figure 81 - EICP 0.5M using pure water only as the dissolving fluid, leading to stepwise microcryst propagation of cubic and cubo-rhombohedral calcite.

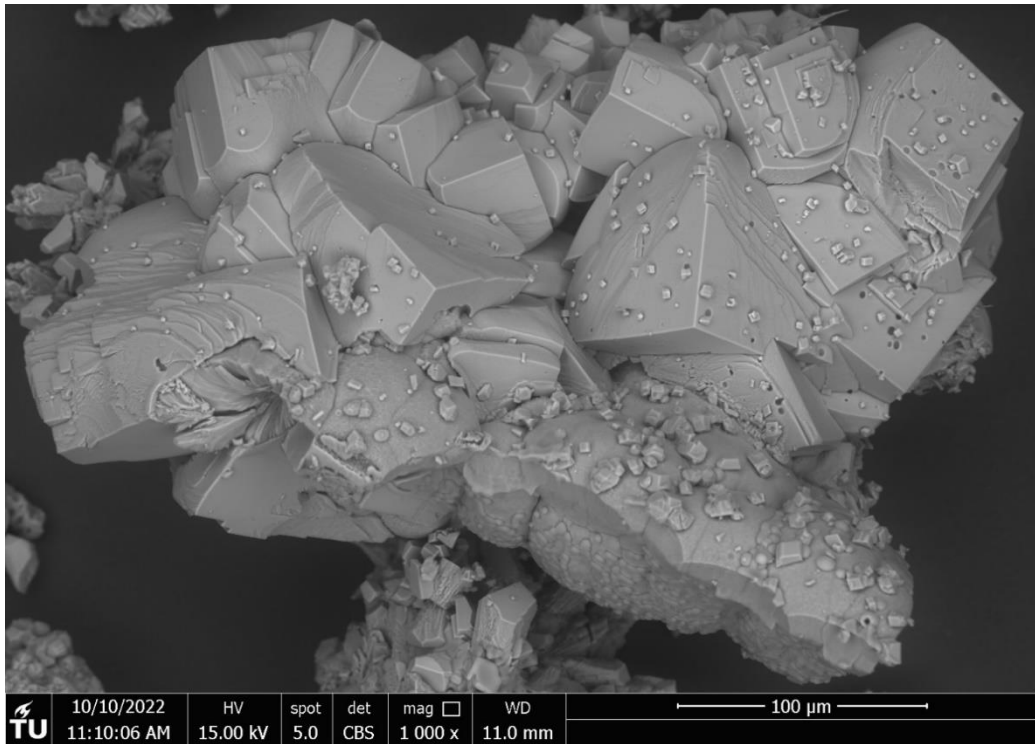


Figure 82 - Rhombohedral calcite macrocrystals with rounded $\{110\}$ and $\{100\}$ crystal planes. Intergrowth of cubic calcite nanocrystals clads the planar faces of the c-axis $\{104\}$. The mesocrystals favor low nucleation rates and ~ 150 micron crystals.

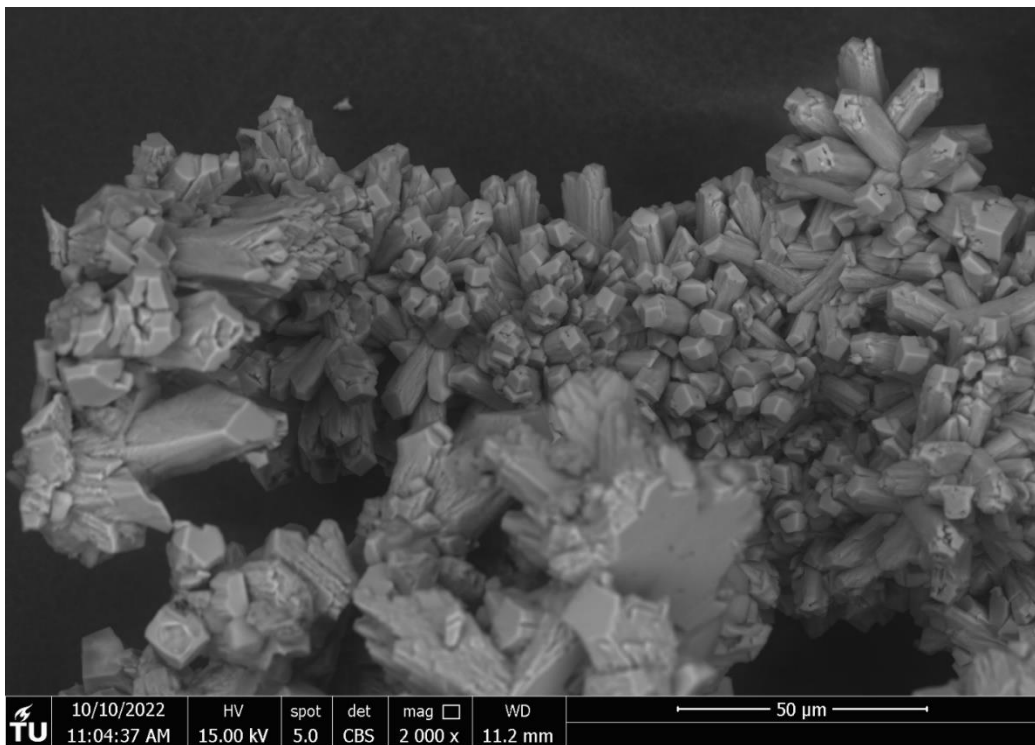


Figure 83 - Aragonite rods expanding to ~ 50 micron long crystals, intercalated by ~ 5 - 10 micron cubic calcite crystals. The growth expands out of the nucleation plane, notably the cementation surface of the test tube.

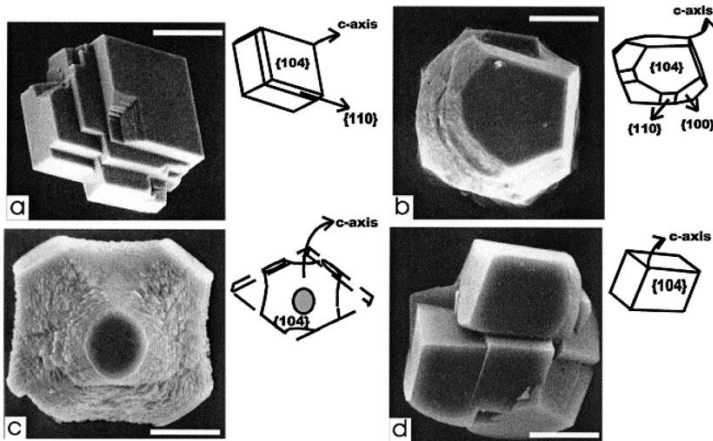


Figure 84 - Modulation of calcite polymorphs in the presence of increasing lysozyme protein concentration after 50h. Specifically images at (a) 0.1mg/ml, (b) 10mg/ml, (c) 25mg/ml, image taken at t_0 for (d) of 10mg/ml (Agudo and Putnis, 2012)

Such difference could be explained by the guanidine molecule. Atomic microscopy research of additives in calcite crystals, has shown that certain molecules alter growth rates and mineral form during biomineralization (Agudo and Putnis, 2012). Molecules such as amino acids, are adsorbed to the surface, reducing diffusive barriers and thus influencing the cation attachment required for crystal growth. In fact, Stephenson *et al.* (2008) have analyzed the variations of calcite morphology, hypothesizing that biomolecules aid surface growth by improving desolvation and ion transport. The modification of the water of solvation at the surface is only due to the hydrophilicity of molecules. Such process only occurs on the mineral surface, and is not incorporated in the matrix bulk (Eldhjah *et al.*, 2006). In fact, XRD analyses performed on all SEM calcium carbonate crystals did not record nitrogen peaks in the target volume. Such recordings support the idea that guanidine is not incorporated in the bulk matrix, but rather acts solely as a surface biomolecule assisting the desolvation of calcium (Ca^{2+}) and carbonate ions (CO_3^{2-}). Therefore, the large calcite polymorphs could be explained by macrostep formation and modulated growth in the c-axis {104}, with rounding of the {110} and {100} crystal planes (Figure 82). Additionally, fast nucleation forms aragonite rods, which expand to ~ 50 micron in length. Such mechanisms are favored in guanidine bearing media, whereas the absence of the additive favors fast nucleation and abundant stepwise growth of ~ 5 -10micron cubic calcite. Ergo, it is postulated that the adsorption of guanidinium to the calcite surface modulates growth, favoring lower nucleation rates and macrostep expansion of large crystal planes.

In conclusion, the addition of 0.25[mol/L] GndHCl biomolecules to EICP enhances the growth and morphology of calcium carbonate crystals. Only the two stable polymorphs are precipitated – calcite and aragonite. Firstly, modulated calcite macromolecules, and secondly aragonite rods intercalated by cubic calcite. The crystals are larger and expand further than pure EICP solutions.

Additional polymorph pH and EC analyses were performed, analyzing the temporal evolution with and without guanidine (Figure 84). To compensate for the extreme vigor of higher activity enzymes, the temporal data verified the slower reaction at 1[g/L]. This recipe allowed for decreased cementation in the syringes during the time consuming injections in D30mm cells (used for UCS tests).

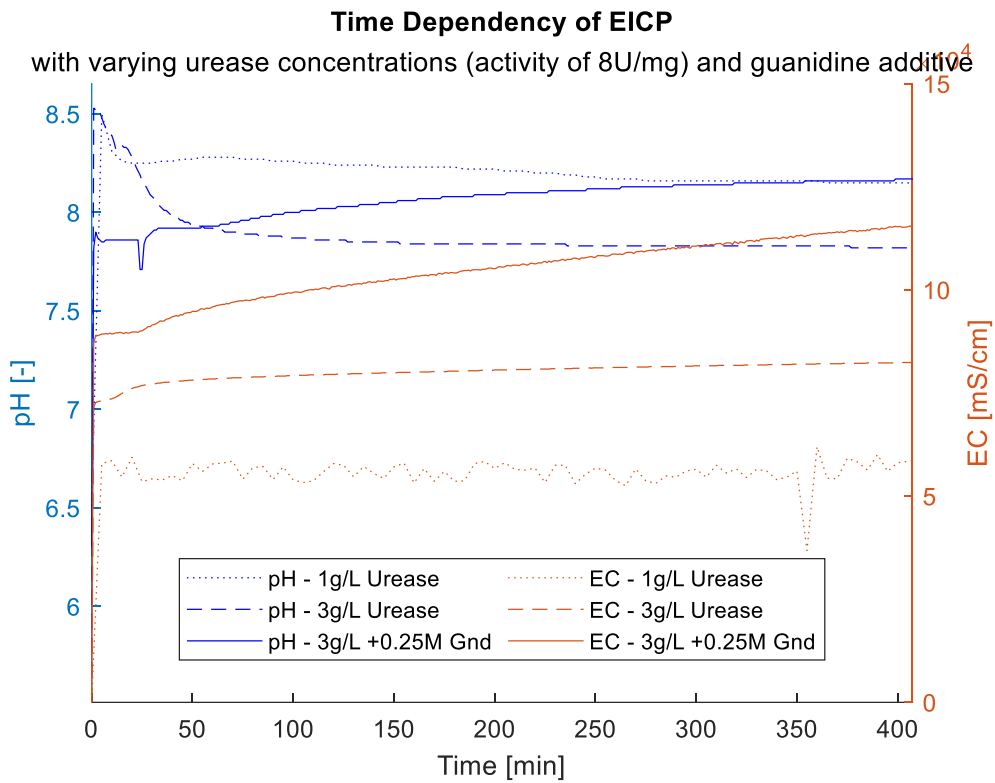
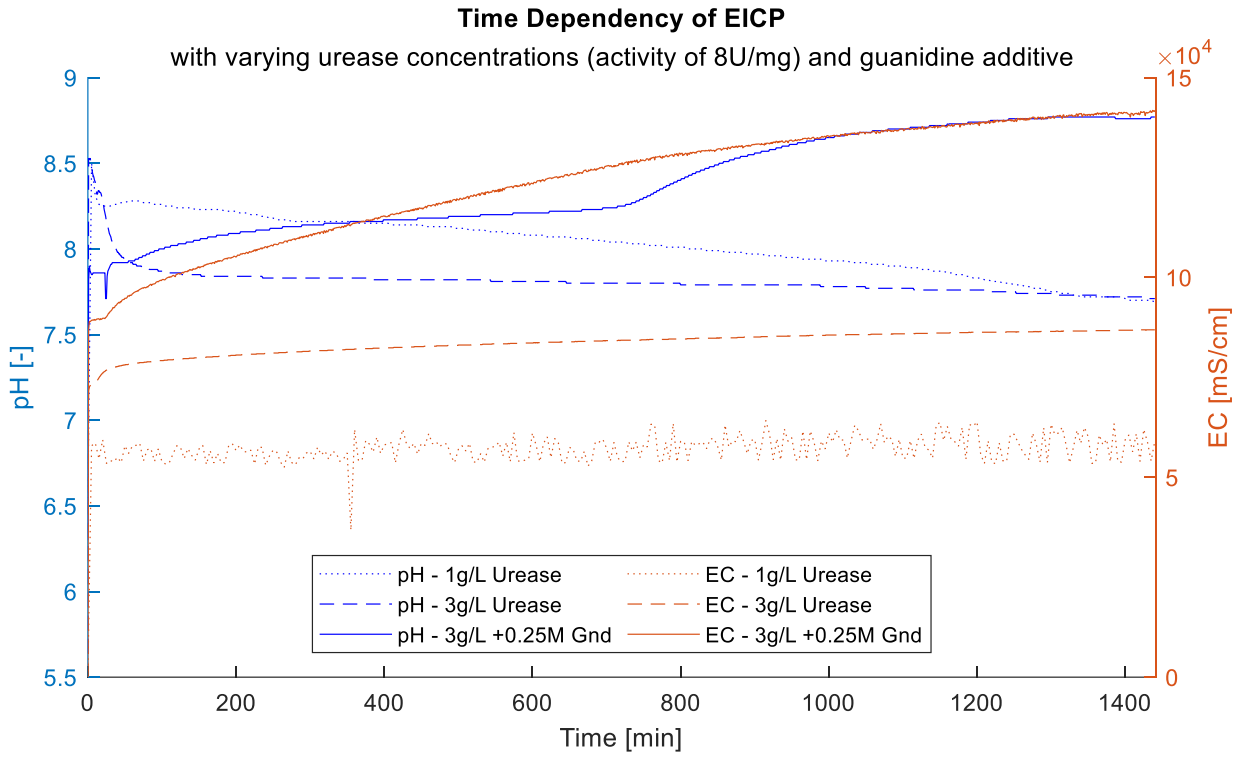


Figure 85 - Temporal evolution of EC and pH of EICP with varying *Canavalia Ensiformis* urease concentrations and 0.25[mol/L] guanidine additive.

8.8 UCS – Additional Images

8.8.1 UCS Sample Preparation

The samples are saturated and treated in 30mm wide injection cells, using EICP recipes catalyzed by the vigorous *Canavalia Ensiformis* urease at 1[g/L]. Two pore volumes are injected per treatment, corresponding to 42mL of fluid. Following guanidinium hydrochloride treatments (only), samples are flushed with two pore volumes of DI water to reduce hydrochloric acid contamination upon extraction and loading.

All samples are tested in saturated conditions to minimize random errors linked to varying suction effects. The Teflon sleeves are slit vertically with a razor to extract the cohesive specimens, which are rapidly placed in the load frame. Thereafter, the UCS tests are performed according to ASTM D2166 at fixed strain rates of 3[mm/min], a rate deemed fast enough to prevent evaporation and development of suction forces. Additionally, images are taken at 5 second intervals from a fixed angle camera placed in front of the apparatus on a tripod.



8.8.2 Failure of 30% Bentonite

See the images taken at peak strength for 30% bentonite specimens on the next page. Untreated samples failed to saturate with DI water, and therefore were loaded at partial saturation (systematic error of the water content physical parameter, leading to systematically greater mechanical parameters induced by suction forces).







Treatment Type →	Water Saturated	Guanidinium Hydrochloride	Bio2Cementation
<p data-bbox="241 252 645 320">30% Bentonite 80% compaction ρ_{dry} 1.35 [g/cm³]</p>			
<p data-bbox="241 818 645 887">30% Bentonite 95% compaction ρ_{dry} 1.56 [g/cm³]</p>			

Figure 86 - Unconfined compressive test peak load, indicating increasingly stiff (left to right) failure mechanisms of 30% bentonite specimens. injected specimens formed preferential flow paths in the cell, failing to saturate over 2 weeks of intervallic DI water injection and curing.

8.9 Equipment

Soil Constituents

Natural sodium bentonite A90 by Sibelco

Quartz Sand M32 (D₅₀ 265µm) by Sibelco

Bio-Cementation

IKA Vibrax VXR Electronic agitator by JK electronics

Alfa Aesar Urea 98+% by ThermoFisher GmbH

Granular Calcium Chloride anhydrous, <7micron, >93% by Sigma-Aldrich

M-prove d=0.001g precision balance by Sartorius AG

Harvard Apparatus PHD | Ultra Syringe Pump – fixed rate injection for BD Plastic 50mL syringes

Multi 3630IDS Digital meter for IDS sensors by WTW, EC sensor TetraCon 925 by WTW, pH-Electrode SenTix94 by WTW

Diaphragm Vacuum Pump 80.0mBar, 230V by Vacuubrand

Cellulose Nitrate Filter pore size 8.0µm by Sartorius AG

Modular Compact Rheometer 302, ANTON PAAR

Clay Inhibitor

Guanide Hydrochloride 6M by Boomlab

Imaging

Micro Computer Tomography by *Phoenix Nanotom 180NF, Resolutie 15 µm (Zs 75, Zd 250), 80kV, 200 tot 240 µA, mode 0, 500ms scantime, Meanvalue of 4 images, Skip 1st image, 1440 images (over 360°)*

Scanning Electron Microscope by *FEI Quanta 650F*

Load Cell

TRI Scan 50 | Advanced Digital Triaxial System - with Mitutoyo Absolute LVDT